

Characterisation of Spontaneous Proximal Tubule  
Formation *in vitro* and Development of a Metastatic  
Clear Cell Renal Cell Carcinoma (ccRCC) Model

Dissertation  
zur Erlangung des Doktorgrades  
der Naturwissenschaften

vorgelegt beim Fachbereich 15  
der Johann Wolfgang Goethe-Universität  
in Frankfurt am Main

von  
Lohitesh Kovooru  
aus Bhilai, Indien

Frankfurt am Main 2023

D30

Vom Fachbereich 15 der  
Johann Wolfgang Goethe-Universität als Dissertation angenommen.

Dekan: Prof. Dr. Sven Klimpel

Gutachter: Prof. Dr. Enrico Schleiff; Prof. Dr. Stefan Eimer

Datum der Disputation: 19<sup>th</sup> June 2023

## Acknowledgement

First and foremost, I would like to express my deep and sincere gratitude to my Ph.D. research supervisor Dr. Christian Pohl for providing me with an excellent platform to pursue my passion. I am obliged to have an opportunity to work under his skilled guidance. I am also grateful for the untiring attention he gave me from initiation till completing my research work. I would also like to thank Dr. Alexandra Stolz for providing the infrastructure and funding support for completing my doctoral studies.

This work would not have been possible without the infrastructural and administrative support from the institute, for which I thank Prof. Dr. Ivan Dikic, Director, Institute of Biochemistry II.

I express my sincere gratitude to Prof. Dr. Enrico Schleiff and Prof. Dr. Stefan Eimer for examining my thesis.

I would like to express my sincere gratitude to Dr. Ludovico Alves, Dr. Javier Garcia-Pardo, Dr. Yi-Lin, and Devang Odedra for their constructive criticism and enthusiastic discussions, which have always been a knowledge-enhancing experience for me.

I want to thank Dr. Christian Münch, Martin Adrian-Allgood, Dr. Rajeshwari Rathore, and Dr. Georg Tascher for helping me perform whole-cell proteomics. I would also like to thank Dr. Adriana Covarrubias for providing me with training in CQ1 Yokogawa microscope.

I want to thank Alok Behera, Vigor Matkovic, and Pramodh Kumar for being a pillar of support during every hurdle I faced in completing this journey.

My sincere thanks to Pablo Sanz, Sara Cano, Dr. Lorène Brunello, Diana Grewe, for being on their toes to help me in any situation.

I want to extend my heartfelt thanks to all the members of the Dikic group. I owe a special thanks to Elvi and Nicole for providing me with the prerequisites for my experiments and the cheerful vibe they bring to the department.

I would also like to thank Shrayans Nalwaya, Anudari Ganbaatar, Arushi Naresh Hegde, Lewis Elson, Dr. Mariana Tellechea, Viktoria Morasch, Paloma Cabrerizo Poveda,

Mukaddes Altinbay, Dr. Vajir Malek, Dr. Priyanka Dutta, Dr. Chaitanya Dingare, Dr. Sandy Maurer, Dr. Patricia Kunz, Heramb Vadhavkar, Anshu Bhattacharya, Dr. Rukmini Mukherjee, Rayene Berkane, Dr. Hung Ho, and Tejasri Lokachari for keeping me motivated during my doctoral studies.

I wish to acknowledge Prof. Rajdeep Chowdhury and Prof. Sudeshna M Chowdhury, Birla Institute of Technology and Science, Pilani (BITS Pilani), and their highly talented lab members Jyothi Nagaraj, Dr. Subhra Dash, Dr. Leena Fageria, and Dr. Heena Saini for introducing me to all the cell culture and molecular biology techniques and budding my interest in research during my post-graduate dissertation work. I would also like to thank Dr. Subhra Dash for constant support and encouragement in completing my Ph.D.

I would also like to thank all the members of Goethe Welcome Centre for their help with the visa process.

I am indebted to my parents' countless blessings and sacrifices and for having faith in my dreams, which made me what I am today. I would also like to thank my grandparents for their blessings. I want to thank my younger brother Sharan Kumar Kovooru, for his care, enduring love, and support in completing this journey.

Lohitesh Kovooru

## Content

Summary	9
Zusammenfassung	15
<b>1. Introduction</b>	<b>22</b>
1.1 Nephrons	22
1.2 Proximal Tubules	23
1.3 Dome formation	25
1.4 Tubulogenesis	28
1.5 Transport mechanisms in proximal tubules	34
1.6 Sodium transport	35
1.7 Chloride transport	36
1.8 Potassium transport	38
1.9 Calcium transport	39
1.10 Phosphate transport	40
1.11 Sulfate transport	41
1.12 Magnesium transport	42
1.13 Bicarbonate transport	42
1.14 Glucose transport	44
1.15 <i>In vitro</i> disease models specific to proximal tubules	47
1.16 Renal cell carcinoma	50
1.17 RENCA cell line	58
1.18 Treatment options for ccRCC	58

<b>2. Materials and Methods</b>	<b>63</b>
2.1 Materials	63
2.2 Maintenance of cell line	70
2.3 Immunoblot	70
2.4 Immunofluorescence	71
2.5 Pharmacological interventions	72
2.5.1 Measurement of major axis, minor axis, and dome area	72
2.5.2 Tube measurement	72
2.6 CRISPR Cas9 Knock-out	72
2.7 Reconstitutions of BAP1 mutation	73
2.8 Whole-cell proteomics	74
2.9 TCGA data analysis	75
2.10 Cloning, expression and purification of BAP1	75
2.10.1 BAP1 structural modelling	76
2.10.2 Evaluation of the BAP1 activity assays using AMC probes	76
<b>3. Results</b>	<b>77</b>
3.1 Self-organized formation of an epithelial-tubular system in LLC-PK1 cells	77
3.2 Differentiation phase-specific proteomics of self-organized morphogenesis	84
3.3 Characterisation of physiologically relevant transport processes by tool compounds	95
3.4 Generation of metastatic ccRCC model in LLC-PK1 cell line using CRISPR	99
3.5 Phenotypic characterisation of knockouts and mutants	101
3.6 Proteomics of engineered <i>in vitro</i> knockout and mutant models of metastatic ccRCC	105
3.7 Molecular characterisation of cell polarity loss	105
3.8 Role of EMT in ccRCC progression	107

3.9 Cytoskeleton contribution in the development of metastatic ccRCC	110
3.10 Investigation of potential signaling cascades involved in development of metastatic ccRCC	115
3.10.1 Cell Cycle	115
3.10.2 Hippo Signaling	116
3.10.3 ERK pathway	116
3.11 Misregulation of SLC genes in engineered metastatic ccRCC model representative of aggressive clinical ccRCC	120
3.12 Biochemical analysis of BAP1 mutations	124
<b>4. Discussion</b>	127
4.1 <i>In vitro</i> proximal tubule model	127
4.2 Luminogenesis process in proximal tubules	127
4.3 Presence of specific markers in different stages of proximal tubule development	129
4.4 Role of transporters in proximal tubule development	130
4.5 Stepwise-edited, metastatic clear cell RCC model developed using differentiated proximal tubule cells	132
4.6 Loss of lumen formation is an early event in metastatic ccRCC development	134
4.7 Epithelial to mesenchymal transition: step towards metastatic ccRCC progression	135
4.8 Activation of oncogenic pathways in metastatic ccRCC	136
4.8.1 Cell Cycle	136
4.8.2 Hippo pathway	137
4.8.3 MAPK pathway	138
4.9 Correlation of engineered <i>in vitro</i> metastatic CCRCC model with patient sample data	139
4.10 Missense mutations in BAP1 catalytic domain cause metastatic ccRCC	139
4.11 Future Work	140
<b>5. References</b>	142
<b>6. List of abbreviations</b>	174

<b>7. List of figures</b>	182
<b>8. List of tables</b>	184



## Summary

Epithelial cells enable essential physiological functions, including absorption, morphogenesis, secretion, and transport. To execute these functions, epithelial cells often form three-dimensional shapes that include curved sheets of cells surrounding a pressurized fluid-filled lumen. These three-dimensional tissues (called domes) are essential for organ function, but when they are not working properly, developmental defects, inflammation, and cancer can ensue. Recently, it has been shown that the cells that form domes show active superelasticity on micropatterned plates.

We show here that the immortalized renal proximal tubule epithelial cell line, LLC-PK1, stereotypically forms tubules in 10 days. Tubule formation takes place in 4 stages. When cells are plated on a culture dish, they form a monolayer on the 1st day; on the 3rd day, three-dimensional structures are formed, called domes; and after the 4.5th day, these domes start fusing to begin the transition stage and transit to the tubule stage. At the end of the 10th day, differentiated, elongated, and matured tubes form (Figure 3.1). Therefore, tubule formation is a self-organized, stereotypic morphogenetic program under long-term, unperturbed tissue culture conditions.

We propose that tubulogenesis is a two-step process in proximal tubules by doming and wrapping. The process begins with dome formation, and as the cell layers come together in the transition stage at the edge of the dome, this leads to the formation of the lumen of the eventual tubule (Figure 3.4). We also found that F-actin provides the mechanical strength during the formation of these three-dimensional structures during tubule formation (Figure 3.5).

To better understand this 4-step process on a molecular level, we performed proteomics of tubule formation to identify the different proteins that play a significant role in proximal tubule development. Importantly, we identified proximal tubule markers like synaptopodin, angiotensin 1-10, collectrin, polycystin 1, and polycystin 2. These proteins play an important role in renal tube formation and differentiation (Figure 3.8).

Cell division is carried out by highly conserved cyclin-CDK complexes, which phosphorylate various cellular components. Cyclin-CDKs act differently depending on the

cell cycle phase and work cooperatively to create DNA replication and cytokinesis. Therefore, we identified that cyclin-B1, marker of proliferation Ki-67, the RAD51 recombinase, and proliferating cell nuclear antigen (PCNA) are upregulated in the monolayer stage, and the expression decreases as tubule formation takes place (Figure 3.9).

The proximal tubule reabsorbs 60-65% of the glomerulus filtrate. Therefore, it requires a lot of energy generated by using the fatty acid oxidation (FAO) pathway. In our model, we found FAO expression is higher than that of the other metabolic pathways (Figure 3.11). We found expression of an intricate protein network in mitochondria, which we interpret as a sign of mitochondrial homeostasis being vital for the FAO pathway to work (Figure 3.12).

Furthermore, we also identified different types of transporters at each stage of proximal tubule formation (Figure 3.13), and we could recognize different cytoskeletal components playing a significant role in each stage of proximal tubule formation, for instance, at the monolayer stage, vimentin expression is high, and its expression is reduced as tubules form (Figure 3.14). Hence, this 2D system, at this step of characterization, seems suitable to use to study differential transport protein expression and how this might relate to physiological functions and syndromes.

Next, we inhibited different transporters using specific inhibitors and analyzed the effect on dome and tubule formation. We identified that Na<sup>+</sup>/K<sup>+</sup> ATPase and vacuolar H<sup>+</sup> ATPase play a significant role in the process of epithelial dynamics. Digoxin (a Na<sup>+</sup>/K<sup>+</sup> ATPase inhibitor) treatment inhibits dome and tubule formation. Bafilomycin (a v-ATPase inhibitor) treatment demonstrated a delay in dome and tube formation (Figure 3.15, 3.16, 3.17). Therefore, this study shows that this 2D proximal tubule novel system can be used for screening of pharmacological leads in the context of specific aspects of kidney physiology.

Despite the recent success in growing kidney organoids, they are not well suited to investigate various pathophysiological conditions *in vitro* for several reasons: They grow in 3D and form a tissue that later needs to be dissected/cleared and stained to investigate pathophysiological changes. Moreover, organoids require complex and expensive

protocols for generation and are challenging to use in screening approaches. Therefore, we set out to demonstrate feasibility for our 2D system using normal renal epithelial cells, which are the origin of various pathological conditions, to study pathophysiological conditions.

Kidney cancer is a type of cancer that has been increasing in recent years. Clear cell Renal Cell Carcinoma (ccRCC) accounts for up to 80% of all kidney cancers. Invasion, metastasis, and tumor progression is still poorly understood in this cancer. A significant problem in many cancers, including RCC, is the inability to target early stages of tumorigenesis if genetic risk factors have been identified. Although many inherited predispositions are known for RCCs, it has been suggested that after the tumor-initiating mutation or deletion, alterations in signaling cascades will lead to epigenetic reprogramming, which, dependent on the mutational landscape, ultimately drive the transition to malignancy.

Therefore, we used normal, immortalized renal proximal tubule LLC-PK1 cells and created oncogenic deletions/mutations through CRISPR-Cas9-mediated genome editing. Having obtained these cells, we could identify adaptation profiles of engineered cell lines that resemble metastatic ccRCC profiles. To do so, we first deleted the von Hippel Lindau tumor suppressor (VHL) and then introduced BRCA1 associated protein-1 (BAP1) mutations that are patient-specific to engineer metastatic ccRCC cell models (Figure 3.18, 3.19, 3.20).

We stained the cells with anti-ZO-1 antibodies, monitoring cell junctions, to inspect the alterations in the morphology of the cells and recognized the absence of tubule formation and the emergence of pleomorphic morphology in the engineered cell line (Figure 3.21).

After this, we also stained the cells with phalloidin to investigate the formation of stress fibers. Stress fibers provide cells with migrating and invasive properties so they can metastasize to other body parts. We found stress fiber formation in the mutated cell line and increased cytoskeleton length and branching points. Elevated cytoskeleton length and branching points help cells to grow abnormally and to obtain the ability to migrate and invade, which are the hallmarks of metastatic cancers (Figure 3.22).

Establishing apicobasal epithelial polarity is required for proper development and function of the kidney. Polarity complexes help to direct and to retain certain proteins at apical, basolateral, or tight junctions. Cell polarity is a significant step in proximal tubule formation, but it is lost and considered one of the initial steps during cancer development. We identified a severe deregulation of Par, Scribble, and Crumbs protein complexes in the VHL knockout cell line (Figure 3.24).

Metastasis is when cells from the primary tumor break off and disseminate to other body parts, including the blood and lymph vessels. The process occurs in most types of cancer and is promoted by epithelial-mesenchymal transition (EMT). It is a cellular process by which epithelial cells lose their apicobasal polarity and cell-cell adhesion and gain migratory and invasive properties to become mesenchymal cells. Since we could identify loss of polarity, we further searched for additional signs of EMT.

We could demonstrate that epithelial markers like E-cadherin (CDH1) and occludin (OCLN) are downregulated in the lines harboring ccRCC mutations (Figure 3.25). We also identified various mesenchymal markers like  $\beta$ -catenin (CTNNB1), desmin (DES), desmoplakin (DSP), FERM, ARH/RhoGEF and Pleckstrin domain protein 1 (FARP1), fibronectin 1 (FN1), integrin subunit alpha 5 (ITGA5), keratin 14 (KRT14), keratin 18 (KRT18), transgelin (TAGLN), and vimentin (VIM) as being upregulated in our ccRCC model cell lines (Figure 3.25). Deregulation of the above proteins is associated with a reduction in overall survival of the metastatic ccRCC.

In cancer cells, EMT markers' dysregulation is often associated with high invasiveness and metastasis. Elevated invasive behavior requires the loss of intercellular adhesion, which could arise from intracellular signaling, a decrease in adhesive strength, or aberrant interactions with the extracellular matrix (ECM). The EMT markers that we discuss in our study interact with ECM and lead to the metastatic state. We can therefore assume that our cell lines with ccRCC resemble tumor cells with metastatic potential.

The cytoskeleton is an essential part of cells that also serves as a framework for the cell to maintain or change its shape. The cytoskeleton comprises three prominent types of filaments: microfilaments, intermediate filaments, and microtubules; this filamentous

network extends throughout the cytoplasm, connects with the plasma membrane, responds to external stimuli and signals, and provides cells with dynamic structural modifications. Certain cancers are characterized by a loss of regulation in cytoskeletal function, which allow abnormal cells to grow, migrate or invade.

We identified dysregulation of all three types of cytoskeletal filaments. We found deregulation of actin alpha 1 (ACTA1) and actin beta-like 2 (ACTBL2) expressions in the mutated cell lines (Figure 3.26a). We also identified that Keratins are deregulated in metastatic cell lines. As described above, the intermediate filament protein Vimentin was upregulated, its expression is prominent in mesenchymal cells (Figure 3.26b). Microtubules are the tracks for dynein and kinesin motor proteins and are also found to be dysregulated in the metastatic ccRCC cell line (Figure 3.26c). They are reported to be overexpressed or under-expressed in many cancers, suggesting that distinct members have different functions. Therefore, engineered cell lines can be used to elucidate the role of the cytoskeleton in metastatic ccRCC.

Cancer is characterized by a deregulation of essential molecular pathways that leads to abnormal gene expression and growth. It is often caused by one or more genetic events that provide a selective growth advantage to cancer cells. Genetic mutations in signaling pathways that control cell-cycle progression, cell growth, and apoptosis are common tell-tales of cancer. We analyzed the alterations in three signaling cascades: Cell cycle, Hippo, and mitogen-activated protein kinase (MAPK) pathways. In the cell cycle pathway, we identified CDK7, CDC16, CDC23, and CDC27 as deregulated in the engineered cell lines. This may lead to abrupt cell division (Figure 3.27a). The Hippo signaling pathway plays an essential role in organogenesis, and we showed the increase of yes-associated protein 1 (YAP1) and TEA domain family member 1 (TEAD1) (Figure 3.27b). We could also identify that misregulation in MAPK pathways frequently occurs in AKT, Kirsten rat sarcoma viral oncogene homolog (KRAS), ras-related protein, epidermal growth factor receptor (EGFR), growth factor receptor bound protein 2 (GFRBP2), neurofibromin, and transforming growth factor beta receptor 2 (TGF $\beta$ R2) in the extracellular signal-regulated kinase pathway (Figure 3.27c).

Solute carriers (SLC) are essential to transport small molecules. Defects in any of these transporters can lead to severe pathological conditions. The expression patterns and prognostic values of the SLC transporters' role in metastatic ccRCC still need to be determined. Therefore, we analyzed the expression levels of SLC family members and their correlation with prognosis in ccRCC patients with Gene Expression Profiling Interactive Analysis (GEPIA) data. We found that SLC12A9, SLC25A13, SLC25A44, SLC29A1, and SLC30A9 are significantly downregulated in metastatic ccRCC cell lines compared to those in normal tissues and associated with overall survival (OS) and disease-free survival (DFS) in ccRCC patients (Figure 3.28).

Furthermore, we showed that BAP1 cancer-associated mutants (i.e., V24D, E31A, V43G, and G185R) lost the ubiquitin activity against the Ub-AMC substrate. We also indicated mutations impacting renal tubule formation are all present in the catalytic domain of BAP1. These mutations abrogated BAP1 activity, which suggests that BAP1 substrate processing is vital for proximal tubule differentiation (Figure 3.29).

In summary, we here characterize morphogenetic, cytoskeletal, and early oncogenic changes during metastatic ccRCC tumorigenesis in a novel *in vitro* system that will allow us and others in future to test pharmacological compounds with direct dynamical readouts not possible *in vivo*. These cell models can also be used to introduce other deletions/mutations of essential proteins responsible for metastatic ccRCC, thus expanding the horizon of possible cellular models of ccRCC. Notably, our model can also be used to reduce the need for studying renal physiology in animal models.

## Zusammenfassung

Epithelzellen übernehmen essentielle physiologische Funktionen, die die Absorption, Morphogenese, Sekretion und den Transport einschließen. Um diese Funktionen auszuführen, bilden Epithelzellen oft eine dreidimensionale Form, welche eine gekrümmte Zellschicht umfasst, die ein mit Flüssigkeit gefülltes Lumen umgibt. Diese dreidimensionalen Gewebeteile, Halbzysten (englisch *dome*) genannt, sind für Organfunktionen unerlässlich. Wenn sie nicht richtig arbeiten, kann dies zu Entwicklungsstörungen, Entzündungen und Krebs führen. Kürzlich wurde gezeigt, dass *dome*-bildende Zellen auf mikrostrukturierten Platten eine aktive Superelastizität aufweisen.

Wir zeigen hier, dass die immortalisierte Epithelzelllinie des proximalen Nierentubulus, LLC-PK1, stereotypisch innerhalb von 10 Tagen Tubuli, (Geweberöhrchen) ausbildet. Die Röhrenbildung oder Tubulogenese erfolgt in vier Stufen: (1) Wenn die Zellen auf eine Kulturschale plattiert werden, bilden sie am ersten Tag eine eine Zelle dicke Schicht (*monolayer*); (2) am dritten Tag bilden sich dreidimensionale Strukturen, Halbzysten (*domes*); und (3) nach dem vierten bis fünften Tag beginnen diese Halbzysten zu verschmelzen, was ein Übergangsstadium darstellt, dass in (4) die Tubulogenese übergeht. Am Ende des zehnten Tages bilden sich differenzierte, verlängerte und ausgereifte Röhren aus (Abbildung 3.1). Daher ist die Tubulogenese ein selbstorganisiertes, stereotypisch morphogenetisches Programm unter langfristigen, ungestörten Gewebekulturbedingungen.

Die Tubulogenese könne wir in diesem Zusammenhang als einen zweistufigen Prozess beschrieben, der aus Halbzystenbildung (*doming*) und Einfaltung (*wrapping*) besteht. Der Prozess beginnt mit einer Halbzystenbildung und sobald die Zellschichten in der Übergangsphase am Rande der Halbzyste zusammenkommen, führt dies zur Bildung des Lumens des späteren Tubulus (Abbildung 3.4). Die Zellen erstrecken sich über die gesamte Länge des Epithels, das eine apikale Verengung erfährt. Dies führt zu einer Einstülpung, welche sich vertieft bevor sich aus den Zellen eine neue Röhre formt (Abbildung 3.5).

Durch eine Proteomanalyse der vier Stadien der proximalen Tubulusbildung, konnten die verschiedenen Proteine identifiziert werden, die bei der Entwicklung der proximalen Tubuli eine wichtige Rolle spielen. Dabei konnten wir proximale Tubulusmarker wie synaptopodin, angiotensin 1-10, collectrin, polycystin 1 und polycystin 2 in einer Stufen-abhängigen Muster nachweisen. Diese Proteine spielen eine wichtige Rolle bei der Bildung und Differenzierung der Nierenkanäle, was (Abbildung 3.8) die physiologische Relevanz des hier dargestellten zellulären Systems unterstreicht.

Bei der hier verwendeten Zelllinie handelt es sich um eine nicht viral oder durch Onkogene immortalisierte Linie. Daher wurde untersucht, wie sich die Regulation des Zellzyklus während der vier Stufen der Morphogenese ändern. Wir konnten zeigen, dass Cyclin-B1, der Proliferationsmarker Ki-67, die Rekombinase RAD51 und das proliferating cell nuclear antigen (PCNA) im Einzellschicht-Stadium hochreguliert sind und deren Expression mit der Tubulusbildung abnimmt, somit verlassen die Zellen während der Morphogenese kontinuierlich den Zellzyklus in eine *gap phase* (Abbildung 3.9).

In der Niere reabsorbieren die proximalen Tubuli 60-65 % des Glomerulusfiltrats. Daher benötigen sie viel Energie, die über den Fettsäureoxidationsweg (FAO) gewonnen wird. In unserem Modell ist die FAO-Expression höher als die der anderen Stoffwechselwege (Abbildung 3.11). Im Vergleich zu anderen zytosolischen Organellen fanden wir in den Mitochondrien außerdem ein kompliziertes Proteinnetzwerk, da die mitochondriale Homöostase für die Funktion des FAO-Stoffwechselwegs unerlässlich ist (Abbildung 3.12).

Neben der Expression organspezifischer Marker, dem Verlassen des Zellzyklus ist dies ein dritter Indikator für das Nachvollziehen eines entwicklungsbiologisch regulierten Vorgangs in Form eines selbstorganisierten Prozesses *in vitro*. Zudem konnten wir als vierten Indikator verschiedene Arten von Transportern in jedem Stadium der proximalen Tubulusbildung identifizieren, die für die Nierenphysiologie von Bedeutung sind (Abbildung 3.13). Das Zytoskelett spielt eine wesentliche Rolle bei der Bildung des proximalen Tubulus. Wir haben festgestellt, dass verschiedene Zytoskelette in jeder Phase der Bildung des proximalen Tubulus eine wichtige Rolle spielen. Zum Beispiel ist die Expression von Vimentin im Einzellschicht-Stadium hoch und nimmt mit der Bildung



des Tubulus ab (Abbildung 3.14). In unseren Augen kann dieses 2D-System daher verwendet werden, um die Rolle der einzelnen Transporter und die mit der Transporteraktivität verbundenen Krankheiten zu untersuchen.

Bei der Hemmung verschiedener Transporter mit Hilfe von Inhibitoren und der Analyse der Auswirkungen auf die Halbzyten- und Röhrenbildung, stellten wir fest, dass die  $\text{Na}^+/\text{K}^+$ -ATPase und die vakuoläre  $\text{H}^+$ -ATPase eine wichtige Rolle im Prozess der Epitheldynamik spielen. Die Behandlung mit Digoxin ( $\text{Na}^+/\text{K}^+$ -ATPase-Inhibitor) hemmt die Halbzyten- und Röhrenbildung. Die Behandlung mit Bafilomycin ( $\text{H}^+$ -ATPase-Inhibitor) führte zu einer Verzögerung der Halbzyten- und Röhrenbildung (Abbildung 3.15, 3.16, 3.17). Diese pharmakologischen Effekte zeigen, dass dieses neuartige 2D-System des proximalen Tubulus für das Hochdurchsatz-Screening von Leitstrukturen in der Pharmaforschung verwendet werden kann.

Trotz der jüngsten Erfolge bei der Kultivierung von Nierenorganoiden sind diese aus mehreren Gründen nicht gut geeignet, um verschiedene pathophysiologische Bedingungen *in vitro* zu untersuchen: Sie wachsen in 3D und bilden ein Gewebe, das später präpariert und gefärbt werden muss, um pathophysiologische Veränderungen zu untersuchen. Außerdem ist die Organoidbildung komplex sowie kostenintensiv und für Screening-Ansätze nur schwer zu verwenden. Daher haben wir das 2D-System unter Verwendung normaler Nierenepithelzellen etabliert, die der Ursprung verschiedener pathologischer Zustände sind, einschließlich des Klarzellen RCC.

Nierenkrebs ist eine Krebsart, die in den letzten Jahren zugenommen hat. Das klarzellige Nierenzellkarzinom (ccRCC) macht bis zu 80 % aller Nierenkrebserkrankungen aus. Vorgänge wie Invasion, Metastasierung und Tumorprogression sind immer noch nicht ausreichend verstanden. Ein signifikantes Problem bei vielen Krebsarten, darunter auch beim Nierenzellkarzinom, ist die Unfähigkeit, frühe Stadien der Tumorentstehung anzugehen, wenn genetische Risikofaktoren identifiziert wurden. Obwohl viele vererbte Prädispositionen für Nierenkrebs bekannt sind, wurde vermutet, dass nach der den Tumor auslösenden Mutation oder Deletion, Veränderungen in den Signalkaskaden zu einer epigenetischen Umprogrammierung führen, die in Abhängig von der Mutationslandschaft, letztlich den Übergang zur Bösartigkeit vorantreibt.

Daher verwendeten wir normale, immortalisierte Zellen des proximalen Nierentubulus LLC-PK1 und erzeugten diese Deletionen/Mutationen durch eine CRISPR-Cas9-vermittelte Genomeditierung. Nachdem wir diese Zellen erhalten hatten, untersuchten wir die Anpassungsprofile der manipulierten Zelllinien, und konnten zeigen, dass diese den Profilen des metastasierten ccRCC ähneln. Um die metastasierenden ccRCC-Zellmodelle zu entwickeln, entfernten wir zunächst den von Hippel Lindau Tumorsuppressor (VHL) und führten dann Mutationen im BRCA1-assoziierten Protein-1 (BAP1)-Mutationen ein, die patientenspezifisch sind (Abbildung 3.18, 3.19, 3.20).

Um die Veränderungen in der Morphologie der Zellen zu untersuchen, färbten wir die Zellen mit ZO-1 an und erkannten, dass die Tubulusbildung ausblieben, sich jedoch pleomorphe Morphologien in den manipulierten Zellen zeigten (Abbildung 3.21).

Anschließend färbten wir die Zellen auch mit Phalloidin, um die Bildung von Stressfasern zu untersuchen. Stressfasern verleihen den Zellen Wanderungsfähigkeit und invasive Eigenschaften, so dass sie in andere Körperteile metastasieren können. In der mutierten Zelllinie entdeckten wir die Bildung von Stressfasern sowie eine erhöhte Skelettlänge und Verzweigungspunkte. Erhöhte Skelettlänge und Verzweigungspunkte tragen dazu bei, dass die Zellen abnormal wachsen und die Fähigkeit zur Migration und Invasion erlangen, was die Kennzeichen von metastasierenden Krebsarten sind (Abbildung 3.22).

Die Etablierung der apikobasalen epithelialen Polarität verbessert die Entwicklung und Funktion der Niere. Die Polaritätskomplexe tragen dazu bei, Proteine an apikalen, basolateralen oder engen Verbindungsstellen zu lenken und zu halten. Die Zellpolarität ist ein wichtiger Schritt bei der Bildung der proximalen Tubuli, geht jedoch verloren und gilt als einer der ersten Schritte bei der Krebsentwicklung. In der VHL-Knockout-Zelllinie konnten wir eine vollständige Deregulierung der Par-, Scribble- und Crumbs-Proteinkomplexe feststellen (Abbildung 3.24).

Von einer Metastasierung spricht man, wenn sich Zellen des Primärtumors ablösen und sich in andere Körperteile, einschließlich der Blut- und Lymphgefäße, ausbreiten. Dieser Prozess tritt bei den meisten Krebsarten auf und wird durch den epithelial-mesenchymalen Übergang (EMT) gefördert. Dabei handelt es sich um einen zellulären

Prozess, bei dem Epithelzellen ihre apikobasale Polarität und Zell-Zell-Adhäsion verlieren und migratorische und invasive Eigenschaften erlangen, um zu mesenchymalen Zellen zu werden.

Wir konnten zeigen, dass Epithelmarker wie E-cadherin (CDH1) und Occludin (OCLN) in metastasierenden ccRCC-Zelllinien herunterreguliert sind (Abbildung 3.25). Wir haben auch festgestellt, dass verschiedene mesenchymale Marker wie  $\beta$ -Catenin (CTNNB1), desmin (DES), desmoplakin (DSP), FERM, ARH/RhoGEF und Pleckstrin domain protein 1 (FARP1), fibronectin-1 (FN1), integrin subunit alpha 5 (ITGA5), keratin 14 (KRT14), keratin 18 (KRT18), transgelin (TAGLN) und vimentin (VIM) im metastasierenden ccRCC-Modell hochreguliert sind (Abbildung 3.25). Eine Deregulierung der oben genannten Proteine ist mit einer Verminderung der Gesamtüberlebensdauer des metastasierten ccRCC verbunden. In Krebszellen ist die Dysregulation von EMT-Markern häufig mit einer hohen Invasivität und Metastasierung verbunden. Ein erhöhtes invasives Verhalten setzt den Verlust der interzellulären Adhäsion voraus. Dieser könnte durch intrazelluläre Signalübertragung, eine Abnahme der Adhäsionskraft oder aberrante Interaktionen mit der extrazellulären Matrix (ECM) entstehen. Die EMT-Marker, die wir in unserer Studie diskutiert haben, interagieren mit der ECM und führen zu einem metastatischen Zustand.

Das Zytoskelett ist ein wesentlicher Zellbestandteil, der auch als Gerüst für die Zelle dient, um ihre Form zu erhalten und ihr Halt zu geben. Das Zytoskelett besteht aus drei wichtigen Filamenten: Mikrofilamente, Intermediärfilamente und Mikrotubuli. Dieses filamentöse Netzwerk erstreckt sich über das gesamte Zytoplasma, ist mit der Plasmamembran verbunden, reagiert auf äußere Reize und Signale und ermöglicht den Zellen dynamische strukturelle Veränderungen. Bestimmte Krebsarten zeichnen sich durch einen Verlust der Regulierung der natürlichen Zytoskelettfunktion aus, der es abnormalen Zellen ermöglicht, zu wachsen, zu wandern oder einzudringen.

Wir haben die Fehlregulierung aller drei Arten von Zytoskelettfilamenten festgestellt. Dabei entdeckten wir eine Deregulierung der actin alpha 1 (ACTA1) und actin beta-like 2 (ACTBL2) Expression in den mutierten Zelllinien (Abbildung 3.26a). Auch haben wir festgestellt, dass die Keratine in den metastatischen Zelllinien dereguliert sind. Vimentin ist ein Intermediärfilament, dessen Expression in mesenchymalen Zellen zu finden ist

(Abbildung 3.26b). Mikrotubuli bilden Zytoskelettelemente auf denen Dynein- und Kinesin-abhängiger Transport stattfinden kann und diese sind in der metastasierenden ccRCC-Zelllinie fehlreguliert (Abbildung 3.26c). Es wird berichtet, dass sie bei vielen Krebsarten über- oder unterexprimiert sind, was darauf hindeutet, dass verschiedene Vertreter unterschiedliche Funktionen haben. Somit bietet es sich an künstlich hergestellte Zelllinien zu verwenden, um die Rolle des Zytoskeletts bei metastasierendem ccRCC zu erforschen.

Krebs ist durch eine Deregulierung wesentlicher molekularer Signalwege gekennzeichnet, die zu einer abnormalen Genexpression und Wachstum führt. Krebs wird häufig durch ein oder mehrere genetische Ereignisse verursacht, die den Krebszellen einen selektiven Wachstumsvorteil verschaffen. Genetische Mutationen in Signalwegen, die das Fortschreiten des Zellzyklus, das Zellwachstum und die Apoptose kontrollieren, sind häufige Anzeichen für Krebs. Wir haben die Veränderungen in drei Signalkaskaden analysiert: Zellzyklus, Hippo und Mitogen-aktivierte Proteinkinase (MAPK)-Signalweg. Im Signalweg des Zellzyklus haben wir festgestellt, dass verschiedene CDK7, CDC16, CDC23 und CDC27 in den manipulierten Zelllinien dereguliert sind. Dies kann zu einer abrupten Zellteilung führen (Abbildung 3.27a). Der Hippo-Signalweg spielt eine wesentliche Rolle bei der Organogenese. Außerdem zeigten wir einen Anstieg des Yes-assoziierten Proteins 1 (YAP1) und des TEA-Domänen-Familienmitglieds 1 (TEAD1) (Abbildung 3.27b). Wir können ferner aufzeigen, dass eine Fehlregulierung im MAPK-Signalweg häufig bei AKT, Kirsten rat sarcoma viral oncogene homolog (KRAS), Ras-bezogenem Protein, epidermalem Wachstumsfaktor-Rezeptor (EGFR), Wachstumsfaktor-Rezeptor-gebundenem Protein 2 (GFRBP2), Neurofibromin und Transformations-Wachstumsfaktor-Beta-Rezeptor 2 (TGF $\beta$ R2) im extrazellulären Signalregulierten Kinase-Signalweg auftritt (Abbildung 3.27c).

Solute Carriers (SLCs) sind für den Transport kleiner Moleküle beim Menschen unerlässlich. Defekte bei einem dieser Transporter können zu schweren pathologischen Bedingungen führen. Die Expressionsmuster und der prognostische Wert der Rolle der SLC-Transporter beim metastasierten ccRCC müssen noch ermittelt werden. Daher haben wir die Expressionsniveaus von Mitgliedern der SLC-Familie und ihre Korrelation

mit der Prognose bei ccRCC-Patienten mit Hilfe der „Gene Expression Profiling Interactive Analysis“ (GEPIA) untersucht. Wir fanden heraus, dass SLC12A9, SLC25A13, SLC25A44, SLC29A1 und SLC30A9 in metastatischen ccRCC-Zelllinien im Vergleich zu normalem Gewebe signifikant herunterreguliert sind und mit dem Gesamtüberleben (OS) und dem krankheitsfreien Überleben (DFS) bei ccRCC-Patienten in Verbindung stehen (Abbildung 3.28).

Wir konnten zeigen, dass Mutanten der Ubiquitinligase BAP1, die mit diesem Krebs speziell assoziiert sind (d. h. V24D, E31A, V43G und G185R), die Ubiquitin-Aktivität gegenüber dem Ub-AMC-Substrat verloren haben. Außerdem haben wir festgestellt, dass alle Mutationen, die sich auf die Bildung von Nierentubuli auswirken, in der katalytischen Domäne von BAP1 auftreten. Diese Mutationen setzten die BAP1-Aktivität außer Kraft, was darauf hindeutet, dass die Verarbeitung des BAP1-Substrats für die Differenzierung der proximalen Tubuli entscheidend ist (Abbildung 3.29).

Wir charakterisieren Veränderungen im Zytoskelett sowie morphogenetische und frühe onkogene Veränderungen, während der metastasierenden ccRCC-Tumorgenese in einem neuartigen *in-vitro*-System. Dieses ermöglicht es uns verschiedene chemische Sonden mit direkten dynamischen Messwerten zu testen, was *in vivo* nicht möglich ist. Letztendlich kann dieses Zellmodell auch verwendet werden, um andere Deletionen/Mutationen von essentiellen Proteinen einzuführen, die für das metastasierende ccRCC verantwortlich sind, um so den Horizont möglicher zellulärer Modelle des ccRCC zu erweitern.

# 1 Introduction

Fluid balance and regulation of osmotic gradients play an essential role in tissue homeostasis. The kidney maintains fluid and electrolyte homeostasis and fluid dynamics, as it reabsorbs about 99% of filtered electrolytes and solutes generated inside the body [1]. No other organ has the fine-tuned capacity to spontaneously respond to changes of systemic electrolyte levels, imbalanced fluid homeostasis, or alterations in blood pressure or pH. The proximal and distal tubular segments of nephrons are responsible for this remarkable responsiveness of the kidney: Proximal tubules re-absorb 65% of the filtered load, which includes amino acids, solutes, and smaller peptides and proteins, the majority of bicarbonates, and glucose [2].

## 1.1 Nephrons

Nephrons are the anatomical units responsible for kidney function. The characterization of the nephron has changed significantly ever since it was first observed and described by William Bowman in the human kidney, while the model laid down by Ernest Henry Starling remains primarily unchanged and has partly enabled modern era renal physiology [3]. Early findings indicated that an individual nephron is broadly divided into renal corpuscle and renal tubule. The renal corpuscle can be further sub-divided into the glomerulus and Bowman's capsule; the glomerulus is an intricate, capillary cluster (tuft), cupped by the Bowman's capsule (Figure 1.1a) [4]. The renal corpuscle is responsible for the first step of filtration, handling ultrafiltration; it hinders most blood proteins and cells while allowing small molecules (~25kDa) to pass through its membrane [5]. The renal tubule emerges from the Bowman's capsule and is composed of different regions: the proximal tubule, the loop of Henle, the distal convoluted tubule, and the connecting tubule [4, 6].

As nephrons are heterogenous in nature, location and structural characteristics are considered as appropriate methodology to classify them. Depending on the localization of the glomerular tuft, superficial cortical nephrons and juxtamedullary or deep nephrons can be discriminated (Figure 1.1b). Other attempts have been made to classify nephrons further. Nephrons were labelled short/long, based on the relative length of their loop of

Henle; the length of the loop of Henle also overlaps with a localization bias, with a higher density of short nephrons in the superficial cortex and long nephrons in the juxtamedullary region [4].

Apical microvilli of the proximal tubule form the brush border at the luminal surface of renal epithelial cells. These brush border microvilli can reach 2-3  $\mu\text{m}$  in length, approximately 4000 in number, equally spaced, densely packed, and nearly identical in height [7]. Since most of the filtrate is re-absorbed by the proximal tubule, this increased surface area is likely to assist in managing large volumes of fluid, allowing an efficient contact with transporters and enzyme arrays arranged across the microvilli. Microvilli also act as mechano-sensors in which hydrodynamic torque is conveyed to the actin cytoskeleton and modulates sodium re-absorption in proximal tubules [8].

## 1.2 Proximal Tubules

The ultra- and micro-structure of proximal tubules has been extensively reported in the literature. Proximal convoluted tubules on the cortex connect directly to the glomerulus through Bowman's capsule, while proximal straight tubules localize to the inner cortex and outer medulla [4]. Due to technical limitations of *in vivo* methodologies for kidney studies (such as micro-puncture or micro-perfusion), most of the functional information on proximal tubules applies to the easily accessible proximal convoluted tubules of superficial nephrons.

By high-resolution light microscopy, three connected, structurally discrete segments (S1, S2, S3) of the proximal tubule have been characterized. S1 comprises proximal and middle sections of the convoluted tube. S2 includes the distal portion of the convoluted tubule and the distal portion of the straight tubule. S3 encompasses the distal section of the straight tube [9]. When considering the morphological differences between nephrons due to species and/or kidney localization, it becomes apparent that even this segmentation is subject to variability [10, 11]. Juxtamedullary nephrons' convoluted tubules contain S1 and S2, S3 is only found in straight tubules; superficial nephron's convoluted tubules also contain S1 and S2, but S2 extends into the straight tubule, preceding S3 [12-14].



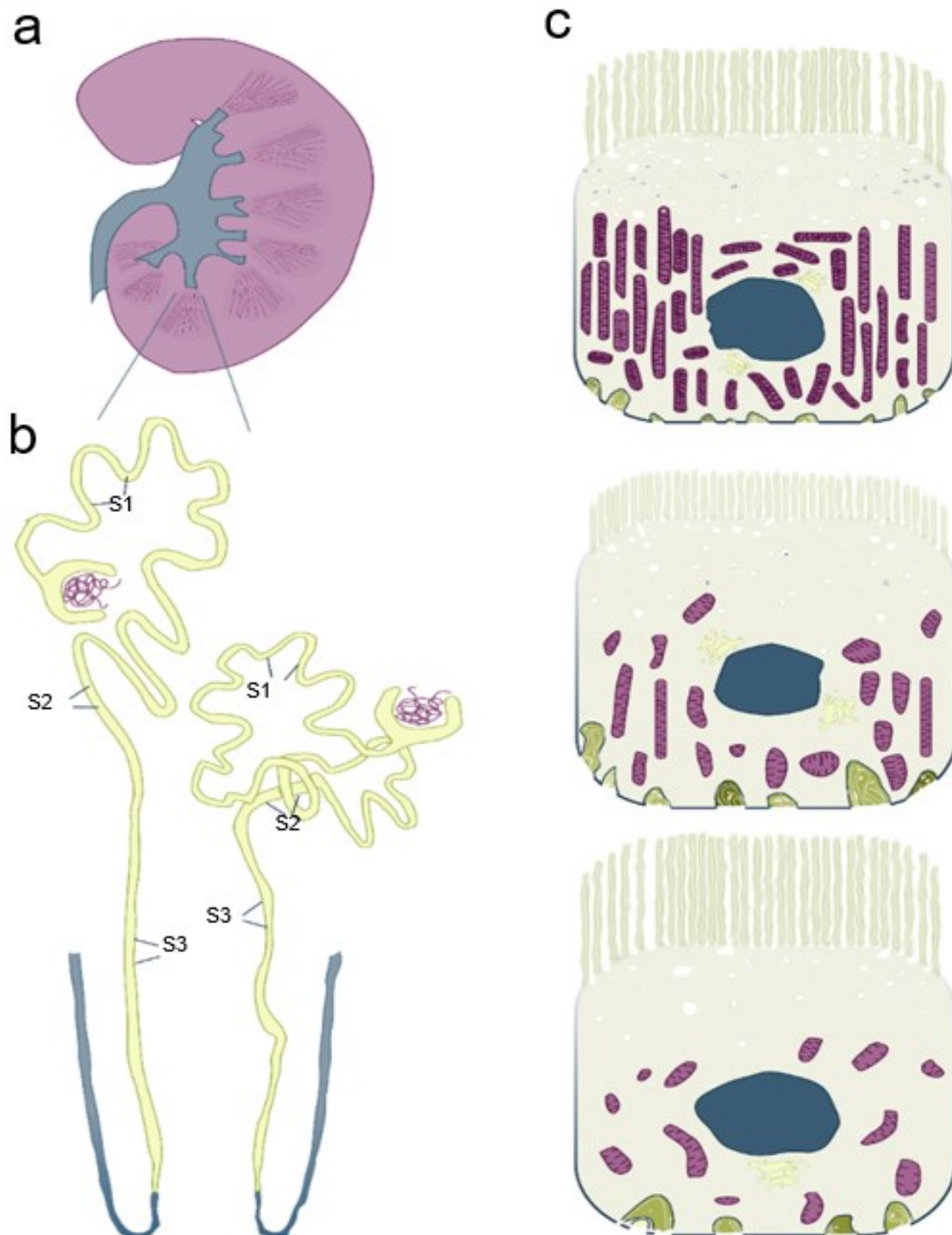


**Figure 1.1 Graphical representation of the kidney.** (a, b) Diagram of the cut surface of a bisected kidney, depicting renal pyramid from where nephrons originate (top) as well as schematic representation of proximal tubular S1–S3 segments in superficial (bottom left) and juxtamedullary nephrons (bottom right). (c) Difference between S1, S2 and S3 segments: S1 segment has taller and wider brush border membranes



with abundant microvilli, prominent endocytic compartments, and a well-developed vacuolar-lysosomal system. The S1 segment has a larger network of elongated mitochondria and well-developed Golgi apparatuses with extensive invaginations on the basolateral membranes. In S2 segments, brush borders are short with less abundant microvilli, less prominent endocytic compartments, and less developed vacuolar-lysosomal system. The S2 segment has small mitochondria and less developed Golgi apparatuses with less extensive invagination. In the S3 segment, the brush border appears to be shorter with least abundant microvilli, endocytic compartments are less prominent and least developed vacuolar-lysosomal system. The S3 segment has smaller mitochondria and the least prominent Golgi apparatuses with the least extensive invaginations.

Although there is variance between nephronic classification as discussed above, the segments of proximal tubules across different nephron classes share fundamental features. Generally, as complexity decreases and morphology changes over the length of the proximal tubule, so does the capacity for volume transport. There is an intricate folding pattern in S1 and S2, with a particularly high density of microvilli in the apical region on S1. The numerous mitochondria in S1 and S2 are organized alongside lateral cell processes, while they are scattered in the cytosol in S3. Moreover, there are also subtle differences between S1 and S2, for instance, a gradual reduction of mitochondria and interdigitation density, whereas S3 shows additional changes such as cuboid cell shapes with a little extension of the apical membrane surface area [9]. Electron microscopy has provided further insights into the cytosolic differences between segments. The subapical region is more pronounced in S1/S2 when compared to S3, with endosomes and lysosomes localizing deeper into the cytoplasm. While endosomes and lysosomes show lesser density and lower degree of organization in S3, there is an increased number of peroxisomes in the latter segment (Figure 1.1c) [9].

### **1.3 Dome formation**

Proximal tubule formation is the central event in kidney organogenesis. Development of proximal tubules is not well understood because of a lack of proper models. There is a need to develop morphologically well-characterized proximal tubule models that can be used to study various changes in the protein expression during the development of proximal tubules. Recently, several *in vitro* models which have been developed to study proximal tubule formation use micropatterned substrates [15, 16].

Domes are discrete structures in which the cells are detached from the culture dish due to the accumulation of fluid that indicates the development of a polarized phenotype and its role in transport of ions [17]. These domes are formed due to the active vectorial trans-epithelial ion transport indicating the differentiated polarized phenotype, which involves the formation of tight junctional complexes [18]. There are various cell lines that are known to form domes (Table 1.1). There are 3 renal cell lines known to form domes: Madin–Darby canine kidney (MDCK), proximal-like porcine kidney cells (LLC-PK1), and opossum kidney cells (OK). However, the role of dome formation is not well studied in nephrotic segments.

Table 1.1 Cell lines reported to from domes

Tissue of origin	Cell line	Reference
Choroid plexus	Primary rat choroid plexus	[19]
Kidney	MDCK (dog kidney)	[20]
Cervix	Human cervical carcinoma	[21]
Mammary	Primary neoplastic mouse mammary	[22]
Bladder	Rat bladder carcinoma	[23]
Colon	Human colon carcinoma (SW-48 cells)	[24]
Stomach	Primary rat glandular stomach	[25]
Mammary	RAMA 25 (rat mammary)	[26]
Kidney	LLC- PK1 (pig kidney)	[27]
Lung	Primary pulmonary alveolar type II cells	[28]
Oral	Primary pig oral epithelia	[29]

Colon	Human colorectal adenocarcinoma (Caco2 cells)	[30]
Kidney	Opossum kidney proximal tubular	[31]
Mammary	LA7 (clonal derivative of RAMA 25)	[32]

The OK cell line was isolated from the proximal tubule of an adult female *Didelphis marsupialis virginiana* to study the X chromosome inactivation process [33]. However, this cell line was soon discovered to manifest various characteristics of proximal tubules. It displayed various receptors like alpha 2 adrenergic, atrial natriuretic peptide (ANP), parathyroid hormone (PTH), and serotonin receptors [34, 35]. The OK cell line is also known to form domes and dexamethasone treatment increases dome formation, suggesting that dexamethasone promotes differentiation of the renal epithelium [31].

MDCK cells were isolated from an adult female *Canis familiaris*. Initially, domes that were observed in this cell line were described as ulcers. However, microscopic analysis revealed that they are not ulcers but are hemispherical vesicles with distinct apico-basal cell polarity [20]. These polarized cells resemble renal epithelial cells, whereas the cell culture medium is analogous to the glomerulus filtrate. This cell line is widely used for high throughput screening, toxicological studies, and virus production for vaccine development [36, 37]. These cells are also used in studying cell motility, cell polarity, and cell-cell junction dynamics. Recently, it has been found that dome cells in MDCK monolayers have superelastic properties when grown in confined geometry. The active superelastic property provides a means to epithelial cells to undergo extreme deformation under constant tension. Actin cortical dilution of the epithelial cells was suggested to be responsible for cellular superstretching [38].

LLC-PK1 cells were derived from the proximal tubule of *Sus scrofa*. These cells express  $\gamma$ -glutamyl transpeptidase, leucine aminopeptidase, and megalin, all markers of proximal

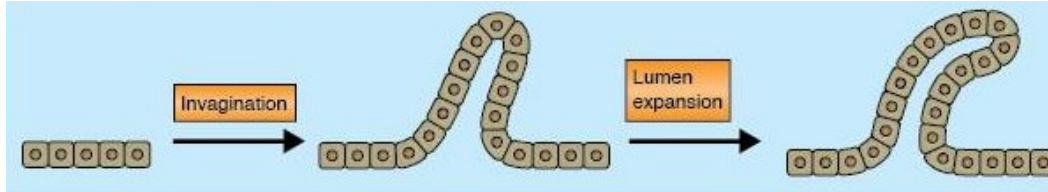
tubules [27, 39]. Like MDCK cells, they also form domes and exhibit apical-basal polarity. LLC-PK1 cells also produce plasminogen activators [40].

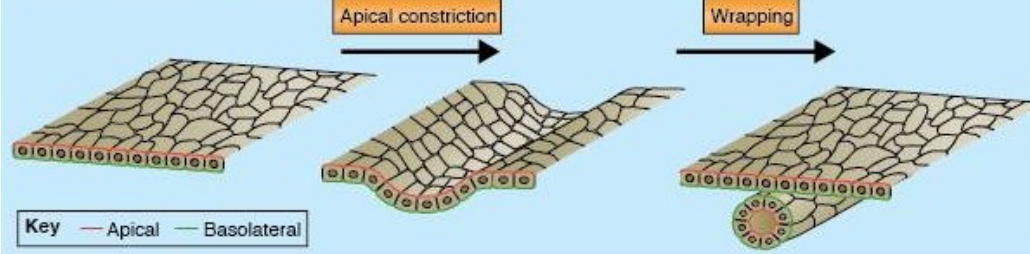
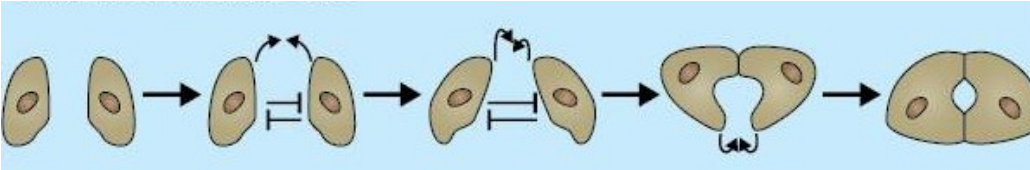
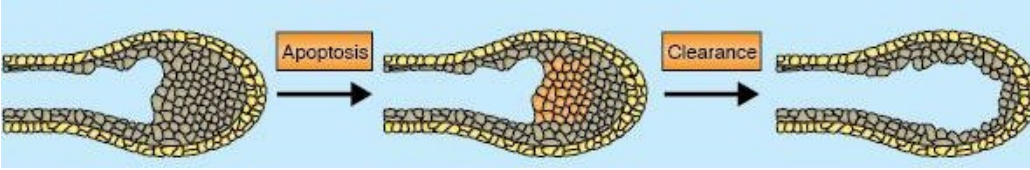
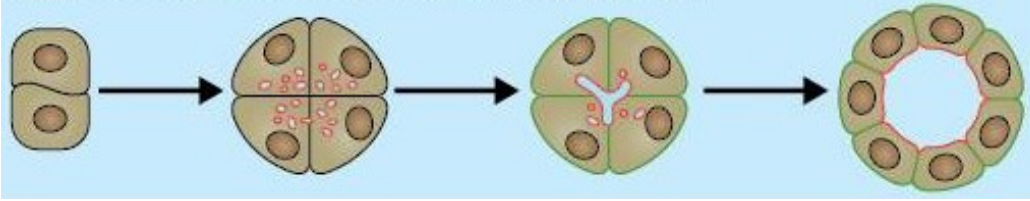
Cells that are isolated from other tissues were also reported to form domes (Table 1). For example, LA7 is clonally derived from the cell line Rama-25, isolated from a mammary adenocarcinoma induced in Sprague-Dawley rats by 7,12-dimethylbenz(a)anthracene (DMBA). This cell line is known to form domes and two strongly expressed proteins were identified, namely, heat shock protein 90 (HSP90) and annexin I [32]. Interestingly, these two proteins are expressed during lactation and this *in vitro* model can be used to study lobulo-alveolar development.

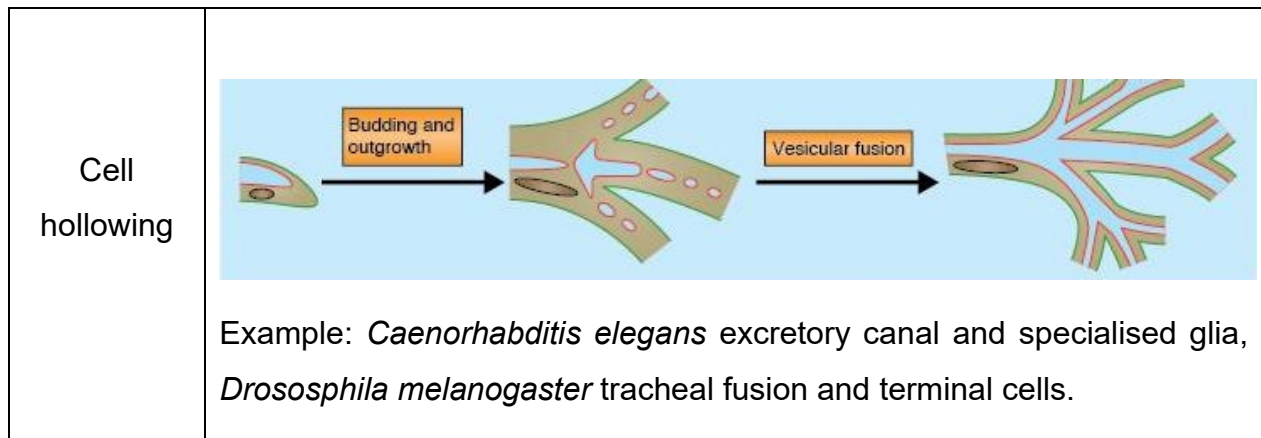
### 1.4 Tubulogenesis

Tubulogenesis is an important process that generates the topological requirements to help transport nutrients and waste through the body. Some tubules contain lumens enclosed by a single cell whereas some comprise multiple cells joined by junction proteins. Various mechanisms of lumen formation have been discussed (Table 1.2). Major tubulogenesis processes and structures involved on a cellular level are cell polarity, vesicular trafficking, and cytoskeletal dynamics.

Table 1.1 Mechanism of lumen formation, adapted from Iruela-Arispe et al, 2013 [41]

Mechanism	Process
Budding	 <p>Example: Mammalian kidney, lung, angiogenesis, <i>Drososphila melanogaster</i> salivary gland, trachea, hindgut and dorsal appendages.</p>

<p>Wrapping</p>	 <p>Example: Neural tube formation.</p>
<p>Lumen entrapment</p>	 <p>Example: Drosophila embryonic heart.</p>
<p>Cavitation</p>	 <p>Example: Mammalian mammary gland.</p>
<p>Cord hollowing</p>	 <p>Example: MDCK tubules, vertebrate vasculature, Zebrafish and <i>Ciona</i> notochord.</p>



Cell polarity: Cell polarity is an essential phenomenon in epithelial cells. It is described by separating the plasma membrane into particular apical and basolateral domains, segregated by adherens and tight junctions [41]. Extracellular cues from the extracellular matrix and adjoining cells, communicated by integrins and cadherins, are significant for the commencement step. Localisation of PAR and Crumbs complexes in the apical domain and the DLG/Scribble complex in the basolateral domain are important cell polarity determinants (Figure 1.2 and Table 1.3) [42]. Defects in any of the protein complexes can disrupt apico-basal polarity and result in cancer. Transforming growth factor beta (TGF- $\beta$ ) signaling can reduce the expression of Par-3 in proximal tubular cells by inducing miR-491-5p, implying that TGF- $\beta$  can disrupt cell polarity [43]. One of the most direct connections between cell polarity disruption and epithelial-mesenchymal transition (EMT) is probably the discovery that TGF- $\beta$  receptors directly interact with Par6 at the level of adherens junctions [43].

Vesicular trafficking: Vesicular trafficking is essential for lumen formation. Vesicular trafficking in proximal tubule cells is an acidification-dependent process that correlates with the interaction between intra-endosomal acidification-dependent V-ATPase and arf nucleotide-binding site opener (ARNO). V-ATPase a2- and c-subunits have been identified as integral endosomal membrane proteins that interact with cytosolic ARNO and ADP-ribosylation factor 6 (Arf6), respectively. This acidification-dependent process may be essential for protein trafficking along the renal proximal tubule cells' endosomal degradation pathway [44]. In MDCK cells, vesicular trafficking of podocalyxin (PODXL)

occurs during the formation of pre-apical patch. Podocalyxin knockdown MDCK cells showed abnormal lumen formation [45, 46].

Cytoskeleton: Cytoskeletal proteins play significant roles in supporting the tubule's structure. Cytoskeletal proteins play significant roles in supporting the tubule's structure. Apical plasma membranes with microvilli on proximal tubule cells provide a large surface area for unidirectional solute transport from lumen to blood. The major structural solute component is F-actin, and its integrity is critical in normal absorptive and secretory functions as well as the regulation of cellular events such as cell shape stability, cell motility, and the distribution of integral membrane proteins [47]. Actin has been shown to interact with ion transport molecules such as basolateral  $\text{Na}^+/\text{H}^+$  exchanger type 1 (NHE1) and apical  $\text{Na}^+/\text{H}^+$  exchanger type 3 (NHE3), which are mediated by the  $\text{Na}^+$  gradient generated by basolateral  $\text{Na}^+/\text{K}^+$ -ATPase. Similarly, this interaction is required for controlling vesicle movement as well as the uptake of macromolecular signaling complex assembly at the apical membrane [47]. Afadin (AFDN) is an F-actin binding protein and adaptor to nectins. Recently, it has been identified that advancement from pre-apical domains to a coordinated apical surface requires afadin. Deletion of afadin in developing nephrons of mice leads to delay in polarization and lumen formation [48].



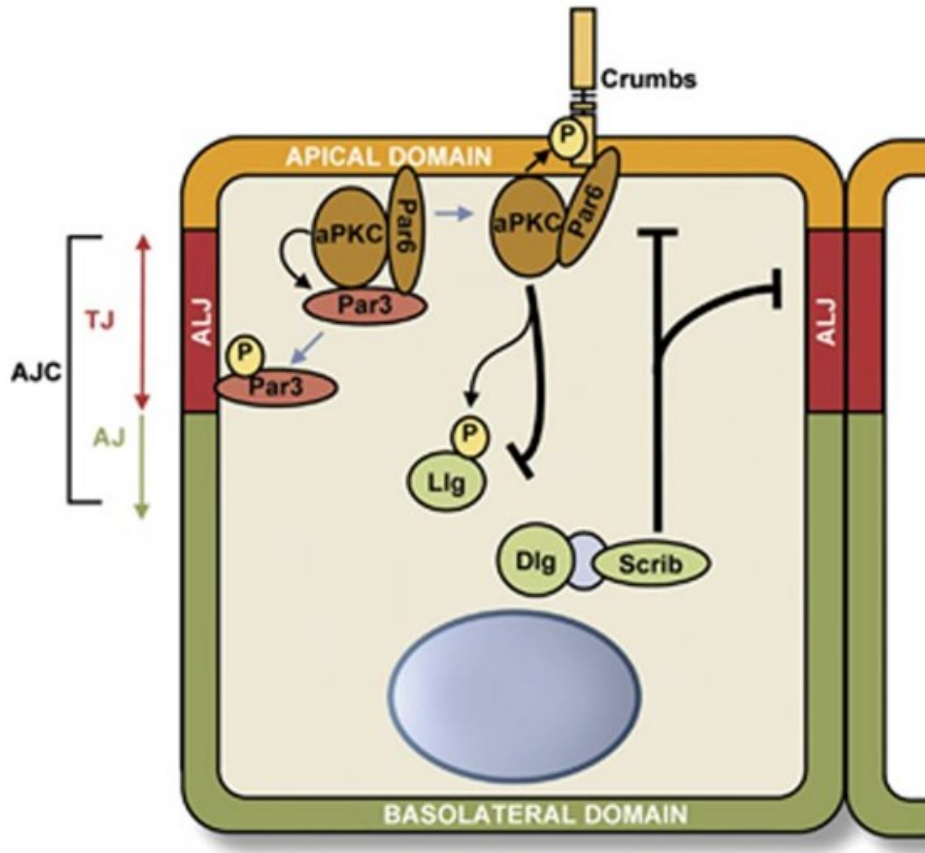


**Figure 1.1 Significant determinants of apicobasal property.** The Par and Crb complexes localize apically, and components of these complexes can interact with the subapical region. The Par complex kinase aPKC phosphorylates Lgl, restricting the Scrib complex to the basolateral side of the cell, where it localizes cortically with the other members of the Scrib complex. Lgl inhibits aPKC at the basolateral side of the cell. AJ: adherens junctions; ALJ: apical/lateral junction; TJ: tight junctions (Figure adapted from Royer et al, 2011) [49].

Table 1.2 Proteins present in different complexes responsible for apical-basal polarity

Complex	Protein
Crumbs	Crumbs (Crb)
	Protein associated with Lin-7 1 (PALS1)
	PALS1-associated tight junction protein (PATJ)
Par	Partitioning defective-3 (Par3)
	Partitioning defective-6 (Par6)



	atypical protein kinase C (aPKC)
Scribble	Scribble (SCRIB)
	Discslarge (Dlg)
	Lethal giant larvae (Lgl)

The glomerular ultrafiltrate, which is isotonic to plasma, is delivered to the proximal tubule. The proximal tubule is in charge of reclaiming the glomerular filtrate in bulk. The proximal tubule is highly permeable to water, and the luminal fluid remains isotonic to plasma throughout this nephron segment [50].

The rate of proximal tubule reabsorption mechanism in the neonate is significantly lower than in the adult segment. Nephrons form in utero and in preemies. Nephron formation is centrifugal, with juxtamedullary nephrons maturing much faster than those in the superficial cortex [51]. Proximal tubular transport increases with development in both superficial and juxtamedullary nephrons, but the increase is greater in the superficial nephrons. Like in adults, transport is isotonic in neonates [52]. Most cells in the body contain aquaporin 1 water channels, which ensure that intracellular and extracellular osmolality are equal. The combined rate of transport of the individual solutes absorbed determines the rate of volume absorption by proximal tubular transport. Most of the solute transport occurs as a result of active transport, but passive solute transport occurs along the paracellular pathway.

As the kidney develops, there is a greater degree of differentiation from the most proximal ureteric bud (UB) epithelium (tip) to the more distal (trunk). This could be due to the UB's growth pattern, in which tip cells serve as progenitors for the entire epithelium [53].

During metanephric development, pharmacological inhibition of  $\gamma$ -secretase defined a window in which Notch activity is required for the fixation of proximal cell identity [54]. These cells are further subdivided into podocyte precursors (which will lose Notch activity, possibly due to an increase in the Notch antagonist COUP-TFII) and proximal tubule precursors (which will gain Notch activity) [55, 56]. Surprisingly,  $\gamma$ -secretase inhibition

applied to the SB does not prevent the emergence of molecularly identifiable proximal cell types, implying that these identities are fixed by the time the SB is visible. Notch activation involves  $\gamma$ -secretase-mediated proteolysis and the formation of neo-epitopes, some of which are antibody-recognizable. These antibodies detected cleaved Notch1 in the renal vesicle, indicating that Notch1 is activated early in the nephrogenesis process [57].

When lim homeobox 1 (LHX1) is deactivated in the metanephric mesenchyme (MM), renal vesicles (RVs) form that express fibroblast growth factor 8 (FGF8), paired box gene 8 (PAX8), and Wnt family member 4 (WNT4) but lack the distal-specifying factor POU class 3 homeobox 3 (POU3F3) and the Notch ligand delta like canonical notch ligand 1 (DLL1) [58]. The failure of Lhx1/RVs to regionalize along the P/D axis stops nephron development at this stage, and no S-shaped bodies (SB) form. In chimera experiments, Lhx1<sup>-/-</sup> embryonic stem cells (ESC) can contribute to the entire RV, but in the mature nephron, Lhx1<sup>-/-</sup> cells can only form the Bowman's capsule and podocytes, the most proximal cells in the nephron. This suggests that Lhx1 not only controls distal tubule, but also sets up the mid-proximal area (the proximal tubule). Because lhx1 activates dll1, it may start a process that depends on Notch and identifies proximal tubules and podocytes. dll1 hypomorphic animals lose proximal segments and have a significant alleviation in nephron numbers [55]. Thus, dll1 is the primary Notch ligand to act in the RV; lhx1 acts downstream of Wnt signaling during mesenchymal epithelial transition (MET) and upstream of brn1 (inducing distal fates) and Notch (inducing proximal fates) in nephron segmentation [59, 60].

In the absence of Notch, podocytes function normally after the proximal nephron forms. While blocking Notch signaling may help prevent glomerulosclerosis, Notch1 and Notch2 cell-autonomously regulate proximal tubular diameter by keeping the division plane perpendicular to the basement membrane. Proximal tubule cysts form in the absence of Notch1 and Notch2 and can form papillary renal cell carcinoma-like structures. Wnt9b and Wnt7 also regulate proximal tubule diameter and loop of Henle elongation [53].

## **1.5 Transport mechanisms in proximal tubules**

Most of the filtered volume is re-absorbed at the proximal tubule through active transport, passive solvent drag, or paracellular electro-diffusion. The filtered fluid and its constituents

are re-absorbed into the peri-tubular capillaries assisted by specific basolateral transporters.

Within the context of proximal tubules, re-absorption predominantly occurs in S1 in a  $\text{Na}^+$  dependent manner. In the first phase,  $\text{Na}^+$ -driven re-absorption of glucose, amino acids, and other solutes leads to export of  $\text{Na}^+$ , which results in electronegative polarization of the epithelium. This polarization creates a transepithelial potential difference, which in turn drives chloride re-absorption and re-absorption of sodium; in this step, re-absorption of glucose and other solutes occurs together with sodium and chloride import in a paracellular manner [61-63].

In the second phase, paracellular and transcellular re-absorption of sodium and chloride occurs; however, these are far from being the sole ionic modulators of proximal tubule re-absorption. S1 also re-absorbs bicarbonate when the concentration of bicarbonate and coupled solutes decrease intracellularly. This leads to charge reversal, from negative polarization during the first to positively charged at the end of the second phase. Together with a chemical gradient between lumen and peritubular space, this process drives sodium transport and paracellular re-absorption of chloride [61, 62, 64]. The importance of this passive pathway cannot be understated; it is responsible for around 40% of S2 and S3 proximal tubule re-absorption. This robust, redundant system of active and passive transport can explain how proximal tubules can re-absorb approximately 60% of sodium and chloride with relatively low expression of the sodium potassium pump ( $\text{Na}^+/\text{K}^+$  ATPase) when compared to other regions of the nephron [65].

## **1.6 Sodium transport**

Sodium is the principal cation present at a lower concentration intracellularly than in the extracellular space. Sodium regulates fluid and electrolyte balance, blood pressure, excitability of muscle and nerve cells, blood clotting process and plays a significant role in maintaining extra cellular fluid volume. Sodium transport in the proximal tubule is inextricably intertwined with chloride, potassium, phosphorus, sulfate, bicarbonate, phosphorus, protons, calcium, glucose, and amino acids transport (Figure 1.3a).

Sodium is re-absorbed in proximal tubules via a transcellular pathway mediated by the energy-dependent sodium-potassium adenosine triphosphatase ( $\text{Na}^+/\text{K}^+$ -ATPase). This  $\text{Na}^+/\text{K}^+$ -ATPase is expressed in the basolateral membrane of proximal tubules and more strongly expressed in proximal convoluted tubules than in the proximal straight tubules [66-70].  $\text{Na}^+/\text{K}^+$ -transport is electrogenic due to a stoichiometry of 3  $\text{Na}^+$  to 2  $\text{K}^+$ . The  $\text{Na}^+/\text{K}^+$ -ATPase keeps the intracellular sodium low by extruding it, thereby maintaining the electrochemical gradient. This leads to the passive entry of sodium via different sodium co-transporters and antiporters present across the apical sodium-dependent phosphate transporter 2 (PiT2), sodium-dependent phosphate transport protein 2A (NaPi-IIa), sodium-dependent phosphate transport protein 2C (NaPi-IIc), sodium/sulphate symporters (NaSi1), sodium/hydrogen antiporter 3 (NHE3), sodium/glucose cotransporter 1 (SGLT1), sodium/glucose cotransporter 2 (SGLT2) and basolateral sodium/calcium exchanger 1 (NCX1) membrane. Sodium also exits the renal tubular cell through the sodium/bicarbonate cotransporter 1 (NBCe1). Exit of sodium is balanced by exit of chloride, maintaining the electroneutrality of transcellular sodium and chloride transport [71, 72].

## 1.7 Chloride transport

Chloride is an anion, present in lower concentrations in the cytosol than at the extracellular space. Chloride permeability of intracellular membranes plays a pivotal role in the re-absorption of low molecular weight proteins via receptor-mediated endocytosis and intracellular membrane trafficking in proximal tubules [73]. Regulation of extracellular fluid volume and maintenance of blood pressure depends entirely on the re-absorption of chloride with sodium along the nephron [74]. Active sodium transport, directly or indirectly, regulates chloride re-absorption in proximal tubules. Active transcellular and passive paracellular transport are the two key mechanisms through which proximal tubules absorb two-thirds of the chloride from the filtrate [62].

In proximal tubules, the intracellular chloride concentration is higher than it is supposed to be at its electrochemical equilibrium. Therefore, transcellular chloride absorption must rely on an active apical process guiding chloride into the cell [75]. Functional *in vitro* studies demonstrated that an anion transporter (CFEX) could mediate this by performing various

exchanges like chloride-hydroxide exchange, chloride-bicarbonate exchange, chloride-formate exchange, and chloride-oxalate exchange (Figure 1.3b) [76].

Chloride-formate transport is electroneutral, whereas chloride-oxalate transport is electrogenic [77]. For the chloride-formate exchange to occur, the internal/external formate ratio must exceed the internal/external chloride ratio. Oxalate presents different challenges, as the chloride-oxalate exchanger is electrogenic. Thus, mechanisms must drive formate and oxalate inside the cell at concentrations above their electrochemical equilibrium. Additionally, the concentrations of formate and oxalate in the biological fluid are very low i.e., 5-50  $\mu\text{M}$  and 1-5  $\mu\text{M}$ , respectively. Therefore, recycling these anions across the apical membrane is crucial to preserve their intracellular accumulation [78]. Formate-chloride transport requires a sodium gradient and depends on acidification and the activities of NHE3 [79].

The molecular actors of chloride ion transport across the basolateral membrane are unknown. However, different transport mechanisms have been proposed as likely candidates. The first proposed mechanism of chloride exit occurs through chloride potassium symporters (KCC3 and KCC4). The central role of the KCC3 co-transporter is fluid re-absorption and serosal transport of chloride ions. KCC3 and KCC4 are expressed from the S1 to the S3 segment across the basolateral membrane of proximal tubules [80, 81]. KCC3 is predominantly expressed in proximal tubules, whereas KCC4 is also expressed in other nephronic elements [80]. The stoichiometry of KCC3 and KCC4 is  $\text{K}^+:\text{Cl}^-$  and they therefore belong to the family of electroneutral cation-chloride co-transporters [82].

Sodium-independent chloride/bicarbonate transport has also been reported as a path for chloride exit. Micro-perfusion studies in S3 segments of rabbits showed that  $\text{HCO}_3^-$  ions are extruded at the expense of  $\text{Cl}^-$  ion import. It is theorized that chloride ions exit into the lumen and recur to the peritubular space through tight junctions [83]. Under the prevailing ion concentration gradient condition, this mechanism can support chloride entry and bicarbonate exit rather than chloride exit [84].

## 1.8 Potassium transport

Potassium ions are essential for various cellular processes. Cell growth and division, DNA, and protein synthesis require a high intracellular concentration of this ion [85, 86].  $K^+$  regulates intracellular pH and cell volume [87-89] and membrane potential and cellular excitability [90]. An imbalance in intracellular  $K^+$  concentration disrupts the acid-base balance, which alters the activity of many enzymes, ultimately impinging on metabolic pathways.

$K^+$  is absorbed across the proximal tubules primarily through solvent drag and diffusion [91, 92]: Active sodium re-absorption guides net fluid absorption; potassium absorption by solvent drag, in turn, depends on the net fluid absorption [93]. The net fluid flow down the proximal tubules changes the trans-epithelial voltage from negative in the S1 segment to positive in S2 and S3 segments [94, 95]. This shift in trans-epithelial voltage induces potassium diffusion via a low resistance paracellular pathway. In addition,  $K^+$  re-absorption can also occur by diffusion through tight junctions [96]. It has been estimated that 20% of  $K^+$  re-absorption is active, 20% is by solvent drag, and 60% is by paracellular diffusion [96-98].

The exit of  $K^+$  from cells into the tubule lumen mainly through a conductive pathway or chloride potassium symporter (KCl) (Figure 1.3b). Intracellular microelectrode and patch-clamp experiments on apical tubule membranes revealed that potassium exits the cells through a conductive pathway [99]. This conductive pathway extrudes potassium from cells into the lumen due to an electrochemical gradient of potassium across the apical membrane. When cells depolarize, apical potassium channels stabilize the apical membrane voltage since potassium channels are voltage sensitive. Therefore, when the apical membrane depolarizes, there will be a reduction in membrane potential, which will activate potassium channels and ultimately lead to the cell's re-polarization [100]. Potassium channels also regulate cell volume in proximal tubules [101]. Activation of sodium-glucose transporters elevates the intracellular sodium and glucose concentration, alongside cell volume; cell swelling activates apical and basolateral potassium channels to expel potassium into the lumen, thereby restoring cell volume [100]. Studies have reported that the apical potassium channel is closed during basal conditions, opening only

to restore cell volume [102]. Therefore, potassium transported by the  $\text{Na}^+/\text{K}^+$  ATPase is primarily recycled by potassium channels present in the basolateral membrane. As such, the exit of potassium ions from the apical membrane is highly controversial.

## 1.9 Calcium transport

Calcium is an essential cation required for the formation of bones and teeth, muscle contraction, nerve impulsion/transmission, blood clotting, regulation of heartbeat, and fluid balance within cells; calcium also acts as a second messenger in various signaling pathways [103]. As such, the calcium concentration in plasma must be tightly regulated through absorption of calcium in the intestine, re-absorption by the kidney, and storage in bones; 60-70% of calcium is re-absorbed by the proximal tubules from the glomerular filtrate [104-106]. Micro-perfusion studies showed that two-thirds of the calcium load is re-absorbed by the end of the accessible proximal convoluted tube. The majority of calcium is re-absorbed paracellularly, but 20-30 % are re-absorbed by a transcellular process in proximal tubules [107].

Paracellular transport occurs either by solvent drag or by diffusion [108]. The tubular fluid to glomerular ultrafiltrate ( $\text{TF}/\text{UF}_{\text{Ca}}$ ) ratio of calcium in early superficial proximal convoluted tubule is 1.0, whereas it rises to 1.1-1.2 in the late convoluted tube [109, 110]. This suggests that the glomerular ultrafiltration of calcium follows the ultrafiltration of sodium and water [110]. Accordingly, the transcellular re-absorption of sodium ions and water provides the concentration gradient for paracellular calcium re-absorption, via the tight junction channel protein claudin 2. Claudin 2 is a cation-selective pore regulating calcium re-absorption in proximal tubules [111]. Claudin 2 knock-out mice show reduced re-absorption of  $\text{Na}^+$ ,  $\text{Cl}^-$  and water; they also display hypercalciuria, confirming that claudin 2 has a peculiar role in regulating paracellular transport of calcium [112].

The extrusion of calcium in proximal tubules is mediated by NCX and the plasma membrane calcium ATPase (PMCA), a P-type ATPase family member (Fig 1.3c). NCX1 and PMCA are present in the basolateral membrane of proximal tubules [113]. NCX has a high capacity for calcium transport, but a low affinity for calcium, whereas PMCA has a low transport capacity for calcium but a high affinity for calcium. The stoichiometry of

NCX1 is  $3\text{Na}^+:1\text{Ca}^{2+}$  and it is therefore electrogenic [114]. The  $\text{Na}^+/\text{Ca}^{2+}$  ratio depends on the electrochemical gradient generated by sodium through the  $\text{Na}^+/\text{K}^+$  ATPase, and thus, ATP is indirectly required for the extrusion of calcium [115]. NCX1 is sensitive to fluctuations in the intracellular and peritubular sodium concentration. PMCA1 and 4 are predominantly present in proximal tubules, but only PMCA1 can mediate efflux of calcium.

### 1.10 Phosphate transport

Inorganic phosphate is essential for metabolic regulation, bioenergetics, and structures such as bones and membranes. In addition, phosphate maintains the acid-base balance through urinary buffering, making nearly complete re-absorption of filtered phosphorus an important function of the proximal tubule [116, 117]. Micro-puncture experiments showed that the accessible portion of the proximal tubule re-absorbs 76% of phosphate [118]. In proximal tubules, phosphate transport exhibits both axial and inter-nephronal heterogeneity. Regarding axial heterogeneity, phosphate re-absorption is three to four times higher in the S1 than the S2 segment and even lower for the S3 portion [119, 120]. Micro-perfusion studies suggest that the phosphate transport rates per unit length are similar for the segments derived from superficial and juxtamedullary nephrons. Inter-nephronal heterogeneity seems mainly due to differences in superficial and juxtamedullary nephrons' lengths or axial composition [120].

Phosphate re-absorption is a unidirectional, transcellular process and depends on the presence of sodium ions. Various *in vitro* and *in vivo* studies showed that phosphate transport across the apical membrane needs sodium ions. Tubules require these sodium ions to activate the binding process of phosphate to the transport site. *In vivo* and *in vitro* micro-perfusions experiments and studies with proximal tubular brush border membrane vesicles assisted in decoding sodium-dependent transport of phosphate [121-123]. PiT2, NaPi-IIa, and NaPi-IIc are the three main Na/Pi co-transporters present on proximal tubules (Figure 1.3c). PiT2 is localized in the S1 segment and to a lesser extent in S2 [124, 125]. The stoichiometry of PiT2 is  $2\text{Na}^+:1\text{HPO}_4$ , which is electrogenic [126]. Under normal physiological conditions, phosphate re-absorption by PiT2 is minimal, but the activity of PiT2 transporters increases at acidic pH [126, 127]. Therefore, PiT2-mediated phosphate re-absorption may play a principal role in acidotic conditions. The precise role



of PiT2 in phosphate re-absorption and its regulation remains to be determined. NaPi-IIa expression is higher in S1 and decreases towards the S3 segment. NaPi-IIc is expressed only in the S1 segment [124]. Na/Pi-co-transport by NaPi-IIa is electrogenic due to a stoichiometry of  $3\text{Na}^+ : 1\text{HPO}_4^{2-}$ , while NaPi-IIc is electroneutral due to a stoichiometry of  $2\text{Na}^+ : 1\text{H}_2\text{PO}_4^{2-}$  [128]. Both co-transporters function similarly with higher rates at more alkaline pH [129-131].

How phosphate is exported at the basolateral membrane is currently unknown. In a canine model, experimental corroboration suggests that phosphate uptake at the basolateral membrane differs from uptake in brush border membrane vesicles [132]. Basolateral membranes lacked pH sensitivity, however, showed sodium-dependency. An electrogenic process, a sodium gradient-dependent transport mechanism, could mediate basolateral entry of phosphate rather than exit. Such a mechanism will most likely not lead to net transcellular transport of phosphate. However, this process may be involved in protecting proximal tubules from the limited availability of intraluminal phosphate [133].

### **1.11 Sulfate transport**

Inorganic sulfate is essential for cellular metabolism, bone, and cartilage formation. Detoxification of endogenous and exogenous compounds in the liver requires sulfate. Sulfate is necessary for the maintenance of the integrity of cell membranes and the synthesis of matrix material. Like phosphate, sulfate is freely filtered, with the rate of re-absorption and secretion determining the urinary excretion rate along the proximal tubule [134]. Sulfate re-absorption is an active, saturable and regulated trans-epithelial process [135, 136]. Micro-puncture studies in isolated brush border and basolateral membrane vesicles established that sulfate transport strictly depends on a sodium ion gradient across the brush border membrane, and basolateral exit of sulfate relies on sulfate/anion co-transport [132, 137, 138].

NaSi1 is found in proximal tubules' apical brush border membrane. NaSi1 is detected more in proximal convoluted tubules (e.g., S1 and S2 segments) than on straight proximal tubules (e.g., S3 segment) [139, 140].  $\text{Na}^+$ /sulfate co-transport by NaSi1 is electrogenic through a stoichiometry of  $3\text{Na}^+ : 1\text{SO}_4^{2-}$  [141].

Sulfate is re-absorbed by the basolateral Sulfate anion transporter 1 (SAT1) channel in exchange for bicarbonate (Figure 1.3d). SAT1 also transports oxalate and chloride but only has low efficiency and affinity for chloride transport. Oxalate interacts with SAT1 with higher affinity, but the concentration of oxalate (1-5  $\mu\text{M}$ ) is less at the basolateral membrane than that of bicarbonate (25 mM), which provides evidence for exchange between intracellular sulfate and extracellular bicarbonate [142].

### **1.12 Magnesium transport**

Magnesium is an essential co-factor for various enzymes, important for cytoskeletal re-arrangements, neuromuscular excitability, and a key regulator of various ion channels and transporters [143]. 70-80% of magnesium is freely filtered by the glomerulus and approximately 20% is re-absorbed by proximal tubules [144]. Magnesium re-absorption in proximal tubules is an under-studied subject.

*In vivo* studies revealed that magnesium re-absorption is a linear function of luminal magnesium concentration and is not saturable in proximal convoluted tubules [145]. Magnesium re-absorption diminishes with the volume expansion and changes with sodium and water re-absorption [146, 147]. Luminal magnesium increases because of the water re-absorption, which provides a concentration gradient for diffusive paracellular flux, and thus, magnesium re-absorption [148]. Several lines of evidence show that the proximal tubule has a low permeability rate for magnesium. The efflux of peritubular magnesium into the lumen is very low, which indicates that magnesium re-absorption is probably a trans-cellular rather than a paracellular pathway [148].

### **1.13 Bicarbonate transport**

The primary regulation of pH homeostasis relies on bicarbonate and requires maintaining its proper concentration through re-absorption. The proximal tubule re-absorbs 75% -80% of bicarbonate from the glomerular filtrate and is the main re-absorber of bicarbonate [149]. The main components involved in bicarbonate transport are NHE3, the  $\text{H}^+$ -ATPase NBCe1, and carbonic anhydrase (Figure 1.3e).

The NHE3 exchanger is the main proton exit transporter; NHE3 can be found in the apical region of S1 convoluted, S2 convoluted, and S2 straight tubules [150]. NHE3 is a sodium-

dependent, chloride-independent and electroneutral (1 Na<sup>+</sup> : 1 H<sup>+</sup>) transporter [151]. NHE3-deleted mice show reduced bicarbonate re-absorption in the proximal tubule (~39%) and volume re-absorption [152]. NHE3-null mice are mildly acidotic [152].

An H<sup>+</sup>-ATPase in the apical region of proximal tubules is responsible for proton extrusion [153]. Studies in intact tubes and membrane vesicles established H<sup>+</sup>-secretion as sodium-independent but electrogenic and ATPase-dependent [153, 154].

Bicarbonate exits the proximal tubules through NBCe1. NBCe1-A is expressed in the basolateral membrane of the S1 and S2 segments of the proximal tubule. NBCe1 is electrogenic with a stoichiometry of 3 HCO<sup>3-</sup> : 1 Na<sup>+</sup> [155].

Bicarbonate transport requires adequate carbon dioxide diffusion across cell membranes [156]. *In vivo* microperfusion studies uncovered that carbon dioxide can diffuse across the proximal tubules, in the presence and absence of carbonic anhydrase [157]. Carbonic anhydrase (CA) plays a paramount function in bicarbonate transport along the nephronal segment. Carbonic anhydrases are zinc metalloenzymes that catalyzes the reversible hydration of carbon dioxide to form protons and bicarbonate through the following reaction [158].



Different isoforms of carbonic anhydrase inside cells and at the apical and basolateral membrane of proximal tubules are critical for acid-base transport and bicarbonate re-absorption [159]. CA II is cytoplasmic, while CA IV is a glycosyl-phosphatidylinositol-anchored protein [160]. Both intracellular CA II and apical CA IV play a significant role in transepithelial proton secretion and bicarbonate re-absorption across the proximal tubules [160]. CA IV is also found in the basolateral membrane of proximal tubules for effluxing bicarbonate from the renal tubules [160, 161].

CA IV combines protons with luminal bicarbonate to form carbon dioxide and water. The apical membrane of proximal tubule is permeable to the newly formed carbon dioxide, and carbon dioxide becomes hydrated inside cells under the enzymatic action of CA II to form proton and bicarbonate [162]. CA XII and CA XIV are transmembrane proteins that are found in the proximal tubules [163, 164]. The functional role of these enzymes is unknown.

Transport of proton/bicarbonate in proximal tubules is described as a high capacity, low gradient system. High capacity, because of the large amount of protons secreted per day; low gradient, due to the slight decrease in tubular pH from 7.4 to 6.7-7.0. Paracellular permeability of bicarbonate restricts net bicarbonate re-absorption in late proximal tubules and extrudes bicarbonate from the proximal tubules [165]. Glucose transport

### **1.14 Glucose transport**

Glucose homeostasis is essential for brain function, as this organ uses glucose as its prime metabolic fuel [166]. A large fraction of glucose filtered load is re-absorbed by the proximal tubule [167, 168]. Micro-puncture techniques confirmed that glucose is completely re-absorbed by proximal tubules of amphibians and rats. Glucose re-absorption was ten-fold higher in S2 tubules than S3 tubules whereas found glucose affinity to be higher in S3 tubules than S2 tubules [167].

Three membrane proteins are responsible for glucose transport: SGLT1 and SGLT2 (co-transporters in the apical membrane), and glucose transporter 2 (GLUT2) (uniporter in the basolateral membrane). SGLT2, in S1 and S2 segments, re-absorbs the bulk of glucose; SGLT1 in the S3 segment re-absorbs the remainder. SGLT2 and SGLT1 co-transport sodium and glucose at 1:1 and 2:1 stoichiometry, respectively [169-171]. Glucose re-absorption is a two-stage process. First, SGLTs present across the apical membrane of the proximal tubules re-absorb glucose. This leads to glucose accumulation inside the cells; the glucose concentration gradient across the plasma membrane triggers the second stage: passive exit of glucose via GLUT2 [167, 169]. The basolateral Na<sup>+</sup>/K<sup>+</sup> ATPase exports sodium to maintain its gradient (Figure 1.3f). This self-regulating, gradient-based, two-stage process assures that glucose is completely re-absorbed before reaching the proximal tubules' end.

The role of glucose transporters in renal handling of glucose re-absorption has been studied in knock-out mouse models. SGLT1 knock-out mice re-absorb 98% of the glucose, whereas SGLT2 knock-outs re-absorb only 70%. This establishes that SGLT1 compensates for SGLT2 loss, becoming the bulk re-absorbing transporter for glucose [172]. Double knock-out mice excrete all glucose through their urine [172]. Non-invasive

positron emission tomography (PET) has been used to monitor urinary excretion. 2-deoxy-2-fluoro-[18F]-D-glucose (2-FDG) is a substrate for GLUT2, and methyl-4-fluoro-[18F]-4-deoxy-D-glucopyranoside (Me-4FDG) is a substrate for SGLTs (with only low affinity for GLUT2). The study found no significant change in 2-FDG in GLUT2 knock-out mice compared to wild-type mice. There was urinary loss of Me-4FDG in both SGLT knock-outs. Complete re-absorption of Me-4FDG in wild-type mice, and null re-absorption in GLUT2 knock-out mice confirms the essential role GLUT2 plays in glucose absorption across the proximal tubule [173]. These findings support that SGLTs re-absorb the glucose from the glomerular filtrate, and that GLUT2 is essential for completing glucose absorption across the tubule.

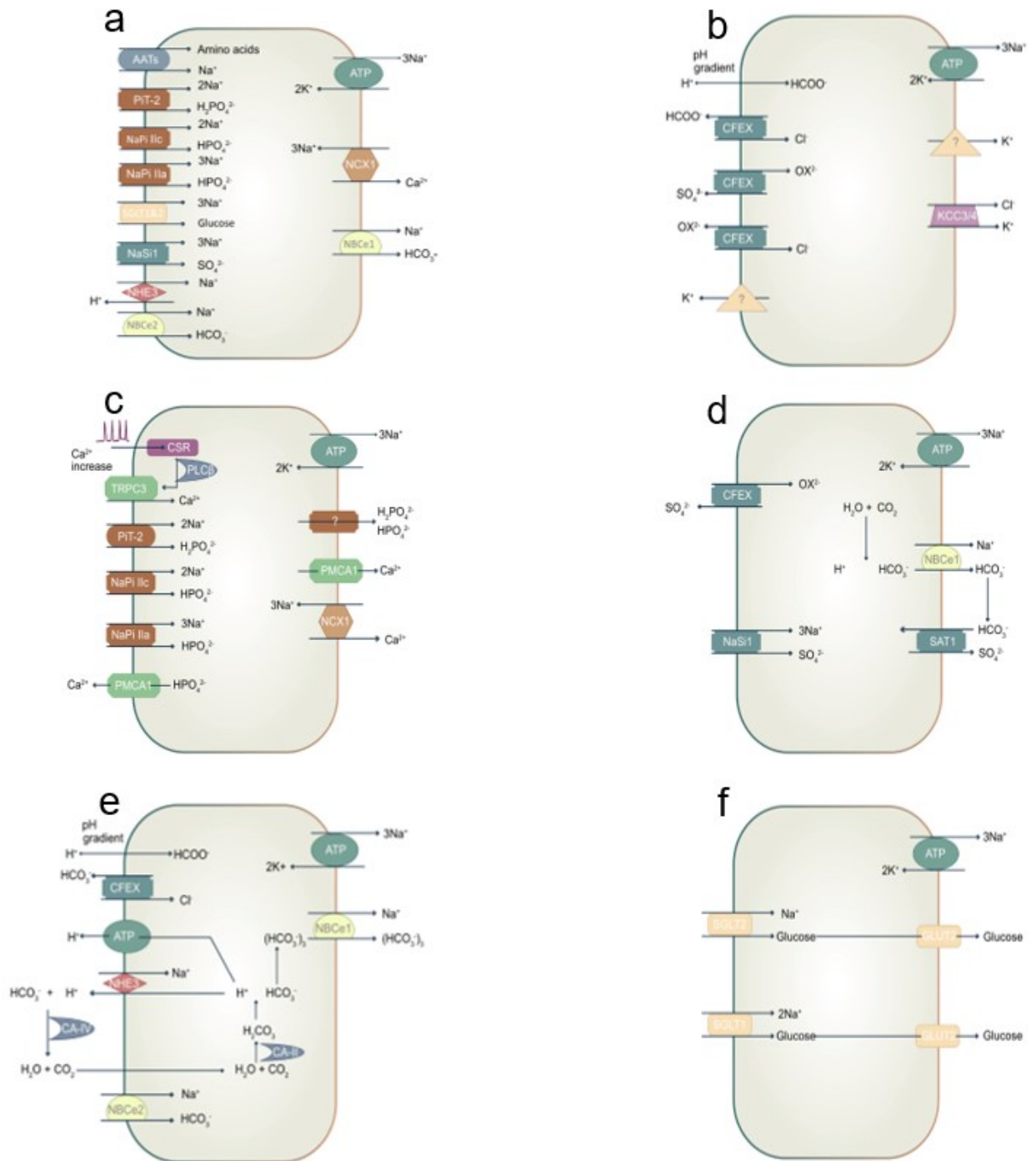


**Figure 1.3 Model depicting the transcellular transport mechanisms of solutes across the luminal and basolateral membrane of proximal tubules.** (a) Sodium enters the proximal tubules with an efflux of amino acids, phosphorus, glucose, bicarbonate, and calcium. Sodium leaves the proximal tubules mainly through the Na<sup>+</sup>/K<sup>+</sup> ATPase and NBCe1. (b) The principal avenue for chloride uptake is through CFEX channels with efflux of oxalate and formate. CFEX is also responsible for the transport of various anions (bicarbonate, hydroxide, lactate, and sulfate). Chloride exit from the proximal tubule is unknown but hypothesis for it have been formulated. The Na<sup>+</sup>/K<sup>+</sup> ATPase mediates potassium reabsorption. Potassium leaves proximal tubules by the KCC symporter and maybe also diffuses out of cells through potassium channels. (c) Calcium enters proximal tubules through transient receptor potential canonical 3, activated by CSR. Calcium exits

proximal tubular cells through PMCA1 and NCX1. (d) Phosphate enters cells via NaPi-IIa, NaPi-IIc, and PiT-2. Phosphate exits proximal tubular cells by an unknown transport pathway. Reabsorption of sulfate is mediated by NaSi1. Sulfate leaves proximal cells via CFEX in exchange for oxalate, chloride or bicarbonate mediated by the SAT1 anion exchanger. (e) Bicarbonate reabsorption is mainly through sodium hydrogen exchanger type 3 and H<sup>+</sup>-ATPase. The breakdown of carbonic acid into water and carbon dioxide by carbonic anhydrase type IV, leads to the diffusion of carbon dioxide in the cytosol of proximal tubules. In the cytosol, carbonic anhydrase converts water and carbon dioxide into carbonic acid where it splits into bicarbonate and a proton, with the latter secreted into the lumen via NHE3 and H<sup>+</sup>-ATPase. Bicarbonate exits the proximal tubules through CFEX and NBCe1. NBCe2 play an important role in apical sodium and bicarbonate cotransport under high-salt conditions. (f) The uptake of glucose from urine is advocated by SGLT2 and SGLT1 and exits by GLUT2 in proximal tubules.

### **1.15 *In vitro* disease models specific to proximal tubules**

As discussed in the above sections, the main function of proximal tubules is re-absorption of the various solutes from the glomerular filtrate. The studies reviewed above capture individual aspects but do not yet provide a complete picture of transport physiology in proximal tubules. Various mechanisms exist for the re-absorption of ions across proximal tubules, but their specific contribution in re-absorption is still unknown.

Defects of the proximal tubule, often hereditary or congenital, impair re-absorption of potassium, phosphorus, sulfate, bicarbonate, protons, calcium, glucose, and amino acids. Acquired defects in the proximal tubule can be drug-induced or related to intrinsic renal diseases.

Development and characterization of renal phenotypes in animal models will help in understanding various pathophysiological conditions related to transport. Various *in vivo* mice models were developed, but their limitations became apparent when the research focused on detecting, alleviating, or understanding human disease. The genetic and phenotypic differences between mice and humans can often be significant enough so that murine models as a translational biomedical research models can be insufficient to represent human disease. If the disease condition is highly dependent on various genetic and epigenetic factors, then even genetically engineered (e.g. humanized) animal models fail to recapitulate the pathophysiological conditions of patients [174].

*In vitro* systems and disease models serve as bio-artificial surrogates for tissues and organs that can be utilized in basic research to investigate fundamental physiology, molecular pathways, and the pathophysiological processes involved in disease

development and progression. Moreover, such *in vitro* systems contribute to research that conforms to the 3R development to reduce the use of animals in research in academia and pharma industry – Replacement, Reduction, Refinement – commanding principles for more ethical research, as they can overcome not only the limitations mentioned above of animal models but also reduce the need for *in vivo* testing [175].

Traditionally, *in vitro* cell cultures are primarily used in cell-based assays due to being more economical, allowing well-controlled experimental design and being scalable since the aforementioned features make them amenable to high-throughput screening. Nonetheless, cultured kidney cells as monolayers in a plastic dishes conflict with the *in vivo* microenvironment: Cells lose significant cooperation with extracellular network proteins and intercellular signs from heterogeneous cell types vital for normal cellular reactions. Moreover, *in vitro* culture addresses a static model, which turns out to be less physiological relevant as supplements are consumed, and metabolic waste accumulates [176].

Primary human renal cells are used because they mimic the renal physiological state more closely. However, these cells have restricted growth capacity and tend to lose their autochthonous phenotype over time. Despite these shortcomings, renal cells are still considered reliable models for studying essential renal cell functions, pathophysiological conditions, and the effects of nephrotoxic agents. Various *in vitro* cell models of proximal tubules are discussed (Table 1.4).

Table 1.3 Different *in vitro* cell types used in biomedical research of proximal tubules (adapted and modified from Yu et al, 2022) [176]

Cell Types	Advantages	Disadvantages
Human kidney 2 (HK2) Human embryonic kidney 293 cells (HEK293) Conditionally immortalized PT epithelial cell line (ciPTEC)	Stable cell lines.  Potentially valuable in toxicity and drug transporter assays.	Limited transport or proximal tubule characteristics.  Low translational impact.



Renal proximal tubule epithelial cell (RPTEC/TERT1)	Polarized tight monolayer formation.	
Human primary renal cells: Fetal renal cells Biopsy-derived renal cells	Complete transporter and metabolic enzyme expression. Polarized tight monolayer formation. Trans-epithelial transport. Broad range of biomarker assays available.	Expression of relevant proteins rapidly decreased. Limiting long-term exposure. Batch-to-batch variation. Limited availability. Translational potential.
Human stem cells: Embryonic stem cells (ESC) induced pluripotent stem cells (iPSC) Urine-derived stem cells (USC)	Can contains a variety of kidney cells (proximal / distal renal tubular cells, endothelial cells, podocytes). Robust proliferative potential.	Not free from ethical and legal issues. Models often immature. Differentiation of non-renal cells is a challenge. Can be contaminated when samples are obtained from female donors.
Animal primary renal cells: Dog (MDCK) Pig (LLC-PK1) Monkey (VERO)	Complete transporter and metabolic enzyme expression. Polarized tight monolayer Formation.	Species differences. Single phenotype in culture – lack of kidney cell type diversity.

	<p>Transepithelial transport.</p> <p>Broad range of biomarker assays is available.</p> <p>Well-established and stable cell line.</p> <p>Formation of polarized tight monolayer.</p>	
--	---	--

The inability of *in vivo* models to mimic human diseases, amalgamated with the inspiration to study various diseases under controlled conditions, has prompted the rise of another field at the convergence among pathology and tissue engineering focused on creating *in vitro* models. Models have been made that can be utilized to concentrate on features of various diseases that happen in basically every organ system of the body.

Non-human cells or established human cell lines, primary cells, and iPSC derived from diseased patients and healthy companions are beginning to be used to develop *in vitro* models to study various pathophysiological conditions. However, several challenges remain because many chronic diseases involve complex interactions between different organs and manifest at the whole-organism level. It won't be easy to model all of these factors, but it might be possible to establish long-term cultures.

There are various *in vitro* models to study pathophysiological conditions of proximal tubules. But, they all need to be micropatterned, have limited growth, and need specific growth factors that can make these models very expensive [177]. Therefore, we developed a self-organised proximal tubule model that can be cultured without needing micropatterning and growth factors. This model can be used to study various pathophysiological conditions related to proximal tubules.

### 1.16 Renal cell carcinoma

Renal cell carcinoma (RCC) originates from renal tubular epithelial cells. Clear cell RCC (ccRCC), papillary RCC (pRCC), chromophobe RCC (chRCC), collecting duct RCC, medullary RCC,

oncocytoma, hereditary leiomyomatosis and RCC (HLRCC) are different known types of RCC [178, 179]. However, clear cell RCC (ccRCC) and papillary RCC (pRCC) are the predominant forms, accounting for ~ 75% and 15-20% respectively [180]. Both originate from proximal tubules.

pRCC is a genetically and histologically heterogeneous disease. Papillary RCC is divided into type 1 pRCC (basophilic cytoplasm) and type 2 pRCC (eosinophilic cytoplasm). High recurrent gains of chromosomes 7 and 17 as well as low recurrent gains of chromosomes 2, 3, 12, 16 or 20 are seen in type 1 pRCC. The MET proto-oncogene (MET), epidermal growth factor receptor (EGFR), and the B-raf proto-oncogene (BRAF) are encoded on chromosome 7 [181]. Somatic mutations of MET are found in non-hereditary papillary renal-cell carcinomas and germline mutations of MET are found in hereditary pRCC patients [181].

Type 2 pRCC is associated with loss of chromosomal arm 22q. This chromosomal arm contains SWI/SNF-related, matrix associated, actin-dependent regulator of chromatin, subfamily B, member 1 (SMARCB1) that encodes a protein of chromatin remodeling SWI/SNF complex and neurofibromin 2 (NF2) is the regulator of the Hippo signaling pathway. Type 2 pRCCs patients have low-frequency mutation in polybromo 1 (PBRM1), SET domain-containing 2 (SETD2), BRCA1 associated protein 1 (BAP1), transcription factor E3 (TFE3) fusions, and enhanced expression of the nuclear erythroid 2-related factor 2 - antioxidant response element (NRF2-ARE) pathway. A novel CpG island methylator phenotype (CIMP) is also found in the distinct subset of type II pRCC and is characterized by mutation in the fumarate hydratase (FH) gene and poor survival rate [181]. Some genetic alterations are found in both type I and type II and are not specific. Cyclin-dependent kinase inhibitor 2A (CDKN2A) loss due to promoter hypermethylation and/or deletion of 9p21.3 chromosomal arm is found in type I pRCC, type II pRCC and unclassified pRCC. NF2 and Salvador family WW domain-containing protein 1 (SAV1) are also mutated in type I pRCC, type II pRCC and unclassified pRCC [181].

In ccRCC, von Hippel–Lindau (VHL) – which encodes pVHL – is the most frequently mutated gene (point mutations, insertions and deletions), besides loss of the 3p25 chromosomal arm and promoter methylation (Figure 1.4) [182]. VHL is the substrate recognition subunit of an E3 ubiquitin ligase complex, whose main function is

ubiquitylation of HIF1 $\alpha$  and HIF2 $\alpha$  as a degradation signal for their proteasomal degradation [183]. Mutation of VHL alone does not cause ccRCC; therefore, other genetic and/or epigenetic events are required to cause ccRCC [184]. Somatic mutation of chromatin-regulating and histone-regulating genes present in 3p21, which includes PBRM1, SETD2, and BAP1 [185-187]. All these genes are tumour suppressor genes. PBRM1 and BAP1 are mutually exclusive and contribute to the sub-classification of ccRCC [187]. PBRM1 mutation leads to extra-renal growth but does not extend beyond Gerota's fascia, whereas BAP1 mutations lead to large tumours, metastasis and a worse prognosis [184, 187]. SETD2 mutations have been associated with metastasis and worse survival prognosis but do not correlate with worse targeted treatment outcomes [188]. Mutations are also found in PI3K–AKT–mTOR pathway genes, CDKN2A (loss of expression), or TP53 [180].

BAP1 is a nuclear-localized histone de-ubiquitinase that binds to the E3 ubiquitin ligase breast cancer gene 1 (BRCA1) really interesting new gene (RING) finger domain – which recruits ubiquitin-loaded E2 ubiquitin conjugating enzymes – and functions as a tumour suppressor gene in various cancers. BAP1 mutations occur in approximately 10% of ccRCC tumours. Interestingly, it has been observed that BAP1 is likely to be a truncation mutation and crucial for the development and pathogenesis of metastatic ccRCC [189]. It has also been found that there is a loss of BAP1 during the pathogenesis of metastatic ccRCC, which indicates the presence of a clone in the primary tumour that had lost BAP1 [190]. However, these findings need to be validated in larger cohorts of metastatic ccRCC tumours.

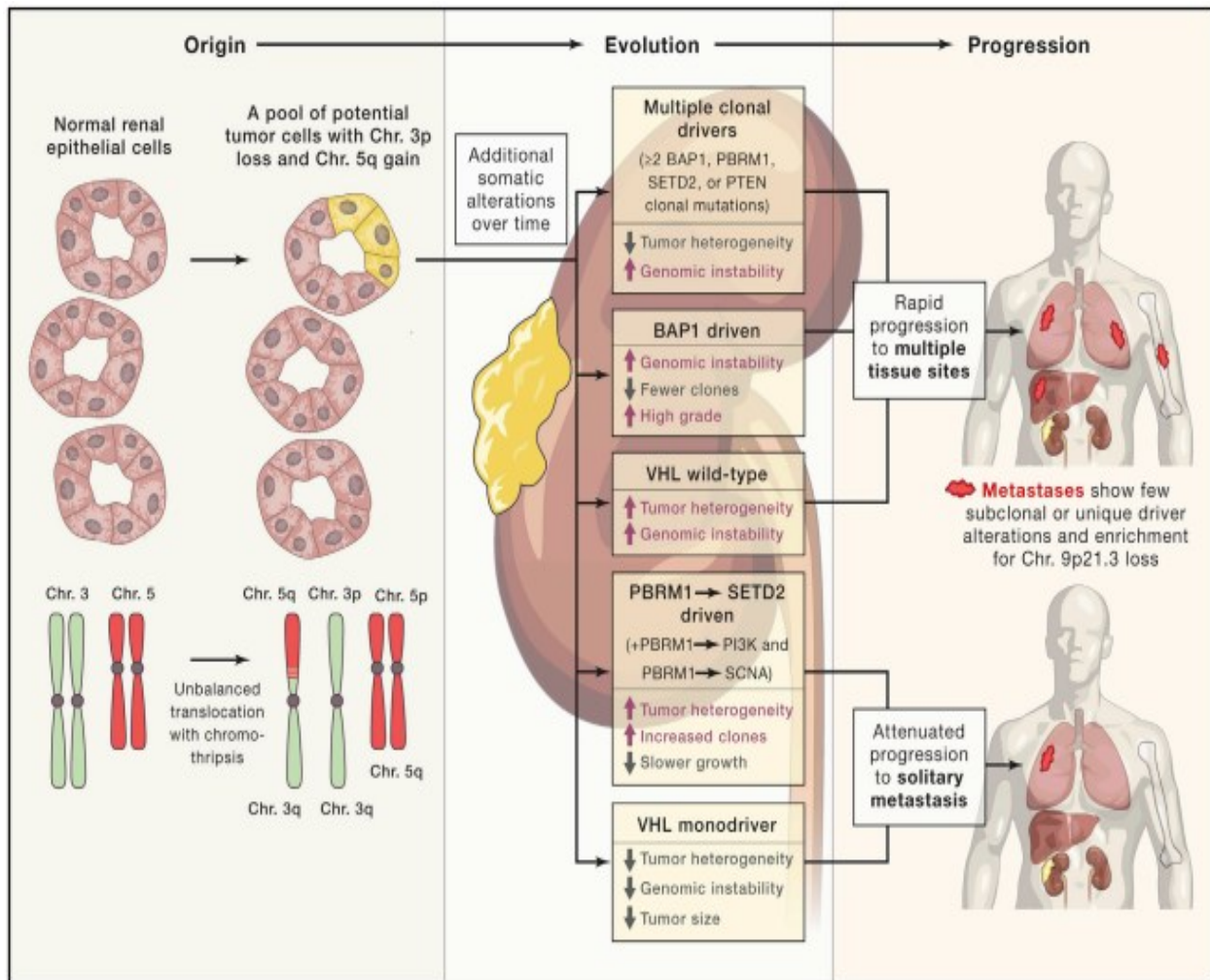


**Figure 1.4 ccRCC Pathophysiology.** Normal renal proximal tubule epithelial cells with a translocation between chromosome number 3 (green) and 5 (red) can result in loss of some part of chromosome 3p and gains in chromosome 5q. These cells divide abruptly and potentially give rise to ccRCC tumours (yellow). Sequencing of multiple ccRCC tumours supports five different evolutionary subtypes and three subtypes based on PBRM1 mutations. ccRCC tumours can manifest multiple clonal drivers; BAP1-driven and VHL wild-type subtypes were plausible to show rapid progression to various tissue sites (red) whereas PBRM1-driven and VHL monodriver tumors are likely to show solitary metastasis. (Figure adapted from Ricketts et al, 2018) [191].

PBRM1 mutations have been known to be present in 40% of metastatic ccRCC tumours, and its loss has been associated with a better survival rate compared to patients who have mutations in BAP1 [189]. Although the number of patients who have mutations in both the genes is lesser in numbers, the overall survival rate is worst compared to those who have mutation only in BAP1 or PBRM1.

Therefore, BAP1 and PBRM1 are likely to be early and critical events in the development and progression to metastasis. Currently, clinical decision-making for the metastatic ccRCC does not depend on the presence or absence of these mutations. The development of models will help in the development of targeted therapy.

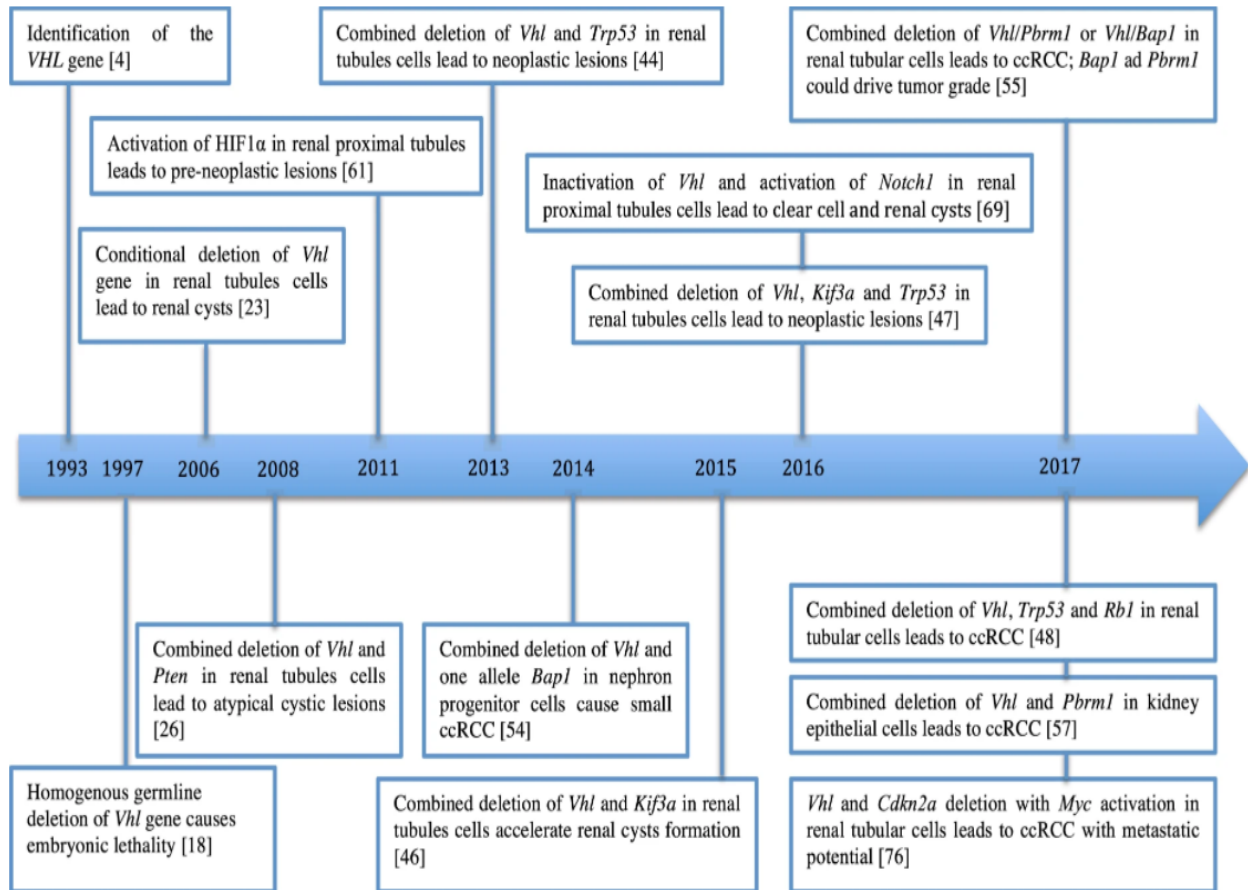


**Figure 1.5 Timeline showing the key events in the development of ccRCC models.** 13 models were developed to study ccRCC, but these models were only able to show lesions and few of the clinical features of ccRCC, depicting the difficulties in successfully progressing in the development of the autochthonous ccRCC model. (Figure adapted from Hou et al, 2018) [192].

The high flexibility of genetic tools currently accessible, makes the investigation of murine models' indispensable. *In vivo* models can emulate a majority of the genetic and epigenetic aberrations found in cancer; in this way, they are significantly instrumental in characterizing the clonal evolution of cancer. A few distinct models are available to study ccRCC, but unfortunately, none shows all the hallmarks of ccRCC (Figure 1.5 and Table 1.4).

A murine Vhl and Bap1 co-knock-out model has been developed to illuminate the combined effects of the inactivation of these genes in nephron progenitor cells. However, these mice died within one month from birth. Subsequently, a new murine model was developed in which both alleles of Vhl have been deleted and one allele of Bap1 has been deleted. These mice were morphologically normal initially, but they started manifesting abnormalities at the start of 1<sup>st</sup> month of age. Tumours in these animals were only 0.25-1.8 mm diameter in size but they were organized in solid cystic form which resembles those in patients with the VHL syndrome. The tumours' cytoplasm was clear and pleomorphic, positive for CAIX, cluster of differentiation 10 (CD10), marker of proliferation Ki-67, cluster of differentiation 31 (CD31), and vimentin (VIM). These results indicate that these models can recapitulate the early stage of human ccRCC [193]. Mice with biallelic deficiency of Vhl and Bap1 were also developed, but they lived approximately for three months and had cystic lesions which were morphologically similar to the previously discussed model.

Table 1.5 The five different GEM models of ccRCC and comparison of the various features (adapted and modified from Hou et al, 2018) [192]

<b>GEM models</b>	<b>Pene- trance</b>	<b>Pathological features</b>	<b>Pathways de- regulation</b>	<b>Tumour aggressive- ness</b>	<b>Ref- erence</b>
Vhl <sup>-/-</sup> Pbrm <sup>-/-</sup>	50%	Positive for CAIX, LTL, CD31, Ki-67; Negative for THP, CD45, cleaved caspase-3de-re.  Clear cytoplasm with lipid and glycogen.	Overexpression of HIF1a and JAK-STAT pathway genes. Hyperactivation of mTORC1 signaling. Reduction in expression of oxidative	Neither local invasion nor metastasis. Transplanted tumour is also not metastatic.	[194]



			phosphorylation genes.		
Vhl <sup>-/-</sup> Pbrm <sup>-/-</sup>	85.7%	Positive for CAIX, LTL, CD10, Ki-67, CD31, vimentin. Moderately clear cytoplasm with lipid and glycogen.	Upregulated HIF1 and HIF2 targeted genes	Not available.	[193]
Vhl <sup>-/-</sup> Bap1 <sup>+/-</sup>	100%	Positive for CAIX, CD10, Ki-67, CD31, vimentin. Clear cytoplasm with lipid and glycogen. Cells with pleomorphisms.	Upregulated HIF1 and HIF2 targeted genes. Over-activation of mTORC1 activity.	Focal lympho-vascular invasion.	[193]
Vhl <sup>-/-</sup> Trp53 <sup>-/-</sup> Rb <sup>-/-</sup>	82%	Positive for CAIX, CD10, CD31, PAX8, vWF, nuclear HIF1 α /HIF2α, pan cytokeratin. Negative for THP, NCC, aquaporin2.	Upregulated HIF1 and HIF2 targeted genes. mTORC1 activity. Overactivation of mTORC1 activity.	Neither local invasion nor metastasis.	[195]



Vhl <sup>-/-</sup> Cdkn2a <sup>-/-</sup> Myc activation	82%	Solid or tightly packed tubule-papillary tumour, high grade, clear cytoplasm, necrotic regions.	Upregulation of Epithelial-mesenchymal transition related genes.	One-third of mice had metastasis.	[196]
--	-----	---	--	-----------------------------------	-------

Ideally, the previously discussed genetically engineered mouse models (GEMM) of ccRCC will help to understand the molecular mechanisms behind tumour progression and metastasis that will lead to the revelation of new biomarkers and to test new medications, which are presently overwhelmed by *in vitro* models and murine xenograft models acquired from ccRCC cell lines or human ccRCC explants. These GEMMs are more beneficial, particularly for the exploration of immunotherapy of RCC, which is impossible on *in vitro* cell lines or immune-compromised xenograft mouse models. An autochthonous GEMM would offer a magnificent chance to explore the viability and track down relevant biomarkers in a genetically controlled setting with regards to a cancer microenvironment and resistant response.

These five ccRCC models were obtained from various combinations of genetic alterations, however, all included Vhl inactivation, underscoring the indispensable role of Vhl in ccRCC tumourigenesis, although Vhl inactivation alone can't proceed ccRCC. BAP1 and PBRM1 represent ccRCC-peculiar tumor-suppressor genes (TSGs) that are not seen in other cancers, demonstrating an explicit mechanism for tumourigenesis of ccRCC. Even though these mice could not depict all the hallmarks of ccRCC, each model may nonetheless conceivably address a subset of ccRCC.

A few attempts were made to create ccRCC mouse models, which unfortunately never fully recreated ccRCC, nevertheless, these models contributed to the understanding of ccRCC: They were able to display some of the signs of ccRCC, like clear cell histology and pre-neoplastic cystic lesions, revealing some insight into the molecular mechanism of ccRCC, however they didn't prompt a bonafide ccRCC. One likely reason for the in part

disappointing result is that conditional knock-out mice with a total loss of protein expression does not necessarily mimic the human disease scenario where mutations produce mutant or truncated proteins with residual activities. The development of clustered regularly interspaced short palindromic repeats (CRISPR)-associated protein 9 (CRISPR-Cas9) can generate the respective mutations and maybe a decent way to establish precisely humanized GEM models. Manipulating genes in a specific order instead of simultaneously mutating can actually be used to recapitulate the evolution of tumourigenesis in ccRCC. Further, these models can help to track deregulated signaling pathways during the evolution process, which will help to develop a deeper understanding of the distinctive genetic signatures and genetic boundaries to design appropriate therapies.

### **1.17 RENCA cell line**

The RENCA cell line was derived from a Balb/cCr mice tumour that emerged spontaneously as a renal cortical adenocarcinoma. This cell line has been recently used to develop metastatic ccRCC. In this study, the authors showed that deleting vhl is responsible for metastasis, but in ccRCC patients, the vhl deletion alone was not able to cause cancer [197]. Therefore, we need to develop a holistic model that will recapitulate not only metastatic ccRCC but which is also able to mimic the evolution of ccRCC.

### **1.18 Treatment options for ccRCC**

The standard therapy for RCC is partial or radical nephrectomy, whereas inoperable and metastatic RCC patients undergo targeted therapy with immune checkpoint inhibitors or targeted agents. Before 2005, cytokine treatment with interferon-alpha (IFN- $\alpha$ ) and afterward, high doses of interleukin 2 (HDIL-2) was viewed as the norm of care for the treatment of metastatic RCC [198]. The median survival rate is between 10 to 15 months [199]. The HDIL-2 complexity or after-effects were needed to be managed in an intensive care unit and mortality rate was found to be between 1% to 5% [198, 200, 201]. However, while HDIL-2 has generally become undesirable, a few clinical trials have proceeded with its utilization in combination with immune checkpoint inhibitors (NCT03729245). RCC is not susceptible to chemotherapeutic drugs or radiotherapy therapies which makes the

urgent need for targeted therapies and immune checkpoint inhibitors (ICI). In the last 15 years, treatment of RCC saw the rapid transformation. There are several Food and Drug Administration (FDA) approved targeted therapies and ICI for the treatment of ccRCC (Table 1.6 and 1.7).

Table 1.6 Monotherapy approved for the treatment of ccRCC (adapted and modified from Khetani et al, 2020) [202]

<b>Drug</b>	<b>Mechanism of action</b>	<b>Line of therapy</b>	<b>Reference</b>
Pazopanib	Tyrosine kinase inhibitor	First	[203]
Sunitinib	Tyrosine kinase inhibitor	First	[204]
Axitinib	Tyrosine kinase inhibitor	First	[205]
Cabozantinib	Inhibitor of multiple TKReceptors	First	[206]
Temsirolimus	mTOR Inhibitor	First	[59]
Pazopanib	Tyrosine kinase inhibitor	Second	[207]
Axitinib	Tyrosine kinase inhibitor	Second	[208]
Sorafenib	Tyrosine kinase inhibitor	Second	[209]
Cabozantinib	Inhibitor of multiple TKReceptors	Second	[206]
Temsirolimus	mTOR inhibitor	Second	[210]
Nivolumab	ICI- Anti PD-1 inhibitor	Second	[211]
Everolimus	mTOR Inhibitor	Third	[212, 213]

Table 1.7 Combinatorial therapy approved for the treatment of ccRCC adapted and modified from Khetani et al, 2020) [202]

<b>Drug</b>	<b>Line of therapy</b>	<b>Reference</b>
Bevacizumab + IFN- $\alpha$	First	[214]
Bevacizumab + IFN- $\alpha$	First	[215]
Nivolumab + Ipilimumab	First	[216]
Pembrolizumab + axitinib	First	[217]
Avelumab + axitinib	First	[218]

Lenvatinib + Everlimus	Second	[219]
------------------------	--------	-------

Combination therapy aims to increase the synergistic effects of the drug, but unfortunately, it also elevates side effects. There are five combinatorial therapies available for clear cell renal cell carcinoma (Table 1.6). The survival rate of monotherapy, as well as combinatorial therapy, is less than three years from starting the therapy. Several combinatorial therapy clinical trials have failed to show significant effects and have caused severe side effects (Table 1.8). Currently, there are seven ongoing clinical trials of combination therapy in ccRCC (Table 1.9). These clinical trials were developed to optimize the treatment regimen and could also be helpful to patients who cannot tolerate TKIs.

Table 1.8 Unsuccessful clinical trials of combinatorial therapy due to severe side effects adapted and modified from Khetani et al, 2020) [202]

Drug	Clinical trial phase	Comments	Reference
Bevacizumab + sunitinib	I	Hypertension, hematologic and vascular toxicities	[220]
Tremelimumb + sunitinib	I	Renal failure	[221]
Everolimus + sorafenib	I	Grade 3 rash with high gastrointestinal toxicity.	[222]
Bevacizumab + everolimus	II	Stomatitis, pulmonary embolism, elevated proteinuria and anorexia.	[223]
Temsirolimus + IFN- $\alpha$	III	No improvement in overall survival rate in comparison to IFN- $\alpha$ .	[59]

Table 1.9 Ongoing clinical trials of combinatorial therapy approved for the treatment of ccRCC adapted and modified from Khetani et al, 2020) [202]

<b>Treatment</b>	<b>ClinicalTrials.gov No.</b>	<b>Completion date</b>	<b>Comments</b>
Nivolumab-cabozantinib	NCT03141177	April 2024	Primary data showed significant improvement in overall survival in comparison to patients who took sunitinib (16.6 vs 8.3 months). Quality of life improved with nivolumab plus cabozantinib in comparison to sunitinib.
Lenvatinib-everolimus or lenvatinib-pembrolizumab	NCT02811861	July 2022	Overall survival was longer with lenvatinib plus pembrolizumab than with sunitinib (23.9 vs. 9.2 months) but was no longer with lenvatinib plus everolimus than with sunitinib. Grade 3 or higher detrimental incidents appeared or aggravated during treatment in 82.4%, 83.1%, and 71.8% of the patients who received lenvatinib plus pembrolizumab, lenvatinib plus everolimus, sunitinib, respectively.
Nivolumab-ipilimumab followed by nivolumab	NCT03793166	September 2022	-
NKTR-214-nivolumab	NCT03729245	June 2024	-

Pazopanib-abexinostat	NCT03592472	June 2022	-
Nivolumab-ipilimumab	NCT03138512	August 2032	-
Nivolumab-ipilimumab	NCT03873402	March 2025	-

As most ccRCC cases are diagnosed in the advanced or metastatic stage, developing a valid biomarker would help decide the treatment option for the patients. We need to currently focus on understanding the deregulated signaling pathways and target the mutated proteins leading to aggressively progressing disease to help develop therapies.

Further, imminent clinical trials are required to assess the clinical utility of recommended pathological signatures. Eventually, biomarkers might permit treatment to be customized to each patient's requirements, empowering patients to get maximal expected advantage while limiting the side effects of the treatment regimen.

Although several studies have previously described protocols for establishing proximal tubules cell primary cultures, these are hampered by frequent hetero-cellular contamination, erroneous cellular differentiation/de-differentiation, and poor viability.

The work presented in this thesis aims to establish and characterize proximal tubule systems to ensure their phenotypic purity and stability. Secondly, by developing a proximal tubule *in vitro* model the evolution of metastatic ccRCC can be recapitulated, by using sequential CRISPR-Cas9-Bsed genome editing and studying proteomic deregulation in the development of metastatic ccRCC.

## 2 Materials and Methods

### 2.1 Materials

Table 2.1 List of cell lines and bacterial strains used in the study

Strain	Reference
LLC-PK1	Merck
HEK 293T	Gift from Anja Bremm, Buchmann Institute of Molecular Life Science, Frankfurt
NEB Stable Competent E. coli	New England Biolabs
BL21(DE3) Competent Cells	New England Biolabs

Table 2.2 List of oligonucleotides used in the study

Oligo name	Sequence (5'-3')	Description
VHL_gRNA1_forward	CACCGGTCCGACGTAATGCCCCG GA	For CRISPR-Cas9 experiments
VHL_gRNA1_reverse	AAACTCCGGGGCATTACGTCGGAC C	For CRISPR-Cas9 experiments
VHL_gRNA2_forward	CACCGGCTGCGCTCGGTGAATTCG C	For CRISPR-Cas9 experiments
VHL_gRNA2_reverse	AAACGCGAATTCACCGAGCGCAGC C	For CRISPR-Cas9 experiments
VHL_gRNA3_forward	CACCGGGTTGTGCGAAGCCTAGTC A	For CRISPR-Cas9 experiments
VHL_gRNA3_reverse	AAACTGACTAGGCTTCGCACAACC C	For CRISPR-Cas9 experiments

BAP1_gRNA1_forward	CACCGAGGTCACGTACAGCGCGAT	For CRISPR-Cas9 experiments
BAP1_gRNA1_reverse	AAACAATCGCGCTGTACGTGACCT C	For CRISPR-Cas9 experiments
BAP1_gRNA2_forward	CACCGGTATTGTCTGACGGTTCAC C	For CRISPR-Cas9 experiments
BAP1_gRNA2_reverse	AAACGGTGAACCGTCAGACAATAC C	For CRISPR-Cas9 experiments
BAP1_gRNA3_forward	CACCGGACCCTTTCGCTTATACCT G	For CRISPR-Cas9 experiments
BAP1_gRNA3_reverse	AAACCAGGTATAAGCGAAAGGGTC C	For CRISPR-Cas9 experiments
U6_forward	GGGCCTATTTCCCATGATTCCTTCA TATTTGC	For verifying gRNA integration into plentiCRISPRv2
G13V_forward	CAGCAGGGTAAACAGAACCGGATC GCTTTCCAG	To create BAP1 cancer-associated mutants
G13V_reverse	CTGGAAAGCGATCCGGTTCTGTTT ACCCTGCTG	To create BAP1 cancer-associated mutants
V24D_forward	TTCCACCTGAACACCTTTATCACCA AAATCTTCAACCAG	To create BAP1 cancer-associated mutants
V24D_reverse	CTGGTTGAAGATTTTGGTGATAAA GGTGTTCAAGGTGGAA	To create BAP1 cancer-associated mutants
E31A_forward	CTCTGCAGATCATAAATCGCTTCCA CCTGAACACCTT	To create BAP1 cancer-associated mutants



E31A_reverse	AAGGTGTTTCAGGTGGAAGCGATTT ATGATCTGCAGAG	To create BAP1 cancer-associated mutants
Y33D_forward	CATTTGCTCTGCAGATCATCAATCT CTTCCACCTGAACAC	To create BAP1 cancer-associated mutants
Y33D_reverse	GTGTTTCAGGTGGAAGAGATTGATG ATCTGCAGAGCAAATG	To create BAP1 cancer-associated mutants
V43G_forward	CAGGAAGATAAAACCATAACCAGG ACCCTGACATTTGCT	To create BAP1 cancer-associated mutants
V43G_reverse	AGCAAATGTCAGGGTCCTGGTTAT GGTTTTATCTTCCTG	To create BAP1 cancer-associated mutants
G128V_forward	GTGCATTACCAATGGCATAAACTTT GCTTTCCGGACTAAAA	To create BAP1 cancer-associated mutants
G128V_reverse	TTTTAGTCCGGAAAGCAAAGTTTAT GCCATTGGTAATGCAC	To create BAP1 cancer-associated mutants
H169V_forward	TAATCGGAACATAGCTAACAAAAAC AAATGCTTCCATTGTACGAACTGC	To create BAP1 cancer-associated mutants
H169V_reverse	GCAGTTCGTACAATGGAAGCATT GTTTTTGTAGCTATGTTCCGATTA	To create BAP1 cancer-associated mutants
F170C_forward	GGAACATAGCTAACACAATGAAAT GCTTCCATTGTACGAACTGCG	To create BAP1 cancer-associated mutants
F170C_reverse	CGCAGTTCGTACAATGGAAGCATT TCATTGTGTTAGCTATGTTCC	To create BAP1 cancer-associated mutants
V171D_forward	CCGGTAATCGGAACATAGCTATCA AAATGAAATGCTTCCATTG	To create BAP1 cancer-associated mutants
V171D_reverse	CAATGGAAGCATTTCATTTTGATAG CTATGTTCCGATTACCGG	To create BAP1 cancer-associated mutants

G185R_forward	CGGATAAACTTTCAGACGATCCAG TTCAAACAGACG	To create BAP1 cancer-associated mutants
G185R_reverse	CGTCTGTTTGAAGTGGATCGTCTG AAAGTTTATCCG	To create BAP1 cancer-associated mutants
W196S_forward	CATCTTCACCCGACGGACCATGAT CAATCGGA	To create BAP1 cancer-associated mutants
W196S_reverse	TCCGATTGATCATGGTCCGTCGGG TGAAGATG	To create BAP1 cancer-associated mutants
N229H_forward	AACTGCCATCAGATGAAAACGAAT ATCGTGATACGGTTCGC	To create BAP1 cancer-associated mutants
N229H_reverse	GCGAACCGTATCACGATATTCGTT TTCATCTGATGGCAGTT	To create BAP1 cancer-associated mutants
V24D_forward	CACTTGCACCCCCTTGTACCGAA ATCTTCCAC	Reconstitution of VHL + BAP1 DKO with BAP1 mutation
V24D_reverse	GTGGAAGATTTTCGGTGACAAGGGG GTGCAAGTG	Reconstitution of VHL + BAP1 DKO with BAP1 mutation
E31A_forward	TGAAGGTCGTAGATCGCCTCCACT TGCACCC	Reconstitution of VHL + BAP1 DKO with BAP1 mutation
E31A_reverse	GGGTGCAAGTGGAGGCGATCTAC GACCTTCA	Reconstitution of VHL + BAP1 DKO with BAP1 mutation
V43G_forward	AGGAAGATAAATCCATATCCAGGG CCCTGACATTTGC	Reconstitution of VHL + BAP1 DKO with BAP1 mutation

V43G_reverse	GCAAATGTCAGGGCCCTGGATATG GATTTATCTTCCT	Reconstitution of VHL + BAP1 DKO with BAP1 mutation
G185R_forward	GACCTTCAGCCTATCCAGCTCAA GAGCCG	Reconstitution of VHL + BAP1 DKO with BAP1 mutation
G185R_reverse	CGGCTCTTTGAGCTGGATAGGCTG AAGGTC	Reconstitution of VHL + BAP1 DKO with BAP1 mutation

Table 2.3 List of plasmids used in the study

Plasmids	Description	Reference
pLentiCRISPRv2 hygromycin	Variant of plentiCRISPRv2 that confers hygromycin resistance	Addgene
pLentiCRISPRv2 neomycin	Variant of plentiCRISPRv2 that confers neomycin resistance	Addgene
psPAX2	2 <sup>nd</sup> generation lentiviral packaging plasmid.	Addgene
pMD2.G	VSV-G lentiviral envelope expressing plasmid.	Addgene
pLVX-M-Flag-BAP1	Express wild type BAP1	Addgene
pTriEx-7	Mammalian expression	Addgene

pLentiCRISPRv2 hygro_VHL_1	VHL_gRNA1 guide sequence is inserted into pLentiCRISPRv2 hygro.	Constructed in this study
pLentiCRISPRv2 hygro_VHL_2	VHL_gRNA2 guide sequence is inserted into pLentiCRISPRv2 hygro.	Constructed in this study
pLentiCRISPRv2 hygro_VHL_3	VHL_gRNA3 guide sequence is inserted into pLentiCRISPRv2 hygro.	Constructed in this study
pLentiCRISPRv2 neo_BAP1_1	BAP1_gRNA1 guide sequence is inserted into pLentiCRISPRv2 neo.	Constructed in this study
pLentiCRISPRv2 neo_BAP1_2	BAP1_gRNA2 guide sequence is inserted into pLentiCRISPRv2 neo.	Constructed in this study
pLentiCRISPRv2 neo_BAP1_3	BAP1_gRNA3 guide sequence is inserted into pLentiCRISPRv2 neo.	Constructed in this study
pLVX-M-Flag-BAP1_V24D	V24D mutation is inserted into pLVX-M-Flag-BAP1	Constructed in this study
pLVX-M-Flag-BAP1_E31A	E31A mutation is inserted into pLVX-M-Flag-BAP1	Constructed in this study
pLVX-M-Flag-BAP1_V43G	V43G mutation is inserted into pLVX-M-Flag-BAP1	Constructed in this study
pLVX-M-Flag-BAP1_G185R	G185R mutation is inserted into pLVX-M-Flag-BAP1	Constructed in this study

pET28a_V24D	V24D mutation is inserted into pET28a	Constructed in this study
pET28a_E31A	E31A mutation is inserted into pET28a	Constructed in this study
pET28a_V43G	V43G mutation is inserted into pET28a	Constructed in this study
pET28a_G185R	G185R mutation is inserted into pET28a	Constructed in this study

Table 2.4 List of antibodies used in the study

Name	Dilution	Application	Reference
VHL	1:500	Immunoblot	Cell Signaling Technology
BAP1	1:1000	Immunoblot	Cell Signaling Technology
Actin	1:1000	Immunoblot	Merck
Goat anti-mouse IgG-HRP	1:2000	Immunoblot	Santa Cruz Biotechnology
Goat anti-rabbit IgG-HRP	1:2000	Immunoblot	Dako
ZO-1	1:250	Immunofluorescence	Santa Cruz Biotechnology
Alexa fluor 488 donkey anti rat	1:500	Immunofluorescence	Santa Cruz Biotechnology
Alexa fluor 647 goat anti mouse	1:500	Immunofluorescence	Santa Cruz Biotechnology

Table 2.5 List of compounds used in the study

Compound	Function	Reference
Digoxin	Na <sup>+</sup> /K <sup>+</sup> ATPase inhibitor	Selleck Chemicals
Bafilomycin	H <sup>+</sup> ATPase inhibitor	Selleck Chemicals
S3226	NHE3 inhibitor	Merck
S0859	Na <sup>+</sup> /HCO <sub>3</sub> <sup>-</sup> inhibitor	Selleck Chemicals
SEA0400	Na <sup>+</sup> /Ca <sup>2+</sup> inhibitor	Selleck Chemicals
Dapagliflozin	SGLTs inhibitor	Selleck Chemicals
R-(+)-DIOA	K <sup>+</sup> /Cl <sup>-</sup> inhibitor	Selleck Chemicals
DIDS	Anionic transport inhibitor	Selleck Chemicals
PF-06869206	PiT2, NaPi-IIa, NaPi-IIc inhibitor	Selleck Chemicals
Pyr3	TRPC3 inhibitor	Selleck Chemicals

## 2.2 Maintenance of cell line

LLC-PK1 cells were cultured at 37°C and 5% CO<sub>2</sub> in Medium 199 (ThermoFisher) supplemented with 10% fetal bovine serum (FBS) and 1% penicillin-streptomycin mixture (Merck). HEK-293T cells were cultured at 37°C and 5% CO<sub>2</sub> in Dulbecco's Modified Eagle's Medium (DMEM-high glucose) with 10% FBS and 1% penicillin-streptomycin mixture (Merck).

## 2.3 Immunoblot

Cells were lysed in NP40 lysis buffer (5 M NaCl, 10% NP-40, 1M Tris (pH 8.0)) and the total protein content was determined using Bradford reagent (Thermo Scientific). The cellular protein lysates were run in 10% SDS PAGE gel and after that transferred to PVDF membrane (Thermo Fisher Scientific). Then, the membrane was blocked using 5% BSA. Membranes were then probed with specific primary antibodies and signals were detected using enhanced chemi-luminescence detection reagents. Finally, a ChemiDoc™ MP

Imaging System (BioRad) was used to detect signals. The primary and secondary antibodies used for immunoblotting are listed above (Table 2.4).

## **2.4 Immunofluorescence**

LLC-PK1 cells were seeded on 2 cm petri dishes and cells were fixed on 1<sup>st</sup> day (monolayer phase), 3<sup>rd</sup> day (dome phase), 4.5<sup>th</sup> day (transition phase), and 10<sup>th</sup> day (tube phase) with 4% paraformaldehyde for 20 minutes at room temperature. Then, cells were incubated in blocking buffer (10% FBS, 0.1% saponin and 0.05% NaN<sub>3</sub> in PBS) for 1 h. Afterwards, the cells were labelled with Phalloidin CruzFluor™ 555 conjugated (Santa Cruz Biotechnology) for 1 h at room temperature. After incubation, PBS wash was performed and ultimately, images were captured using the Leica DMI8 confocal microscope and Zeiss LSM780 confocal microscope, respectively.

In another experiment, LLC-PK1 wild type, VHL KO, VHL +BAP1 double knock out (DKO), reconstituted BAP1 mutation in DKO cell lines were grown on 2 cm petri dishes (Mat Tek Life Sciences) at 70% confluency and cells were fixed on 10<sup>th</sup> day using 4% paraformaldehyde for 20 minutes. Then, cells were incubated in blocking buffer (1% BSA, 0.1% saponin and 0.05% NaN<sub>3</sub> in PBS) for 1h. Following incubation, ZO-1 antibody was added and incubated at 4° overnight. After incubation, cells were incubated with Alexa fluor 488 donkey anti rat secondary antibody for ZO-1 at room temperature for 1 h. Finally, Hoechst was added and incubated for 15 minutes, and images were captured using the Zeiss LSM780 microscope system.

In another set of experiment, LLC-PK1 wild type, VHL KO, VHL +BAP1 DKO, reconstituted BAP1 mutation in DKO cell lines were grown on 96 cell culture plate (Mat Tek Life Sciences) at 70% confluency and cells were fixed on 10<sup>th</sup> day using 4% paraformaldehyde for 20 minutes. Then cells were incubated in a blocking buffer (1% BSA, 0.1% saponin and 0.05% NaN<sub>3</sub> in PBS) for 1 h. Afterwards, the cells were labelled with Phalloidin CruzFluor™ 555 conjugated (Santa Cruz Biotechnology) for 1 h at room temperature. After incubation, PBS wash was performed and ultimately, images were captured using the Leica DMI8 confocal microscope and Zeiss LSM780 confocal microscope respectively. Finally, Hoechst was added and incubated for 15 minutes, and images were captured using the CQ1 Yokogawa system.

## **2.5 Pharmacological interventions**

Cells were grown in Imagelock 96 well plates (Essen BioScience), rinsed in phosphate-buffered saline (PBS), and placed in a fresh medium prior to treatments. Cells were treated with different transport inhibitors (Table 2.5) and after treatment, cells were imaged for 10 days with a 10x objective in an Incucyte<sup>®</sup> S3 (Sartorius) automated microscope. Also, wild type, VHL KO, VHL + BAP1 DKO, reconstituted BAP1 mutation in DKO cell lines were grown in Imagelock 96 well plates and videos were captured for 10 days at in an Incucyte<sup>®</sup> S5 (Sartorius) automated microscope for morphological studies.

### **2.5.1 Measurement of major axis, minor axis, and dome area**

A region of interest containing maximum the dome area was selected for computing major axis, minor axis, and dome area in each condition using Fiji - ImageJ.

### **2.5.2 Tube measurement**

Total tube length, total number of tubes, and branching points were measured using WimTube software (<https://www.wimasis.com/en/products/13/WimTube>).

## **2.6 CRISPR Cas9 Knock-out**

Three gRNAs were designed for VHL and BAP1 using CHOPCHOP software. (<https://chopchop.cbu.uib.no/>). Two oligonucleotides were synthesized for each gRNA (Table 2.2). Then, each gRNA was inserted into pLentiCRISPRv2 using a standard cloning procedure. Briefly, 1.5 µg of pLentiCRISPRv2 was digested using BsmB1. Oligos were annealed by decreasing temperature from 95°C to 10°C in steps of 5°C per minute in PCR. Then, oligos were diluted to 0.5 µM. Annealed oligos were ligated with 100 ng of the digested backbone by adding 2.5 U/µl of T4 DNA ligase (Biolabs) and incubated 10 min at RT. Finally, the ligated product is transformed using NEB Stable Competent E. coli. Ampicillin-resistant colonies were picked and plasmids were isolated using QIAGEN<sup>®</sup> Plasmid midi kits and sequenced using U6 primer.

HEK239T cells were seeded with the confluence of 80-90% confluence. Following day, cells were transfected with 3 guide RNAs (1.1 µg for each gRNA), pPAX2 (2.7 µg), pMD2.G (1 µg) for each gene in 200ul OptiMEM media and 21 µl TurboFect<sup>™</sup>. After 24



h, 1.9 ml supernatant was collected and added 2 ml media. Supernatant was stored at -80°C. After another 24 h, supernatant was collected and stored at -80°C. Supernatant was centrifuged at 170 g for 10 minutes to remove cell debris and finally used for transduction experiment.

LLC-PK1 and LLC-PK1\_VHLKO cells were transduced with 500 µl of lentivirus supernatant and 8 µg per ml of polybrene. After two days, cells were transferred in the selection media. LLC-PK1\_VHL KO was selected using hygromycin (1.5 mg per ml) and LLC-PK1\_VHL KO + BAP1 DKO was selected using hygromycin (1.5 mg per ml), and neomycin (500 µg per ml). Clones were picked, amplified and validated by immunoblotting.

## 2.7 Reconstitutions of BAP1 mutation

V24D, E31A, V43G, G185R were generated using pLVX-M-Flag-BAP1 by site directed mutagenesis using Quick-change site-directed mutagenesis kit. Then, PCR is run according to the below protocol.

Temperature	Time	Number of cycle
95 °C	00:30 sec	x1
95 °C	00:30 sec	x25
55 °C	01:00 min	
68 °C	10:00 min	
72 °C	10:00 min	x1

After PCR, samples were digested with DpnI for 2 h and heat-inactivated at 80°C for 20 minutes. After that, transformation was performed using NEB Stable Competent *E. coli*. Colonies were picked and plasmids were isolated using QIAGEN® Plasmid midi kits. Plasmids were sequenced using U6 primer.

Then, HEK239T cells were seeded with the confluence of 80-90% confluence. Following day, cells were transfected with wild type and mutant plasmids (3.3 µg), pPAX2 (2.7 µg), pMD2.G (1 µg) for each gene in 200 µl OptiMEM media and 21 µl TurboFect™. After 24 h, 1.9 ml supernatant was collected and added 2 ml media. Supernatant was stored at -

80°C. After other 24 h, supernatant was collected and stored at -80°C. Supernatant was centrifuged at 170 g for 10 minutes to remove cell debris and finally used for transduction experiment.

LLC-PK1\_VHL KO + BAP1 DKO is transfected with 750 µl of lentivirus supernatant and 8 µg per ml of polybrene. After two days, cells (LLC-PK1\_VHL KO + BAP1 DKO + reconstituted mutation) were transferred in the selection media and selected using hygromycin (1.5 mg per ml), neomycin (500 µg per ml), and puromycin (3 µg per ml). Clones were selected and validated by immunoblotting.

## **2.8 Whole-cell proteomics**

Cells were collected at four different stages: day 1 (monolayer phase), day 3 (dome phase), day 4.5 (transition phase), and day 10 (tube phase) and then lysed with lysis buffer (2% SDS, 50 mM Tris pH 8, 150 mM NaCl, 10 mM TCEP, 40 mM chloroacetamide including protease inhibitor cocktail complete (Roche)). For whole-cell proteomics of LLC-PK1\_VHL KO, LLC-PK1\_VHL KO + BAP1 DKO + reconstituted mutation (V24D, E31A, V43G, G185R); the lysates were collected at day 10 and then lysed with lysis buffer. Lysates were transferred to 1.5 ml ProteinLoBind tubes (Eppendorf). Samples were incubated for 10 min at 95°C.

Lysates were precipitated using methanol/chloroform, and protein pellet was dissolved using 40 µl digestion buffer (8 M urea, 50 mM Tris pH 8) to reach 1.5 mg per ml concentration. Samples were incubated for 20 minutes at 37°C and protein concentration was estimated using Bradford assay. Then, samples were diluted 1:8 with 1 M urea. After that samples were incubated for overnight at 37 °C. Digestion was stopped using 1% TFA and peptides were purified by tC18 SepPak. 10 µg peptides per sample were TMT labelled with TMTpro™ 16plex Label Reagent Set (ThermoFisher). Finally, according to manufacturer's protocol, 80 µg of pooled peptides were dried and fractionated with Pierce High pH Reversed-Phase Peptide Fractionation Kit (ThermoFisher).

The Orbitrap Fusion Lumos mass spectrometer (ThermoFisher) acquired mass spectrometry data. Proteome Discoverer (PD) 2.4 software (ThermoFisher) was used to analyze raw files. Proteomic analysis and visualization were performed using R studio.

## 2.9 TCGA data analysis

Data from the TCGA was queried using Gene Expression Profiling Interactive Analysis (GEPIA). Downregulated SLC transporters from proteomics data were searched in GEPIA database. SLC transporters with worse overall survival (OS) and disease-free survival (DFS) were retrieved and analyzed.

## 2.10 Cloning, expression and purification of BAP1

The full-length BAP1 synthetic gene containing an N-terminal 6xHis-tag was purchased from Addgene. The sequence corresponding to the catalytic domain of BAP1 (1–238) was cloned into the pTriEx-7 vector. Using this DNA template, a set of mutations on the catalytic domain of BAP1 were generated by site-directed mutagenesis using a Quick-change method (Agilent). The Catalytic domain BAP1 (residues 1–238) and metastatic ccRCC mutants were expressed in *E. coli* BL21 DE3 cells and proteins were purified using a standard His-affinity purification protocol. Briefly, BL21 (DE3) cells containing pET28a-BAP and the different plasmid DNA were grown to 0.6 OD and then induced with 250  $\mu$ M of IPTG at 18°C for overnight. After protein expression, the cells were harvested and pellet was resuspended in lysis buffer containing 50 mM Tris-HCl (pH 8.0), 1 mM MgCl<sub>2</sub>, and 10  $\mu$ g/ml lysozyme. Homogenized solutions were loaded onto 2 mL TALON metal affinity columns (Takara Bioscience) that were previously equilibrated with 50 mM Tris-HCl (pH 8.0), 150 mM NaCl, and 10 mM imidazole. The recombinant proteins (BAP1 and BAP1 single-point mutants) were eluted in 50 mM Tris-HCl, pH 8.0, 300 mM NaCl, 200 mM imidazole. The eluted proteins were dialyzed extensively with 50 mM Tris-HCl pH 8.0, 50 mM NaCl. The purity of the final proteins was verified by SDS-PAGE. All the samples were concentrated up to ~15 mg/ml, flash-frozen and stored at -80 °C until use.

### 2.10.1 BAP1 structural modeling

The structural model of the catalytic domain of BAP1 was generated using deep learningbased modeling with Alpha Fold2. Mutants with relevant implications for protein stability and function were selected to a further biochemical characterization.

### **2.10.2 Evaluation of the BAP1 activity assays using AMC probes**

The catalytic activity of the recombinant BAP1 was evaluated using Ub-AMC, SUMO1-AMC, SUMO2-AMC and ISG15-AMC substrates as previously described elsewhere. In brief, we prepared 10  $\mu$ l reactions containing increasing concentrations of BAP1 (0, 1, 5 and 20  $\mu$ M) diluted in reaction buffer (25 mM Tris-HCl pH 7.5, 150 mM NaCl, 10 mM DTT) and containing the activity-based probes 5  $\mu$ M final concentration. The samples were then incubated for 10 minutes were diluted in dilution buffer (50 mM Tris-HCl 7.5, 150 mM NaCl). All the incubations were conducted at 37 °C and measures of AMC fluorescence emission were taken every 10 seconds using a 384 fluorescence microplate reader PHERAstar FSX, BMG Labtech. To evaluate the activity of the BAP1 cancer-associated single-point mutants, reactions with 5  $\mu$ M enzyme concentration and 5  $\mu$ M substrate Ub-AMC were prepared as described above. In all the cases, substrate hydrolysis and AMC release activity was shown as AMC fluorescence [224].

### 3. Results

#### 3.1 Self-organized formation of an epithelial-tubular system in LLC-PK1 cells

Serendipitously, we observed that porcine LLC-PK1 cells, originating from proximal tubule tissue, could form a network of connected tubules on an epithelial monolayer when cultivated for prolonged periods under standard culture conditions in regular plastic cell culture ware. We then set out to characterize this system, specifically, to study to which degree this system resembles anatomical structures in the kidney: Proximal tubules are specialized structures with selective capabilities defined by the specificity of highly differentiated epithelial cells. All polarized epithelial cells in the tubular system have clearly defined apical and basal plasma membrane domains and lateral surfaces that join sister cells via specialized tight junctions (TJs). TJs are composed of occludin, claudins, and proteins of other junctional adhesion molecule families. Most of these are transmembrane proteins that connect adjoining cells via interactions with their extracellular domains and link to their respective actin cytoskeleton by their cytoplasmic domains. A fundamental feature of TJs is to create a barrier that separates the apical and basolateral elements of epithelial cells.

Perhaps the main properties of epithelial cells are the arrangement of a paracellular barrier for various proteins, ions, and different molecules. This boundary framed by TJs assumes a significant part in physiology, as it permits the development and function of diverse fluid compartments in the organisms and is likewise vital in pathological conditions. The dynamic organization of the TJ is a crucial step in various cellular processes like cell polarity and developmental patterning [225]. Therefore, we stained the cells with zonula occludens-1 (ZO-1) and identified the different stages of proximal tubule formation that will be described in detail below: We first observed formation of a monolayer (day 1), formation of domes in areas of the monolayer (day 3), appearance of a transition stage (day 4.5), after which tubes formed (day 10) (Figure 3.1).



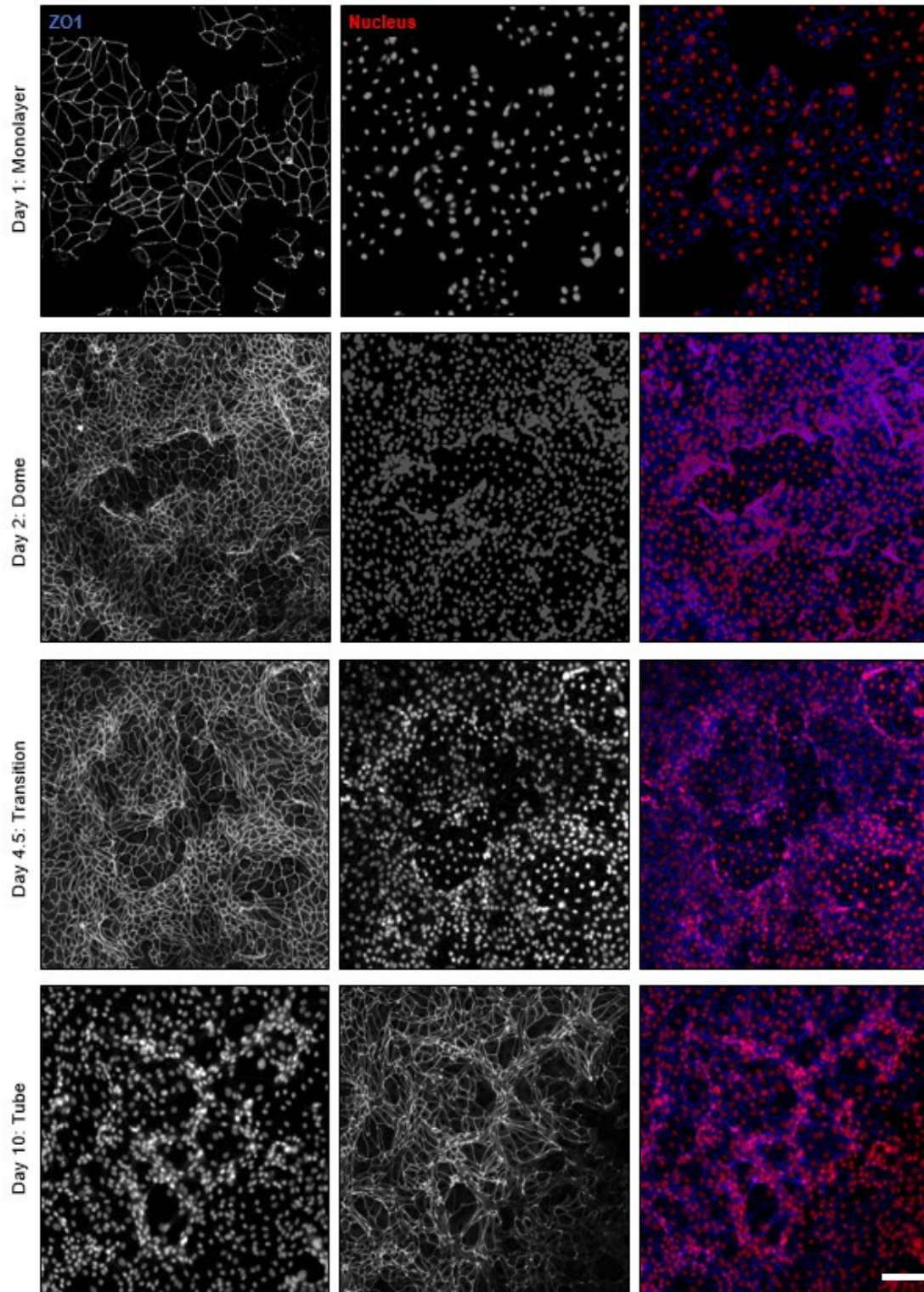


**Figure 3.1 Development of self-organized proximal tubule formation.** We cultured LLC-PK1 cells and fixed the cells using 4% para-formaldehyde at 4 different time points: monolayer stage (day 1), dome stage (day 3), transition stage (day 4.5), and tube stage (day 10). Then, cells were stained with ZO-1 staining (blue) and Nuclei (red), depicting the four stages of proximal tubule formation. Scale bar=50  $\mu$ m.

Tubulogenesis is a 10-day process. It has four different stages: monolayer, dome, transition, and tube. Concerning cell seeding dynamics, we discovered that after reaching confluence (formation of a densely, regularly packed monolayer), monolayer cells formed three-dimensional structures called domes due to fluid accumulation between the monolayer and dish, resulting in the specialized, uni-directional epithelial transport secretory properties. The doming process begins on the 2nd day and ends on the 4th day. In 4.5 days, these domes start fusing, which we called the transition stage. The dynamics during this stage ultimately lead to fully differentiated proximal tubule formation on the 10th day (Figure 3.2).

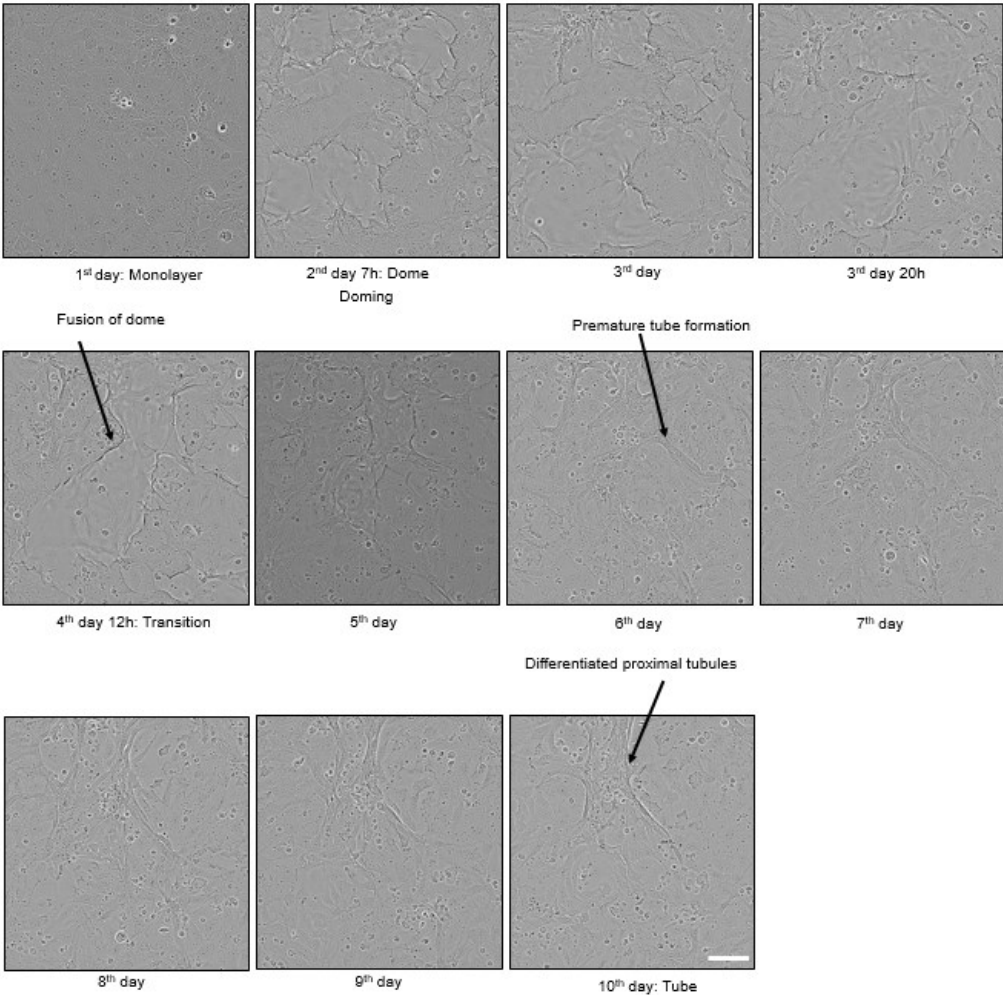


**Figure 3.2 Tubulogenesis process in proximal tubules.** LLC-PK1 were cultured for 10 days in 96 well image lock plates and imaged every hour using Incucyte microscope. Scale bar = 20  $\mu$ m.



We also found these cells have an intrinsically cystic nature. When these cells were plated, they underwent cyst-to-epithelial transformation (Figure 3.3). The cysts are eliminated by apoptosis, and a normal epithelial layer is formed.

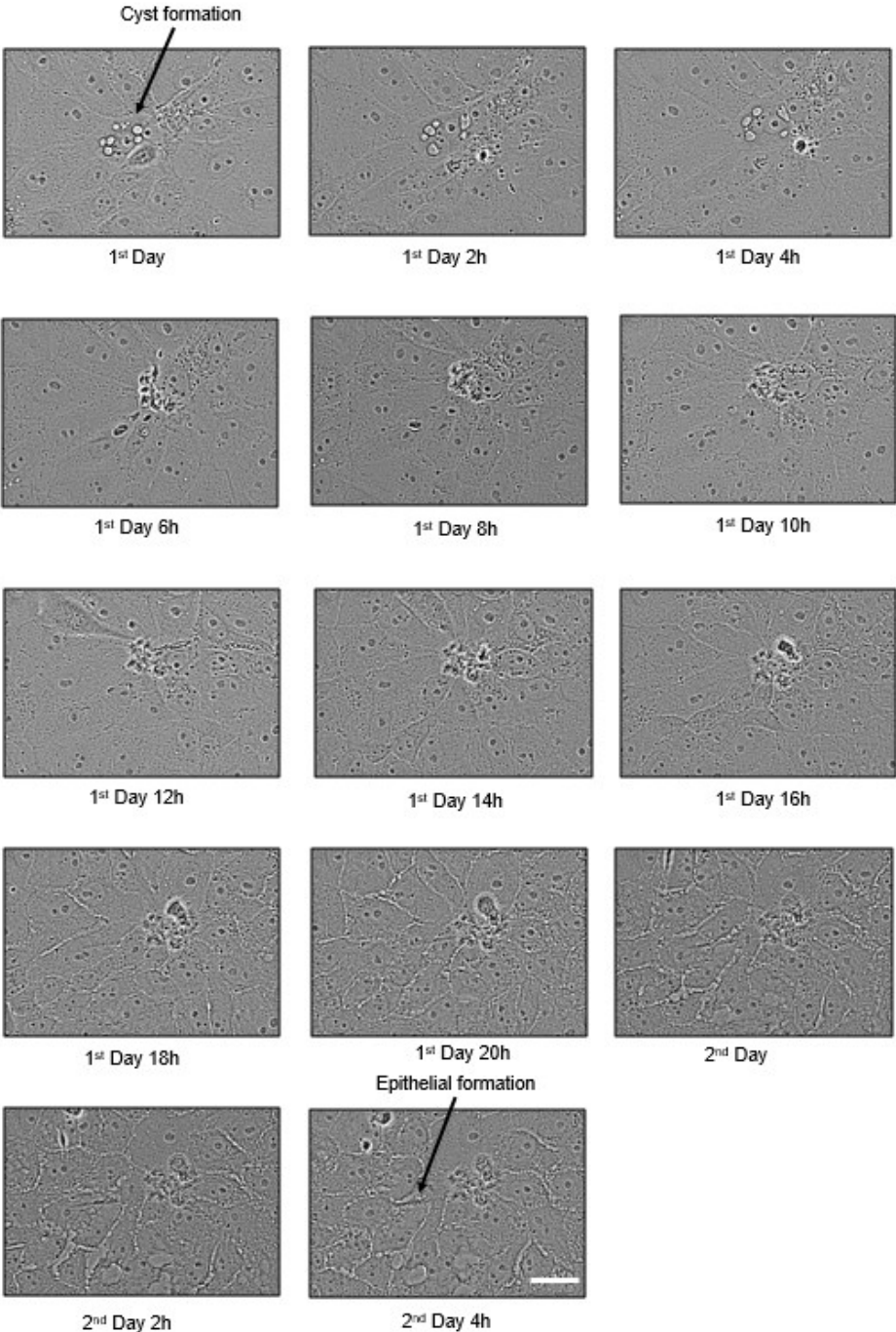


**Figure 3.3 Cystic nature of LLC-PK1.** LLC-PK1 were cultured for 10 days in 96 well image lock plates and imaged every hour using Incucyte microscope. Scale bar = 5  $\mu$ m.



We also set out to identify a potential mechanism of tubulogenesis in this system. Once cells are plated and form a monolayer that is sealed by tight junctions. First, this monolayer vectorially pumps fluid to its basal surface, which leads to local, stochastic upward bending of the layer, called doming. On the 4.5th day, domes fuse and this leads to the transition stage. We termed this fusion stage of domes a wrapping process for the following reason: Tubes form because cells at the edge of a (sometimes fusing) dome connect through stress fibers underneath the dome's cupola. This leads to the creation of a new topology: The cells at the edge contact, form connection that covers the space underneath the dome. This leads to a new topological configuration: Once the dome now shrinks, it can separate from the monolayer and form a tube structure on top of it (Figure 3.4).

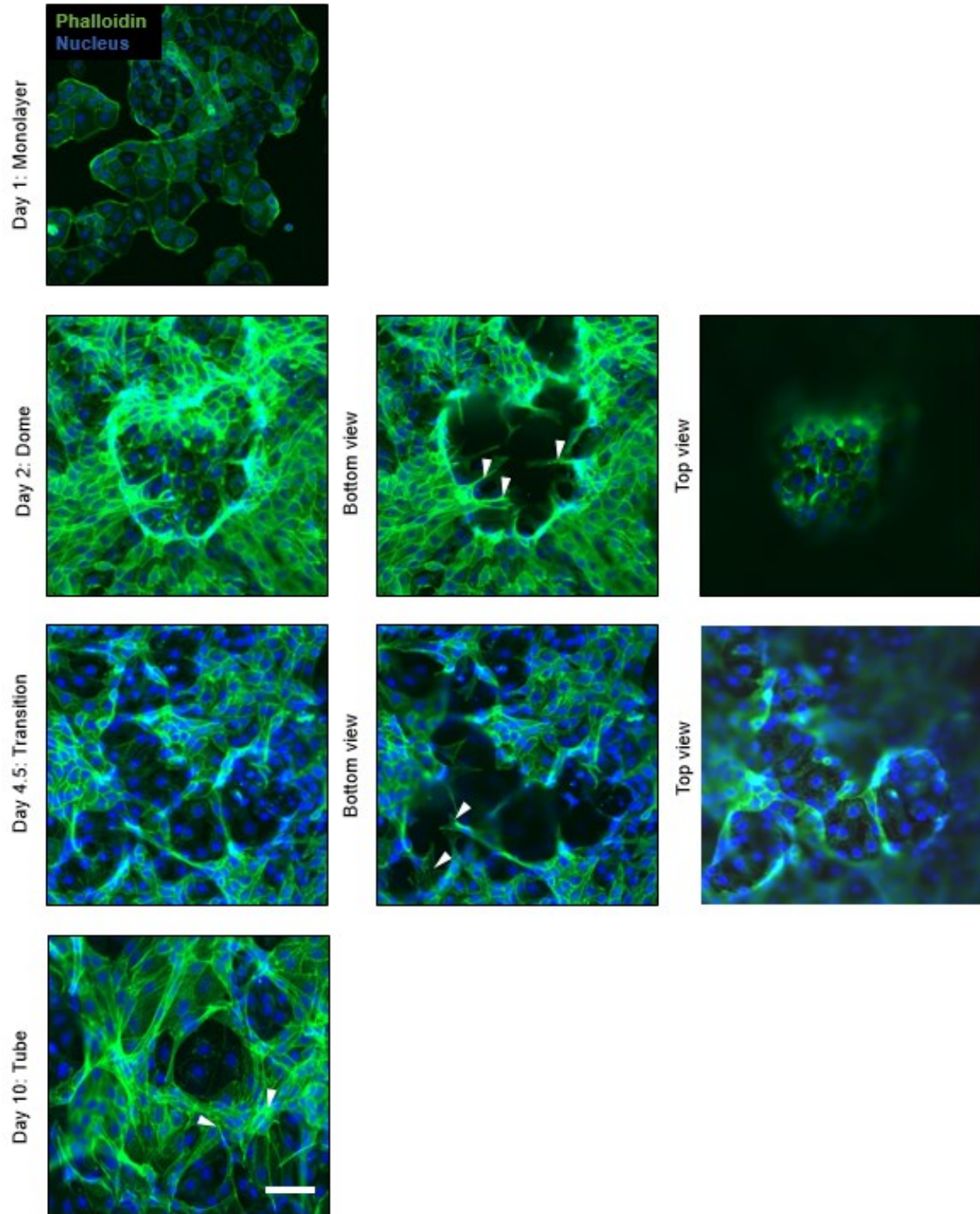


**Figure 3.4 Tubulogenesis process is two-step process.** LLC-PK1 cells were cultured and fixed using 4% paraformaldehyde at 4 different time points: monolayer stage (day 1), dome stage (day 3), transition stage (day 4.5), and tube stage (day 10). Then, cells were stained with with phalloidin (green) and nuclei (blue) staining illustrating proximal tubule formation by doming and wrapping process. Whitearrow indicates stress fibers. Left panel shows maximum projection of each stage and other panels are z stacks of corresponding stage. Scale bar=20 μm.

Through time lapse imaging and by fixing cells at dome stage to monitor the change in the F-actin structure (Figure 3.5). We found that F-actin is diluted and stretched in the sides of the domes whereas in the intermediate point of monolayer and dome it is more concentrated. The F-actin is stretched at the side of the domes is to provide mechanical strength to form 3D structure.

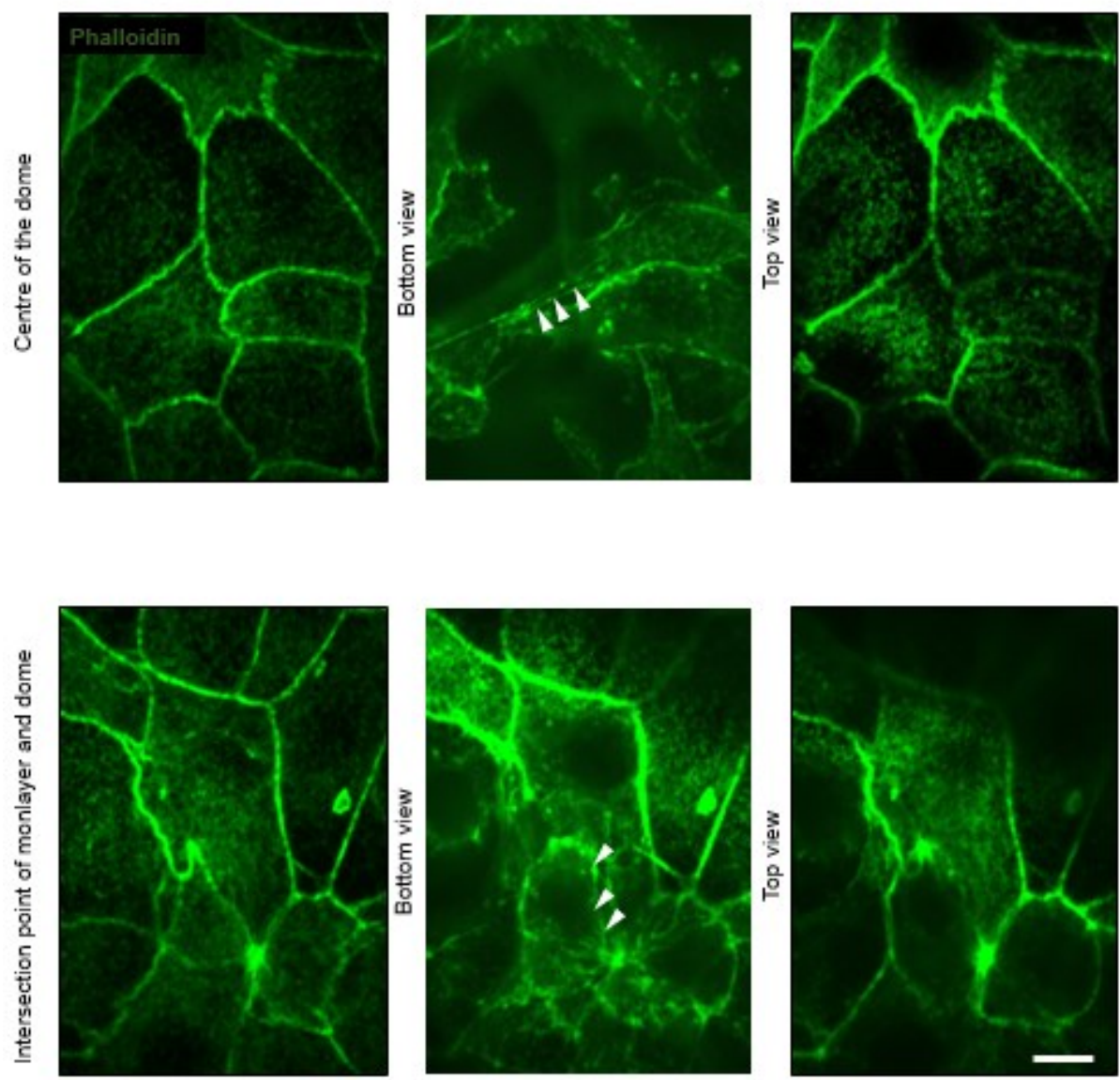


**Figure 3.5 Role of F-actin in dome formation.** LLC-PK1 cells were cultured and fixed using 4% paraformaldehyde at dome stage. Then, cells were stained with with phalloidin stain. illustrating proximal tubule formation by doming and wrapping process. White arrow indicates stress fibers. Left panel shows maximum projection and other panels are z stacks. Scale bar=20  $\mu\text{m}$ .

### 3.2 Differentiation phase-specific proteomics of self-organized morphogenesis

To discover the temporal profile of doming and tubulogenesis during self-organized differentiation, we cultured LLC-PK1 cells and collected cell lysates at 4 different time points: when cells had formed an uninterrupted monolayer (day 1), during dome formation (day 3), during the more static transition phase (day 4.5), and after tubes had formed and the epithelial layer stopped to dome (day 10). Proteins were quantified and analyzed using Proteome Discoverer, and R studio was used for analysis. Principal component analysis and scatter plot analysis showed the expected clustering among replicates; replicates of each cluster are similar to each other (Figure 3.6).

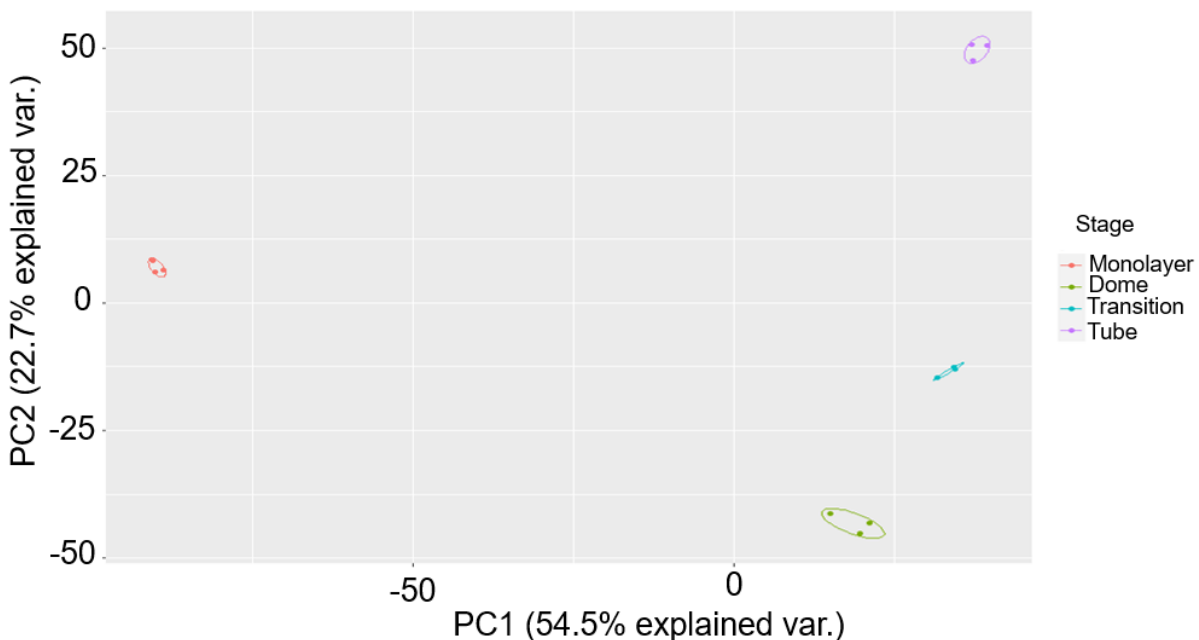


**Figure 3.6 Principal Component Analysis.** We cultured LLC-PK1 cells and collected the lysates at 4 different time points: monolayer stage (day 1), dome stage (day 3), transition stage (day 4.5), and tube stage (day 10). Samples were processed for whole cell proteomics and proteins were quantified using MS/MS, Liquid chromatography-tandem mass spectrometry. Results were visualized using R.

Hierarchical clustering depicted monolayer has large number of proteins that are upregulated in comparison to the other stages. We found upregulated proteins in monolayer from ribosome, RNA transport, replication, and RNA polymerase; in dome and transition state, metabolic pathways are upregulated instead. In the tube state, metabolic pathways, regulation of actin cytoskeleton, and endocytotic proteins are overrepresented

(Figure 3.7). These analyses show that at each phase different pathways plays peculiar roles in the formation of the structure.

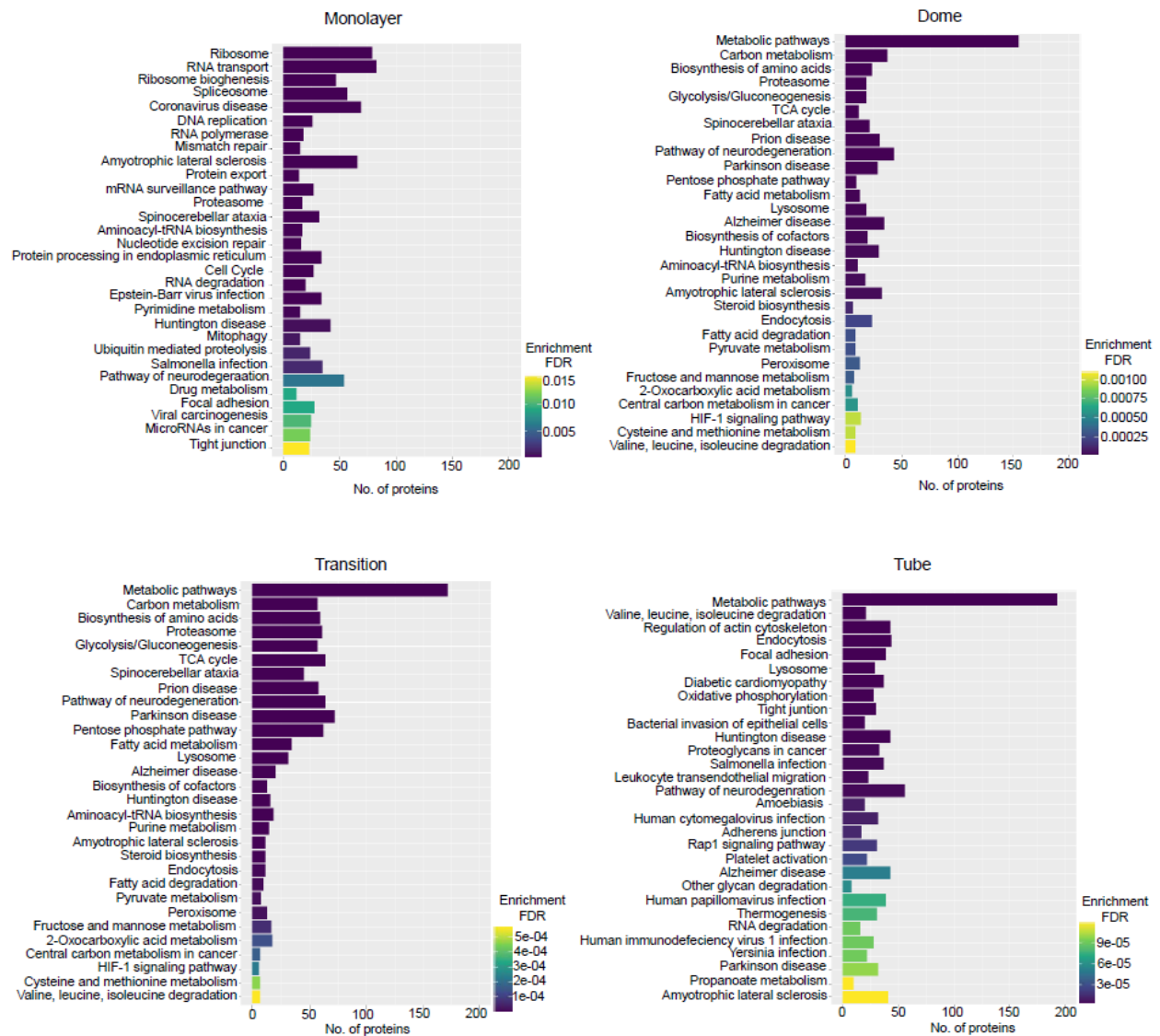


**Figure 3.7 Gene Ontology enrichment analysis.** We cultured LLC-PK1 cells and collected the lysates at 4 different time points: monolayer stage (day 1), dome stage (day 3), transition stage (day 4.5), and tube stage (day 10). Samples were processed for whole-cell proteomics and proteins were quantified using MS/MS, Liquid chromatography-tandem mass spectrometry. Results were visualized using R. Bar plots were plotted to show significantly upregulated proteins at each stage of proximal tubule development. Upregulated proteins were compared within a stage.



After this, we scrutinized specific proximal tubule markers. Interestingly, we could confirm expression of several markers directly implicated in proximal tubule biology: angiotensin 1-10 which is part of the renin-angiotensin system (RAS) and also maintains electrolyte homeostasis [226]; cubilin, which is present in the apical endocytic compartments of the proximal tubules ; collectrin, which is also present in proximal tubule and plays a key role in amino acid re-absorption [227]; and both polycystin 1 (PKD1) and polycystin 2 (PKD2), which are involved in renal tubulogenesis and also in fluid-flow mechanosensation by the primary cilium in proximal tubules (Figure 3.8) [228, 229]. These markers confirm that our proposed model has properties of proximal tubules and is a viable system to study various proximal tubule molecular and biochemical properties.

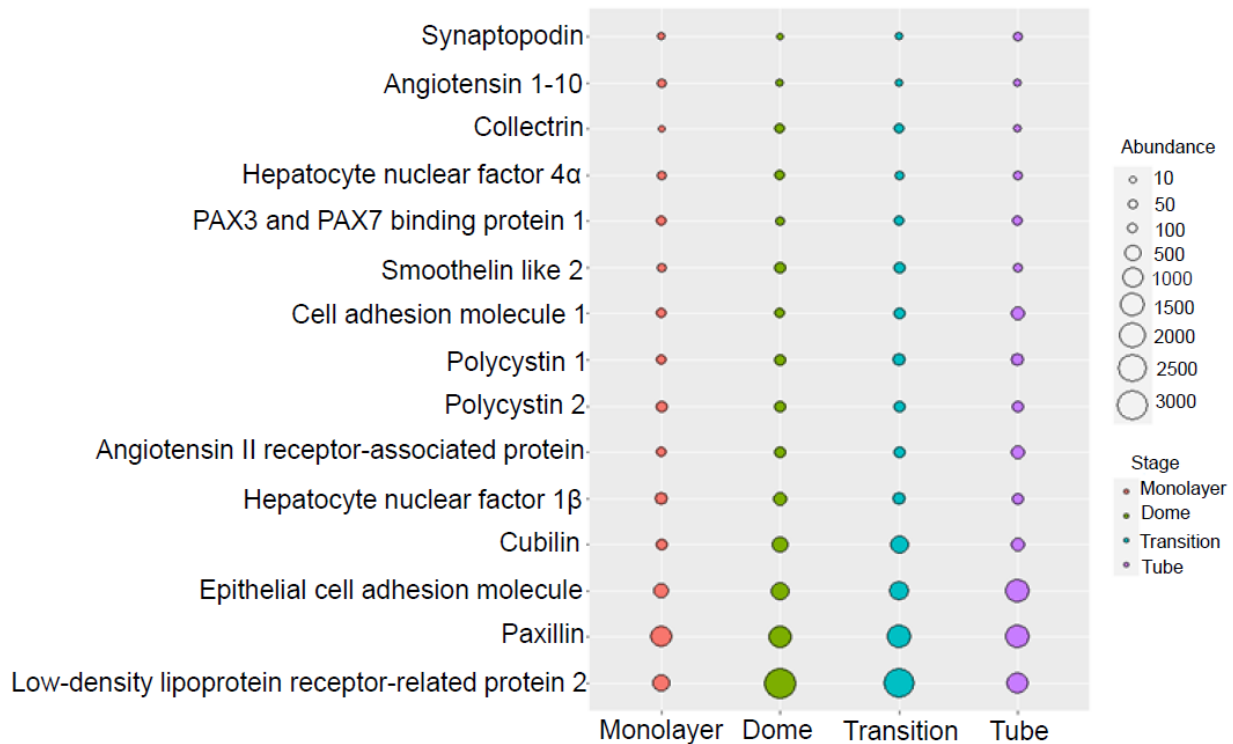


**Figure 3.8 Presence of proximal tubules markers.** We cultured LLC-PK1 cells and collected the lysates at 4 different time points: monolayer stage (day 1), dome stage (day 3), transition stage (day 4.5), and tube stage (day 10). Samples were processed for whole cell proteomics, and proteins were quantified using MS/MS, Liquid chromatography–tandem mass spectrometry. Results were visualized using R.

After that, we analyzed the expression of cell cycle-associated proteins as these are key regulators in differentiation processes. Interestingly, we found that Ki67 abundance is significantly high in monolayer stage in comparison to other three stages [230]. This shows

that in the monolayer stage cells were in dividing state and proliferate but stop proliferating in the tube state (differentiated state). Additionally, the expression of DNA-damage response proteins like proliferating cell nuclear antigen (PCNA) and RAD51 recombinase (RAD51) is substantially high in monolayer stage; PCNA level is inversely correlated to differentiation process. These results manifest that in monolayer stage, cells are in replication phase whereas once they differentiate then there is no replication. Also, expression of Cyclin B1 and cell division cycle 20 (CDC20) homolog is higher in the monolayer in comparison to other stages (Figure 3.9) [231, 232].

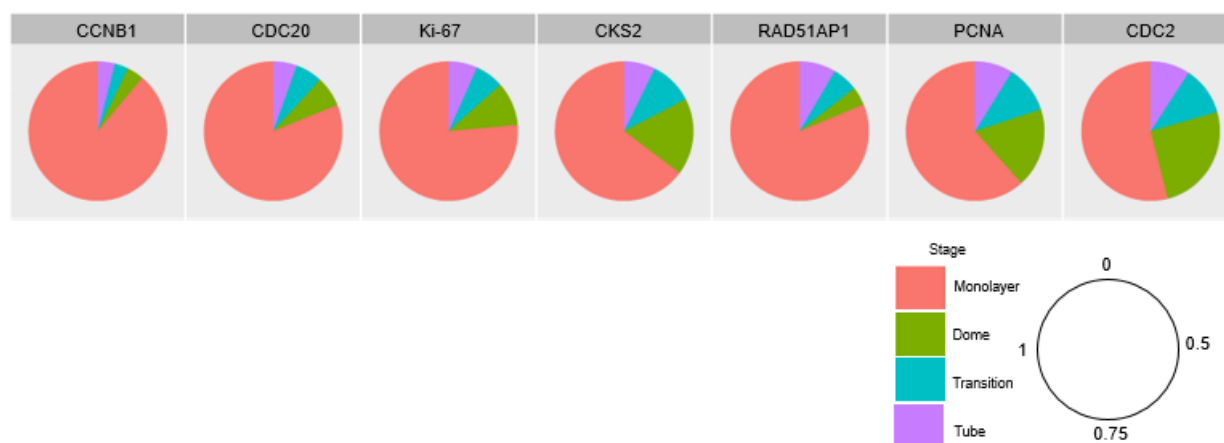


**Figure 3.9 Expression of cell cycle proteins.** We cultured LLC-PK1 cells and collected the lysates at 4 different time points: monolayer stage (day 1), dome stage (day 3), transition stage (day 4.5), and tube stage (day 10). Samples were processed for whole-cell proteomics and proteins were quantified using MS/MS, Liquid chromatography–tandem mass spectrometry. Results were visualized using R. Each circular map represents the expression of a specific cell cycle protein at four different stages of proximal tubule formation.

We also analyzed expression of proteins known to be responsible for luminogenesis. Apicobasal polarity is important for the proper functioning of proximal tubules. The three important polarity complexes are the Crumbs complex, the Par complex, and the Scribble complex. The complexes also serve as scaffolds to direct and retain proteins at the apicobasal membrane or the intervening tight junction [42]. Surprisingly, the Par-3 complex is high at the monolayer state and is slightly reduced in the other three stages (Figure 3.10). Previously, it has been shown that the Par-3 complex plays an essential role in the initial part of cell polarity [226]. The Crumbs complex and the Scribble complex proteins increased from monolayer to tube state (Figure 3.10). We also found expression of PODXL, AFDN, and Sodium-hydrogen antiporter 3 regulator 1 (SLC9A3R1) which are

key regulators of apicobasal polarity. Depleting podocalyxin and SLC9A3R1 caused defects in epithelial polarization [44]. Inhibition of AFDN leads to misorientation of apical-basal cell division in the nephron tubule [227].

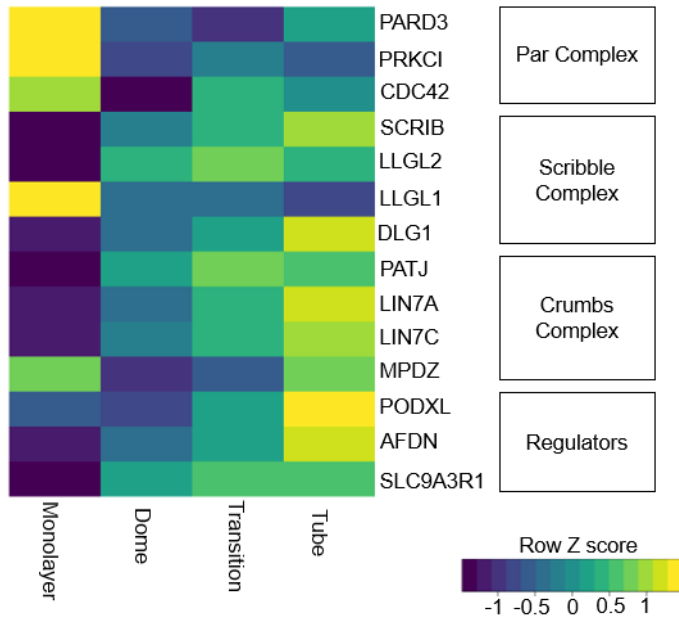
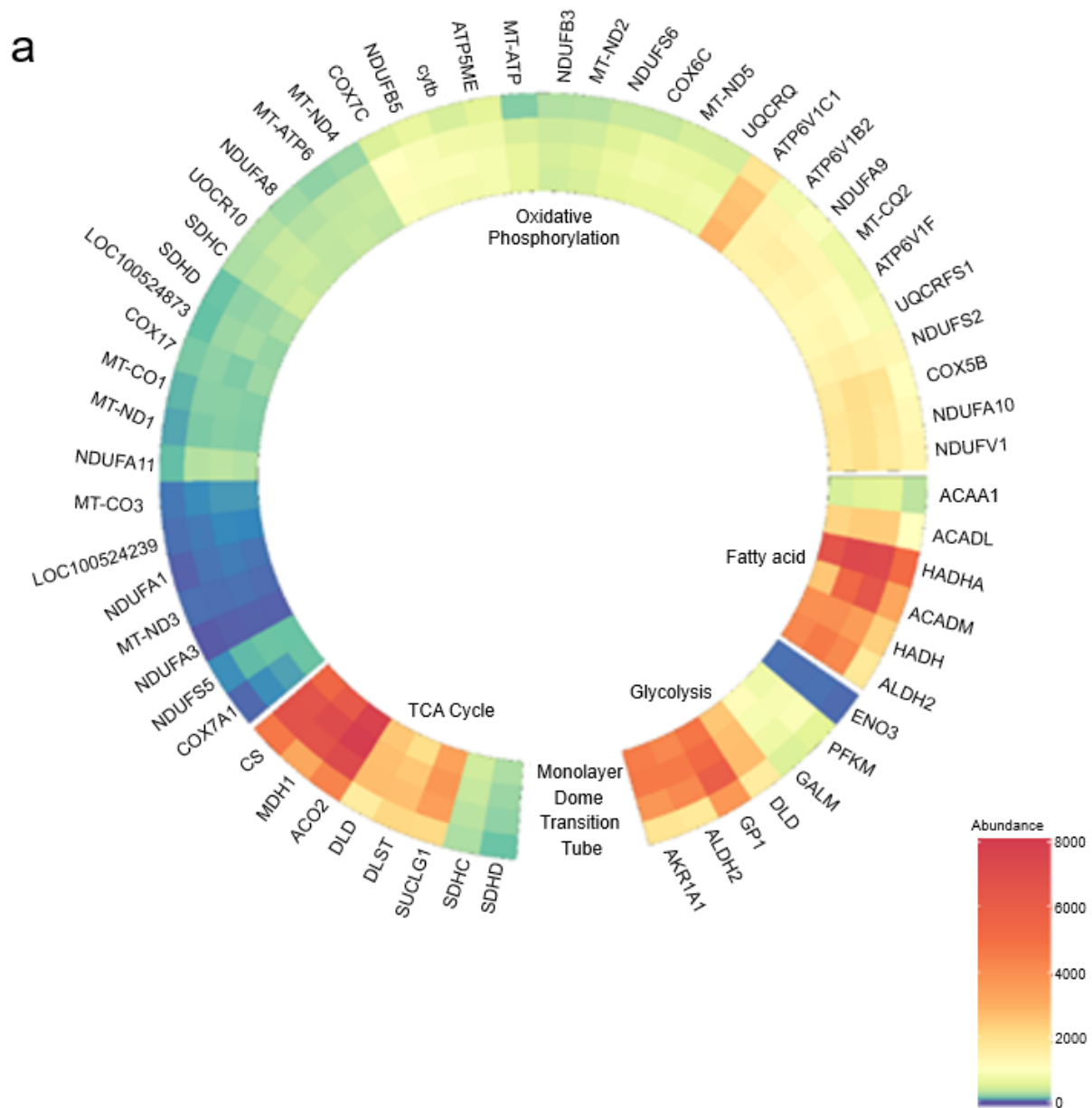


**Figure 3.10 Luminogenesis protein in different stages of the proximal tubule.** We cultured LLC-PK1 cells and collected the lysates at 4 different time points: monolayer stage (day 1), dome stage (day 3), transition stage (day 4.5), and tube stage (day 10). Samples were processed for whole-cell proteomics, and proteins were quantified using MS/MS, Liquid chromatography–tandem mass spectrometry. We screen the proteins responsible for luminogenesis in proximal tubules and visualized using R.

Proximal tubules mainly use four different metabolic pathways to meet the energy needs: glycolysis, fatty acid oxidation (FAO), oxidative phosphorylation, and the tricarboxylic acid (TCA) cycle. Interestingly, we found that cells are metabolically active in dome and transition phase (Figure 3.11a, b). As cells assemble three dimensional structures, and/or fusion of two domes may require more energy in comparison to monolayer (Figure 3.11a, b). The proximal tubule depends on fatty acid oxidation (FAO) since this fuel source yields 106 ATP units in contrast with 36 from glucose metabolism [233]. Due to the enormous mass of proximal tubules, 66% of oxygen utilization in the human kidney comes from FAO [233]. This is also found in our model as FAO protein expression is higher than other metabolic pathways (Figure 3.11b). FAO might be the favoured energy substrate for proximal tubules, yet the kidney is a significant organ for glucose reabsorption, production, and utilization [233]. The majority of the re-absorbed glucose is recovered by SGLTs.



Proximal tubule metabolizes less glucose rather GLUTs allow glucose to move down a concentration gradient back into the circulation [233].



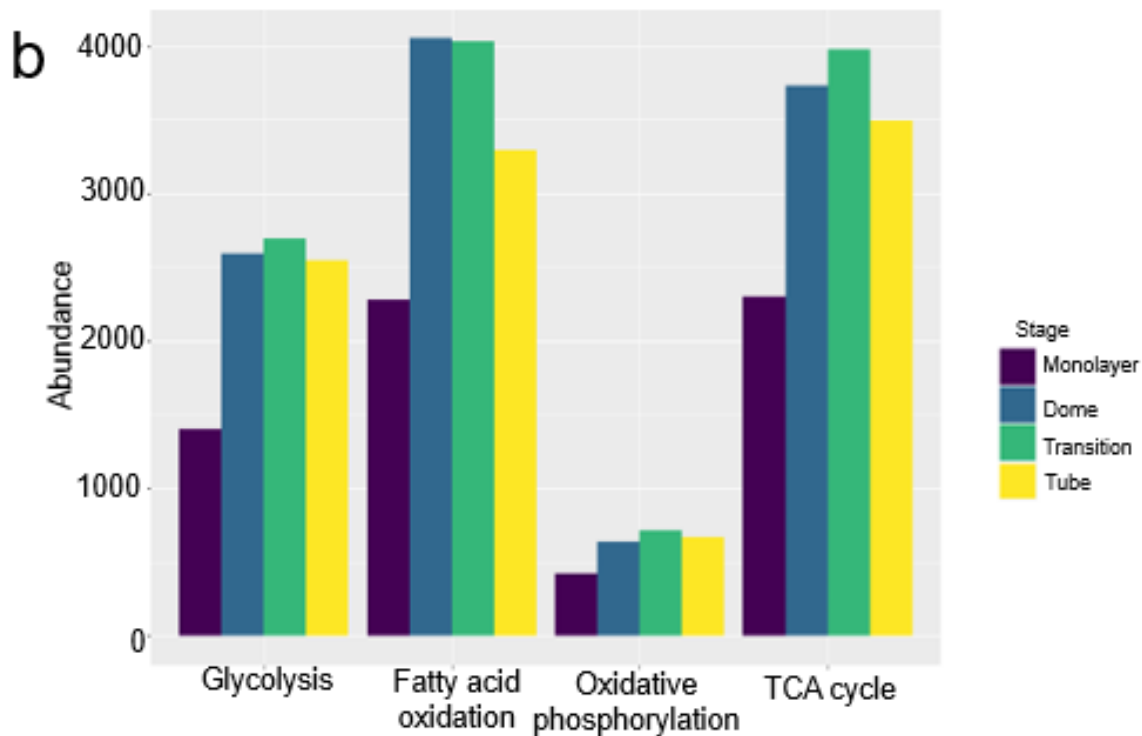


**Figure 3.11 Role of metabolic pathways in proximal tubule development.** We cultured LLC-PK1 cells and collected the lysates at 4 different time points: monolayer stage (day 1), dome stage (day 3), transition stage (day 4.5), and tube stage (day 10). Samples were processed for whole-cell proteomics and proteins were quantified using MS/MS, Liquid chromatography–tandem mass spectrometry. Results were visualized using R. (a) Circular heatmap depicting protein abundances of four metabolic pathways: glycolysis, TCA, oxidative phosphorylation, and fatty acid (b) Bar plot showing protein abundance of all proteins at each phase of 4 different metabolic pathways.

Proximal tubules require more active transport mechanisms than other nephrotic cells as majority of the solute is re-absorbed by the proximal tubule [234]. Therefore, they contain more mitochondria than any other nephrotic structure [234]. Mitochondrial homeostasis is maintained to meet the energy demands of proximal tubules [234]. We selected top 50 upregulated proteins from each stage and found that majority of the upregulated proteins found in the mitochondria and involved in metabolic pathways (Figure 3.12).

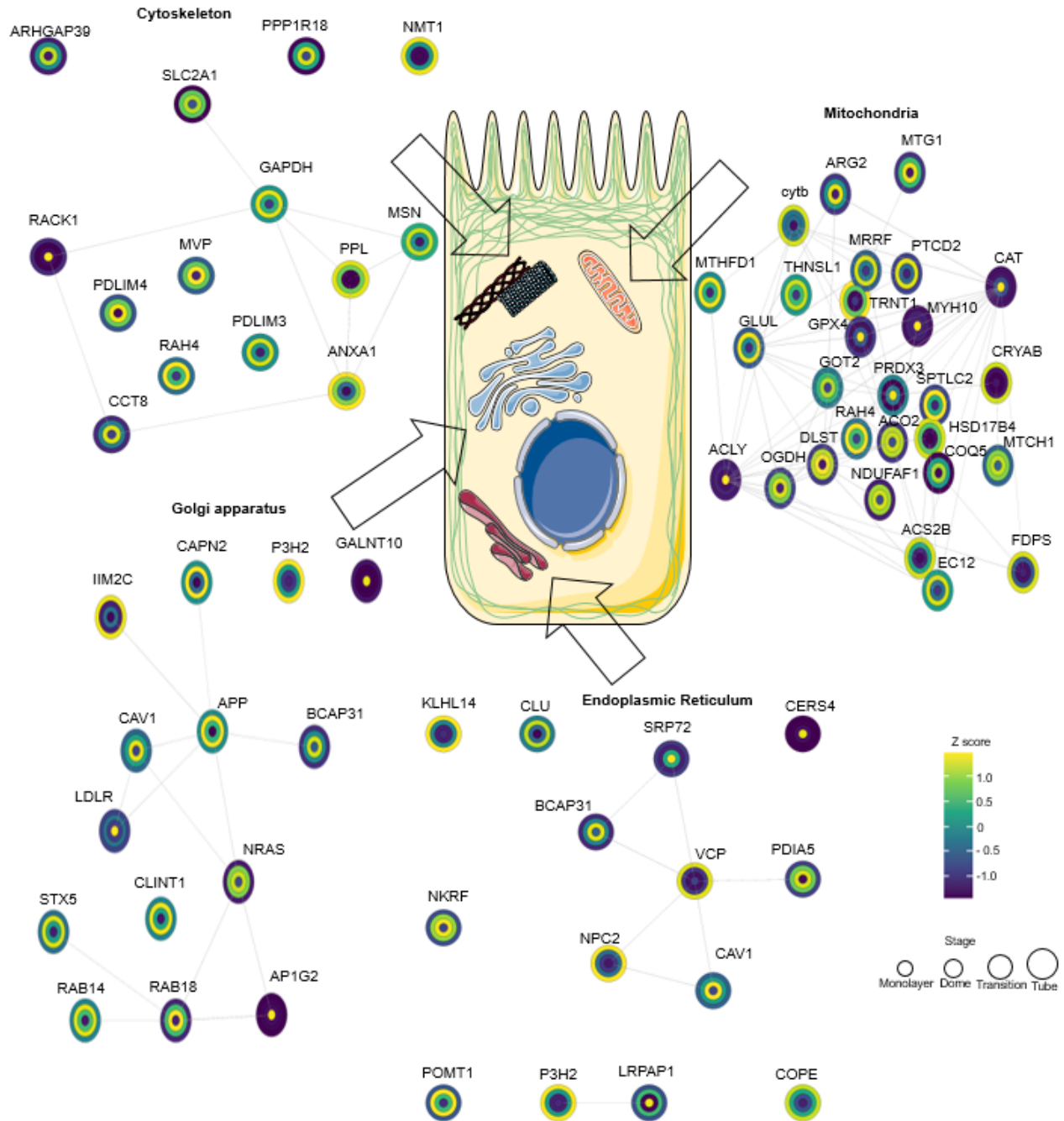


**Figure 3.12 Compartment analysis of proteins that are significantly regulated.** We cultured LLC-PK1 cells and collected the lysates at 4 different time points: monolayer stage (day 1), dome stage (day 3), transition stage (day 4.5), and tube stage (day 10). Samples were processed for whole-cell proteomics and proteins were quantified using MS/MS, Liquid chromatography–tandem mass spectrometry. Results were visualized using R. Each circular map represents the expression of a specific proteins at four different stages of proximal tubule formation. We took top-upregulated proteins expressed in each stage and studied their interaction in different cytosolic cellular compartments.

As proximal tubules are known for their re-absorption capacity, we investigated the presence of different transporters at each phase. We found 145 differentially expressed transporters. Studying these transporters in more detail can help us understand the mechanism of various ions re-absorption during the proximal tubule formation (Figure 3.13). We found that the sodium/potassium-transporting ATPase subunit alpha (ATP1A1) and sodium/potassium-transporting ATPase subunit beta-1 (ATP1B1) are upregulated in the dome phase. This is one of the critical pumps as it is inextricably intertwined with several transporters. Various physiological processes rely upon ATP1A1 subcellular confinement [235]. Depending upon the physiological role of an epithelial sheet, the cellular sorting machinery ensures that ATP1A1 presents either in the apical or the basolateral membrane [235]. Aquaporin-1 (AQP1) is the vital water-transporting protein in cell plasma membranes in the proximal kidney tubule, facilitating transepithelial water transport [236]. It has been found that less AQP1 is expressed in the prenatal kidney than in the differentiated kidney. It has been found that when LLC-PK1 cells became confluent and differentiated, there was a significant increase in SGLT1 levels. These analyses lend support to our finding that AQP1 and SGLT1 can serve as markers of differentiated proximal tubules in our *in vitro* model.

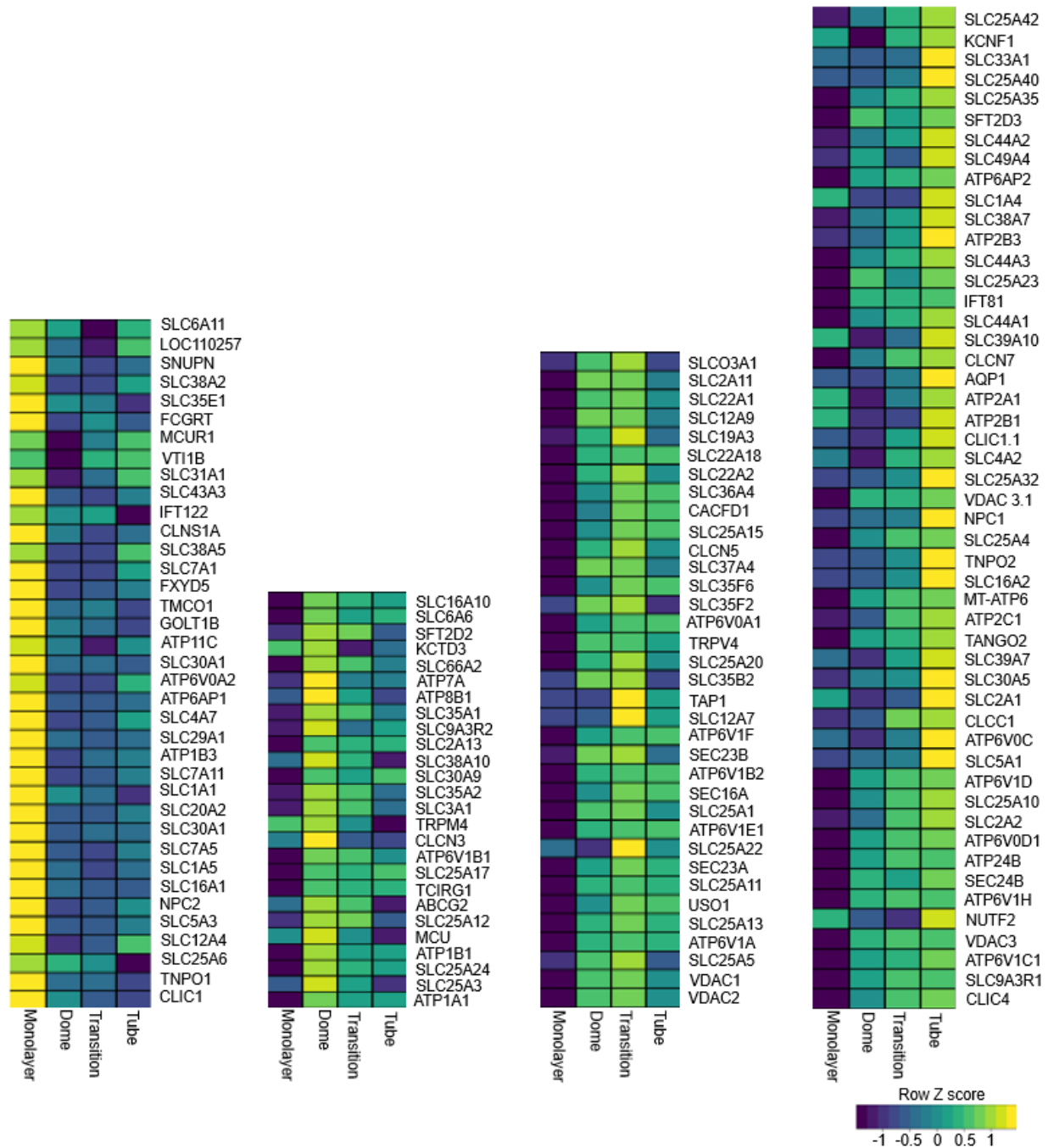


**Figure 3.13 Expression of transporters during proximal tubule formation.** We cultured LLC-PK1 cells and collected the lysates at 4 different time points: monolayer stage (day 1), dome stage (day 3), transition stage (day 4.5), and tube stage (day 10). Samples were processed for whole-cell proteomics and proteins were quantified using MS/MS, Liquid chromatography–tandem mass spectrometry. Results were visualized using R. Heatmap depicting protein expression of various transporters upregulated at different stages. Z-scores were calculated for each row by subtracting the mean and dividing by the standard deviation.

In the monolayer phase, vimentin is first upregulated and ~~gets~~ subsequently downregulated as differentiation proceeds (Figure 3.14). Specifically, in the dome phase, Rho GTPase Activating Protein 18 (ARHGAP18) is upregulated substantially and subsequently reduced in the tube phase (Figure 3.14). ARHGAP18 has been shown to be responsible for the shape of 3D tissues by regulating cortical actomyosin network formation [237]. Ezrin (EZR) plays a key role in cell surface structure, adhesion and migration. EZR is mainly expressed in epithelial tissues. This protein is upregulated in the transition phase (Figure 3.14). During this phase dome cells migrate to fuse with other domes [238]. Also, EZR plays an essential role in solute re-absorption by regulating several transporters present in the apical membrane of proximal tubules [239]. Interestingly, we also found Keratin 8 (KRT8) is significantly upregulated in the tube phase (Figure 3.14). KRT8 dimerizes with KRT18 to form an intermediate filament in simple single-layered epithelial cells [240]. KRTs play an important role in maintaining cellular structural integrity and also in signal transduction and cellular differentiation [240]. Our results provided insights into the role of the cytoskeleton in the proximal tubule differentiation process.

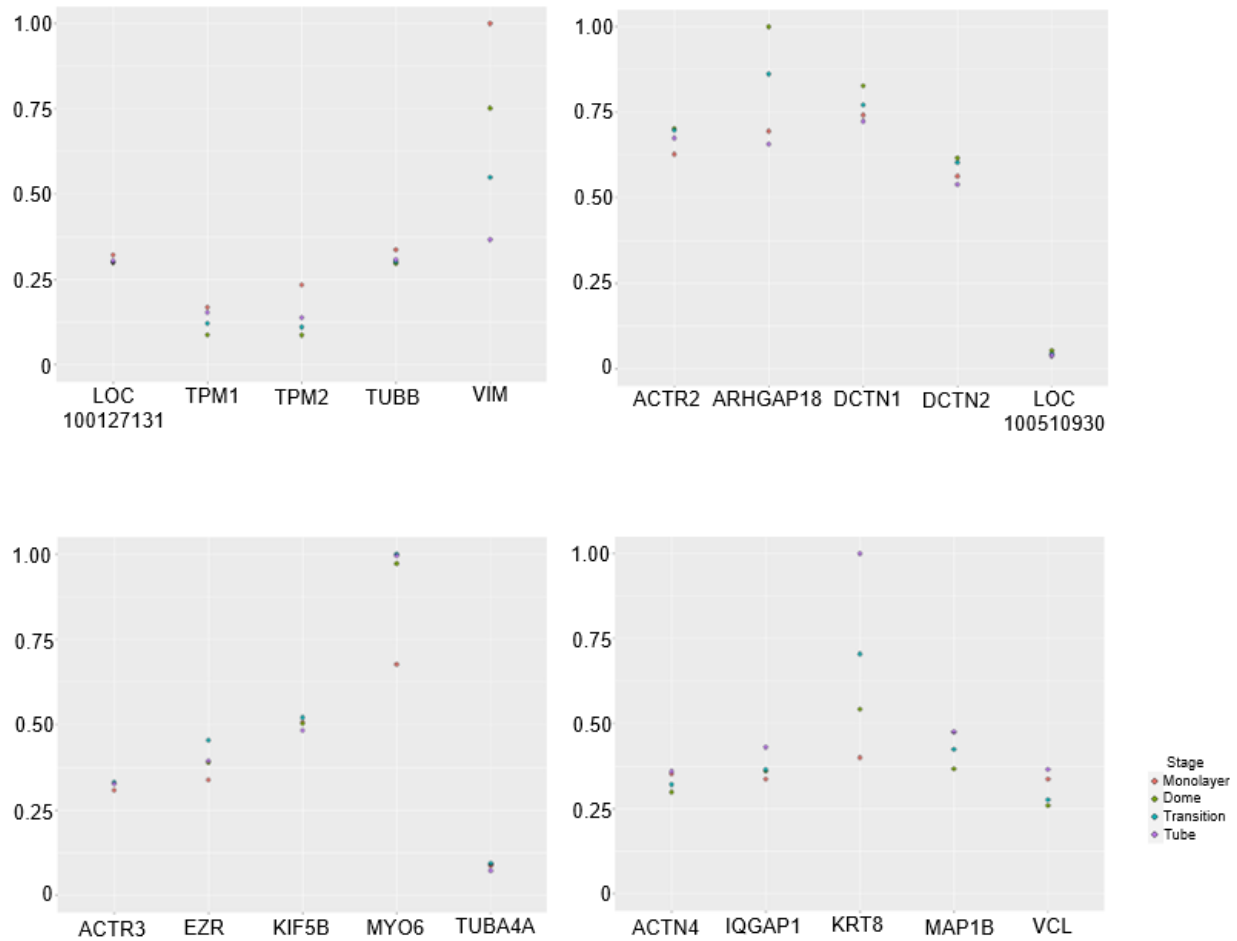


**Figure 3.14 Role of cytoskeleton in the differentiation process of proximal tubules.** Expression of transporters during proximal tubule formation. We cultured LLC-PK1 cells and collected the lysates at 4 different time points: monolayer stage (day 1), dome stage (day 3), transition stage (day 4.5), and tube stage (day 10). Samples were processed for whole-cell proteomics and proteins were quantified using MS/MS, Liquid chromatography–tandem mass spectrometry. Results were visualized using R. Heatmap depicting protein expression of various transporters upregulated at different stages. Z-scores were calculated for each row by subtracting the mean and dividing by the standard deviation.

### 3.3 Characterisation of physiologically relevant transport processes by tool compounds

The main function of the transporters present in the proximal tubule is the reabsorption of ions (See also the "Introduction"). Therefore, we performed a screen to analyze the effect of different transporters on renal tube morphogenesis and differentiation. Interestingly, we found that digoxin ( $\text{Na}^+/\text{K}^+$  ATPase) inhibits the dome and tube formation (Figure 3.15a, b, c). This is mainly due to the dependency of other transporters on the  $\text{Na}^+/\text{K}^+$  ATPase pump.



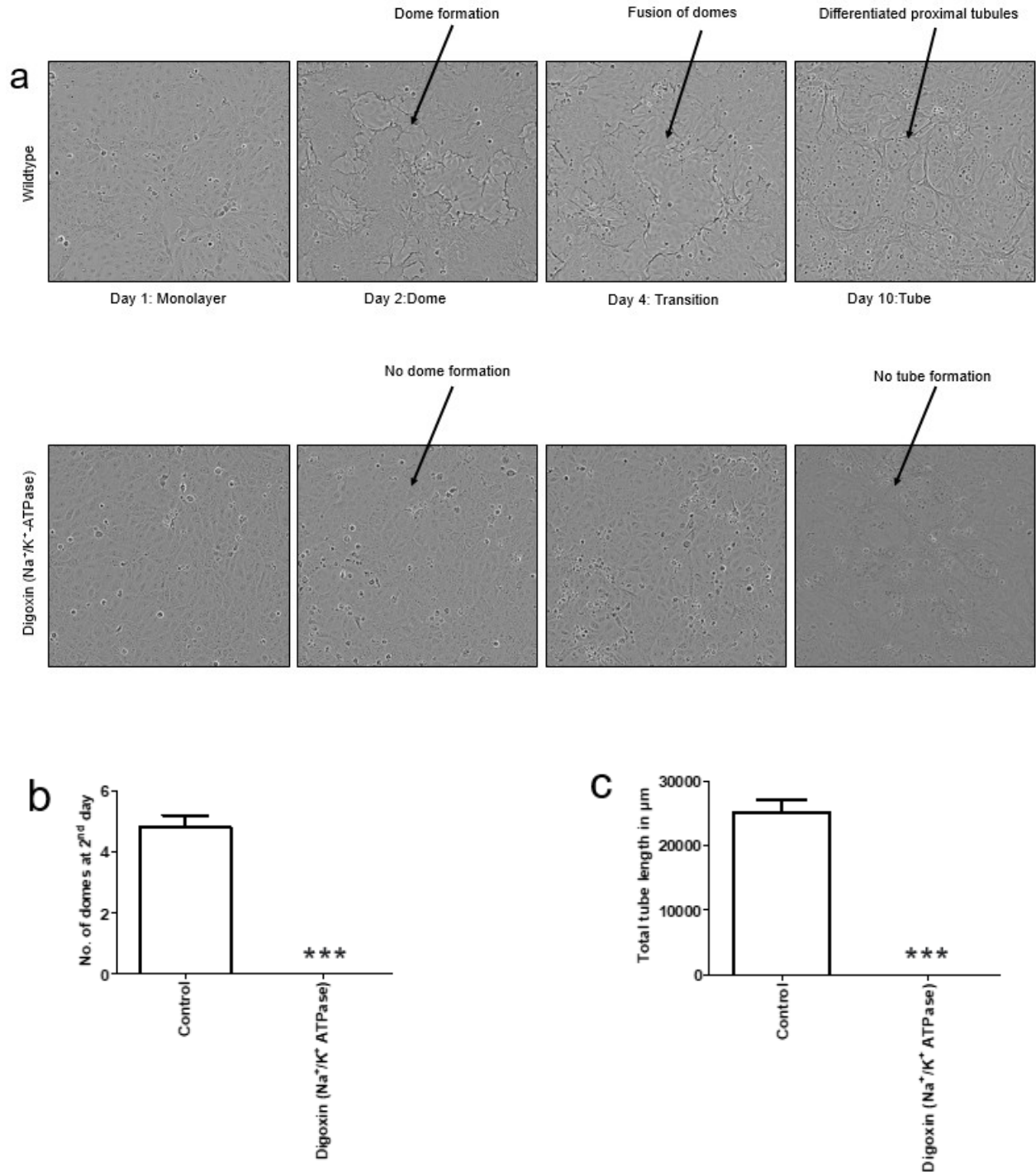


**Figure 3.15 Effect of transport inhibition on proximal tubule development.** (a) We cultured LLC-PK1 cells in imagedlock 96 well plates and treated them with different transport inhibitors (Table 2. 5). After treatment, cells were imaged for 10 days at 10X in Incucyte® S3. Bright field images were captured at 4 different time points i.e. monolayer stage (day 1), dome stage (day 3), transition stage (day 4.5), and tube stage (day 10) to show morphological changes in cells after transport inhibition. (b) We manually counted the number of domes formed at 2<sup>nd</sup> day. Day 10 tube images from incucyte were uploaded in the Wimasis image analysis software, and we measured (c) tube length. The impact of specific treatment compared to



control using Graph Pad Prism software version 5.0. Data represented in mean  $\pm$  SEM (n = 5). In b) and c), \*\*\*P < 0.0001 compared to control, two-tailed paired t-test.

We also evaluated changes in the dome structure and found that bafilomycin treated cells have a significant difference in the dome structure specifically the major and minor axis of the dome whereas all the inhibitors have affected the dome size (Figure 3.16a, b, c, d).

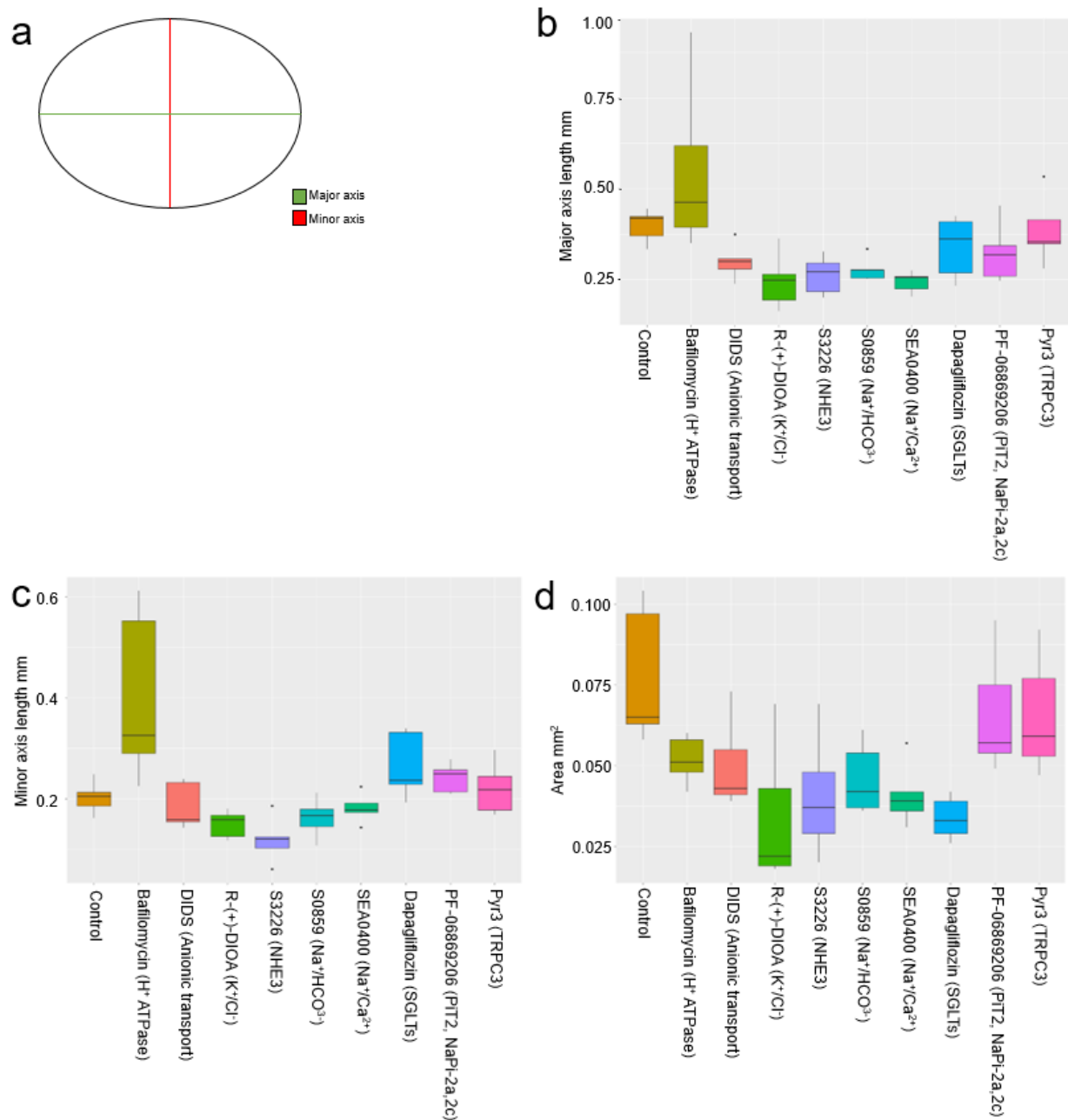


**Figure 3.16 Effect of transporter inhibition on dome formation.** We cultured LLC-PK1 cells in imagelock 96 well plates and treated them with different transport inhibitors. After treatment, time-lapse videos were taken for 10 days at 10X in Incucyte® S3 and (a) we measured major axis, minor axis, and area of dome

when dome is at maximum size. Measurement of (b) major axis, (c) minor axis, and (d) maximum dome area after transporter inhibition. Measurement is performed using Fiji - ImageJ and represented as a box plot with standard error. Results were visualized using R.

After this, we reconnoitred the changes in the tube structure and we found that tube length, number of tubes, and branching point are affected post bafilomycin treatment (Figure 3.17a, b, c). This result shows that transporters not only play a role in the re-absorption mechanism but also play significant roles in the differentiation process of proximal tubules.

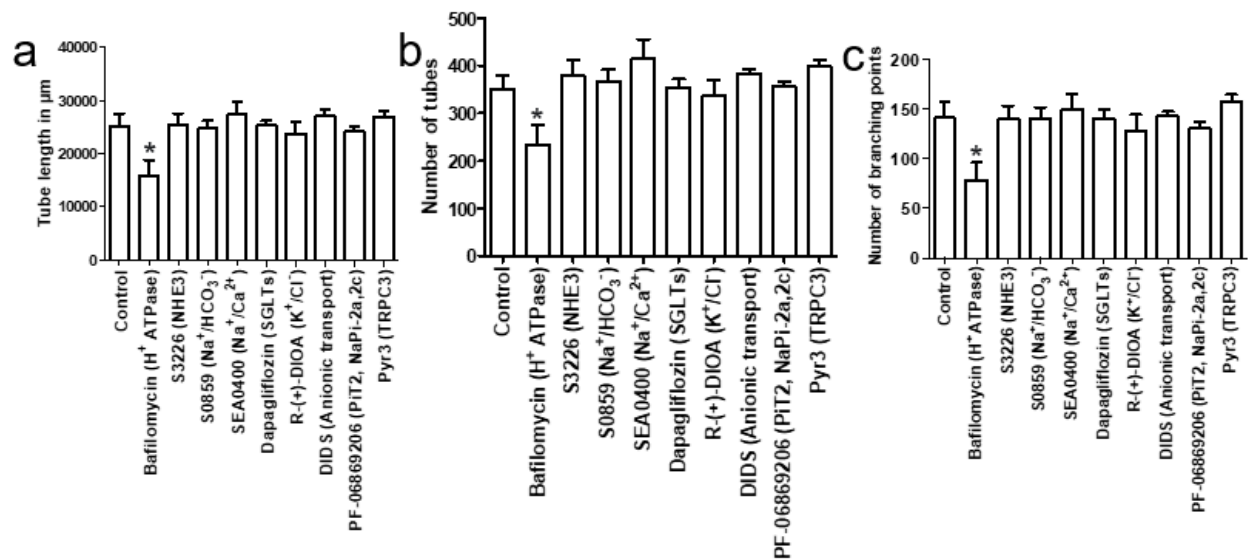


**Figure 3.17 Effect of transporter inhibition on tube formation.** We cultured LLC-PK1 cells in imagelock 96 well plates and treated with different transport inhibitors. After treatment, time-lapse videos were taken for 10 days at 10X in Incucyte® S3. Day 10 tube images from incucyte were uploaded in the Wimasis image analysis software, and (a) tube length, (b) number of tubes, and (c) branching points were measured. Dunnett's multiple comparison test was used as a follow-up to one-way ANOVA to study The impact of specific treatment compared to control using Graph Pad Prism software version 5.0. Data represented in mean ± SEM (n =5). Dunnett's multiple comparison test: \*p<0.05.

Our study revealed different cellular pathways which play specific roles at each phase of proximal tube differentiation and the role of different transporters in the differentiation process. This will enable us to assess new drug targets and also to study drug induced nephrotoxicity. To the best of our knowledge this is the first time to delineate the proximal tubule cellular model without micropatterning that can be used to study the development mechanism of proximal tubule and also to perform *in vitro* toxicological investigations.

### 3.4 Generation of metastatic ccRCC model in LLC-PK1 cell line using CRISPR

ccRCC starts with the loss of VHL. Afterwards, BAP1 mutations can drive the cells towards a metastatic state [181]. Therefore, in the immortalized LLC-PK1 cell line, we deleted the VHL (VHL KO) and then the BAP1 gene in the VHL KO through CRISPR-Cas9 technology, obtaining a VHL + BAP1 double KO (DKO). We then also introduced BAP1 mutations in the VHL + BAP1 DKO. From these cells, we performed Tandem Mass Tag (TMT) proteomics and compared them to the parental cell line. Data from TMT proteomics was compared with data from The Cancer Genome Atlas Program (TCGA). In parallel to proteomic profiling, we also performed *in vitro* differentiation assays to investigate how sequential steps in the presumptive genetic tumor evolution alter cellular differentiation potential and biomechanics (Figure 3.18).

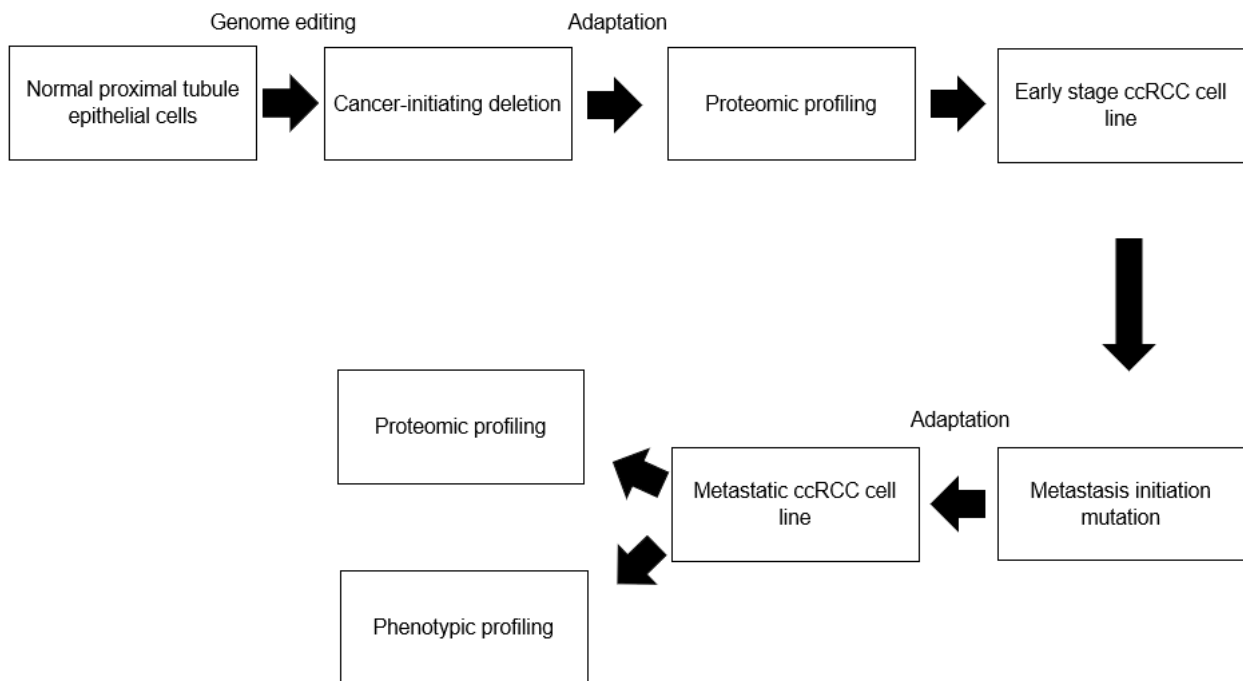


**Figure 3.18 Experimental approach for introducing sequential ccRCC mutations into the genomes of primary proximal tubules with CRISPR-Cas9.** We used CRISPR-Cas9 to build metastatic ccRCC models from LLC-PK1 cell line. First, we knocked out VHL and BAP1 by CRISPR-Cas9 and then reconstituted BAP1 mutations in the VHL + BAP1 double KO (DKO) genetic background. After that, we performed phenotypic studies and proteomic studies to characterise engineered metastatic ccRCC models.

In many cases, VHL is the first gene to become inactivated in ccRCC [184]. Therefore, we designed three sgRNAs against VHL and used these for gene knockouts through

CRISPR-Cas9. VHL KO cells were selected using 1.5 mg hygromycin per ml of culture medium over the course of four weeks. LLC-PK1 wild-type cells and VHL KO cells were assessed for VHL protein levels to determine the effectiveness of VHL KO. Western blots revealed a significant reduction in VHL upon CRISPR-mediated gene modification. These findings indicate that this CRISPR approach can effectively knock out the VHL gene (Figure 3.19).

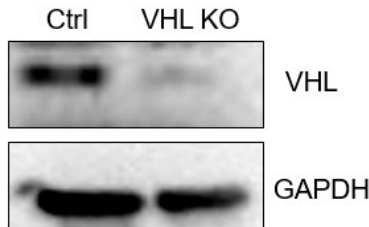


**Figure 3.19 Validation of VHL knockout (VHL KO).** We cultured LLC-PK1 cells, VHL KO, and total cell proteins were collected on day 10. Immunoblot depicting VHL KO in LLC-PK1 cells. GAPDH served as a loading control.

VHL inactivation alone does not cause ccRCC, other additional genetic and/or epigenetic events are required to cause ccRCC [143]. Hence, we introduced BAP1 mutations in the VHL KO cell lines. Again, we employed CRISPR-Cas9 to knockout BAP1 in VHL KO. We selected this knockout using 1.5 mg of hygromycin and 500 µg of neomycin per ml of culture medium for four weeks. After this, we introduced BAP1 mutations in VHL + BAP1 DKO, and clones were selected using 1.5 mg of hygromycin, 500 µg of neomycin, and 3 µg of puromycin per ml of culture medium (Figure 3.20).

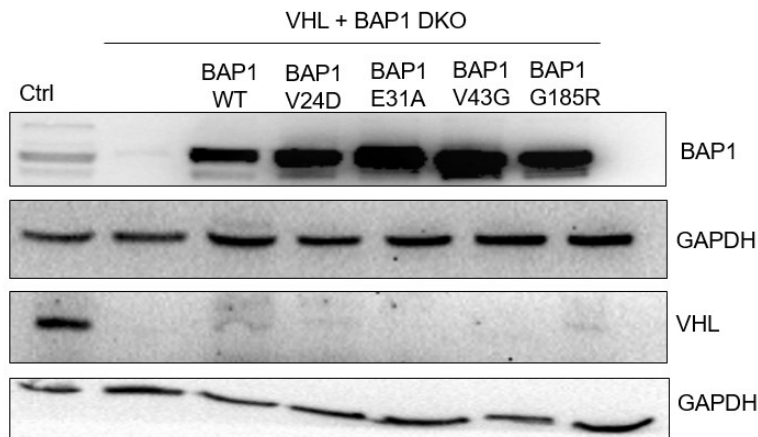


**Figure 3.20 Immunoblot depicting VHL KO, BAP1 knockout (VHL + BAP1 DKO), and reconstituted BAP1 mutations in LLC-PK1 cells.** We cultured LLC-PK1 cells, VHL KO, VHL + BAP1 knockout (DKO), and reconstituted BAP1 mutations in DKO cell lines and total cell proteins were collected on day 10.

Immunoblot depicting the loss of VHL and BAP1 in VHL + BAP1 DKO and reconstitution of BAP1 in VHL + BAP1 DKO. GAPDH served as a loading control.

### **3.5 Phenotypic characterisation of knockouts and mutants**

Human cancers frequently display substantial intra-tumor heterogeneity, including angiogenic, cellular morphology, gene expression, metabolism, motility, proliferative, and ultimately metastatic potential [241].

We stained cells with anti-ZO-1 antibodies (Figure 3.21). The tight junction protein ZO-1 in the wild-type proximal tubule allows to assess proper cell polarity and tubulogenesis [242]. ZO-1 also contributes to ion homeostasis mediated by paracellular transport [243]. We found that mutated cell lines could not form tubular structures and have irregular pleomorphic morphology. Pleomorphism is a hallmark of ccRCC [244]. We also quantified the amount of cells that have different morphology in comparison to wild-type. We found that mutated cell lines have a significant number of pleomorphic cells compared to control cell lines (Figure 3.21b).



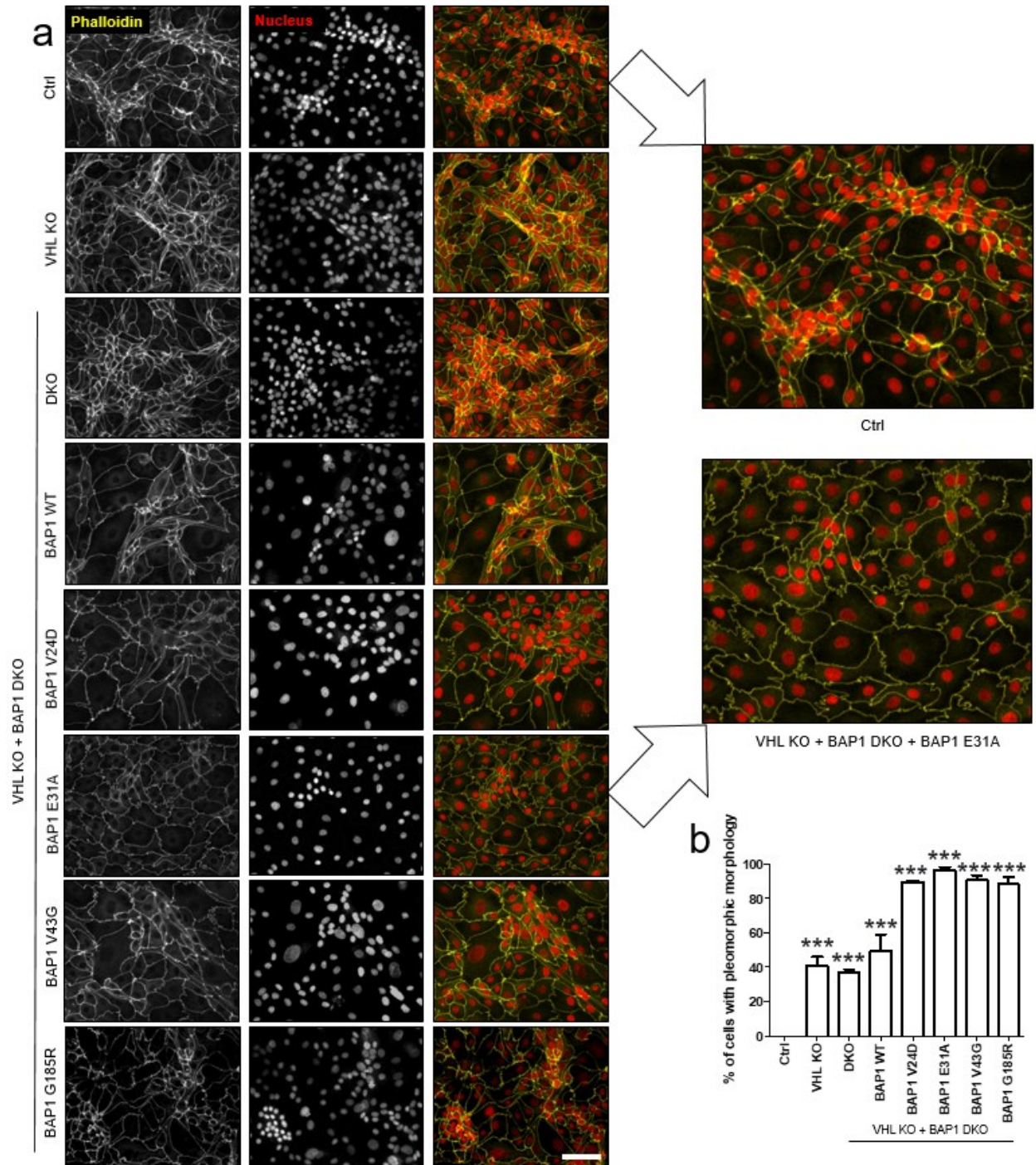


**Figure 3.21 Evaluation of morphological changes.** We cultured LLC-PK1, VHL KO, VHL + BAP1 DKO, and reconstituted BAP1 mutations in VHL + BAP1 DKO cells and were fixed using 4% Paraformaldehyde on day 10. (a) Then, cells were stained with ZO-1 staining (yellow) and Nuclei (red) depicting the morphological changes in the mutants in comparison to the wild-type proximal tubule cell line. Scale bar=20  $\mu$ m. (b) ZO-1 stained cells were counted to compare the changes in the morphology of the cells. Dunnett's multiple comparison test was used as a follow-up to one-way ANOVA to compare wild-type cells to each mutated sample using Graph Pad Prism software version 5.0. Data represented in mean  $\pm$  SEM (n = 100). \*p<0.05, \*\*p<0.01, and \*\*\*p<0.001.

Next, we asked, whether the morphological changes of the mutated cell lines are due to an altered expression of F-actin. We used phalloidin to measure F-actin intensity, branch count, and skeleton length (Figure 3.22). In some cancers with higher actin fibers levels, it has been found that they are highly metastatic and stiff cells [245]. Interestingly, in mutated samples, we found that F-actin intensity is significantly higher in comparison to wild-type (Figure 3.22a). We measured the branch count and skeleton length and found that both increased substantially in mutated samples (Figure 3.22b, c).

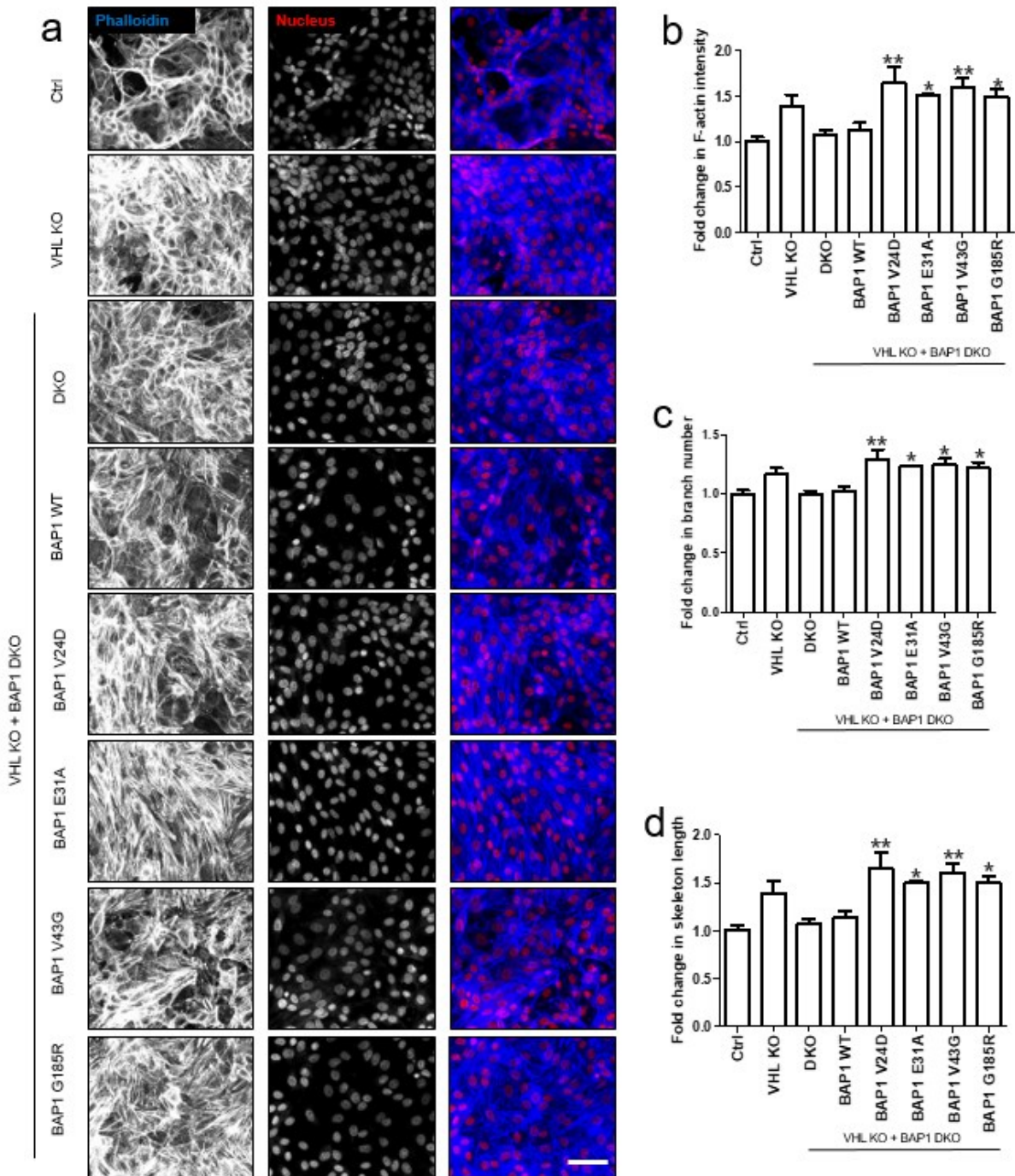


**Figure 3.22 Stress fibers formation.** We cultured LLC-PK1, VHL KO, DKO, and reconstituted BAP1 mutations in DKO cells and were fixed using 4% Paraformaldehyde on day 10. (a) Then, cells were stained with F-actin (blue) and Nuclei (red) illustrating the increase in stress fibers in mutant samples in comparison to wild-type proximal tubule cell line. Scale bar=20  $\mu$ m. (b) F actin intensity, (c) Branch count, and (d) Skeleton length were measured in F-actin stained cells. Dunnett's multiple comparison test was used as a follow-up to one-way ANOVA to compare wild-type cells to each mutated sample using Graph Pad Prism software version 5.0. Data represented in mean  $\pm$  SEM (n = 100). Dunnett's multiple comparison test: \* $p$ <0.05, and \*\* $p$ <0.01.



### 3.6 Proteomics of engineered *in vitro* knockout and mutant models of metastatic ccRCC

To identify changes in the proteomes of VHL KO, VHL + BAP1 DKO, reconstituted BAP1 mutations samples relative to wild-type LLC-PK1 cells, we performed total proteome mass spectrometry (MS) analysis. Principal component analysis showed the expected clustering among replicates and replicates of each cluster were similar to each other (Figure 3.23).

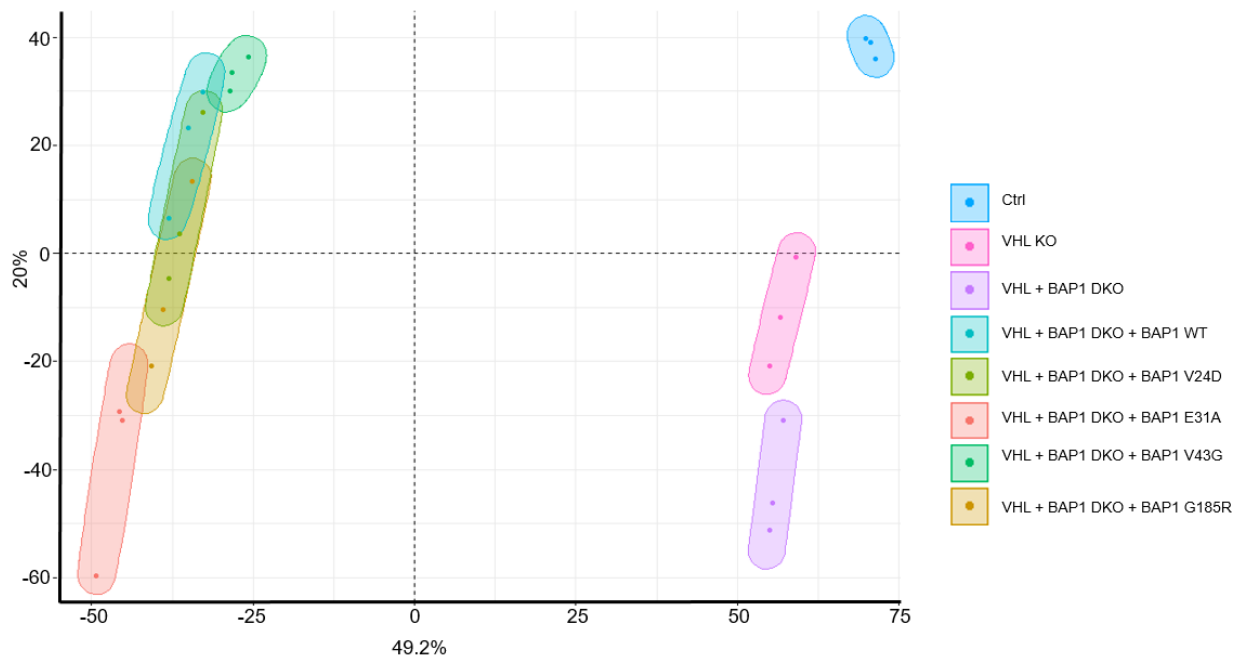


**Figure 3.23 Principal Component Analysis.** We cultured wild-type LLC-PK1, VHL KO, VHL + BAP1 DKO, and reconstituted BAP1 mutations in VHL + BAP1 DKO cells. Lysates were collected on day 10 of cultivation. Samples were processed for whole cell proteomics and proteins were quantified using LC-MS/MS (liquid chromatography-tandem mass spectrometry). Results were visualized using R.

### 3.7 Molecular characterisation of cell polarity loss

Loss of cell differentiation is one of the hallmarks of cancer. The ultimate loss of epithelial phenotype contributes to epithelial-to-mesenchymal transition (EMT) and metastasis [246]. Therefore, we analyzed the cell polarity markers, and interestingly we found that all three complexes are significantly deregulated in mutant cells compared to wild-type cells. In the Scrib complexes, we found SCRIB and LLGL2 to be upregulated in DKO cells expressing mutated forms of BAP1 (Figure 3.24). SCRIB has been shown to be overexpressed in hepatocellular carcinoma (HCC) and plays an essential role in the

dissemination of HCC cells [247]. Recently, in breast cancer, it has been found that LLGL2 (but not LLGL1) is overexpressed, and linked to poor patient survival [248]. For the Crumbs complex, we found that PATJ is upregulated; it has been found that PATJ was upregulated in the urine of ccRCC patients stratified as advanced stage and early grade [249]. PODXL, AFDN, and SLC9A3R were found to be deregulated and their deregulation has been associated with poor prognosis in different cancers [250-252]. This data suggests the involvement of cell polarity complexes as in ccRCC.

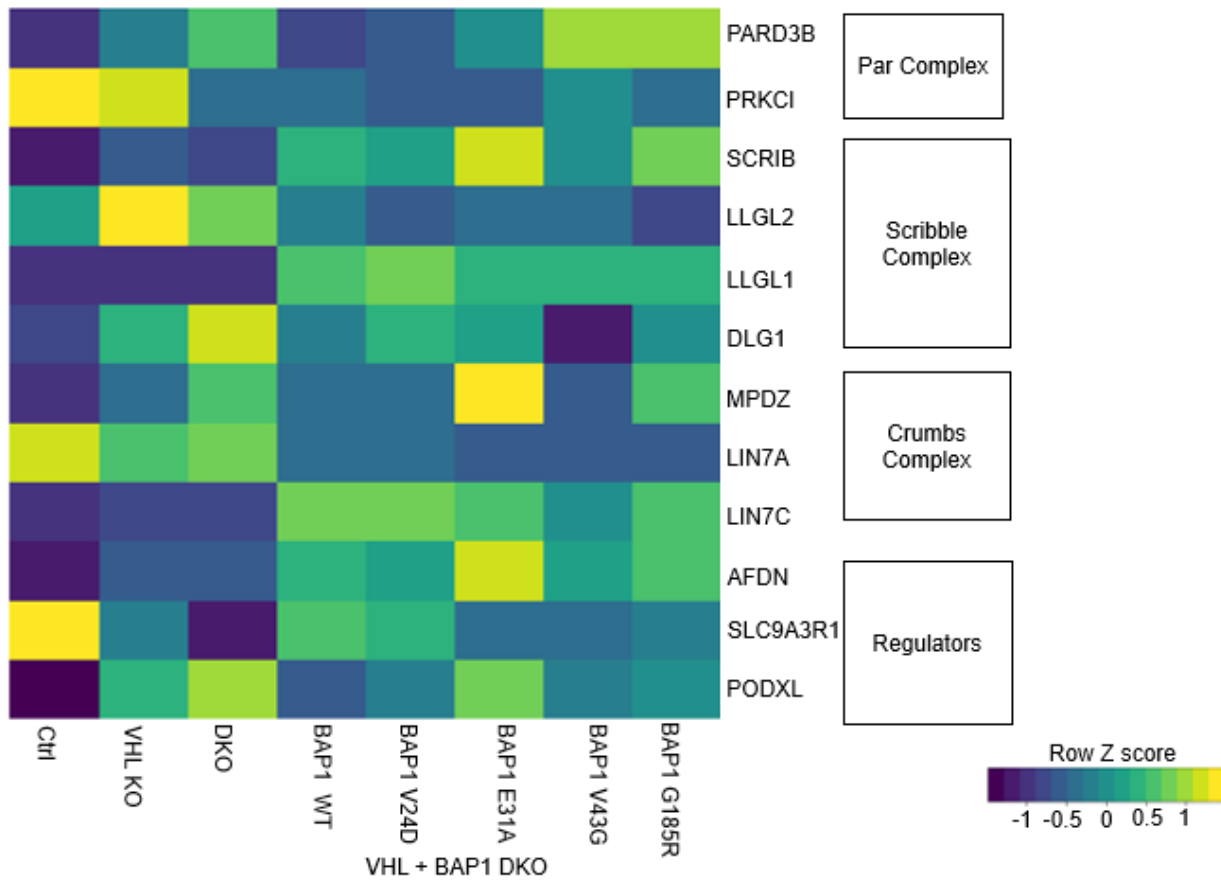


**Figure 3.24 Loss of luminogenesis protein in metastatic ccRCC development.** We cultured wild-type LLC-PK1, VHL KO, VHL + BAP1 DKO, and reconstituted BAP1 mutations in DKO cells and lysates were collected on day 10. Samples were processed for whole cell proteomics and proteins were quantified using MS/MS, Liquid chromatography-tandem mass spectrometry. Heatmap showing the deregulated proteins involved in the luminogenesis in ccRCC cell lines. Results were visualized using R. Z-scores were calculated for each row by subtracting the mean and dividing by the standard deviation.

### 3.8 Role of EMT in ccRCC progression

EMT is the acquisition of mesenchymal features from epithelial cells. This process occurs during embryonic development and adult tissue regeneration and is associated with cancer progression. EMT is highly deregulated during tumor progression [250]. EMT helps the solid tumor to become invasive and metastatic [250].

Therefore, we analyzed the proteins that are involved in the EMT process (Figure 3.25). Interestingly, proteins that are linked to mesenchymal features are significantly upregulated in mutants compared to wild-type cells. Notably, an increase in the expression of mesenchymal markers signifies a reduction in the overall survival rate in ccRCC patients. We also found that DKO cells that overexpress WT BAP1 also have significantly upregulated mesenchymal markers (Figure 3.25). This shows that even if wild-type protein is not present at a normal level, it may cause cancer. Wild-type BAP1 upregulation activates the EMT cascade in esophageal carcinoma and breast cancer [253, 254].

E-cadherin (CDH1) and Occludin (OCLN) are epithelial markers and we found both to be down-regulated in DKO cells that expressing BAP1 mutants but CDH1 is upregulated in DKO cells that expressing E31A BAP1 mutant. Loss of CDH1 and OCLN function or expression plays a relevant role in cancer progression [251]. Downregulation of these epithelial markers decreases cellular adhesion in epithelial cells. As a result, increased cell motility leads to invasion and metastasis [251].

OCLN is a tight junction membrane protein, and it is ubiquitously expressed in epithelial cells, mainly at bicellular junctions. OCLN is considered a tumor suppressor as its deletion or mutations lead to invasive properties of cells [255].

Cytokeratins are Keratin (KRT) proteins found in the intracytoplasmic cytoskeleton of various epithelial cells [252]. KRT-14 and KRT-18 are essential components of intermediate filaments type 1, which help cells withstand mechanical stress. Upregulation of these proteins allows cells to activate the EMT cascade [253].

We also identified that different EMT markers like Cadherin-16 (CDH16),  $\beta$ -catenin (CTNNB1), Desmin (DES), Integrin Subunit Alpha 5 (ITGA5), FARP1 (FERM, ARH/RhoGEF And Pleckstrin Domain Protein 1), Fibronectin (FN1), Transgelin (TAGLN),

and Vimentin (VIM) are significantly deregulated in the metastatic ccRCC model (Figure 3.25). Deregulation of these proteins is positively associated with the clinical stage, tumor stage, and metastasis stage in patients with metastatic ccRCC [254-257].

CDH16 is a member of the cadherin superfamily known as kidney-specific cadherin (ksp-cadherin), which plays an essential role in tubulous formation during embryonic development. CDH16 loss was linked to aneuploidy in clear cell carcinomas. It has also been found that CDH16 can be used to differentiate ccRCC from other types of kidney cancer as CDH16 is downregulated in ccRCC, whereas not in other kinds of kidney cancer [256].

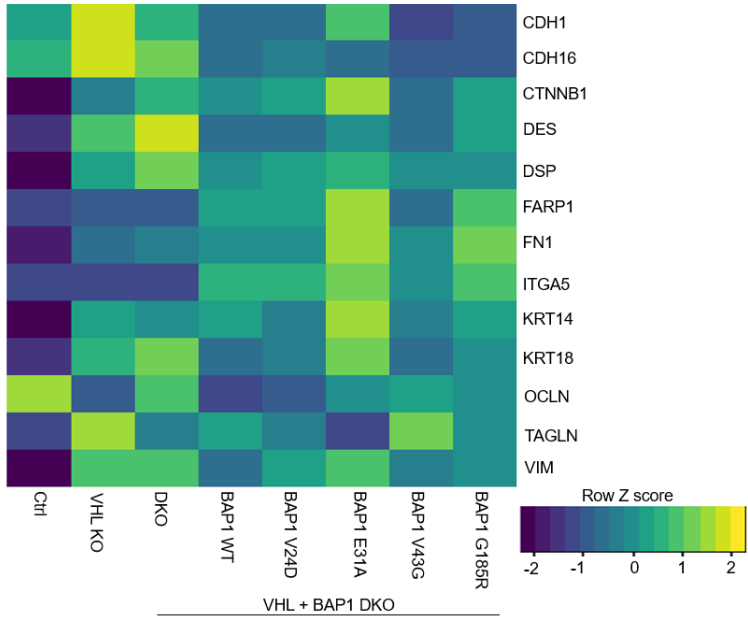
DSP are intercellular junction proteins that help cell-to-cell adhesion and confer resistance against mechanical stress on epithelial cells. DSP is highly upregulated in ccRCC, but the molecular mechanism of desmosomes in metastasis ccRCC is unknown [257].

FARP1 encodes for a protein that contains a FERM (4.2, ezrin, radixin, moesin) domain, a Dbl homology domain, and two pleckstrin homology domains. These domains link the cytoskeleton to the cell membrane. Upregulation of this protein links to the reduction in the overall survival of patients. FARP1 elevates CDC42 activity and facilitates cell migration and invasion by assisting in forming filopodia and invadopodia [258].

Fibronectin-1 (FN1) is an ECM glycoprotein protein with diverse functions in growth and development, adhesion, migration, and wound healing. FN1 intensifies metastasis in ccRCC by upregulating the cluster of differentiation 276 (CD276). CD276 is highly expressed in tumor vasculature and metastatic lymph nodes of ccRCC patients [259].

These results suggest that our engineered model shows a de-regulation of proteins involved in EMT similarly to what has been found in patient sample data.

a



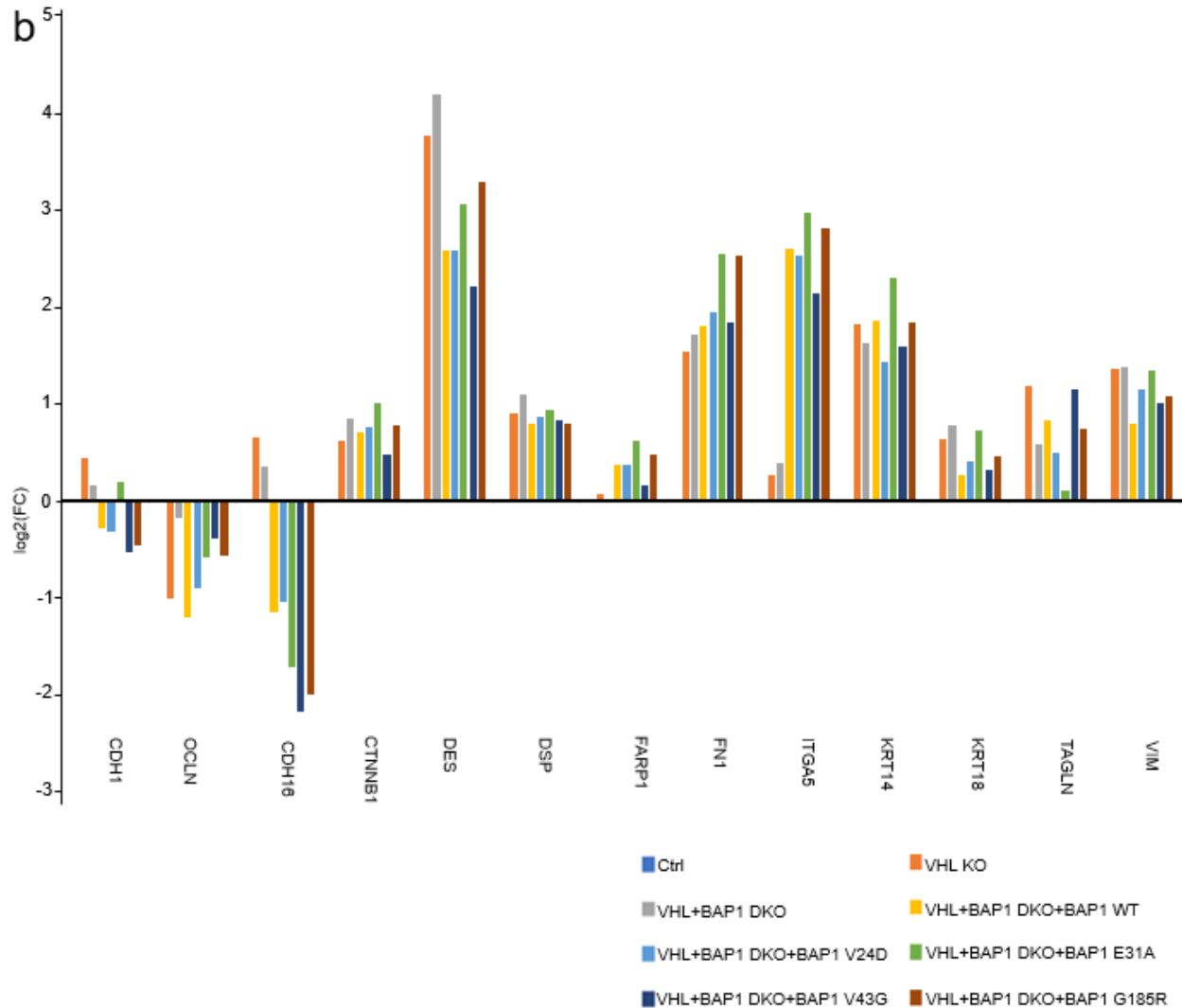


**Figure 3.25 Expression of EMT markers.** We cultured wild-type LLC-PK1, VHL KO, VHL + BAP1 DKO, and reconstituted BAP1 mutations in DKO cells and lysates were collected on day 10. Samples were processed for whole cell proteomics and proteins were quantified using MS/MS, Liquid chromatography-tandem mass spectrometry. Heatmap illustrating the changes in epithelial and mesenchymal marker proteins in metastatic ccRCC cell lines in compared with wild-type LLC-PK1 cell line. Results were visualized using R. Z-scores were calculated for each row by subtracting the mean and dividing by the standard deviation. (b) The graph demonstrates the mean of log 2-fold change for EMT markers.

### 3.9 Cytoskeleton contribution in the development of metastatic ccRCC

Cell migration is an essential process from embryogenesis to cell death [260]. These processes are strictly regulated by various proteins that assist in the correct functioning of the cells. In cancer, this process is deregulated and facilitates the dissemination of tumor cells leading to the activation of the metastasis cascade. Cytoskeletal components like

microfilaments, microtubules, and intermediate filaments and their related proteins must synchronize orderly to form cellular protrusions, like lamellipodia, filopodia, and invadopodia, that help the tumor to metastasize [260, 261].

Actin is an essential structural protein that has a role in various cellular functions such as cell division, chromatin remodeling, vesicle trafficking, and migration [262]. Aberrant actin isoform expression leads to neoplastic transformation by driving tumor growth and advancing to the metastasis stage [260].

We established that Actin alpha 1 (ACTA1) is deregulated in metastatic ccRCC cell lines. DKO cells expressing the V24D and V43G mutants showed upregulation of ACTA1, whereas it is downregulated in DKO cells expressing the E31A and G185R mutants (Figure 3.26a). In ccRCC, downregulation of ACTA1 is associated with higher tumor metastatic potential (31649873) [263]. Actin beta-like 2 (ACTBL2) is essential for cell motility. Upregulation of ACTBL2 provides a survival advantage via interacting with proteins involved in cell growth arrest, cell migration, and tumorigenesis (Figure 3.26a) [264, 265].

Actin Related Protein 2/3 complex (Arp2/3 complex) is a seven-subunit protein complex that significantly regulates actin polymerization. The seven subunits are Arp2 and Arp3 subunits (ACTR2 and ACTR3), and five accessory subunits, ARPC1 (subunits: ARPC1A and ARPC1B), ARPC2, ARPC3, ARPC4, and ARPC5 (subunits: ARPC5 and ARPC5L) [266, 267]. We identified the deregulation of ARP 2/3 complex subunits in ccRCC (Figure 3.26a). In lung cancer, ARPC5 has been associated with the invasiveness and motility of cancer cells. MicroRNA-133a regulates ARPC5. Restoration of miR-133a or inhibition of ARPC5 reduces the cell's motility [268].

IQ motif containing GTPase activating protein (IQGAP) is an evolutionarily conserved family of proteins interacting with many partners to regulate cytoskeletal dynamics, cytokinesis, cell proliferation, cell migration, and vesicle trafficking [269]. IQGAP has three different isoforms: IQGAP1, IQGAP2, and IQGAP3 [269]. We found both IQGAP1 and IQGAP2 downregulated in engineered metastatic ccRCC (Figure 3.26a) [270-272]. Downregulation of these proteins leads to mis-regulation of critical oncogenic pathways and is associated with worse clinical pathological features in ccRCC.



Myosins are actin-binding motor proteins that use the energy of ATP hydrolysis to generate force and move along the actin filaments. Myosin plays a vital role in cell contractility and aids in vesicle trafficking, RNA localization, and protein localization [273]. The role of myosin has been well studied in different cancers but not in metastatic ccRCC. We identified various myosin proteins that are deregulated in engineered metastatic ccRCC compared to the parental cell line (Figure 3.26a). Therefore, these models can be used to elucidate the role of myosin in the development of metastatic ccRCC.

The intermediate filaments are 10 nm filament width and are intermediate between 6 nm wide actin filaments and 25 nm wide microtubules [274]. Vimentin is a type of intermediate filament that became a canonical marker of EMT, the cellular reprogramming process in which the epithelial cells acquire a mesenchymal phenotype [275]. This change alters their shape, allows for increased motility, and helps tumor cells to migrate [275]. Vimentin promotes invasion and migration via Extracellular signal-regulated kinase (ERK) and Ras-related C3 botulinum toxin substrate 1 (RAC1) signaling pathways [275]. Keratins (KRT) belong to the IF proteins family, where they offer critical structural support for any stress. KRTs dynamically remodel and can undergo reorganization upon diverse mechanical and non-mechanical stimuli to regulate heterogeneous cellular processes, including cell signaling and migration [276]. We also found deregulation of keratin filaments (KRT2, KRT7, KRT8, KRT15, KRT17, KRT18) in the engineered metastatic ccRCC model and associated with poor prognosis (Figure 3.26b).

Dyneins are proteins that walk along MT in cells. Dynein transports cellular cargos, provides forces and displacements essential in cytokinesis and manages the beat of eukaryotic cilia and flagella [277]. We found the majority of the dynein proteins are downregulated (Figure 3.26c).

The kinesin superfamily proteins (KIFs) carry membranous organelles and protein complexes in a microtubule and ATP-dependent manner. Kinesins engage in several cellular functions, including cytokinesis and the transport of macromolecules [278]. Increasing evidence also supports their role in cancer genesis [279]. We identified various kinesin proteins that are mis-regulated in engineered metastatic ccRCC cell lines (Figure 3.26c). KIF2A localizes to spindle poles and disassembles at the minus ends of

microtubules. It promotes the progression of cancer via activation of the AKT signaling pathway [280, 281].

The metastatic ccRCC models can be used to understand the contribution of cytoskeleton proteins in cancer development. The above results validate that engineered metastatic ccRCC cell lines can be used to identify biomarkers and develop therapies to treat metastatic ccRCC.

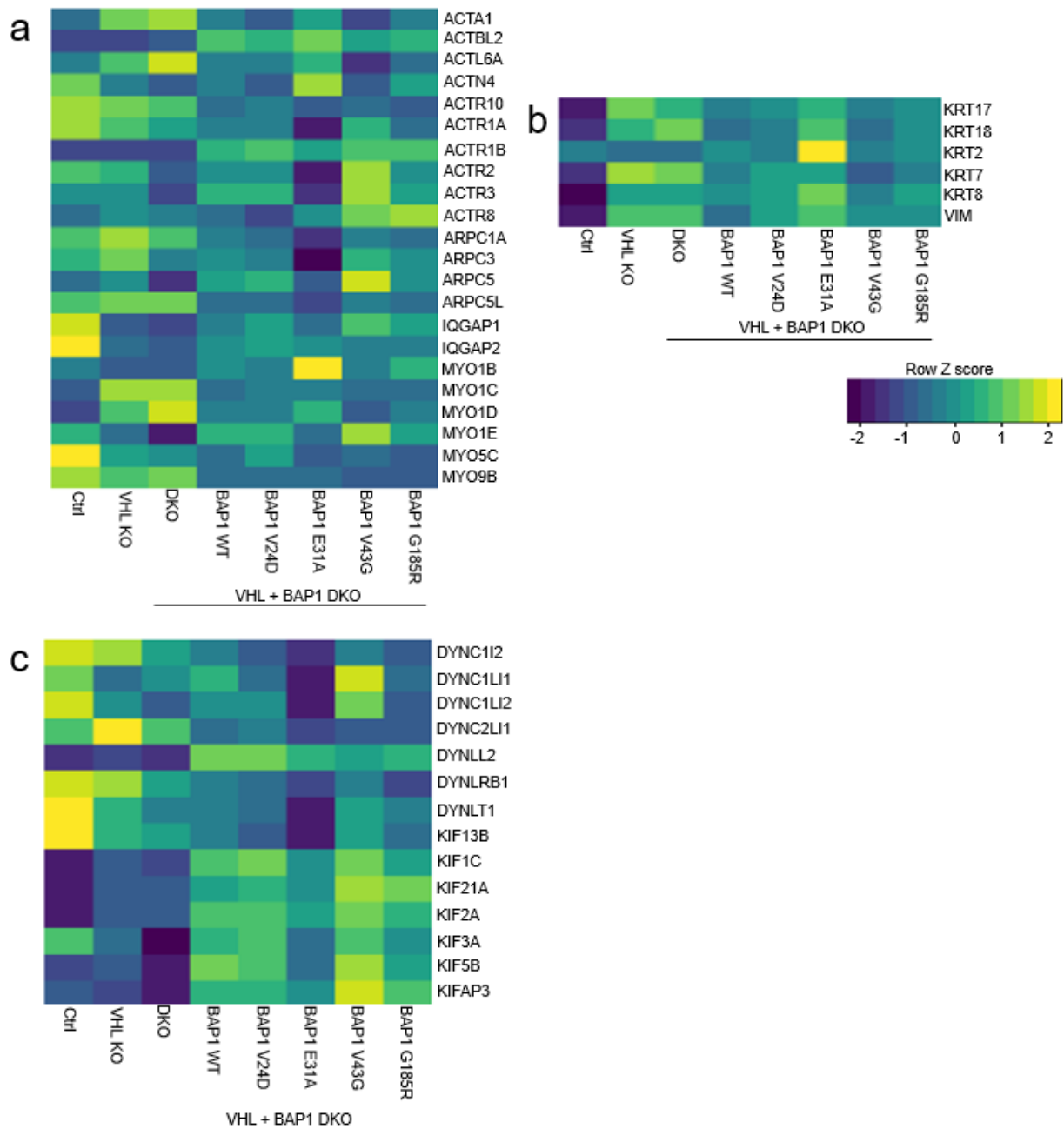


**Figure 3.26 Deregulation of cytoskeleton proteins.** We cultured wild-type LLC-PK1, VHL KO, VHL + BAP1 DKO, and reconstituted BAP1 mutations in DKO cells and lysates were collected on day 10. Samples were processed for whole cell proteomics and proteins were quantified using MS/MS, Liquid chromatography-tandem mass spectrometry. We showed the altered expression of cytoskeleton proteins into three different heatmaps: (a) microfilaments (actin and myosin), (b) intermediate filaments, and (c) microtubules (kinesin and dynein). Results were visualized using R. Z-scores were calculated for each row by subtracting the mean and dividing by the standard deviation.

## 3.10 Investigation of potential signaling cascades involved in development of metastatic ccRCC

Somatic and genetic changes to signaling pathways in cancer cells control the processes that lead to tumorigenesis and put them in the context of distorted signaling cascades that help cancer develop and metastasize.

### 3.10.1 Cell Cycle

Several cyclins and Cyclin-dependent kinases (CDKs) tightly regulate cell division to corroborate the production of two genetically identical cells. Cell cycle checkpoints act as DNA surveillance mechanisms that halt the accumulation and spread of genetic errors during cell division. Checkpoints can prevent cell cycle progression, irreparable DNA damage, commence cell cycle exit or activate cell death cascade. Cancer-related mutations that disrupt cell cycle control enable continuous cell division, primarily by impairing the ability of cells to exit the cell cycle. Cyclins bind to CDKs and form cyclin-CDK complexes. This complex gives signals to cells in order to enter the next cell cycle phase. Defects in the cyclins and CDKs cause genomic and chromosomal instability, leading to cancer [282]. We found downregulation of CDK7, CDC16, CDC23, and upregulation of CDC27 that may cause unscheduled cell proliferation in engineered cell line compared to wild-type cell line (Figure 3.27a). CDK7 shapes the trimeric complex with cyclin H and Menage A Trois 1 (MAT1) that functions as a Cdk-activating kinase (CAK). It is a crucial component of the transcription factor TFIIH, which is involved in DNA repair [283]. CDC16, CDC23, and CDC27 are components of the anaphase-promoting complex (APC) complex, which acts as a protein ubiquitin ligase. The APC complex is a cyclin degradation system that controls the exit of cells from mitosis [284]. CDC27 upregulation elevates stemness in cancer stem cells, whereas its downregulation may escalate cancer cell survival and chemoresistance [285]. We also found the upregulation of Proliferating cell nuclear antigen (PCNA), RAD21 Cohesin Complex Component (RAD21), Structural maintenance of chromosomes 3 (SMC3), and S-phase kinase-associated protein 1 (SKP1) and its upregulation is associated with the proliferation, invasion, and metastasis in various cancer (Figure 3.27a) [286-289]. We also found proteins that are upregulated in a few mutations and downregulated in other mutants. For example, DKO cells

expressing the E31A mutant showed upregulation of BUB1B, whereas it is downregulated in DKO cells expressing the V43G mutant (Figure 3.27a). BUBR1 overexpression plays a critical role in the cytogenetic and morphologic progression of ccRCC [290].

### **3.10.2 Hippo Signaling**

Hippo signaling controls organ size by regulating cell proliferation, apoptosis, and self-renewal. Several lines of evidence showed that the Hippo pathway is a sensor rather than a typical ligand-receptor pathway. The hippo pathway receives various molecular cues to ensure that the epithelial cell maintains its fate. This pathway relies on different morphogens, such as those involved in cell polarity or tissue's mechanical stress. These inputs help with developmental control and the homeostasis of adult tissues by regulating their regeneration [291].

Dysfunctional Hippo signaling plays a role in the maintenance and progression of human cancers, but data involving clear cell renal cell carcinoma (ccRCC) have been limited. We found high Yes-associated protein 1 (YAP1) and TEA domain family member 1 (TEAD1) protein levels, which has been previously reported breast cancer and melanoma (Figure 3.27 b). The evidence implicates aberrant Hippo signaling in ccRCC is linked to proliferation, invasiveness, and metastasis [292].

Cell polarity is a prerequisite for epithelial tissue formation. Many lines of evidence suggest that polarity perturbations can favour cancer, with the mechanism still unclear. Studies have uncovered intricate interactions between the conserved hippo tumor suppressor pathway and apico-basal polarity determinants [293]. Deregulation of the network of hippo signaling leads to massive over proliferation in cells [294].

In our study, we found deregulation of the hippo signaling pathway and disruption of apico-basal polarity, which further supports the notion that hippo signaling and apico-basal polarity complexes are also interconnected in our model (Figure 3.27b).

### **3.10.3 ERK pathway**

The Ras/Raf/MAPK (MEK)/ERK pathway is the essential signaling pathway among all Mitogen-activated protein kinase (MAPK) pathways [295]. ERK belongs to the MAPK family cascade that controls cell growth and differentiation by transmitting extracellular

signals to intracellular targets. MAPKs are central signaling cascade components that regulate cellular functions such as cell proliferation, differentiation, and stress responses [295]. Deregulation of the ERK cascade is the most common trigger for cancer, with mutations of this pathway occurring in most types. Ras mutations (mainly KRAS) are the most common mutations that affect cancer. They are found in 30% of all cancers and 10% of cancer patients. Rapidly Accelerated Fibrosarcoma (RAF) mutations have been found in 8% of cancers, and MEK is rare in 1% [295].

The AKT protein is the central signaling cascade system involved in various cellular processes. There are three different isoforms of AKT, and elevated expression of AKT1, AKT2, and AKT3 has been observed in multiple types of cancer [296]. Surprisingly, AKT2 is downregulated in ccRCC patients (Figure 3.27c) [297].

Kirsten rat sarcoma viral oncogene homolog (KRAS) transmits signals and is essential in regulating cellular signaling events. It can relay signals and activate MAPK, necessary for cell development, growth, survival, and differentiation [298]. Interestingly, our study found that KRAS is downregulated, and another study also concluded the same (Figure 3.27 c) [299].

Ras-related protein (RRAS) is a type of GTPase and is reported to be involved in amplifying integrin function, regulation of cell adhesion, invasion, and migration [300]. Upregulation of RRAS leads to continuous activation of the MAPK pathway and contributes to leukaemogenesis (Figure 3.27c) [301].

RAS p21 protein activator 1 (RASA1), also known as p120-RasGAP, is a RasGAP protein. RASA1 involves actin filament polymerization, blood vessel development, cell apoptosis, and movement. Analysis shows that a low level of RASA1 predicts the prognosis for various cancers, including RCC, indicating that RASA1 can be used to predict the prognosis for patients with metastatic ccRCC (Figure 3.27c) [302].

We also found the deregulation of EGFR, GRB2, NF1, and TGFBR2 which are known regulators of the ERK pathway (Figure 3.27c).

Epidermal Growth Factor Receptor (EGFR) is a receptor tyrosine kinase that can autocross-phosphorylate, which initiates a downstream cascade signal. ccRCC depends on over-expression or mutations in EGFR to drive malignancy [303].

Growth factor receptor bound protein 2 (GRB2) is a molecular adaptor initially discovered for its role in cell proliferation, survival, angiogenesis, and differentiation. Recent studies show that Grb2 plays a significant role in tumor malignancies. RTKs can activate Ras at plasma membranes by recruitment of GRB2/Son of Sevenless (SOS) complexes. Upregulation of Grb2 causes continuous activation of the Ras pathway, leading to cancer cell growth [304].

The Neurofibromin (NF1) gene loss of function leads to tumor predispositions. NF1 inactivation caused by the hypoxia and hypoxia-associated factor-mediated proteasomal degradation leads to the abruption in the Ras-ERK pathway in ccRCC [305].

TGF- $\beta$  is an essential factor in cancerous tumors that signals through heteromeric complexes of type I and type II (TGFBR1, TGFBR2) receptors, activating members of the Small mothers against decapentaplegic (SMAD) family [306]. TGF $\beta$ R2 is a transmembrane protein with a protein kinase domain, which recruits and phosphorylates TGF $\beta$ R1 forming a heterodimeric complex, and binds TGF- $\beta$ . Mutations in any of these proteins will result in tumor growth or metastasis [306]. In ccRCC, upregulation of TGF $\beta$ R2 expression is associated with proliferation, invasiveness, and metastatic potential of ccRCC [307].



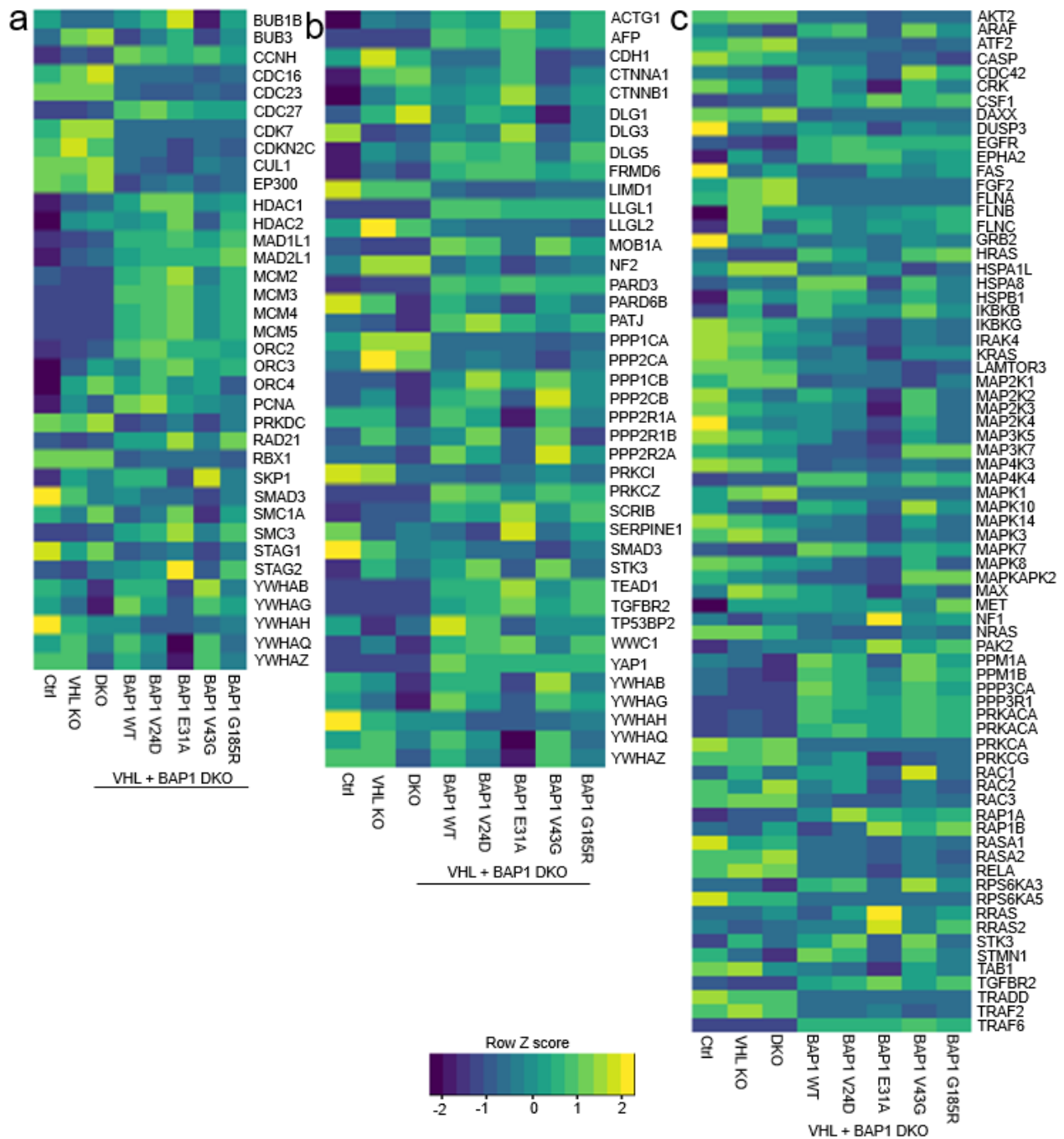


**Figure 3.27 Analysis of the role of the oncogenic pathway.** We cultured wild-type LLC-PK1, VHL KO, VHL + BAP1 DKO, and reconstituted BAP1 mutations in DKO cells and lysates were collected on day 10. Samples were processed for whole cell proteomics and proteins were quantified using MS/MS, Liquid chromatography-tandem mass spectrometry. We showed the expression of different pathway proteins in three different heatmaps: (a) Cell cycle, (b) Hippo pathway, and (c) ERK pathway. Results were visualized using R. Z-scores were calculated for each row by subtracting the mean and dividing by the standard deviation.

### **3.11 Misregulation of SLC genes in engineered metastatic ccRCC model representative of aggressive clinical ccRCC**

The solute carrier (SLC) superfamily consists of different types of transporters that are ubiquitously expressed in various organs and mediate the uptake of small molecule substrates in a facilitative manner [308]. The vital function of SLC proteins is to maintain the reabsorption of various ions across proximal tubules; dysregulation of these transport proteins can cause neoplasm in proximal tubules [309]. We identified 107 different SLC proteins misregulated in engineered cell lines compared with wild-type cells. Therefore, we analyzed the expression levels of SLC family members and correlated them with prognosis in ccRCC patients with data from GEPIA. We identified significantly downregulated SLC proteins compared with wild-type cell line: SLC12A9, SLC25A13, SLC25A44, SLC29A1, and SLC30A9, are associated with OS and DFS in ccRCC patients (Figure 3.28).

Solute Carrier Family 12 Member 9 (SLC12A9) encodes Potassium-Chloride Transporter 9. Potassium-Chloride Transporter 9 is involved in cell volume homeostasis and inorganic ion transmembrane transport [310]. As per our knowledge, this is the first report that showed the downregulation of SLC12A9 might be associated with metastatic ccRCC

Solute Carrier Family 25 Member 13 (SLC25A13) is an electrogenic Aspartate/Glutamate antiporter that plays an essential role in malate–aspartate shuttle. SLC25A13 was negatively associated with the depth of tumor invasion and metastasis in colorectal cancer [311].

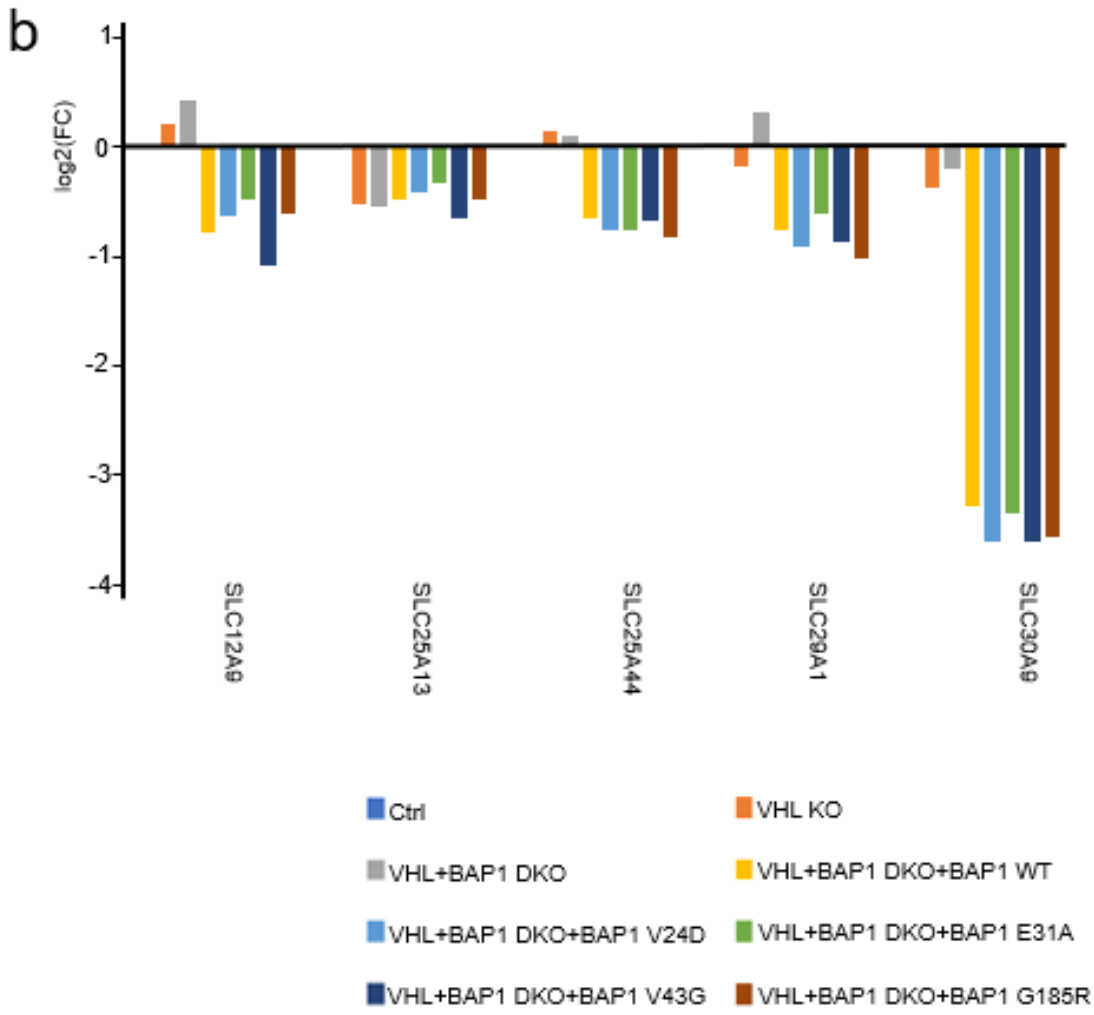
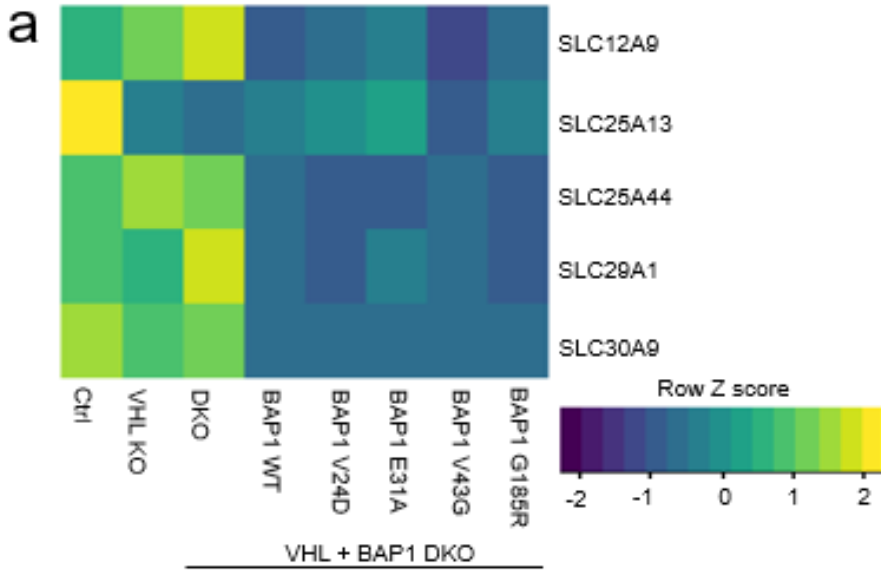
Solute Carrier Family 25 Member 44 (SLC25A44) belongs to the mitochondrial carrier proteins and transports branched-chain amino acid (BCAA) into mitochondria. Inactivation of the AMPK-GATA3-ECHS1 pathway induces Fatty Acid Synthesis (FAS) that downregulates BCAA and helps in the progression of metastatic ccRCC [312].

Solute Carrier Family 29 Member 1 (SLC29A1) is an equilibrative nucleoside transporter. This protein encodes a transmembrane glycoprotein that localizes to the mitochondrial and plasma membranes and intercedes the cellular uptake of nucleosides from the

surrounding medium. Increased expression of SLC29A1 improved survival in pancreatic cancer patients treated with gemcitabine [313].

Solute Carrier Family 30 Member 9 (SLC30A9) encodes for zinc transporter (ZnT) responsible for maintaining zinc homeostasis by transporting zinc from the cytosol to organelles and the extracellular space to avoid toxicity. Some ZnT proteins have been involved in breast, pancreatic, and prostate cancers. Loss of function of SLC30A9 has been seen in cerebro-renal syndrome [314].

These studies showed that deregulated SLC proteins elevate cancer hallmarks and provide a functional advantage to tumor cells. Although previous literature has demonstrated that the SLC family plays a vital role in the prognosis of various cancers, not many studies have considered their role in ccRCC. Our work indicates a correlation between ccRCC outcome and the SLC family. However, the underlying mechanism remains equivocal and should be the subject of future studies.



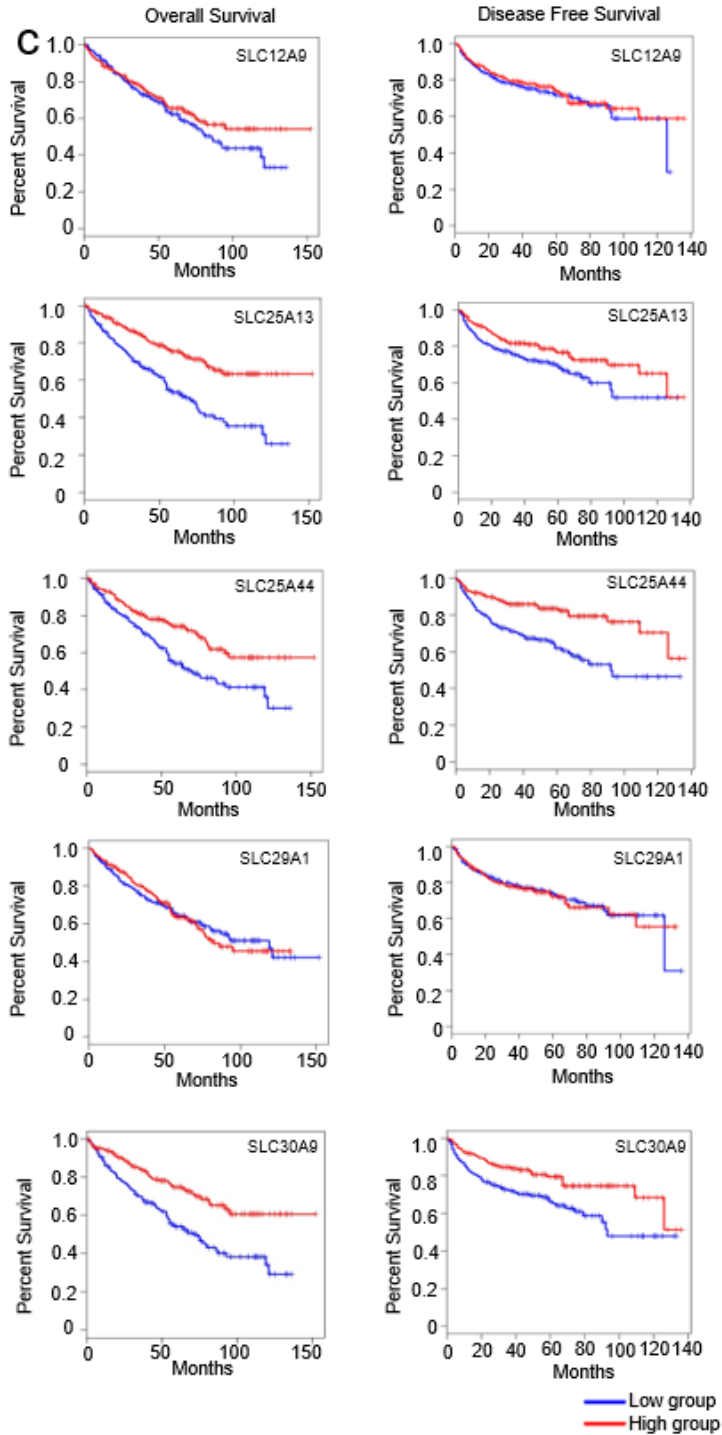


**Figure 3.28 SLC based prognostic biomarkers for ccRCC.** (a) We cultured wild-type LLC-PK1, VHL KO, VHL + BAP1 DKO, and reconstituted BAP1 mutations in DKO cells and lysates were collected on day 10. Samples were processed for whole cell proteomics and proteins were quantified using MS/MS, Liquid chromatography-tandem mass spectrometry. We depicted the 5 SLC transporters in heatmap that are downregulated in mutants' comparison to wild-type and are correlated with the OS and/or DFS of patients. Results were visualized using R. Z-scores were calculated for each row by subtracting the mean and dividing by the standard deviation. (b) The graph demonstrates the mean of log 2-fold change for five SLC transporters. Bonferroni test was used as a follow-up to two-way ANOVA to compare control cells to each

mutated sample. Bonferroni test: \*\*\* $p < 0.001$ . (c) Kaplan-Meier survival curves for OS and DFS according to the expression level of SLC family genes in ccRCC (GEPIA).

### 3.12 Biochemical analysis of BAP1 mutations

BAP1 is a relevant tumor suppressor protein involved in cell growth, DNA damage response and transcriptional regulation. BAP1 belongs to the ubiquitin C-terminal hydrolases (UCH) DUB subfamily of cysteine proteases and is part of the Polycomb repression (PR-DUB) complex, which requires the activation by deubiquitinase adaptor domain of ASXL1 [315].

The domain structure of BAP1 and the structure of BAP1 is predicted to contain a catalytic domain (CD), together with a long C-terminal coiled-coil region (Figure 3.29a). Since no experimental structures are currently available, we modelled the structure of human BAP1 using AlphaFold2 [316]. The model structure of BAP1 displays a typical CD with high homology to the CD of other UCHs enzymes from the same family, such as UCH-L1, UCH-L3 or UCH-L5 (UCH37) (Figure 3.29b, c). Such fold represents the minimum fold required for substrate binding (i.e. Ub) and hydrolysis [317]. Interestingly, the structure of the CD of BAP1 also shows the presence of a characteristic crossover loop, which is unique for UCHs (Figure 3.29b). This loop is positioned over the active site and plays an important role in Ub hydrolysis, as shown for the *Drosophila* ortholog Calypso. It also shows the conservation of relevant active site residues (Figure 3.29b), suggesting that BAP1 is a catalytically active protein able to cleave Ub and Ub-substrates. The structural model of BAP1 also revealed the location of cancer-associated missense mutations, suggesting that these mutations are likely to have an impact on the catalytic activity of the protein.

The catalytic domain of BAP1 (BAP1<sub>1-238</sub>) and four single-point mutants were expressed and purified. We performed biochemical studies using fluorogenic AMC-based probes, namely AMC-Ub, AMC-SUMO1, AMC-SUMO2 and AMC-ISG15 substrates, in order to evaluate the substrate specificity of this enzyme. In agreement with previous studies, we have shown that the purified BAP1 catalytic domain (BAP1<sub>1-238</sub>) is a deubiquitinating enzyme that cleaves exclusively Ub-conjugated AMC substrates (Figure 3.29d). BAP1

catalytic domain was active only against Ub-AMC substrates, confirming that this protein has a strict deubiquitinase activity. We considered four mutations (i.e., V24D, E31A, V43G, and G185R) in our study. We looked through the cBioPortal and found two BAP1 mutations that are common in patients (E31A and G185R). The other two mutations we looked at for our study (V24D and V43G) were found in the literature [187, 318]. Activity assays with BAP1 cancer-associated mutants showed that these proteins are largely inactive towards a typical Ub-AMC substrate (Figure 3.29e). These BAP1 mutations appear at interaction surfaces with Ub (V24D, E31A, and V43G) or located at the catalytic site of the enzyme (G185R). Ultimately, these critical mutations lead to reduced levels of PR-DUB activity in BAP1.



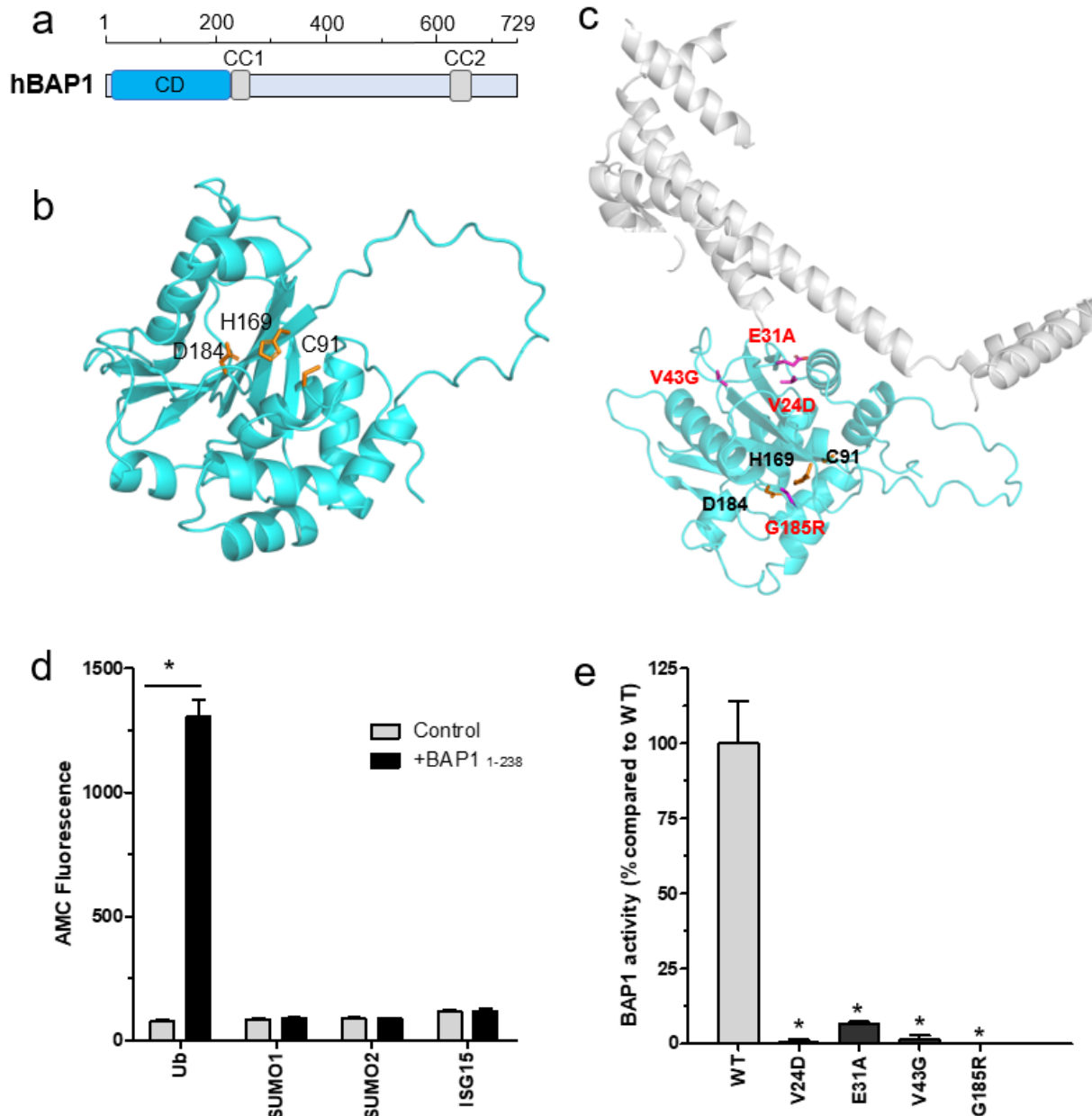


**Figure 3.29 Effect of cancer-associated missense mutations on the catalytic activity of BAP1.** (a) Domain organization of human BAP1. The catalytic domain of BAP1 is shown in cyan. The catalytic domain of BAP1 is followed by two predicted coiled-coil regions are shown in grey. (b) Model structure of the catalytic domain of BAP1 showing the position of relevant active site residues (*i.e.* C91, H169, and D184). Side chains of these residues are shown as orange sticks. (c) Selected cancer-associated missense mutations mapped onto the modeled structure of BAP1. BAP1 model structure was generated with AlphaFold2. Note that C-terminal disordered regions with a low-confidence prediction have been removed for clarity. (d) Catalytic activity of BAP1 catalytic domain against different AMC-substrates (*i.e.* Ub-AMC, SUMO1-AMC, SUMO2-AMC, or ISG15-AMC). All the substrates were assayed at a final concentration of 1  $\mu$ M. (e) Effect of cancer-associated missense mutations on BAP1 activity. In all cases, the enzyme concentration was 25 nM. The final Ub-AMC concentration was 5  $\mu$ M. In d) and e), data are shown as mean  $\pm$  SEM ( $n = 3$  independent experiments). In d) \* $P < 0.05$  compared to control, two-tailed paired t-test. In e), \* $p < 0.05$  compared to WT, one-way ANOVA.

## 4. Discussion

### 4.1 *In vitro* proximal tubule model

The foundation of a completely practical human-based renal proximal tubule *in vitro* test framework would be of extraordinary interest to the fields of physiological science and pharmacological exploration.

LLC-PK1 cells have been derived from juvenile male Hampshire pig kidneys to generate cells that could produce plasminogen activators. Monolayer cultures have been reported to form domes (100-1000  $\mu\text{m}$  in diameter), and it has been shown that they polarize apicobasal with apical microvilli and the basal side facing the culture dish [319]. More importantly, around the time of their generation, it was evident that LLC-PK1 cells maintain an epithelial-like morphology through several years in culture, unlike many other kidney-derived cell lines. It was also shown by electron microscopy that the cells are already in the monolayer stage and form rosettes which exhibit ultrastructural characteristics of tubules; including a basal lamina-like material. Active trans-epithelial transport and responsiveness to vasopressin and calcitonin, a small apical negative potential, opposite to the polarity of MDCK monolayers, glucose transport like in proximal tubules, and many other features characteristic of kidney epithelia have also been reported [320].

In addition, we here report that this spontaneously immortalized, normal kidney proximal tubule epithelial cells can be used as an *in vitro* differentiation system that ultimately yields functional proximal tubules on an epithelial layer. Specifically, the formation of these tubules requires approximately ten days and a transition of the epithelium from a stochastically oscillating, dome-forming system to a more static epithelial layer overlaid by tubules (Figure 3.1). In contrast to earlier studies, which used micropatterning to develop proximal tubules, tubulogenesis in this system is self-organised.

### 4.2 Luminogenesis process in proximal tubules

Tubules represent prevalent epithelial topology in metazoa. There is significant diversity in the anatomy of tubules. Tubules can contain lumens encased by a single cell, while others include multiple cells that "seal" the lumens via auto-or intercellular junctions. The formation of a lumen can occur by budding, wrapping, entrapment, cavitation, and

hollowing [321]. In general, the formation of tubules by budding or wrapping starts with a fully polarized epithelium, whereas entrapment, cavitation, or hollowing is initiated by non-polarized cell(s) [321]. In this work, we present evidence that tubulogenesis in the LLC-PK1 model occurs by doming and wrapping. Doming precedes the wrapping process in proximal tubules. The doming process starts when the monolayer reaches 80-90% confluence, and then several domes fuse so that they can form tubes (Figure 3.4). Renal proximal tubules are pre-patterned through tissue oscillations. Dome edges are stabilized, and tubes are patterned at the same site where domes were previously formed.

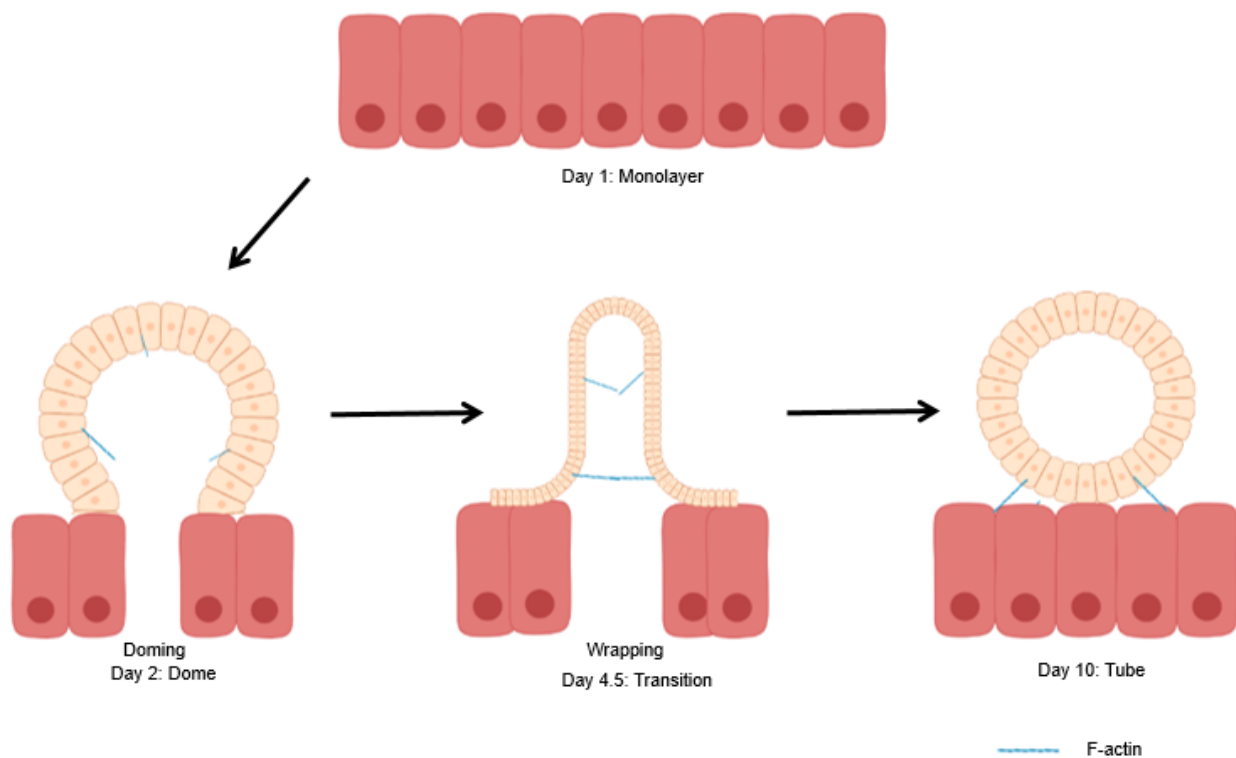


**Figure 4.1: Proposed model of tubulogenesis in proximal tubules.** Cells are plated and form a monolayer that is sealed by tight junctions. This monolayer vectorially pumps fluid to its basal surface, which leads to local, stochastic upward bending of the layer, called doming. These domes fuse and wrap to create tubes. These tubes become mature and elongated on the 10th day. The figure was created with Biorender.

Apical-basal polarity is essential for proper tubule formation. Three major polarity complexes serve as the core proteins initiating the lumenogenesis process. The complexes are the apical Crumbs, and Par complexes, and the basolateral Scribble complex [322]. The antagonism of the apical compared to the basolateral complexes is

mediated by protein-protein interactions that define the apical-basolateral boundary that forms at the tight junctions [322]. Par complex proteins are high in the monolayer stage, whereas Crumbs and apical complex proteins are high in the tube stage (Figure 3.11).

### **4.3 Presence of specific markers in different stages of proximal tubule development**

The self-organized model expresses different proximal tubule-specific markers and exhibits transport proteins that can be correlated to the *in vivo* functions of proximal tubules.

We found that our system expresses various proximal tubule markers like Synaptopodin, Smoothelin like 2, and Paxillin which play an essential role in renal tubule morphogenesis (Figure 3.8) [323-325].

There is a strong association between the cell cycle and the components expected to execute cell fate decisions in various developmental processes [326]. We established that proteins responsible for proliferation are significantly higher in the monolayer stage than in the tube stage. Proteins linked to cell proliferation, Cyclin-B1, Ki-67, RAD51, and PCNA are high in the monolayer stage (Figure 3.9).

The metabolic rate for the kidney is high because it requires sufficient energy to re-absorb nutrients, remove waste from the blood, maintain acid-base homeostasis, and regulate blood pressure [233]. To facilitate the re-absorption of various ions, many ATP-consuming transporters are needed. Abundant mitochondria are present in proximal tubules to generate the necessary ATP. Therefore, the proximal tubule depends on FAO compared to glucose metabolism as FAO produces more ATP units than any other metabolic pathways (Figure 3.11) [233].

We also identified the presence of various transporters in the self-organized proximal tubule model. These transporters play a significant role in the re-absorption of multiple ions. Mitochondria provide energy to the Na<sup>+</sup>/K<sup>+</sup>-ATPase to generate ion gradients across the cellular membrane [234]. This model expresses several transporters that can be studied to identify their mechanism of action (Figure 3.13).

The cytoskeleton is composed of dynamically assembled and disassembled protein structures, called filaments. The main classes of the cytoskeleton are microtubules, actin filaments, and intermediate filaments. The cytoskeleton provides stability and integrity to the cell structure [327]. The actin cytoskeleton, which lines the plasma membrane, has been shown to play critical roles in epithelial cell function. These roles include the processes of exocytosis and endocytosis, as well as direct and indirect interactions (via actin-binding proteins) with membrane-bound transporters, channels, and AQP isoforms [6]. Vimentin expression is only observed in three different conditions: 1) during the early stage of proximal tubule development, 2) in ccRCC, and 3) in the regenerating phase after ischemic or toxic renal injury. In the early stage, we also identified the expression of vimentin [328]. ERM (Ezrin–Radixin–Moesin) proteins characteristic as plasma membrane–actin cytoskeleton linkers and take part in the formation of specialised domain of the plasma membrane. The role of ezrin in tubulogenesis process is studied in LLC-PK1. Ezrin interacts with p85, the regulatory subunit of PI3K. When examined for tubulogenesis, cells overproducing a mutant Y353F ezrin undergo apoptosis. The apoptotic phenotype of cells is rescued with the transfection of constitutively activated PI3K. These results showed the role of ezrin in tubulogenesis process [329]. We identified various cytoskeletons proteins that play a significant role in each stage of proximal tubule development (Figure 3.14).

Suitable model systems are crucial to investigating disease mechanisms and testing potential drugs and drug targets for diseases associated with the proximal tubules. This model can be used to study different genetic and acquired diseases of proximal tubules.

#### **4.4 Role of transporters in proximal tubule development**

We also inhibited some specific transporters to understand how the tubulogenesis process is affected. We identified that the inhibition of Na<sup>+</sup>/K<sup>+</sup>-ATPase by digoxin treatment hinders the dome and tube formation. The secretory transport of digoxin across LLC-PK1 monolayers grown on permeable filters was studied. Digoxin's total and specific basolateral to apical (B-A) flux was reduced by metabolic inhibitors, while the apical to basolateral (A-B) flux was increased. Our findings suggest that digoxin is secreted transepithelially in renal tubules via an energy-dependent, carrier-mediated process [330].

The apical membrane of LLC-PK1 was found to be expressing human P-glycoprotein. Digoxin is transported by human P-glycoprotein, implying a molecular mechanism for digoxin secretion in the renal tubules [331]. Digoxin is primarily excreted in the urine, unchanged. Although clearance appears to be well correlated with glomerular filtration rate, tubular handling of digoxin is thought to play a significant role in clinically relevant drug interactions. The *in vivo* multiple indicator dilution technique revealed that digoxin is extracted from the peritubular circulation and secreted into the urine [332].

Bafilomycin A1 (H<sup>+</sup>-ATPase inhibitor) can permeate into the organelles of living cells via the plasma membranes without killing the cells, allowing us to study the V-ATPase, organelle acidification, and the various functions of the central vacuolar system *in vivo*. Bafilomycin A1 has been shown to effectively inhibit lysosome acidification and the degradation of an endocytosed protein *in vivo* [333]. In LLC-PK1, Bafilomycin A1 blocks the recycling pathway of AQP2 in a perinuclear compartment adjacent to the Golgi, indicating a role for vesicle acidification in both constitutive and regulated recycling of AQP2. The colocalization of AQP2 with clathrin following bafilomycin treatment suggests that the compartment in which recycling AQP2 is inhibited may be the trans-Golgi rather than the cis- and medial-Golgi cisternae [334].

We also analyzed the effect of inhibition of transporters on dome and tube formation. We found that bafilomycin-treated cells affected the dome size and tube length (Figure 3.16, 3.17). Together, we can conclude that if dome size is affected, it will affect the tube formation. The inhibitors that we used in our study are FDA approved, but they affect tube formation. Therefore, we cannot outweigh their side effects. Continuous use of these drugs in patients may cause nephrotoxicity and will compromise re-absorption capacity of proximal tubules.

Therefore, our self-organised system will allow us to perform constant, low dose exposure studies to predict longer therapy regimens and study acute and chronic toxicity, empowering us to acquire a more detailed forecast of tissue-level clinical results. We expect this will affect the pre-clinical medication revelation pipeline, facilitating the forestalling of exorbitant disappointments in late-stage clinical studies. We propose that this novel system can be used to investigate various genetic and acquired diseases of the

proximal tubule, as it offers the unique ability to recapitulate emergent properties while being accessible to high-content screening in pre-clinical studies.

One more significant part of *in vitro* investigations concerning the kidney is the capacity of cell models to anticipate the potential human kidney response to different drugs. These investigations incorporate the assessment of potential drug-induced toxicity, studies of drug-drug interactions, and the evaluation of therapeutic impacts of the drugs in a specific condition. Renal proximal tubules are central parts coordinating nutrient recovery and waste removal from the body, including most drugs and their metabolites. Hence, nephrotoxicity is a considerable concern during any drug development process, especially since renal insult is frequently perceived late during clinical trials. Therefore, our *in vitro* proximal tubule model can study the effect of various drugs and generate models for different genetic and acquired diseases of proximal tubules.

#### **4.5 Stepwise-edited, metastatic clear cell RCC model developed using differentiated proximal tubule cells**

We developed a strategy to introduce different series of cancer-associated mutations sequentially into healthy, differentiated proximal tubules in culture. This study demonstrates the ability to use the lentiviral CRISPR approach to manipulate a cell line *in vitro* and generate an improved metastatic ccRCC tumour model *in vitro* to study the genetic landscape of metastatic ccRCC.

We showed the fitness advantage by which malignant growth drives clonal expansion in human tumorigenesis that could be exploited to produce multipotent disease models from the primary cell line in a stepwise way. This model-building technique applies to diseases emerging from differentiated cells, which might not have adequate replication potential to develop large populations from a single cell.

This study exemplifies the ability to use a lentiviral CRISPR-Cas12 approach to develop progressive series of mutant metastatic ccRCC models *in vitro*. There are several noteworthy aspects of the mutants we developed. Since VHL inactivation and BAP1 mutations are clinically central hallmarks of metastatic ccRCC [187], we have used LLC-



PK1 self-organised system to develop genetically similar metastatic ccRCC model to what is seen in patients.

ccRCC has been classified into seven evolutionary subtypes, which may be related to clinical outcome. Two subtypes were identified by the presence of multiple clonal drivers or the BAP1 mutation. They had lower levels of intratumor heterogeneity (ITH) and higher levels of genomic instability, which were linked to metastasis and worse clinical outcomes. Overall survival was worst for a rare subtype that didn't have any driver changes, like a loss of VHL function, and had more ITH and genomic instability, as well as a higher stage and grade of tumor [335].

The remaining four subtypes were less aggressive: an early PBRM1 mutation followed by any of SETD2, PI3K, or somatic copy number alterations characterized slow-growing primary tumors with high ITH, and tumors in which VHL was the sole driver were indolent, with decreased ITH, genome instability, and size. The majority of small renal masses in the cohort had low ITH and genome instability, but some fell into less benign subtypes and could progress without surgery [335].

There was some evidence of immune evasion, as indicated by the loss of heterozygosity at the HLA locus, in populations with the capacity to develop metastases. Especially, genomic instability was significantly elevated, along with an increase in ploidy. Instability was linked to chromosome 9p and 14q losses, which were both markers for metastatic potential. Both 9p and 14q losses were predominantly subclonal in the primary tumors, suggesting that they may be missed by single biopsy approaches [182, 335, 336].

In the evolutionary subgroups of primary tumors, rapid spread to multiple metastatic sites was linked to multiple clonal drivers and BAP1 subtypes with less diversity and more genomic instability. This category includes VHL wild-type tumors, which had high levels of genomic instability. In these subtypes, metastatic competence is acquired early in the development of the primary tumor, resulting in rapid dissemination, surgical failure, an inadequate response to systemic therapy, and early death [182, 336].

In contrast, metastatic competence developed slowly in subclonal populations of the four primary subtypes with high heterogeneity and lower levels of genome instability, where

only one or a few metastases were seen. Metastatic capacity increases exponentially over time and may eventually result in widespread disease. For patients in these groups, surgical removal of the primary tumor prior to systemic therapy may remove the "evolutionary sink" from which metastatic mutations arise, thereby alleviating the danger of future metastatic seeding. This is because removing the primary tumor would get rid of the "evolutionary sink" from which mutations in metastatic tumors come [182, 336].

The significance of studying combinations of mutations while connecting cancer genotypes to phenotypes is featured by our observations of how the effect of a given single mutation relies on the genetic setting.

#### **4.6 Loss of lumen formation is an early event in metastatic ccRCC development**

Epithelial cells are profoundly coordinated structures at cellular and tissue levels, disrupted in carcinoma. Apical-basal membrane polarity outlines different cell membrane compartments, with an apical membrane facing the lumen and a basolateral membrane that contacts adjacent cells and the extracellular matrix (ECM) [42]. Polarity complexes establish distinct membrane domains that are fundamental in organizing and coordinating intracellular signaling pathways for proper growth control, tissue organization and inhibition of metastasis [337].

Par complex comprises a core scaffold, Par3, that recruits the adaptor protein Par6 and its effector kinase, aPKC. After being recruited by Par3, Par6 and aPKC separate from Par3 and partner with the Crumbs complex at the apical film in mature epithelial cells [42]. The Scrib complex acts to limit the spatial association of the apical complexes mutually [72]. Several lines of evidence indicate apical-basal polarity is a barrier to carcinogenesis. Inactivation or mislocalization of individual polarity proteins in the epithelium is adequate to actuate pre-malignancy and can speed up tumour progression [338]. Vhl inactivation disrupted the lumen formations in metastatic ccRCC development (Figure 3.24).

## 4.7 Epithelial to mesenchymal transition: step towards metastatic ccRCC progression

EMT is a biological phenomenon in which epithelial cells dedifferentiate to mesenchymal cells. During the EMT process, epithelial cells lose their polarity, cytoskeletal structure, and cell-cell adhesion but gain the ability to migrate like mesenchymal cells [339]. Moreover, a few studies showed that EMT is linked to a worse survival outcome (Figure 3.25, 4.2) [340].

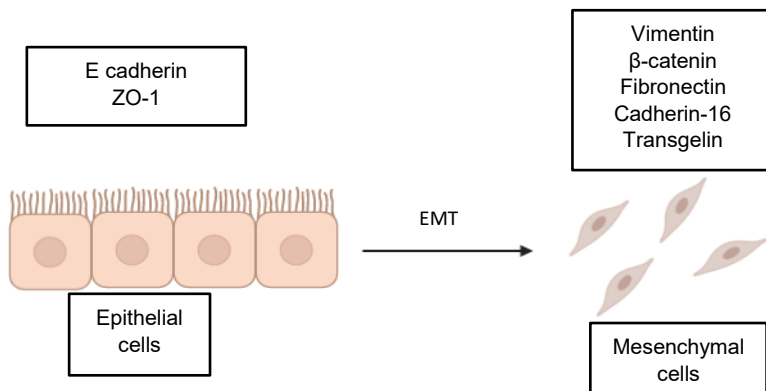


**Figure 4.2 EMT process during ccRCC development.** During EMT, epithelial cells lose their polarity and interconnections between cells and basement membrane. The key mesenchymal proteins get upregulated and the expression of epithelial markers gets downregulated.

The cytoskeleton comprises actin, microtubules, and intermediate filaments that provide structural stability and mechanical strength necessary to maintain cell integrity [341]. During cancer development, the cytoskeleton remodels to help the cell invade and metastasis [342]. Actin filaments, microtubules, and intermediate filaments play significant roles in EMT.

Restructuring the actin cytoskeleton is fundamental for metastasis and in the conversion of epithelial cells to mesenchymal cells. Filopodia are finger-like protrusions formed during the EMT process at the leading edge of migrating cells that play an essential antennal function during motility and invasion [343]. Actin fibers bundle hexagonally and provide rigidity to filopodia [344].

Intermediate filaments are significantly rearranged during the EMT process, switching from cytokeratin-rich to vimentin-rich networks. During the EMT process, intermediate

filaments undergo a considerable reorganization, changing from networks rich in cytokeratin to networks rich in vimentin. Vimentin is a type III intermediate filament that is significantly upregulated during EMT and E-cadherin is one type of cell adhesion epithelial molecule that regulates EMT [345].

Microtubules are  $\alpha/\beta$ -tubulin heterodimers involved in proliferation, migration, and invasion. Cancer cells penetrate the basal membrane by forming unique structures called invadopodia. Microtubules were required for the function of invadopodia-related structures [346].

Many of the distinctive EMT effector molecules are subcellular structural proteins that distinguish a cell's identity as either epithelial or mesenchymal. Important molecular parts of these structures are regulated at different degrees during EMT. For example, the genes encoding various epithelial junction proteins, such as E-cadherin, ZO-1 are down-regulated and mesenchymal proteins are upregulated (Figure 4.3). Our study evaluated different EMT markers that are deregulated in ccRCC cell lines compared to wild-type proximal tubule cell lines. These cell models can shed light on the molecular basis of metastasis and conclusively link metastasis to ccRCC (Figure 3.26).

## **4.8 Activation of oncogenic pathways in metastatic ccRCC**

Deregulated signaling pathways always accompany cancer. Modifications in proto-oncogenes and TSGs lead to altered signal transduction that underlies malignant growth and multiplication of cells.

### **4.8.1 Cell Cycle**

The regulation of the cell cycle focuses on two processes that take place at various stages of the cycle: the process by which genomic DNA is replicated and its subsequent segregation between daughter cells [282].

It is often assumed that cancer cells are not in control of their cell cycles and that many if not all, cell cycle checkpoints need to be defective for a cell to become cancerous [347]. A recent study has shown that only certain aspects of cell cycle control must be disrupted

for cancer cells to continue dividing. This study also indicates that most cell cycle regulators are essential for cancer cell survival [282].

We identified different cell cycle control proteins, such as cyclins and CDKs, checkpoint signaling whose mutations cause errors and propagation of genetic alteration (Figure 3.27a).

One of the most important cancer biomarkers is the cell cycle engine, since it is located downstream from the point where oncogenic signaling networks converge. The abnormal cell proliferation that distinguishes metastatic ccRCC results from its dysregulation.

#### **4.8.2 Hippo pathway**

The Hippo signaling pathway, a critical regulator of organ size control, is evolutionarily conserved. Recently, it has been conveyed that Hippo signaling exerts oncogenic potential in human malignancies. However, somatic mutations of the Hippo pathway core components are rare, but germ-line mutations exist [348]. Upregulation of YAP has been found in many human cancers and deregulation of the Hippo signaling pathway causes it to overproduce YAP [348].

Deregulation of Hippo signaling can induce the expression of at least three distinct classes of genes.

The first class corresponds to genes with cell-autonomous roles in cell proliferation or survival, such as the cell death inhibitor *diap1*, the microRNA *bantam*, and the cell-cycle regulators *cyclin E*, and *E2F Transcription Factor 1 (E2F1)* [349-351].

The second type of gene governs the Hippo pathway's upstream regulators which are *Kibra*, *Expanded*, *Crumbs*, and *Four-jointed* [352-355]. Feedback regulation for the upstream components has been suggested as an important way to maintain steady-state levels of signaling strength.

The third set of genes includes the heparan sulfate proteoglycans *Dally* and *Dally-like*, as well as the cell surface proteins *E-cadherin*, *Serrate* (a Notch ligand), *Wingless*, *Vein* (an EGFR ligand), and *Serrate*. These proteins are both involved in regulating the extracellular

diffusion and signaling effectiveness of secreted morphogens like Hedgehog, Decapentaplegic, and Wingless [354-357].

In our engineered metastatic ccRCC model, we identified several deregulated proteins from the above classes, which validates that the metastatic model aligns with real-time patient data (Figure 3.27b).

### **4.8.3 MAPK pathway**

ERK is a crucial intermediary in intracellular signal transduction networks to transmit signals from extracellular stimuli such as growth factors, hormones, and neurotransmitters to their desired cells. As new evidence suggests, activation of ERK encourages cell proliferation and confers a survival advantage on cells, giving it a vital role in human cancer [358].

The Ras family of small GTPases is essential for MAPK signaling. There are three different Ras isoforms: H-Ras, K-Ras, and N-Ras. The varied actions, molecular functions, and effector preferences of these Ras isoforms result in distinct physiological processes in various tissues [359]. The RAF/MEK/ERK kinase cascade is located downstream of small GTPases. It contains two pseudokinases, KSR1 and KSR2, as well as the RAF isoforms CRAF, BRAF, and ARAF [360].

Under normal conditions, ERK signaling is regulated by feedback loops at multiple levels, indispensable for modulating cell growth and homeostasis. Basal-like breast, hepatic, melanoma, colorectal, non-small cell lung, uveal melanoma, and pancreatic cancer involve deregulated ERK. We also found that the ERK pathway is completely deregulated in metastatic ccRCC. Deregulated MAPK signaling is caused directly by genetic modifications of its upstream apparatus, including RTKs, Ras, and BRAF, or indirectly by those independent of Ras or RAF [360]. It significantly promotes the proliferation, invasiveness, and metastatic potential of ccRCC (Figure 3.27c) [361].

## **4.9 Correlation of engineered *in vitro* metastatic CCRCC model with patient sample data**

The SLC family of proteins plays a significant role in the transportation of ions along the renal tubule. Also, the SLC family is responsible for mediating housekeeping functions by transporting substrates for metabolism across the proximal tubules [362]. Deregulation of specific transporters can cause severe diseases. Therefore, we focused on studying how transporters and metastatic ccRCC are related. Our study found that SLC12A9, SLC25A13, SLC25A44, SLC29A1, and SLC30A9 exhibited abnormal changes in engineered cell lines (Figure 3.28).

SLC family proteins are also associated with chemotherapeutic drug transport in colorectal, hepatocyte, and pancreatic cancers [363]. Therefore, further studies can be done to identify the drugs that can modulate SLCs and may help to develop anti-cancer drugs. The downregulation of the above SLC proteins was associated with the clinical stage, OS, and DFS. In our study, we systematically investigated the expression patterns of the SLC family in metastatic ccRCC-engineered cell lines.

We provided a facilitated understanding of the complex molecular biological properties and heterogeneity of ccRCC. Collectively, our interrogation of clinical sources clearly showed that the five biomarkers derived from our engineered metastatic ccRCC model are downregulated in the ccRCC tumor tissues and that they forecast a significantly poorer outcome in ccRCC patients. These proteins may be potential targets for therapeutic purposes for detection for clinical diagnosis, prognosis, and treatment of ccRCC patients.

## **4.10 Missense mutations in BAP1 catalytic domain cause metastatic ccRCC**

As discussed above, BAP1 is a prominent tumor suppressor, and our selected mutations affected renal tubule formation. Using our model structure for BAP1, we mapped onto the structure of all four missense mutations found in patients (Figure 3.29a, b, c). We found that all the mutations are located on the CD of the protein, with all four mutations mapped onto two different functionally relevant regions. One such mutation (G185R in Figure 3.29c) is located in the enzyme's catalytic site. Thus, it is tempting to speculate that the highly positive side chain of Arg located near the catalytic triad may impede substrate

hydrolysis. Another set of mutations (V24D, E31A, and V43G in Figure 3.29c) are found at the protein surface within a region involved in Ub binding. Similarly, with respect to G185R, these mutations are likely to interfere with BAP1 activity by altering substrate recognition and binding.

Therefore, studying the catalytic activities of these mutant variants can provide interesting information to explain the phenotypes observed in our renal *in vitro* models. To comprehensively evaluate the effects of these cancer-related mutations on BAP1 enzymatic activity, we expressed all four BAP1<sub>(1-238)</sub> mutant proteins and evaluated their activity against the Ub-AMC substrate. All four mutants showed a drastic reduction in the rate of hydrolysis of the Ub-AMC substrate compared to the WT protein. Previous reports showed that BAP1 deubiquitinating capacity had been associated with its tumor suppressor activity [364]. Here we show that patient-derived mutations impacting renal tubule formation are all mapped on the catalytic domain of BAP1. These mutations abolished BAP1 deubiquitinase activity, which suggests that BAP1 substrate processing is required for cell differentiation and proper renal tubule formation.

#### **4.11 Future Work**

*In vitro* cell culture cell lines are widely used in proximal tubules to study pathophysiology, pharmacology, and toxicology. We have developed the *in vitro* proximal tubule system that can be used to study various diseases associated with proximal tubules and identify new therapeutic targets. The model can be used to study the re-absorption of various ions across proximal tubules, which will help better understand the functions of transporters.

Despite the recent success in growing kidney organoids, they are not well suited to investigate RCC evolution *in vitro* for several reasons: They grow in 3D and form a tissue that later needs to be dissected/cleared, and stained to examine pathophysiological changes [365]. Moreover, organoids require complex and expensive protocols for generation and are challenging to use in screening approaches. Therefore, we have investigated whether the generation of kidney structures in 2D can be achieved by using normal renal epithelial cells which are cells that are the origin of the clear cell RCC. The



genome-edited cell models are acquiescent with selection marker-based experiments, including pooled genetic perturbations, genome-wide genetic screens, comparative molecular studies, and those with high content readouts. Applying such methodologies in these forms of the model with matched genetic controls may help discover therapeutic targets.

Multiple genes are responsible for the development of metastatic ccRCC. This study highlights the functional importance of two genes in developing metastatic ccRCC. However, practically, the outcome of metastatic ccRCC pathogenesis involves various genes that need to be mimicked through future appropriate studies. Nevertheless, our study provides decisive pointers to the probable molecular effects and reveals insights into crucial aspects of metastatic ccRCC.

The current study mainly focuses on Vhl and Bap1 and the evolution of metastatic ccRCC. However, additional genes can be inactivated to assess the effect of therapeutic response of the complex gene interaction because single mutations cannot explain resistance to therapies.

Screening assays can be developed to evaluate the angiogenic and immunosuppressive potential of the lead compounds. Epigenetic modulators can also be used to perform proliferation/differentiation screens and angiogenesis/macrophage differentiation inhibition.

Based on the results from these screens, compounds can be tested on animal models and others *in vivo* translational approaches. This will develop a toolset of differently staged tumor cells and differentiation assays that will allow the screening of epigenetic modifiers for their differential roles during tumor evolution. Ultimately, this should lead to identifying epigenetic modifications as early tumor biomarkers.

## 5 References

1. Bockenhauer, D. and R. Kleta, *Tubulopathy meets Sherlock Holmes: biochemical fingerprinting of disorders of altered kidney tubular salt handling*. *Pediatric Nephrology*, 2021: p. 1-9.
2. Lin, N.Y., et al., *Renal reabsorption in 3D vascularized proximal tubule models*. *Proceedings of the National Academy of Sciences*, 2019. **116**(12): p. 5399-5404.
3. Mezzogiorno, A., V. Mezzogiorno, and V. Esposito, *History of the nephron*. *American journal of nephrology*, 2002. **22**(2-3): p. 213-219.
4. IMAI, M., et al., *A standard nomenclature for structures of the kidney*. *Kidney international*, 1988. **33**: p. 1-7.
5. Maack, T., et al., *Renal filtration, transport, and metabolism of low-molecular-weight proteins: a review*. *Kidney international*, 1979. **16**(3): p. 251-270.
6. Kumaran, G.K. and I. Hanukoglu, *Identification and classification of epithelial cells in nephron segments by actin cytoskeleton patterns*. *The FEBS journal*, 2020. **287**(6): p. 1176-1194.
7. Welling, L.W. and D.J. Welling, *Surface areas of brush border and lateral cell walls in the rabbit proximal nephron*. *Kidney international*, 1975. **8**(6): p. 343-348.
8. Du, Z., et al., *Mechanosensory function of microvilli of the kidney proximal tubule*. *Proceedings of the National Academy of Sciences*, 2004. **101**(35): p. 13068-13073.
9. Maunsbach, A.B., *Observations on the segmentation of the proximal tubule in the rat kidney: Comparison of results from phase contrast, fluorescence and electron microscopy*. *Journal of ultrastructure research*, 1966. **16**(3-4): p. 239-258.
10. Madsen, K.M. and C.H. Park, *Lysosome distribution and cathepsin B and L activity along the rabbit proximal tubule*. *American Journal of Physiology-Renal Physiology*, 1987. **253**(6): p. F1290-F1301.
11. Zhai, X.Y., et al., *Digital three-dimensional reconstruction and ultrastructure of the mouse proximal tubule*. *Journal of the American Society of Nephrology*, 2003. **14**(3): p. 611-619.
12. Schafer, J.A. and D.W. Barfuss, *The study of pars recta function by the perfusion of isolated tubule segments*. *Kidney international*, 1982. **22**(5): p. 434-448.

13. Schmidt, U. and U. Dubach, *Differential enzymatic behaviour of single proximal segments of the superficial and juxtamedullary nephron*. Zeitschrift für die gesamte experimentelle Medizin einschließlich experimentelle Chirurgie, 1969. **151**(2): p. 93-102.
14. Woodhall, P.B., et al., *Relationship between para-aminohippurate secretion and cellular morphology in rabbit proximal tubules*. The Journal of clinical investigation, 1978. **61**(5): p. 1320-1329.
15. Bosch-Fortea, M., et al., *Micropattern-based platform as a physiologically relevant model to study epithelial morphogenesis and nephrotoxicity*. Biomaterials, 2019. **218**: p. 119339.
16. Terryn, S., et al., *A primary culture of mouse proximal tubular cells, established on collagen-coated membranes*. American Journal of Physiology-Renal Physiology, 2007. **293**(2): p. F476-F485.
17. Rotoli, B., et al., *Employment of confocal microscopy for the dynamic visualization of domes in intact epithelial cell cultures*. Cells Tissues Organs, 2002. **170**(4): p. 237-245.
18. Shlyonsky, V., et al., *Differentiation of epithelial Na<sup>+</sup> channel function: an in vitro model*. Journal of Biological Chemistry, 2005. **280**(25): p. 24181-24187.
19. Cameron, G., *Secretory activity of the chorioid plexus in tissue culture*. The Anatomical Record, 1953. **117**(1): p. 115-125.
20. Leighton, J., et al., *Secretory Activity and Oncogenicity of a Cell Line (MDCK) Derived from Canine Kidney*. Science, 1969. **163**(3866): p. 472-473.
21. Auersperg, N., *Histogenetic behavior of tumors. I. Morphologic variation in vitro and in vivo of two related human carcinoma cell lines*. Journal of the National Cancer Institute, 1969. **43**(1): p. 151-173.
22. McGrath, C.M., *Cell organization and responsiveness to hormones in vitro: genesis of domes in mammary cell cultures*. American Zoologist, 1975. **15**(2): p. 231-236.
23. Toyoshima, K., et al., *Conditions of cultivation required for the formation of hemicysts in vitro by rat bladder carcinoma R-4909*. Cancer research, 1976. **36**(8): p. 2800-2806.

24. McCombs III, W.B., et al., *Morphologic and immunologic studies of a human colon tumor cell line (SW-48)*. *Cancer*, 1976. **38**(6): p. 2316-2327.
25. Huh, N., T. Takaoka, and H. Katsuta, *Establishment of epithelial cell lines from rat glandular stomachs*. *The Japanese journal of experimental medicine*, 1977. **47**(5): p. 413-424.
26. Lever, J., *Cyclic AMP and inducers of mammalian cell differentiation stimulate dome formation in mammary and renal epithelial cell cultures*. *Hormones and cell culture*, 1979. **6**: p. 727.
27. Mullin, J.M., et al., *Sugar transport in the LLC-PK1 renal epithelial cell line: Similarity to mammalian kidney and the influence of cell density*. *Journal of cellular physiology*, 1980. **104**(3): p. 375-389.
28. Mason, R.J., et al., *Transepithelial transport by pulmonary alveolar type II cells in primary culture*. *Proceedings of the National Academy of Sciences*, 1982. **79**(19): p. 6033-6037.
29. Birek, C., et al., *Dome formation by oral epithelia in vitro*. *In vitro*, 1982. **18**(4): p. 382-392.
30. Grasset, E., et al., *Epithelial properties of human colonic carcinoma cell line Caco-2: electrical parameters*. *American Journal of Physiology-Cell Physiology*, 1984. **247**(3): p. C260-C267.
31. Rizzoli, R. and J.P. Bonjour, *Effect of dexamethasone on parathyroid hormone stimulation of cyclic AMP in an opossum kidney cell line*. *Journal of cellular physiology*, 1987. **132**(3): p. 517-523.
32. Zucchi, I., et al., *Dome formation in cell cultures as expression of an early stage of lactogenic differentiation of the mammary gland*. *Proceedings of the National Academy of Sciences*, 2002. **99**(13): p. 8660-8665.
33. Koyama, H., et al., *Establishment and characterization of a cell line from the American opossum (*Didelphys virginiana*)*. *In vitro*, 1978. **14**(3): p. 239-246.
34. Teitelbaum, A. and G. Strewler, *Parathyroid hormone receptors coupled to cyclic adenosine monophosphate formation in an established renal cell line*. *Endocrinology*, 1984. **114**(3): p. 980-985.

35. Cheng, L., et al., *Dopamine stimulation of cAMP production in cultured opossum kidney cells*. American Journal of Physiology-Renal Physiology, 1990. **258**(4): p. F877-F882.
36. Takada, K., et al., *A humanized MDCK cell line for the efficient isolation and propagation of human influenza viruses*. Nature microbiology, 2019. **4**(8): p. 1268-1273.
37. Liu, J., et al., *Use of MDCK cells for production of live attenuated influenza vaccine*. Vaccine, 2009. **27**(46): p. 6460-6463.
38. Latorre, E., et al., *Active superelasticity in three-dimensional epithelia of controlled shape*. Nature, 2018. **563**(7730): p. 203-208.
39. Nielsen, R., et al., *Characterization of a kidney proximal tubule cell line, LLC-PK1, expressing endocytotic active megalin*. Journal of the American Society of Nephrology, 1998. **9**(10): p. 1767-1776.
40. Wohlwend, A., et al., *LLC-PK1 cells: cloning of phenotypically stable subpopulations*. American Journal of Physiology-Cell Physiology, 1986. **250**(5): p. C682-C687.
41. Iruela-Arispe, M.L. and G.J. Beitel, *Tubulogenesis*. Development, 2013. **140**(14): p. 2851-2855.
42. Campanale, J.P., T.Y. Sun, and D.J. Montell, *Development and dynamics of cell polarity at a glance*. Journal of cell science, 2017. **130**(7): p. 1201-1207.
43. Zhou, Q., et al., *TGF- $\beta$ -induced MiR-491-5p expression promotes Par-3 degradation in rat proximal tubular epithelial cells*. Journal of Biological Chemistry, 2010. **285**(51): p. 40019-40027.
44. Hurtado-Lorenzo, A., et al., *V-ATPase interacts with ARNO and Arf6 in early endosomes and regulates the protein degradative pathway*. Nature cell biology, 2006. **8**(2): p. 124-136.
45. Meder, D., et al., *Gp135/podocalyxin and NHERF-2 participate in the formation of a preapical domain during polarization of MDCK cells*. The Journal of cell biology, 2005. **168**(2): p. 303-313.

46. Ferrari, A., et al., *ROCK-mediated contractility, tight junctions and channels contribute to the conversion of a preapical patch into apical surface during isochoric lumen initiation*. Journal of cell science, 2008. **121**(21): p. 3649-3663.
47. Figueiredo, J., I. Bertels, and J. Gontijo. *Actin cytoskeletal and functional studies of the proximal convoluted tubules after preservation*. in *Transplantation proceedings*. 2008. Elsevier.
48. Yang, Z., et al., *De novo lumen formation and elongation in the developing nephron: a central role for afadin in apical polarity*. Development, 2013. **140**(8): p. 1774-1784.
49. Royer, C. and X. Lu, *Epithelial cell polarity: a major gatekeeper against cancer?* Cell Death & Differentiation, 2011. **18**(9): p. 1470-1477.
50. Gattineni, J. and M. Baum, *Developmental changes in renal tubular transport—an overview*. Pediatric nephrology, 2015. **30**(12): p. 2085-2098.
51. Evan, A.P., V. Gattone 2nd, and G.J. Schwartz, *Development of solute transport in rabbit proximal tubule. II. Morphologic segmentation*. American Journal of Physiology-Renal Physiology, 1983. **245**(3): p. F391-F407.
52. Haworth, J. and M.S. Macdonald, *Reducing sugars in the urine and blood of premature babies*. Archives of Disease in Childhood, 1957. **32**(165): p. 417.
53. Costantini, F. and R. Kopan, *Patterning a complex organ: branching morphogenesis and nephron segmentation in kidney development*. Developmental cell, 2010. **18**(5): p. 698-712.
54. Cheng, H.-T., et al.,  *$\gamma$ -Secretase activity is dispensable for mesenchyme-to-epithelium transition but required for podocyte and proximal tubule formation in developing mouse kidney*. 2003.
55. Cheng, H.-T., et al., *Notch2, but not Notch1, is required for proximal fate acquisition in the mammalian nephron*. 2007.
56. Suh, J.M., et al., *The expression profiles of nuclear receptors in the developing and adult kidney*. Molecular endocrinology, 2006. **20**(12): p. 3412-3420.
57. Kopan, R., H.-T. Cheng, and K. Surendran, *Molecular insights into segmentation along the proximal–distal axis of the nephron*. Journal of the American Society of Nephrology, 2007. **18**(7): p. 2014-2020.

58. Kobayashi, A., et al., *Distinct and sequential tissue-specific activities of the LIM-class homeobox gene Lim1 for tubular morphogenesis during kidney development*. 2005.
59. Hudes, G., et al., *Temsirolimus, interferon alfa, or both for advanced renal-cell carcinoma*. New England Journal of Medicine, 2007. **356**(22): p. 2271-2281.
60. Nakai, S., et al., *Crucial roles of Brn1 in distal tubule formation and function in mouse kidney*. 2003.
61. Neumann, K.H. and F. Rector, *Mechanism of NaCl and water reabsorption in the proximal convoluted tubule of rat kidney*. The Journal of clinical investigation, 1976. **58**(5): p. 1110-1118.
62. Alpern, R., K.J. Howlin, and P. Preisig, *Active and passive components of chloride transport in the rat proximal convoluted tubule*. The Journal of clinical investigation, 1985. **76**(4): p. 1360-1366.
63. Kokko, J.P., *Proximal tubule potential difference. Dependence on glucose, HCO<sub>3</sub>, and amino acids*. The Journal of clinical investigation, 1973. **52**(6): p. 1362-1367.
64. Barratt, L., et al., *Factors governing the transepithelial potential difference across the proximal tubule of the rat kidney*. The Journal of clinical investigation, 1974. **53**(2): p. 454-464.
65. Katz, A., A. Doucet, and F. Morel, *Na-K-ATPase activity along the rabbit, rat, and mouse nephron*. American Journal of Physiology-Renal Physiology, 1979. **237**(2): p. F114-F120.
66. Scherzer, P. and M.M. Popovtzer, *Segmental localization of mRNAs encoding Na-K-ATPase  $\alpha$ 1 and  $\beta$ 1 subunits in the diabetic rat kidneys using RT-PCR*. American Journal of Physiology-Renal Physiology, 2001.
67. Clapp, W.L., et al., *Segmental localization of mRNAs encoding Na<sup>+</sup>-K<sup>+</sup>-ATPase  $\alpha$ - and  $\beta$ -subunit isoforms in rat kidney using RT-PCR*. Kidney international, 1994. **46**(3): p. 627-638.
68. Salyer, S.A., et al., *Aldosterone regulates Na<sup>+</sup>, K<sup>+</sup> ATPase activity in human renal proximal tubule cells through mineralocorticoid receptor*. Biochimica et Biophysica Acta (BBA)-Molecular Cell Research, 2013. **1833**(10): p. 2143-2152.



69. Kashgarian, M., et al., *Monoclonal antibody to Na, K-ATPase: immunocytochemical localization along nephron segments*. *Kidney international*, 1985. **28**(6): p. 899-913.
70. Takada, T., et al., *Quantitative immunogold localization of Na, K-ATPase along rat nephron*. *Histochemistry*, 1992. **98**(3): p. 183-197.
71. Baum, M. and C. Berry, *Evidence for neutral transcellular NaCl transport and neutral basolateral chloride exit in the rabbit proximal convoluted tubule*. *The Journal of clinical investigation*, 1984. **74**(1): p. 205-211.
72. Berry, C.A. and F.C. Rector Jr, *Electroneutral NaCl absorption in the proximal tubule: mechanisms of apical Na-coupled transport*. *Kidney international*, 1989. **36**(3): p. 403-411.
73. Devuyst, O. and A. Luciani, *Chloride transporters and receptor-mediated endocytosis in the renal proximal tubule*. *The Journal of physiology*, 2015. **593**(18): p. 4151-4164.
74. Hamlyn, J. and M. Blaustein, *Sodium chloride, extracellular fluid volume, and blood pressure regulation*. *American Journal of Physiology-Renal Physiology*, 1986. **251**(4): p. F563-F575.
75. Planelles, G., *Chloride transport in the renal proximal tubule*. *Pflügers Archiv*, 2004. **448**(6): p. 561-570.
76. Petrovic, S., et al., *Identification of an apical exchanger in rat kidney proximal tubule*. *American Journal of Physiology-Cell Physiology*, 2003. **285**(3): p. C608-C617.
77. Karniski, L.P. and P.S. Aronson, *Anion exchange pathways for Cl-transport in rabbit renal microvillus membranes*. *American Journal of Physiology-Renal Physiology*, 1987. **253**(3): p. F513-F521.
78. Aronson, P.S. and G. Giebisch, *Mechanisms of chloride transport in the proximal tubule*. *American Journal of Physiology-Renal Physiology*, 1997. **273**(2): p. F179-F192.
79. Wang, T., et al., *Mechanisms of stimulation of proximal tubule chloride transport by formate and oxalate*. *American Journal of Physiology-Renal Physiology*, 1996. **271**(2): p. F446-F450.



80. Melo, Z., et al., *Molecular evidence for a role for K<sup>+</sup>-Cl<sup>-</sup> cotransporters in the kidney*. American Journal of Physiology-Renal Physiology, 2013. **305**(10): p. F1402-F1411.
81. Mercado, A., et al., *NH<sub>2</sub>-terminal heterogeneity in the KCC3 K<sup>+</sup>-Cl<sup>-</sup> cotransporter*. American Journal of Physiology-Renal Physiology, 2005. **289**(6): p. F1246-F1261.
82. Mount, D.B., et al., *Cloning and characterization of KCC3 and KCC4, new members of the cation-chloride cotransporter gene family*. Journal of Biological Chemistry, 1999. **274**(23): p. 16355-16362.
83. Kondo, Y. and E. Frömter, *Evidence of chloride/bicarbonate exchange mediating bicarbonate efflux from S3 segments of rabbit renal proximal tubule*. Pflügers Archiv, 1990. **415**(6): p. 726-733.
84. Edwards, J.C., *Chloride transport*. Comprehensive Physiology, 2011. **2**(2): p. 1061-1092.
85. Ledbetter, M.L.S. and M. Lubin, *Control of protein synthesis in human fibroblasts by intracellular potassium*. Experimental cell research, 1977. **105**(2): p. 223-236.
86. Lopez-Rivas, A., E.A. Adelberg, and E. Rozengurt, *Intracellular K<sup>+</sup> and the mitogenic response of 3T3 cells to peptide factors in serum-free medium*. Proceedings of the National Academy of Sciences, 1982. **79**(20): p. 6275-6279.
87. Burnell, J.M., et al., *THE EFFECT IN HUMANS OF EXTRACELLULAR p H CHANGE ON THE RELATIONSHIP BETWEEN SERUM POTASSIUM CONCENTRATION AND INTRACELLULAR POTASSIUM*. The Journal of clinical investigation, 1956. **35**(9): p. 935-939.
88. Völkl, H. and F. Lang, *Effect of potassium on cell volume regulation in renal straight proximal tubules*. The Journal of membrane biology, 1990. **117**(2): p. 113-122.
89. Kelley, S., R. Thomas, and P. Dunham, *Candidate inhibitor of the volume-sensitive kinase regulating K-Cl cotransport: the myosin light chain kinase inhibitor ML-7*. The Journal of membrane biology, 2000. **178**(1): p. 31-41.
90. Urrego, D., et al., *Potassium channels in cell cycle and cell proliferation*. Philosophical Transactions of the Royal Society B: Biological Sciences, 2014. **369**(1638): p. 20130094.

91. Kibble, J.D., et al., *Effect of barium on potassium diffusion across the proximal convoluted tubule of the anesthetized rat*. American Journal of Physiology-Renal Physiology, 1995. **268**(4): p. F778-F783.
92. Wilson, R., M. Wareing, and R. Green, *The role of active transport in potassium reabsorption in the proximal convoluted tubule of the anaesthetized rat*. The Journal of physiology, 1997. **500**(1): p. 155-164.
93. Wareing, M., et al., *Estimated potassium reflection coefficient in perfused proximal convoluted tubules of the anaesthetized rat in vivo*. The Journal of physiology, 1995. **488**(1): p. 153-161.
94. Shirley, D., et al., *Transepithelial electrochemical gradients in the proximal convoluted tubule during potassium depletion in the rat*. The Journal of physiology, 1998. **513**(2): p. 551-557.
95. Frömter, E. and K. Geßner, *Free-flow potential profile along rat kidney proximal tubule*. Pflügers Archiv, 1974. **351**(1): p. 69-83.
96. Weinstein, A.M., *Modeling the proximal tubule: complications of the paracellular pathway*. American Journal of Physiology-Renal Physiology, 1988. **254**(3): p. F297-F305.
97. Weinstein, A.M., *Convective paracellular solute flux. A source of ion-ion interaction in the epithelial transport equations*. The Journal of general physiology, 1987. **89**(3): p. 501-518.
98. Weinstein, A.M., *A mathematical model of the rat proximal tubule*. American Journal of Physiology-Renal Physiology, 1986. **250**(5): p. F860-F873.
99. Greger, R. and H. Gögelein, *Role of K<sup>+</sup> conductive pathways in the nephron*. Kidney international, 1987. **31**(5): p. 1055-1064.
100. Hebert, S.C., et al., *Molecular diversity and regulation of renal potassium channels*. Physiological reviews, 2005. **85**(1): p. 319-371.
101. Kawahara, K., *A stretch-activated K<sup>+</sup> channel in the basolateral membrane of Xenopus kidney proximal tubule cells*. Pflügers Archiv, 1990. **415**(5): p. 624-629.
102. Giebisch, G. and W. Wang, *Potassium transport: from clearance to channels and pumps*. Kidney international, 1996. **49**(6): p. 1624-1631.

103. Pravina, P., D. Sayaji, and M. Avinash, *Calcium and its role in human body*. International Journal of Research in Pharmaceutical and Biomedical Sciences, 2013. **4**(2): p. 659-668.
104. Duarte, C.G. and J.F. Watson, *Calcium reabsorption in proximal tubule of the dog nephron*. American Journal of Physiology-Legacy Content, 1967. **212**(6): p. 1355-1360.
105. Lassiter, W.E., C.W. Gottschalk, and M. Mylle, *Micropuncture study of renal tubular reabsorption of calcium in normal rodents*. American Journal of Physiology-Legacy Content, 1963. **204**(5): p. 771-775.
106. Bushinsky, D.A., *Contribution of intestine, bone, kidney, and dialysis to extracellular fluid calcium content*. Clinical Journal of the American Society of Nephrology, 2010. **5**(Supplement 1): p. S12-S22.
107. Rouse, D., R. Ng, and W.N. Suki, *Calcium transport in the pars recta and thin descending limb of Henle of the rabbit, perfused in vitro*. The Journal of clinical investigation, 1980. **65**(1): p. 37-42.
108. Ng, R., D. Rouse, and W.N. Suki, *Calcium transport in the rabbit superficial proximal convoluted tubule*. The Journal of clinical investigation, 1984. **74**(3): p. 834-842.
109. Agus, Z.S., et al., *Effects of parathyroid hormone on renal tubular reabsorption of calcium, sodium, and phosphate*. American Journal of Physiology-Legacy Content, 1973. **224**(5): p. 1143-1148.
110. Sutton, R. and J. Dirks, *The renal excretion of calcium: a review of micropuncture data*. Canadian journal of physiology and pharmacology, 1975. **53**(6): p. 979-988.
111. Schnermann, J., Y. Huang, and D. Mizel, *Fluid reabsorption in proximal convoluted tubules of mice with gene deletions of claudin-2 and/or aquaporin1*. American Journal of Physiology-Renal Physiology, 2013. **305**(9): p. F1352-F1364.
112. Muto, S., et al., *Claudin-2-deficient mice are defective in the leaky and cation-selective paracellular permeability properties of renal proximal tubules*. Proceedings of the National Academy of Sciences, 2010. **107**(17): p. 8011-8016.
113. Reilly, R.F., et al., *Immunolocalization of the Na<sup>+</sup>/Ca<sup>2+</sup> exchanger in rabbit kidney*. American Journal of Physiology-Renal Physiology, 1993. **265**(2): p. F327-F332.

114. Talor, Z. and J. Arruda, *Partial purification and reconstitution of renal basolateral Na<sup>+</sup>-Ca<sup>2+</sup> exchanger into liposomes*. Journal of Biological Chemistry, 1985. **260**(29): p. 15473-15476.
115. Gmaj, P., H. Murer, and R. Kinne, *Calcium ion transport across plasma membranes isolated from rat kidney cortex*. Biochemical Journal, 1979. **178**(3): p. 549-557.
116. Takeda, E., et al., *The regulation and function of phosphate in the human body*. Biofactors, 2004. **21**(1-4): p. 345-355.
117. Hamm, L.L., N. Nakhoul, and K.S. Hering-Smith, *Acid-base homeostasis*. Clinical Journal of the American Society of Nephrology, 2015. **10**(12): p. 2232-2242.
118. Strickler, J.C., et al., *Micropuncture study of inorganic phosphate excretion in the rat*. The Journal of clinical investigation, 1964. **43**(8): p. 1596-1607.
119. Dennis, V.W., P.B. Woodhall, and R.R. Robinson, *Characteristics of phosphate transport in isolated proximal tubule*. American Journal of Physiology-Legacy Content, 1976. **231**(3): p. 979-985.
120. McKEOWN, J.W., P.C. Brazy, and V.W. Dennis, *Intrarenal heterogeneity for fluid, phosphate, and glucose absorption in the rabbit*. American Journal of Physiology-Renal Physiology, 1979. **237**(4): p. F312-F318.
121. Baumann, K., et al., *Renal phosphate transport: inhomogeneity of local proximal transport rates and sodium dependence*. Pflügers Archiv, 1975. **356**(4): p. 287-297.
122. Hoffmann, N., M. Thees, and R. Kinne, *Phosphate transport by isolated renal brush border vesicles*. Pflügers Archiv, 1976. **362**(2): p. 147-156.
123. Cheng, L. and B. Sacktor, *Sodium gradient-dependent phosphate transport in renal brush border membrane vesicles*. Journal of Biological Chemistry, 1981. **256**(4): p. 1556-1564.
124. Picard, N., et al., *Acute parathyroid hormone differentially regulates renal brush border membrane phosphate cotransporters*. Pflügers Archiv-European Journal of Physiology, 2010. **460**(3): p. 677-687.
125. Villa-Bellosta, R., et al., *The Na<sup>+</sup>-Pi cotransporter PiT-2 (SLC20A2) is expressed in the apical membrane of rat renal proximal tubules and regulated by dietary Pi*. American Journal of Physiology-Renal Physiology, 2009. **296**(4): p. F691-F699.

126. Ravera, S., et al., *Deciphering PiT transport kinetics and substrate specificity using electrophysiology and flux measurements*. American Journal of Physiology-Cell Physiology, 2007. **293**(2): p. C606-C620.
127. Villa-Bellosta, R. and V. Sorribas, *Compensatory regulation of the sodium/phosphate cotransporters NaPi-IIc (SCL34A3) and Pit-2 (SLC20A2) during Pi deprivation and acidosis*. Pflügers Archiv-European Journal of Physiology, 2010. **459**(3): p. 499-508.
128. Nielsen, S., et al., *CHIP28 water channels are localized in constitutively water-permeable segments of the nephron*. Journal of Cell Biology, 1993. **120**(2): p. 371-383.
129. Segawa, H., et al., *Growth-related renal type II Na/Pi cotransporter*. Journal of Biological Chemistry, 2002. **277**(22): p. 19665-19672.
130. de la Horra, C., et al., *Molecular determinants of pH sensitivity of the type IIa Na/Pi cotransporter*. Journal of Biological Chemistry, 2000. **275**(9): p. 6284-6287.
131. Ullrich, K.J., G. Rumrich, and S. Klöss, *Phosphate transport in the proximal convolution of the rat kidney*. Pflügers Archiv, 1978. **377**(1): p. 33-42.
132. Schwab, S.J., S. Klahr, and M.R. Hammerman, *Na<sup>+</sup> gradient-dependent Pi uptake in basolateral membrane vesicles from dog kidney*. American Journal of Physiology-Renal Physiology, 1984. **246**(5): p. F663-F669.
133. Schwab, S.J., S. Klahr, and M.R. Hammerman, *Uptake of Pi in basolateral vesicles after release of unilateral ureteral obstruction*. American Journal of Physiology-Renal Physiology, 1984. **247**(4): p. F543-F547.
134. Goudsmit Jr, A., M.H. Power, and J.L. Bollman, *The excretion of sulfates by the dog*. American Journal of Physiology-Legacy Content, 1939. **125**(3): p. 506-520.
135. Lin, J.H. and G. Levy, *Renal clearance of inorganic sulfate in rats: Effect of acetaminophen-induced depletion of endogenous sulfate*. Journal of pharmaceutical sciences, 1983. **72**(3): p. 213-217.
136. Dudas, P.L. and J.L. Renfro, *Transepithelial sulfate transport by avian renal proximal tubule epithelium in primary culture*. American Journal of Physiology-Regulatory, Integrative and Comparative Physiology, 2002. **283**(6): p. R1354-R1361.

137. Turner, R.J., *Sodium-dependent sulfate transport in renal outer cortical brush border membrane vesicles*. American Journal of Physiology-Renal Physiology, 1984. **247**(5): p. F793-F798.
138. Schneider, E., J. Durham, and B. Sacktor, *Sodium-dependent transport of inorganic sulfate by rabbit renal brush-border membrane vesicles. Effects of other ions*. Journal of Biological Chemistry, 1984. **259**(23): p. 14591-14599.
139. Custer, M., H. Murer, and J. Biber, *Nephron localization of Na/SO<sub>4</sub><sup>2-</sup>-cotransport-related mRNA and protein*. Pflügers Archiv, 1994. **429**(2): p. 165-168.
140. Biber, J., et al., *Immunolocalization of Na/SO<sub>4</sub>-cotransport (NaSi-1) in rat kidney*. Pflügers Archiv, 1996. **432**(3): p. 373-378.
141. Busch, A.E., et al., *Electrogenic cotransport of Na<sup>+</sup> and sulfate in Xenopus oocytes expressing the cloned Na<sup>+</sup> SO<sub>4</sub><sup>(2-)</sup> transport protein NaSi-1*. Journal of Biological Chemistry, 1994. **269**(17): p. 12407-12409.
142. Krick, W., et al., *Ability of sat-1 to transport sulfate, bicarbonate, or oxalate under physiological conditions*. American Journal of Physiology-Renal Physiology, 2009. **297**(1): p. F145-F154.
143. Wolf, F.I. and V. Trapani, *Cell (patho) physiology of magnesium*. Clinical science, 2008. **114**(1): p. 27-35.
144. Le Grimellec, C., et al., *Simultaneous Mg, Ca, P, K, Na and Cl analysis in rat tubular fluid*. Pflügers Archiv, 1973. **340**(3): p. 181-196.
145. Wong, N., J.H. Dirks, and G.A. Quamme, *Tubular reabsorptive capacity for magnesium in the dog kidney*. American Journal of Physiology-Renal Physiology, 1983. **244**(1): p. F78-F83.
146. Poujeol, P., et al., *Influence of extracellular fluid volume expansion on magnesium, calcium and phosphate handling along the rat nephron*. Pflügers Archiv, 1976. **365**(2): p. 203-211.
147. Quamme, G.A. and C.M. Smith, *Magnesium transport in the proximal straight tubule of the rabbit*. American Journal of Physiology-Renal Physiology, 1984. **246**(5): p. F544-F550.



148. Quamme, G. and J. Dirks, *Intraluminal and contraluminal magnesium on magnesium and calcium transfer in the rat nephron*. American Journal of Physiology-Renal Physiology, 1980. **238**(3): p. F187-F198.
149. Santella, R.N., F.J. Gennari, and D.A. Maddox, *Metabolic acidosis stimulates bicarbonate reabsorption in the early proximal tubule*. American Journal of Physiology-Renal Physiology, 1989. **257**(1): p. F35-F42.
150. Amemiya, M., et al., *Expression of NHE-3 in the apical membrane of rat renal proximal tubule and thick ascending limb*. Kidney international, 1995. **48**(4): p. 1206-1215.
151. Biemesderfer, D., et al., *NHE3: a Na<sup>+</sup>/H<sup>+</sup> exchanger isoform of renal brush border*. American Journal of Physiology-Renal Physiology, 1993. **265**(5): p. F736-F742.
152. Schultheis, P.J., et al., *Renal and intestinal absorptive defects in mice lacking the NHE3 Na<sup>+</sup>/H<sup>+</sup> exchanger*. Nature genetics, 1998. **19**(3): p. 282-285.
153. Kinne-Saffran, E., R. Beauwens, and R. Kinne, *An ATP-driven proton pump in brush-border membranes from rat renal cortex*. The Journal of membrane biology, 1982. **64**(1): p. 67-76.
154. Kurtz, I., *Apical Na<sup>+</sup>/H<sup>+</sup> antiporter and glycolysis-dependent H<sup>+</sup>-ATPase regulate intracellular pH in the rabbit S3 proximal tubule*. The Journal of clinical investigation, 1987. **80**(4): p. 928-935.
155. Maunsbach, A.B., et al., *Immunoelectron microscopic localization of the electrogenic Na/HCO<sub>3</sub> cotransporter in rat and ambystoma kidney*. Journal of the American Society of Nephrology, 2000. **11**(12): p. 2179-2189.
156. Schwartz, G.J., et al., *Carbon dioxide permeability of rabbit proximal convoluted tubules*. American Journal of Physiology-Renal Physiology, 1981. **240**(3): p. F231-F244.
157. Lucci, M.S., et al., *Direct evaluation of the permeability of the rat proximal convoluted tubule to CO<sub>2</sub>*. American Journal of Physiology-Renal Physiology, 1982. **242**(5): p. F470-F476.
158. Meldrum, N.U. and F.J. Roughton, *Carbonic anhydrase. Its preparation and properties*. The Journal of physiology, 1933. **80**(2): p. 113-142.

159. Brown, D., X.L. Zhu, and W.S. Sly, *Localization of membrane-associated carbonic anhydrase type IV in kidney epithelial cells*. Proceedings of the National Academy of Sciences, 1990. **87**(19): p. 7457-7461.
160. Purkerson, J., A. Kittelberger, and G. Schwartz, *Basolateral carbonic anhydrase IV in the proximal tubule is a glycosylphosphatidylinositol-anchored protein*. Kidney international, 2007. **71**(5): p. 407-416.
161. Krapf, R., et al., *Basolateral membrane Na/base cotransport is dependent on CO<sub>2</sub>/HCO<sub>3</sub> in the proximal convoluted tubule*. The Journal of general physiology, 1987. **90**(6): p. 833-853.
162. Musa-Aziz, R., R. Occhipinti, and W.F. Boron, *Evidence from simultaneous intracellular-and surface-pH transients that carbonic anhydrase II enhances CO<sub>2</sub> fluxes across Xenopus oocyte plasma membranes*. American Journal of Physiology-Cell Physiology, 2014. **307**(9): p. C791-C813.
163. Kaunisto, K., et al., *Carbonic anhydrase XIV: luminal expression suggests key role in renal acidification*. Kidney international, 2002. **61**(6): p. 2111-2118.
164. Kyllönen, M.S., et al., *Localization of carbonic anhydrase XII to the basolateral membrane of H<sup>+</sup>-secreting cells of mouse and rat kidney*. Journal of Histochemistry & Cytochemistry, 2003. **51**(9): p. 1217-1224.
165. Preisig, P.A. and R. Alpern, *Contributions of cellular leak pathways to net NaHCO<sub>3</sub> and NaCl absorption*. The Journal of clinical investigation, 1989. **83**(6): p. 1859-1867.
166. Mergenthaler, P., et al., *Sugar for the brain: the role of glucose in physiological and pathological brain function*. Trends in neurosciences, 2013. **36**(10): p. 587-597.
167. Barfuss, D.W. and J.A. Schafer, *Differences in active and passive glucose transport along the proximal nephron*. American Journal of Physiology-Renal Physiology, 1981. **241**(3): p. F322-F332.
168. Frohnert, P.P., et al., *Free flow micropuncture studies of glucose transport in the rat nephron*. Pflügers Archiv: European Journal of Physiology, 1970. **315**(1): p. 66-85.



169. Turner, R.J. and A. Moran, *Further studies of proximal tubular brush border membrane D-glucose transport heterogeneity*. The Journal of membrane biology, 1982. **70**(1): p. 37-45.
170. Hediger, M.A., et al., *Expression cloning and cDNA sequencing of the Na<sup>+</sup>/glucose co-transporter*. Nature, 1987. **330**(6146): p. 379-381.
171. Kanai, Y., et al., *The human kidney low affinity Na<sup>+</sup>/glucose cotransporter SGLT2. Delineation of the major renal reabsorptive mechanism for D-glucose*. The Journal of clinical investigation, 1994. **93**(1): p. 397-404.
172. Powell, D.R., et al., *Improved glycemic control in mice lacking Sglt1 and Sglt2*. American Journal of Physiology-Endocrinology and Metabolism, 2013.
173. Sala-Rabanal, M., et al., *Revisiting the physiological roles of SGLTs and GLUTs using positron emission tomography in mice*. The Journal of physiology, 2016. **594**(15): p. 4425-4438.
174. Benam, K.H., et al., *Engineered in vitro disease models*. Annual Review of Pathology: Mechanisms of Disease, 2015. **10**: p. 195-262.
175. Khademhosseini, A. and R. Langer, *A decade of progress in tissue engineering*. Nature protocols, 2016. **11**(10): p. 1775-1781.
176. Yu, P., et al., *Drug-Induced Nephrotoxicity Assessment in 3D Cellular Models*. Micromachines, 2021. **13**(1): p. 3.
177. Fransen, M.F., et al., *Bioprinting of kidney in vitro models: cells, biomaterials, and manufacturing techniques*. Essays in Biochemistry, 2021. **65**(3): p. 587-602.
178. Manley, B.J. and A.A. Hakimi, *Molecular profiling of renal cell carcinoma: Building a bridge towards clinical impact*. Current opinion in urology, 2016. **26**(5): p. 383.
179. Yusenko, M.V., et al., *High-resolution DNA copy number and gene expression analyses distinguish chromophobe renal cell carcinomas and renal oncocytomas*. BMC cancer, 2009. **9**(1): p. 1-10.
180. Ricketts, C.J., et al., *The cancer genome atlas comprehensive molecular characterization of renal cell carcinoma*. Cell reports, 2018. **23**(1): p. 313-326. e5.
181. Network, C.G.A.R., *Comprehensive molecular characterization of papillary renal-cell carcinoma*. New England Journal of Medicine, 2016. **374**(2): p. 135-145.

182. Mitchell, T.J., et al., *Timing the landmark events in the evolution of clear cell renal cell cancer: TRACERx renal*. Cell, 2018. **173**(3): p. 611-623. e17.
183. Zhang, Q. and H. Yang, *The roles of VHL-dependent ubiquitination in signaling and cancer*. Frontiers in oncology, 2012. **2**: p. 35.
184. Hakimi, A.A., et al., *Clinical and pathologic impact of select chromatin-modulating tumor suppressors in clear cell renal cell carcinoma*. European urology, 2013. **63**(5): p. 848-854.
185. Varela, I., et al., *Exome sequencing identifies frequent mutation of the SWI/SNF complex gene PBRM1 in renal carcinoma*. Nature, 2011. **469**(7331): p. 539-542.
186. Dalgliesh, G.L., et al., *Systematic sequencing of renal carcinoma reveals inactivation of histone modifying genes*. Nature, 2010. **463**(7279): p. 360-363.
187. Peña-Llopis, S., et al., *BAP1 loss defines a new class of renal cell carcinoma*. Nature genetics, 2012. **44**(7): p. 751-759.
188. Manley, B.J., et al., *Integration of recurrent somatic mutations with clinical outcomes: a pooled analysis of 1049 patients with clear cell renal cell carcinoma*. European urology focus, 2017. **3**(4-5): p. 421-427.
189. Eckel-Passow, J.E., et al., *BAP1 and PBRM1 in metastatic clear cell renal cell carcinoma: tumor heterogeneity and concordance with paired primary tumor*. BMC urology, 2017. **17**(1): p. 1-7.
190. Joseph, R.W., et al., *Loss of BAP1 protein expression is an independent marker of poor prognosis in patients with low-risk clear cell renal cell carcinoma*. Cancer, 2014. **120**(7): p. 1059-1067.
191. Ricketts, C.J. and W.M. Linehan, *Multi-regional sequencing elucidates the evolution of clear cell renal cell carcinoma*. Cell, 2018. **173**(3): p. 540-542.
192. Hou, W. and Z. Ji, *Generation of autochthonous mouse models of clear cell renal cell carcinoma: mouse models of renal cell carcinoma*. Experimental & molecular medicine, 2018. **50**(4): p. 1-10.
193. Gu, Y.-F., et al., *Modeling renal cell carcinoma in mice: Bap1 and Pbrm1 inactivation drive tumor grade*. Cancer discovery, 2017. **7**(8): p. 900-917.
194. Nargund, A.M., et al., *The SWI/SNF protein PBRM1 restrains VHL-loss-driven clear cell renal cell carcinoma*. Cell reports, 2017. **18**(12): p. 2893-2906.

195. Harlander, S., et al., *Combined mutation in Vhl, Trp53 and Rb1 causes clear cell renal cell carcinoma in mice*. Nature medicine, 2017. **23**(7): p. 869-877.
196. Bailey, S.T., et al., *MYC activation cooperates with Vhl and Ink4a/Arf loss to induce clear cell renal cell carcinoma*. Nature communications, 2017. **8**(1): p. 1-12.
197. Schokrpur, S., et al., *CRISPR-mediated VHL knockout generates an improved model for metastatic renal cell carcinoma*. Scientific reports, 2016. **6**(1): p. 1-13.
198. Allard, C.B., et al. *Contemporary trends in high-dose interleukin-2 use for metastatic renal cell carcinoma in the United States*. in *Urologic Oncology: Seminars and Original Investigations*. 2015. Elsevier.
199. Vachhani, P. and S. George, *VEGF inhibitors in renal cell carcinoma*. Clin Adv Hematol Oncol, 2016. **14**(12): p. 1016-28.
200. Margolin, K.A. *Interleukin-2 in the treatment of renal cancer*. in *Seminars in oncology*. 2000.
201. Eklund, J.W. and T.M. Kuzel, *Interleukin-2 in the treatment of renal cell carcinoma and malignant melanoma*. Cytokines and Cancer, 2005: p. 263-287.
202. Khetani, V.V., et al., *Combination drug regimens for metastatic clear cell renal cell carcinoma*. World Journal of Clinical Oncology, 2020. **11**(8): p. 541.
203. Sternberg, C.N., et al., *A randomised, double-blind phase III study of pazopanib in patients with advanced and/or metastatic renal cell carcinoma: final overall survival results and safety update*. European journal of cancer, 2013. **49**(6): p. 1287-1296.
204. Motzer, R.J., et al., *Overall survival and updated results for sunitinib compared with interferon alfa in patients with metastatic renal cell carcinoma*. Journal of clinical oncology, 2009. **27**(22): p. 3584.
205. Hutson, T.E., et al., *Axitinib versus sorafenib in first-line metastatic renal cell carcinoma: overall survival from a randomized phase III trial*. Clinical genitourinary cancer, 2017. **15**(1): p. 72-76.
206. Choueiri, T.K., et al., *Cabozantinib versus sunitinib as initial targeted therapy for patients with metastatic renal cell carcinoma of poor or intermediate risk: the alliance A031203 CABOSUN trial*. Journal of Clinical Oncology, 2017. **35**(6): p. 591.

207. Hainsworth, J.D., et al., *Pazopanib as second-line treatment after sunitinib or bevacizumab in patients with advanced renal cell carcinoma: a Sarah Cannon Oncology Research Consortium Phase II Trial*. *Clinical genitourinary cancer*, 2013. **11**(3): p. 270-275.
208. Motzer, R.J., et al., *Axitinib versus sorafenib as second-line treatment for advanced renal cell carcinoma: overall survival analysis and updated results from a randomised phase 3 trial*. *The Lancet Oncology*, 2013. **14**(6): p. 552-562.
209. Escudier, B., *TARGET Study Group*. *Sorafenib in advanced clear-cell renal-cell carcinoma*. *N. Engl. J. Med.*, 2007. **357**: p. 203.
210. Hutson, T.E., et al., *Randomized phase III trial of temsirolimus versus sorafenib as second-line therapy after sunitinib in patients with metastatic renal cell carcinoma*. *Journal of clinical oncology*, 2014. **32**(8): p. 760.
211. Escudier, B., et al., *CheckMate 025 randomized phase 3 study: outcomes by key baseline factors and prior therapy for nivolumab versus everolimus in advanced renal cell carcinoma*. *European urology*, 2017. **72**(6): p. 962-971.
212. Motzer, R.J., et al., *Phase 3 trial of everolimus for metastatic renal cell carcinoma: final results and analysis of prognostic factors*. *Cancer*, 2010. **116**(18): p. 4256-4265.
213. Motzer, R.J., et al., *Efficacy of everolimus in advanced renal cell carcinoma: a double-blind, randomised, placebo-controlled phase III trial*. *The Lancet*, 2008. **372**(9637): p. 449-456.
214. Escudier, B., et al., *Bevacizumab plus interferon alfa-2a for treatment of metastatic renal cell carcinoma: a randomised, double-blind phase III trial*. *The Lancet*, 2007. **370**(9605): p. 2103-2111.
215. Rini, B.I., et al., *Phase III trial of bevacizumab plus interferon alfa versus interferon alfa monotherapy in patients with metastatic renal cell carcinoma: final results of CALGB 90206*. *Journal of clinical oncology*, 2010. **28**(13): p. 2137.
216. Motzer, R., et al., *CheckMate 214 investigators*. *Nivolumab plus ipilimumab versus sunitinib in first-line treatment for advanced renal cell carcinoma: extended follow-up of efficacy and safety results from a randomised, controlled, phase 3 trial*. *Lancet Oncol*, 2019. **20**(10): p. 1370-1385.

217. Rini, B.I., et al., *Pembrolizumab plus axitinib versus sunitinib for advanced renal-cell carcinoma*. New England Journal of Medicine, 2019. **380**(12): p. 1116-1127.
218. Motzer, R.J., et al., *Avelumab plus axitinib versus sunitinib for advanced renal-cell carcinoma*. New England Journal of Medicine, 2019. **380**(12): p. 1103-1115.
219. Motzer, R.J., et al., *Lenvatinib, everolimus, and the combination in patients with metastatic renal cell carcinoma: a randomised, phase 2, open-label, multicentre trial*. The lancet oncology, 2015. **16**(15): p. 1473-1482.
220. Feldman, D.R., et al., *Phase I trial of bevacizumab plus escalated doses of sunitinib in patients with metastatic renal cell carcinoma*. Journal of clinical oncology, 2009. **27**(9): p. 1432.
221. Rini, B.I., et al., *Phase 1 dose-escalation trial of tremelimumab plus sunitinib in patients with metastatic renal cell carcinoma*. Cancer, 2011. **117**(4): p. 758-767.
222. Harzstark, A.L., et al., *A phase 1 study of everolimus and sorafenib for metastatic clear cell renal cell carcinoma*. Cancer, 2011. **117**(18): p. 4194-4200.
223. Hainsworth, J.D., et al., *Phase II trial of bevacizumab and everolimus in patients with advanced renal cell carcinoma*. Journal of clinical oncology, 2010. **28**(13): p. 2131-2136.
224. Shin, D., et al., *Papain-like protease regulates SARS-CoV-2 viral spread and innate immunity*. Nature, 2020. **587**(7835): p. 657-662.
225. Cereijido, M., et al., *Role of tight junctions in establishing and maintaining cell polarity*. Annual Review of Physiology, 1998. **60**(1): p. 161-177.
226. Fountain, J.H. and S.L. Lappin, *Physiology, renin angiotensin system*. 2017.
227. Bröer, S., *The role of the neutral amino acid transporter B0AT1 (SLC6A19) in Hartnup disorder and protein nutrition*. IUBMB life, 2009. **61**(6): p. 591-599.
228. Nickel, C., et al., *The polycystin-1 C-terminal fragment triggers branching morphogenesis and migration of tubular kidney epithelial cells*. The Journal of clinical investigation, 2002. **109**(4): p. 481-489.
229. Raghavan, V. and O.A. Weisz, *Flow stimulated endocytosis in the proximal tubule*. Current opinion in nephrology and hypertension, 2015. **24**(4): p. 359.
230. Sun, X. and P.D. Kaufman, *Ki-67: more than a proliferation marker*. Chromosoma, 2018. **127**(2): p. 175-186.

231. Gavet, O. and J. Pines, *Activation of cyclin B1–Cdk1 synchronizes events in the nucleus and the cytoplasm at mitosis*. Journal of Cell Biology, 2010. **189**(2): p. 247-259.
232. Robbins, J.A. and F.R. Cross, *Regulated degradation of the APC coactivator Cdc20*. Cell division, 2010. **5**(1): p. 1-9.
233. Gewin, L.S., *Sugar or Fat? Renal Tubular Metabolism Reviewed in Health and Disease*. Nutrients, 2021. **13**(5): p. 1580.
234. Bhargava, P. and R.G. Schnellmann, *Mitochondrial energetics in the kidney*. Nature Reviews Nephrology, 2017. **13**(10): p. 629-646.
235. Clausen, M.V., F. Hilbers, and H. Poulsen, *The structure and function of the Na, K-ATPase isoforms in health and disease*. Frontiers in physiology, 2017. **8**: p. 371.
236. Hara-Chikuma, M. and A. Verkman, *Aquaporin-1 facilitates epithelial cell migration in kidney proximal tubule*. Journal of the American Society of Nephrology, 2006. **17**(1): p. 39-45.
237. Porazinski, S., et al., *YAP is essential for tissue tension to ensure vertebrate 3D body shape*. Nature, 2015. **521**(7551): p. 217-221.
238. Song, Y., et al., *Ezrin mediates invasion and metastasis in tumorigenesis: A review*. Frontiers in Cell and Developmental Biology, 2020: p. 1321.
239. Hatano, R., et al., *Ezrin, a membrane cytoskeletal cross-linker, is essential for the regulation of phosphate and calcium homeostasis*. Kidney international, 2013. **83**(1): p. 41-49.
240. Karantza, V., *Keratins in health and cancer: more than mere epithelial cell markers*. Oncogene, 2011. **30**(2): p. 127-138.
241. Marusyk, A. and K. Polyak, *Tumor heterogeneity: causes and consequences*. Biochimica et Biophysica Acta (BBA)-Reviews on Cancer, 2010. **1805**(1): p. 105-117.
242. Odenwald, M.A., et al., *ZO-1 interactions with F-actin and occludin direct epithelial polarization and single lumen specification in 3D culture*. Journal of cell science, 2017. **130**(1): p. 243-259.



243. Rajasekaran, S.A., K.W. Beyenbach, and A.K. Rajasekaran, *Interactions of tight junctions with membrane channels and transporters*. Biochimica et Biophysica Acta (BBA)-Biomembranes, 2008. **1778**(3): p. 757-769.
244. Sirohi, D., et al., *Histologic Growth Patterns in Clear Cell Renal Cell Carcinoma Stratify Patients into Survival Risk Groups*. Clinical Genitourinary Cancer, 2022. **20**(3): p. e233-e243.
245. Kita, K., et al., *Cytoskeletal Actin Structure in Osteosarcoma Cells Determines Metastatic Phenotype via Regulating Cell Stiffness, Migration, and Transmigration*. Current Issues in Molecular Biology, 2021. **43**(3): p. 1255-1266.
246. Gandalovičová, A., et al., *Cell polarity signaling in the plasticity of cancer cell invasiveness*. Oncotarget, 2016. **7**(18): p. 25022.
247. Wan, S., et al., *Cytoplasmic localization of the cell polarity factor scribble supports liver tumor formation and tumor cell invasiveness*. Hepatology, 2018. **67**(5): p. 1842-1856.
248. Saito, Y., et al., *LLGL2 rescues nutrient stress by promoting leucine uptake in ER+ breast cancer*. Nature, 2019. **569**(7755): p. 275-279.
249. Santorelli, L., et al., *Does the Urinary Proteome Reflect ccRCC Stage and Grade Progression?* Diagnostics, 2021. **11**(12): p. 2369.
250. He, S., et al., *PODXL might be a new prognostic biomarker in various cancers: a meta-analysis and sequential verification with TCGA datasets*. BMC cancer, 2020. **20**(1): p. 1-13.
251. Tabariès, S., et al., *Afadin cooperates with Claudin-2 to promote breast cancer metastasis*. Genes & development, 2019. **33**(3-4): p. 180-193.
252. Centonze, M., C. Saponaro, and A. Mangia, *NHERF1 between promises and hopes: overview on cancer and prospective openings*. Translational oncology, 2018. **11**(2): p. 374-390.
253. Qin, J., et al., *BAP1 promotes breast cancer cell proliferation and metastasis by deubiquitinating KLF5*. Nature communications, 2015. **6**(1): p. 1-12.
254. Wang, F., et al., *BAP1 promotes viability and migration of ECA109 cells through KLF5/CyclinD1/FGF-BP1*. FEBS open bio, 2021. **11**(5): p. 1497-1503.

255. Osanai, M., et al., *Epigenetic silencing of occludin promotes tumorigenic and metastatic properties of cancer cells via modulations of unique sets of apoptosis-associated genes*. *Cancer research*, 2006. **66**(18): p. 9125-9133.
256. Lennartz, M., et al. *Reduced CDH16 expression is linked to poor prognosis in clear cell renal cell carcinoma* 16. in *Urologic Oncology: Seminars and Original Investigations*. 2022. Elsevier.
257. Strauss, P., et al., *A multiomics disease progression signature of low-risk ccRCC*. *Scientific Reports*, 2022. **12**(1): p. 1-15.
258. Hirano, T., et al., *FARP1 boosts CDC42 activity from integrin  $\alpha\beta 5$  signaling and correlates with poor prognosis of advanced gastric cancer*. *Oncogenesis*, 2020. **9**(2): p. 1-14.
259. Xie, J., et al., *Fibronectin enhances tumor metastasis through B7-H3 in clear cell renal cell carcinoma*. *FEBS Open bio*, 2021. **11**(11): p. 2977-2987.
260. Fife, C., J. McCarroll, and M. Kavallaris, *Movers and shakers: cell cytoskeleton in cancer metastasis*. *British journal of pharmacology*, 2014. **171**(24): p. 5507-5523.
261. Antonipillai, J., *Cytoskeletal molecules play a major role in cancer progression*. *ARCHIVOS DE MEDICINA*, 2017. **2**(2): p. 9.
262. Perrin, B.J. and J.M. Ervasti, *The actin gene family: function follows isoform*. *Cytoskeleton*, 2010. **67**(10): p. 630-634.
263. Ni, W.-D., et al., *Tenascin-C is a potential cancer-associated fibroblasts marker and predicts poor prognosis in prostate cancer*. *Biochemical and biophysical research communications*, 2017. **486**(3): p. 607-612.
264. Topalov, N.E., et al., *Actin Beta-Like 2 as a new mediator of proliferation and migration in epithelial ovarian cancer*. *Frontiers in oncology*, 2021. **11**.
265. Ghazanfar, S., et al., *Identification of actin beta-like 2 (ACTBL2) as novel, upregulated protein in colorectal cancer*. *Journal of proteomics*, 2017. **152**: p. 33-40.
266. Pollard, T.D. and C.C. Beltzner, *Structure and function of the Arp2/3 complex*. *Current opinion in structural biology*, 2002. **12**(6): p. 768-774.
267. Pizarro-Cerdá, J., et al., *The diverse family of Arp2/3 complexes*. *Trends in cell biology*, 2017. **27**(2): p. 93-100.



268. Lan, D., et al., *MiR-133a is downregulated in non-small cell lung cancer: a study of clinical significance*. European journal of medical research, 2015. **20**(1): p. 1-8.
269. Hedman, A.C., J.M. Smith, and D.B. Sacks, *The biology of IQGAP proteins: beyond the cytoskeleton*. EMBO reports, 2015. **16**(4): p. 427-446.
270. Lin, X., et al., *Construction of a novel multigene panel potentially predicting poor prognosis in patients with clear cell renal cell carcinoma*. Cancers, 2020. **12**(11): p. 3471.
271. White, C.D., et al., *IQGAP1 and IQGAP2 are reciprocally altered in hepatocellular carcinoma*. BMC gastroenterology, 2010. **10**(1): p. 1-10.
272. Kumar, D., et al., *Reduced expression of IQGAP2 and higher expression of IQGAP3 correlates with poor prognosis in cancers*. PloS one, 2017. **12**(10): p. e0186977.
273. Titus, M.A., *Myosin-driven intracellular transport*. Cold Spring Harbor Perspectives in Biology, 2018. **10**(3): p. a021972.
274. Herrmann, H. and U. Aebi, *Intermediate filaments: structure and assembly*. Cold Spring Harbor Perspectives in Biology, 2016. **8**(11): p. a018242.
275. Usman, S., et al., *Vimentin is at the heart of epithelial mesenchymal transition (EMT) mediated metastasis*. Cancers, 2021. **13**(19): p. 4985.
276. Haines, R.L. and E.B. Lane, *Keratins and disease at a glance*. Journal of cell science, 2012. **125**(17): p. 3923-3928.
277. Sakakibara, H. and K. Oiwa, *Molecular organization and force-generating mechanism of dynein*. The FEBS journal, 2011. **278**(17): p. 2964-2979.
278. Hirokawa, N. and R. Takemura, *Kinesin superfamily proteins and their various functions and dynamics*. Experimental cell research, 2004. **301**(1): p. 50-59.
279. Rath, O. and F. Kozielski, *Kinesins and cancer*. Nature reviews cancer, 2012. **12**(8): p. 527-539.
280. Li, X., et al., *Prognostic significance of KIF2A and KIF20A expression in human cancer: A systematic review and meta-analysis*. Medicine, 2019. **98**(46).
281. Zhang, X., et al., *KIF2A promotes the progression via AKT signaling pathway and is upregulated by transcription factor ETV4 in human gastric cancer*. Biomedicine & Pharmacotherapy, 2020. **125**: p. 109840.

282. Matthews, H.K., C. Bertoli, and R.A. de Bruin, *Cell cycle control in cancer*. Nature Reviews Molecular Cell Biology, 2022. **23**(1): p. 74-88.
283. Peissert, S., et al., *Structural basis for CDK7 activation by MAT1 and Cyclin H*. Proceedings of the National Academy of Sciences, 2020. **117**(43): p. 26739-26748.
284. Kraft, C., et al., *Mitotic regulation of the human anaphase-promoting complex by phosphorylation*. The EMBO journal, 2003. **22**(24): p. 6598-6609.
285. Kazemi-Sefat, G.E., et al., *The importance of CDC27 in cancer: molecular pathology and clinical aspects*. Cancer cell international, 2021. **21**(1): p. 1-11.
286. Cardano, M., C. Tribioli, and E. Prosperi, *Targeting proliferating cell nuclear antigen (PCNA) as an effective strategy to inhibit tumor cell proliferation*. Current Cancer Drug Targets, 2020. **20**(4): p. 240-252.
287. Xu, H., et al., *Enhanced RAD21 cohesin expression confers poor prognosis and resistance to chemotherapy in high grade luminal, basal and HER2 breast cancers*. Breast Cancer Research, 2011. **13**(1): p. 1-10.
288. Thompson, L.L., et al., *Aberrant SKP1 Expression: Diverse Mechanisms Impacting Genome and Chromosome Stability*. Frontiers in Cell and Developmental Biology, 2022: p. 529.
289. Ghiselli, G., *SMC3 knockdown triggers genomic instability and p53-dependent apoptosis in human and zebrafish cells*. Molecular Cancer, 2006. **5**(1): p. 1-13.
290. Pinto, M., et al., *Overexpression of the mitotic checkpoint genes BUB1 and BUBR1 is associated with genomic complexity in clear cell kidney carcinomas*. Analytical Cellular Pathology, 2008. **30**(5): p. 389-395.
291. Yu, F.-X. and K.-L. Guan, *The Hippo pathway: regulators and regulations*. Genes & development, 2013. **27**(4): p. 355-371.
292. Schütte, U., et al., *Hippo signaling mediates proliferation, invasiveness, and metastatic potential of clear cell renal cell carcinoma*. Translational oncology, 2014. **7**(2): p. 309-321.
293. Genevet, A. and N. Tapon, *The Hippo pathway and apico-basal cell polarity*. Biochemical Journal, 2011. **436**(2): p. 213-224.

294. Zhao, B., K. Tumaneng, and K.-L. Guan, *The Hippo pathway in organ size control, tissue regeneration and stem cell self-renewal*. Nature cell biology, 2011. **13**(8): p. 877-883.
295. Guo, Y.J., et al., *ERK/MAPK signalling pathway and tumorigenesis*. Experimental and therapeutic medicine, 2020. **19**(3): p. 1997-2007.
296. Song, M., et al., *AKT as a Therapeutic Target for CancerChallenging Cancer Therapy by Targeting AKT*. Cancer research, 2019. **79**(6): p. 1019-1031.
297. Yuan, L., et al., *Identification of key genes and pathways in human clear cell renal cell carcinoma (ccRCC) by co-expression analysis*. International Journal of Biological Sciences, 2018. **14**(3): p. 266.
298. Pantsar, T., *The current understanding of KRAS protein structure and dynamics*. Computational and structural biotechnology journal, 2020. **18**: p. 189-198.
299. Wei, X., et al., *Redox Metabolism-Associated Molecular Classification of Clear Cell Renal Cell Carcinoma*. Oxidative medicine and cellular longevity, 2022. **2022**.
300. Gawecka, J.E., et al., *R-Ras regulates migration through an interaction with filamin A in melanoma cells*. PloS one, 2010. **5**(6): p. e11269.
301. Flex, E., et al., *Activating mutations in RRAS underlie a phenotype within the RASopathy spectrum and contribute to leukaemogenesis*. Human molecular genetics, 2014. **23**(16): p. 4315-4327.
302. Zhang, R.-L., et al., *RASA1 inhibits the progression of renal cell carcinoma by decreasing the expression of miR-223-3p and promoting the expression of FBXW7*. Bioscience reports, 2020. **40**(7).
303. Wang, S., Z.-h. Yu, and K.-q. Chai, *Identification of EGFR as a novel key gene in clear cell renal cell carcinoma (ccRCC) through bioinformatics analysis and meta-analysis*. BioMed research international, 2019. **2019**.
304. Giubellino, A., T.R. Burke, and D.P. Bottaro, *Grb2 signaling in cell motility and cancer*. Expert opinion on therapeutic targets, 2008. **12**(8): p. 1021-1033.
305. Green, Y.S., et al., *Hypoxia-Associated Factor (HAF) Mediates Neurofibromin Ubiquitination and Degradation Leading to Ras–ERK Pathway Activation in HypoxiaHAF Degrades Neurofibromin and Activates Ras–ERK in Hypoxia*. Molecular Cancer Research, 2019. **17**(5): p. 1220-1232.

306. Padua, D. and J. Massagué, *Roles of TGF $\beta$  in metastasis*. Cell research, 2009. **19**(1): p. 89-102.
307. Parker, A.S., et al., *Lower expression levels of the transforming growth factor beta receptor type II protein are associated with a less aggressive tumor phenotype and improved survival among patients with clear cell renal cell carcinoma*. Human pathology, 2007. **38**(3): p. 453-461.
308. Pizzagalli, M.D., A. Bensimon, and G. Superti-Furga, *A guide to plasma membrane solute carrier proteins*. The FEBS journal, 2021. **288**(9): p. 2784-2835.
309. Winter, S., et al., *Methylomes of renal cell lines and tumors or metastases differ significantly with impact on pharmacogenes*. Scientific reports, 2016. **6**(1): p. 1-15.
310. Caron, L., et al., *Cloning and functional characterization of a cation-Cl<sup>-</sup>-cotransporter-interacting protein*. Journal of Biological Chemistry, 2000. **275**(41): p. 32027-32036.
311. Miyo, M., et al., *Metabolic adaptation to nutritional stress in human colorectal cancer*. Scientific reports, 2016. **6**(1): p. 1-13.
312. Peng, H., Y. Wang, and W. Luo, *Multifaceted role of branched-chain amino acid metabolism in cancer*. Oncogene, 2020. **39**(44): p. 6747-6756.
313. Mohelnikova-Duchonova, B. and B. Melichar, *Human equilibrative nucleoside transporter 1 (hENT1): do we really have a new predictive biomarker of chemotherapy outcome in pancreatic cancer patients?* Pancreatology, 2013. **13**(6): p. 558-563.
314. Kleyner, R., et al., *Autosomal recessive SLC30A9 variants in a proband with a cerebrorenal syndrome and no parental consanguinity*. Molecular Case Studies, 2022. **8**(2): p. a006137.
315. Masclef, L., et al., *Roles and mechanisms of BAP1 deubiquitinase in tumor suppression*. Cell Death & Differentiation, 2021. **28**(2): p. 606-625.
316. Jumper, J., et al., *Highly accurate protein structure prediction with AlphaFold*. Nature, 2021. **596**(7873): p. 583-589.
317. Komander, D., M.J. Clague, and S. Urbé, *Breaking the chains: structure and function of the deubiquitinases*. Nature reviews Molecular cell biology, 2009. **10**(8): p. 550-563.

318. Guo, G., et al., *Frequent mutations of genes encoding ubiquitin-mediated proteolysis pathway components in clear cell renal cell carcinoma*. *Nature genetics*, 2012. **44**(1): p. 17-19.
319. Mills, J.W., et al., *Localization of [3H] ouabain-sensitive Na<sup>+</sup> pump sites in cultured pig kidney cells*. *American Journal of Physiology-Cell Physiology*, 1979. **236**(3): p. C157-C162.
320. Perantoni, A. and J.J. Berman, *Properties of Wilms' tumor line (TuWi) and pig kidney line (LLC-PK1) typical of normal kidney tubular epithelium*. *In vitro*, 1979. **15**(6): p. 446-454.
321. Marciano, D.K., *A holey pursuit: lumen formation in the developing kidney*. *Pediatric nephrology*, 2017. **32**(1): p. 7-20.
322. Pieczynski, J. and B. Margolis, *Protein complexes that control renal epithelial polarity*. *American Journal of Physiology-Renal Physiology*, 2011. **300**(3): p. F589-F601.
323. Hachimi, M., et al., *Smoothelin-like 2 inhibits Coronin-1B to stabilize the apical actin cortex during epithelial morphogenesis*. *Current Biology*, 2021. **31**(4): p. 696-706. e9.
324. Patrie, K.M., et al., *Interaction of two actin-binding proteins, synaptopodin and  $\alpha$ -actinin-4, with the tight junction protein MAGI-1*. *Journal of Biological Chemistry*, 2002. **277**(33): p. 30183-30190.
325. Matsuura, S., et al., *Expression of focal adhesion proteins in the developing rat kidney*. *Journal of Histochemistry & Cytochemistry*, 2011. **59**(9): p. 864-874.
326. Soufi, A. and S. Dalton, *Cycling through developmental decisions: how cell cycle dynamics control pluripotency, differentiation and reprogramming*. *Development*, 2016. **143**(23): p. 4301-4311.
327. Ambriz, X., P. De Lanerolle, and J. Ambrosio, *The mechanobiology of the actin cytoskeleton in stem cells during differentiation and interaction with biomaterials*. *Stem cells international*, 2018. **2018**.
328. Terzi, F., et al., *Normal tubular regeneration and differentiation of the post-ischemic kidney in mice lacking vimentin*. *The American journal of pathology*, 1997. **150**(4): p. 1361.

329. Gautreau, A., et al., *Ezrin, a plasma membrane–microfilament linker, signals cell survival through the phosphatidylinositol 3-kinase/Akt pathway*. Proceedings of the National Academy of Sciences, 1999. **96**(13): p. 7300-7305.
330. Ito, S., et al., *Energy-dependent transport of digoxin across renal tubular cell monolayers (LLC-PK1)*. Canadian journal of physiology and pharmacology, 1993. **71**(1): p. 40-47.
331. Tanigawara, Y., et al., *Transport of digoxin by human P-glycoprotein expressed in a porcine kidney epithelial cell line (LLC-PK1)*. Journal of Pharmacology and Experimental Therapeutics, 1992. **263**(2): p. 840-845.
332. Ito, S., G. Koren, and P. Harper, *Handling of digoxin and ouabain by renal tubular cells (LLC-PK1)*. Journal of Pharmacology and Experimental Therapeutics, 1992. **262**(1): p. 109-113.
333. Yoshimori, T., et al., *Bafilomycin A1, a specific inhibitor of vacuolar-type H (+)-ATPase, inhibits acidification and protein degradation in lysosomes of cultured cells*. Journal of Biological Chemistry, 1991. **266**(26): p. 17707-17712.
334. Gustafson, C.E., et al., *Recycling of AQP2 occurs through a temperature-and bafilomycin-sensitive trans-Golgi-associated compartment*. American Journal of Physiology-Renal Physiology, 2000. **278**(2): p. F317-F326.
335. Turajlic, S., et al., *Deterministic evolutionary trajectories influence primary tumor growth: TRACERx renal*. Cell, 2018. **173**(3): p. 595-610. e11.
336. Turajlic, S., et al., *Tracking cancer evolution reveals constrained routes to metastases: TRACERx renal*. Cell, 2018. **173**(3): p. 581-594. e12.
337. Chatterjee, S.J. and L. McCaffrey, *Emerging role of cell polarity proteins in breast cancer progression and metastasis*. Breast Cancer: Targets and Therapy, 2014. **6**: p. 15.
338. Lee, M. and V. Vasioukhin, *Cell polarity and cancer–cell and tissue polarity as a non-canonical tumor suppressor*. Journal of cell science, 2008. **121**(8): p. 1141-1150.
339. Savagner, P., *The epithelial–mesenchymal transition (EMT) phenomenon*. Annals of oncology, 2010. **21**: p. vii89-vii92.



340. Zhong, W., et al., *Identification of Epithelial–Mesenchymal Transition-Related lncRNA With Prognosis and Molecular Subtypes in Clear Cell Renal Cell Carcinoma*. *Frontiers in Oncology*, 2020. **10**: p. 2619.
341. Hardin, J., G.P. Bertoni, and L.J. Kleinsmith, *Becker's World of the Cell*, eBook. 2017: Pearson Higher Ed.
342. Aseervatham, J., *Cytoskeletal remodeling in cancer*. *Biology*, 2020. **9**(11): p. 385.
343. Gross, S.R., *Actin binding proteins: their ups and downs in metastatic life*. *Cell adhesion & migration*, 2013. **7**(2): p. 199-213.
344. Aramaki, S., et al., *Filopodia formation by crosslinking of F-actin with fascin in two different binding manners*. *Cytoskeleton*, 2016. **73**(7): p. 365-374.
345. Zhang, X., et al., *Novel Insights into the Role of the Cytoskeleton in Cancer*. *Cytoskelet. Struct. Dyn. Funct. Dis*, 2017. **64**: p. 259-278.
346. Zhang, P., et al., *Tubulin cofactor A functions as a novel positive regulator of ccRCC progression, invasion and metastasis*. *International journal of cancer*, 2013. **133**(12): p. 2801-2811.
347. Chow, A.Y., *Cell cycle control by oncogenes and tumor suppressors: driving the transformation of normal cells into cancerous cells*. *Nature Education*, 2010. **3**(9): p. 7.
348. Barron, D.A. and J.D. Kagey, *The role of the Hippo pathway in human disease and tumorigenesis*. *Clinical and translational medicine*, 2014. **3**(1): p. 1-10.
349. Wu, S., et al., *hippo encodes a Ste-20 family protein kinase that restricts cell proliferation and promotes apoptosis in conjunction with salvador and warts*. *Cell*, 2003. **114**(4): p. 445-456.
350. Nolo, R., et al., *The bantam microRNA is a target of the hippo tumor-suppressor pathway*. *Current Biology*, 2006. **16**(19): p. 1895-1904.
351. Tapon, N., et al., *salvador Promotes both cell cycle exit and apoptosis in Drosophila and is mutated in human cancer cell lines*. *Cell*, 2002. **110**(4): p. 467-478.
352. Genevet, A., et al., *Kibra is a regulator of the Salvador/Warts/Hippo signaling network*. *Developmental cell*, 2010. **18**(2): p. 300-308.

353. Hamaratoglu, F., et al., *The tumour-suppressor genes NF2/Merlin and Expanded act through Hippo signalling to regulate cell proliferation and apoptosis*. Nature cell biology, 2006. **8**(1): p. 27-36.
354. Genevet, A., et al., *The Hippo pathway regulates apical-domain size independently of its growth-control function*. Journal of cell science, 2009. **122**(14): p. 2360-2370.
355. Cho, E., et al., *Delineation of a Fat tumor suppressor pathway*. Nature genetics, 2006. **38**(10): p. 1142-1150.
356. Zhang, J., et al., *YAP-dependent induction of amphiregulin identifies a non-cell-autonomous component of the Hippo pathway*. Nature cell biology, 2009. **11**(12): p. 1444-1450.
357. Baena-Lopez, L.A., I. Rodríguez, and A. Baonza, *The tumor suppressor genes dachsous and fat modulate different signalling pathways by regulating dally and dally-like*. Proceedings of the National Academy of Sciences, 2008. **105**(28): p. 9645-9650.
358. Lavoie, H., J. Gagnon, and M. Therrien, *ERK signalling: a master regulator of cell behaviour, life and fate*. Nature Reviews Molecular Cell Biology, 2020. **21**(10): p. 607-632.
359. Parker, J.A. and C. Mattos, *The K-Ras, N-Ras, and H-Ras isoforms: unique conformational preferences and implications for targeting oncogenic mutants*. Cold Spring Harbor Perspectives in Medicine, 2018. **8**(8): p. a031427.
360. Yuan, J., et al., *The MAPK and AMPK signalings: interplay and implication in targeted cancer therapy*. Journal of hematology & oncology, 2020. **13**(1): p. 1-19.
361. Salinas-Sánchez, A., et al., *Role of mitogen-activated protein kinase (MAPK) in the sporadic renal cell carcinoma*. Actas Urológicas Españolas (English Edition), 2012. **36**(2): p. 99-103.
362. Lin, L., et al., *SLC transporters as therapeutic targets: emerging opportunities*. Nature reviews Drug discovery, 2015. **14**(8): p. 543-560.
363. Xie, J., et al., *Solute carrier transporters: potential targets for digestive system neoplasms*. Cancer Management and research, 2018. **10**: p. 153.



364. Ventii, K.H., et al., *BRCA1-associated protein-1 is a tumor suppressor that requires deubiquitinating activity and nuclear localization*. *Cancer research*, 2008. **68**(17): p. 6953-6962.
365. Garreta, E., N. Montserrat, and J.C.I. Belmonte, *Kidney organoids for disease modeling*. *Oncotarget*, 2018. **9**(16): p. 12552.

## 6 List of abbreviations

2-FDG	2-deoxy-2- fluoro-[18F]-D-glucose
3R	Replacement, Reduction, Refinement
ACTA1	Actin alpha 1
ACTBL2	Actin beta-like 2
ACTN4	$\alpha$ - actinin-4
ACTR2	Actin-related protein 2
AFDN	Afadin
ARF6	ADP-ribosylation factor 6
ARNO	Arf nucleotide-binding site opener
ANP	Atrial natriuretic peptide
AQP1	Aquaporin-1
ARE	Antioxidant response element
ARHGAP18	Rho GTPase Activating Protein 18
ATP1A1	Sodium/potassium-transporting ATPase subunit alpha-1
ATP1B1	Sodium/potassium-transporting ATPase subunit beta-1
Arp2/3 complex	Actin Related Protein 2/3 complex
BAP1	BRCA1 Associated Protein 1
BCAA	Branched-chain amino acid
BRAF	B-Raf Proto-Oncogene
BRCA1	Breast cancer gene 1

CA	Carbonic anhydrase
CAK	Cdk-activating kinase
CD10	Cluster of differentiation 10
CD276	Cluster of differentiation 276
CD31	Cluster of differentiation 31
CDC20	Cell division cycle 20
CDC42	Cell division control protein 42 homolog
CDH1	E-cadherin
CDH16	Cadherin-16
CDKN2A	Cyclin Dependent Kinase Inhibitor 2A
CDKs	Cyclin-dependent kinases
CFEX	Anion transporter
CIMP	CpG island methylator phenotype
CRISPR-Cas9	Clustered regularly interspaced short palindromic repeats-CRISPR-associated protein 9
CTNNB1	$\beta$ -catenin
CRB	Crumbs
DES	Desmin
DLG	Discslarge
DLL1	Delta like canonical notch ligand 1
DMBA	7,12-Dimethylbenz(a)anthracene
E2F1	E2F Transcription Factor 1

ECM	Extracellular matrix
EGFR	Epidermal growth factor receptor
ERK	Extracellular signal-regulated kinase
ESC	Embryonic stem cells
EZR	Ezrin
FAO	Fatty acid oxidation
FARP1	FERM, ARH/RhoGEF And Pleckstrin Domain Protein 1
FAS	Fatty Acid Synthesis
FDA	Food and Drug Administration
FGF8	fibroblast growth factor 8
FH	Fumarate hydratase
FN1	Fibronectin
GEMM	Genetically engineered mouse models
GEPIA	Gene Expression Profiling Interactive Analysis
GLUT2	Glucose transporter 2
GRB2	Growth factor receptor bound protein 2
HDIL-2	High doses of interleukin 2
HEK293	Human embryonic kidney 293 cells
HK2	Human kidney 2
HLRCC	Hereditary leiomyomatosis and Renal cell carcinoma
HSP90	Heat shock protein 90
IFN- $\alpha$	Interferon-alpha

IQGAP	IQ Motif Containing GTPase Activating Protein
ITGA5	Integrin Subunit Alpha 5
KCC3	Chloride potassium symporters 3
KCC4	Chloride potassium symporters 4
KCI	Chloride potassium symporter
KIFs	Kinesin superfamily proteins
KRAS	Kirsten rat sarcoma viral oncogene homolog
KRT	Keratin
Ki-67	Marker Of Proliferation
Ksp-cadherin	Kidney-specific cadherin
LGL	Lethal giant larvae
LHX1	Lim homeobox 1
MAPK	Mitogen-activated protein kinase
MAT1	Menage A Trois 1
MDCK	Madin–Darby canine kidney
MET	MET Proto-Oncogene
MET	Mesenchymal to Epithelial transition
MM	metanephric mesenchyme
Me-4FDG	Methyl-4-fluoro-[18F]-4-deoxy-D-glucopyranoside
NBCe1	Sodium/Bicarbonate cotransporter 1
NCX1	Sodium/calcium exchanger 1
NF1	Neurofibromin 1

NF2	Neurofibromin 2
NHE3	Sodium/hydrogen antiporter 3
NRF2	Nuclear erythroid 2-related factor 2
Na <sup>+</sup> /K <sup>+</sup> -ATPase	Sodium–potassium adenosine triphosphatase
NaPi-IIa	Sodium-dependent phosphate transport protein 2A
NaPi-IIc	Sodium-dependent phosphate transport protein 2C
NaSi1	Sodium/sulphate Symporters
OCN	Occludin
OK	Opossum kidney cells
PALS1	Protein associated with Lin-7 1
PATJ	PALS1-associated tight junction protein
PAX8	Paired box gene 8
PBRM1	Polybromo 1
PCNA	Proliferating cell nuclear antigen
PET	Positron emission tomography
PKD1	Polycystin 1
PKD2	Polycystin 2
PMCA	Plasma membrane calcium ATPases
PODXL	Podocalyxin
POU3F3	POU class 3 homeobox 3
PTH	Parathyroid hormone

Par3	Partitioning defective-3
Par6	Partitioning defective-6
PiT2	Sodium-dependent phosphate transporter 2
RAC	Ras-related C3 botulinum toxin substrate
RAD21	RAD21 Cohesin Complex Component
RAD51	RAD51 recombinase
RAF	Rapidly Accelerated Fibrosarcoma
RAS	Renin-angiotensin system
RASA1	RAS p21 protein activator 1
RCC	Renal cell carcinoma
RING	Really Interesting New Gene
RPTEC	Renal proximal tubule epithelial cell
RRAS	Ras-related protein
RVs	Renal vesicles
SAT1	Sulfate anion transporter 1
SAV1	Salvador Family WW Domain Containing Protein 1
SCRIB	Scribble
SETD2	SET Domain Containing 2
SGLT1	Sodium/glucose cotransporter 1
SGLT2	Sodium/glucose cotransporter 2
SKP1	S-phase kinase-associated protein 1
SLC	Solute carrier

SLC12A9	Solute Carrier Family 12 Member 9
SLC25A13	Solute Carrier Family 25 Member 13
SLC25A44	Solute Carrier Family 25 Member 44
SLC29A1	Solute Carrier Family 29 Member 1
SLC30A9	Solute Carrier Family 30 Member 9
SLC9A3R1	Sodium-hydrogen antiporter 3 regulator 1
SMAD	Small mothers against decapentaplegic
SMARCB1	SWI/SNF Related, Matrix Associated, Actin Dependent Regulator Of Chromatin, Subfamily B, Member 1
SMC3	Structural maintenance of chromosomes 3
SOS	Son of Sevenless
TAGLN	Transgelin
TBCA	Tubulin-specific chaperone A
TGF- $\beta$	Transforming growth factor beta
TFE3	Transcription factor E3
TJ	Tight junction
TMT	Tandem Mass Tag
TSGs	Tumor suppressor gene
UB	Ureteric bud
UCH	Ubiquitin C-terminal hydrolases
USC	Urine-derived stem cells
VHL	von Hippel–Lindau



VIM	Vimentin
WNT4	Wnt family member 4
ZO-1	Zonula occludens-1
ZnT	Zinc transporter
aPKC	atypical protein kinase C
ccRCC	Clear cell Renal cell carcinoma
chRCC	Chromophobe Renal cell carcinoma
ciPTEC	Conditionally immortalized PT epithelial cell line
iPSC	Induced pluripotent stem cells
pRCC	Papillary Renal cell carcinoma

## 7 List of figures

Figure 1.1 Graphical representation of the Kidney.	24
Figure 2.1 Significant determinants of apicobasal property.	32
Figure 2.3 Model depicting transcellular transportation mechanism of solutes across the luminal and basolateral membrane of proximal tubules.	46
Figure 2.4 ccRCC Pathophysiology.	53
Figure 1.5 Timeline showing the key events in the development of ccRCC models.	54
Figure 3.1 Development of self-organized proximal tubule formation.	78
Figure 3.2 Tubulogenesis process in proximal tubules.	79
Figure 3.3 Cystic nature of LLC-PK1.	80
Figure 3.4 Tubulogenesis process is two-step process.	82
Figure 3.5 Role of F-actin in dome formation.	83
Figure 3.6 Principal Component Analysis.	84
Figure 3.7 Gene Ontology enrichment analysis.	85
Figure 3.8 Presence of proximal tubules markers.	86
Figure 3.9 Expression of cell cycle proteins.	87
Figure 3.10 Luminogenesis protein in different stages of the proximal tubule.	88
Figure 3.11 Role of metabolic pathways in proximal tubule development.	89
Figure 3.12 Compartment analysis of proteins that are significantly regulated.	91
Figure 3.13 Expression of transporters during proximal tubule formation.	93
Figure 3.14 Role of cytoskeleton in the differentiation process of proximal tubules.	95
Figure 3.15 Effect of transport inhibition on proximal tubule development.	96
Figure 3.16 Effect of transporter inhibition on dome formation.	97
Figure 3.17 Effect of transporter inhibition on tube formation.	98
Figure 3.18 Experimental approach for introducing sequential ccRCC mutations into the genomes of primary proximal tubules with CRISPR-Cas9.	99
Figure 3.19 Validation of VHL knockout (VHL KO).	100
Figure 3.20 Immunoblot depicting VHL KO, BAP1 knockout (VHL + BAP1 DKO), and reconstituted BAP1 mutations in LLC-PK1 cells.	100

Figure 3.21 Evaluation of morphological changes.	102
Figure 3.22 Stress fibers formation.	104
Figure 3.23 Principal Component Analysis.	105
Figure 3.24 Loss of luminogenesis protein in metastatic ccRCC development.	106
Figure 3.25 Expression of EMT markers.	109
Figure 3.26 Deregulation of cytoskeleton proteins.	114
Figure 3.27 Analysis of the role of the oncogenic pathway.	119
Figure 3.28 Misregulation of SLC transporters.	122
Figure 3.29 Effect of cancer-associated missense mutations on the catalytic activity of BAP1.	126
Figure 4.1 Proposed model of tubulogenesis in proximal tubules.	128
Figure 4.2 EMT process during ccRCC development.	135

## 8 List of tables

Table 1.1 Cell lines reported to from domes	26
Table 1.2 Mechanism of lumen formation	28
Table 1.3 Proteins present in different complexes responsible for apical-basal polarity	32
Table 1.4 Different <i>in vitro</i> cell types used in biomedical research of proximal tubules	48
Table 1.5 The five different GEM models of ccRCC and comparison of the various features	55
Table 1.6 Monotherapy approved for the treatment of ccRCC	59
Table 1.7 Combinatorial therapy approved for the treatment of ccRCC	59
Table 1.8 Unsuccessful clinical trials of combinatorial therapy due to severe side effects	60
Table 1.9 Ongoing clinical trials of combinatorial therapy approved for the treatment of ccRCC	61
Table 2.1 List of cell lines and bacterial strains used in the study	63
Table 2.2 List of oligonucleotides used in the study	63
Table 2.3 List of plasmids used in the study	67
Table 2.4 List of antibodies used in the study	69
Table 2.5 List of compounds used in the study	70